THE CLIMATOLOGY OF THAILAND AND FUTURE CLIMATE CHANGE PROJECTIONS USING THE REGIONAL CLIMATE MODEL PRECIS

SUJITTRA INTHACHA

This thesis submitted in fulfillment of the requirements
for the degree of Doctor of Philosophy at the University of East Anglia.

School of Environmental Sciences

May 2011

Abstract

The climate of Thailand has not been studied in as much depth as in other parts of continental Southeast Asia. The baseline climate of Thailand during 1961-1990 is first analysed using **daily** observational data from five surface stations, each representing a different region of Thailand, supplemented by the high resolution 0.5° **monthly** gridded observational dataset, CRUTS2.1. The latter leads to a deeper understanding of the spatial variation in seasonal cycles of key climate variables in Thailand. Also revealed is an increase in the number of tropical depressions crossing Thailand during La Niña years. It was found that there is a statistically significant intensification (reduction) of precipitation during La Niña (El Niño) years at Surat Thani (Chiang Mai) in southern (northern) Thailand during ON (JJAS). This work facilitates the Regional Climate Model validation work which follows.

The Providing REgional Climates for Impact Studies regional climate model, PRECIS, was run for the first time over Southeast Asia to specifically study the climate of Thailand. The first phase is model validation during the 1961-1990 baseline period. An ensemble of RCM runs is undertaken to study the sensitivity to the driving GCM. The added value provided by PRECIS in comparison to the coarser driving models is discussed. The possible causes of model bias are investigated. The model projections for the end of this century are undertaken based on high (SRES-A2) and low (SRES-B2) emission scenarios which estimate the range of possible climate change in Thailand. These RCM simulations suggest trends in temperature that are broadly in line with those reported by IPCC. PRECIS A2 and B2 simulations mostly produce small precipitation increases in JJAS and small precipitation increases (decreases) during DJF under the A2 (B2) scenario. Wet season precipitation increases appear to be related to higher rain intensity on fewer rain days.

Statement of Originality

This thesis has not previously been submitted for any degree in other universities. There is no material previously published or written by another author excluding where reference is made. Unless otherwise noted or referenced in the text, the content in this thesis is that of the author.

Sujittra Inthacha May 2011

Acknowledgments

First of all, I would like to profoundly thank Dr. Steve Dorling, my supervisor, for giving me the opportunity to study here in UEA and for being an excellent supervisor who always gave his time to help and support me, especially, during my last year study. I truly appreciate his advice and his attitudes for being an international student. He also gave me an opportunity to participate in an international conference in Malaysia in 2008 which is very helpful for my further research when I return to Thailand.

Regarding the observation data set thanks are due to the Thai Meteorology Department for providing station data set, Climate Research Unit for high resolution gridded data set CRUTS2.1, National Oceanic and Atmospheric Administration for NCAR-NCEP reanalysis data, Tropical Rainfall Measuring Mission for satellite images which are available online and easy to access.

For the tool in this study, I would like to thank the UK Met Office to make the PRECIS, Regional Climate Model, available for public and also kindly organised the PRECIS workshop that I participated in 2006 as well as continue support, in particular David Hein providing excellent technical support with running the model. Further technical support was supplied by Julie Harold and Mike Simon. I also would like to thank Stephen Ag for CDAT technical assistance.

Thanks to the consortium of PRECIS running over SEA, Justin Sentian at University of Malaysia Sabah, Malaysia, Fredolin Tangang and Liew Ju Neng at Universiti Kebangsaan Malaysia and Mohan Kumar Sammathuria at Malaysian Meteorological Department for sharing the PRECIS output.

I would like to give special thanks to my parents for their love and support. Finally, thank to the Thai Royal Government for giving me a scholarship to carry out this project.

Contents

List of Figures

List of Tables

Abbreviations

CDAT- Climate Data Analysis Tools

ECHAM4 – European Centre HAMburg 4; an atmosphere only GCM described in Roeckner et al. (1996)

ECMWF – European Centre for Medium-range Weather Forecasts

ERA40 – ECMWF 45 year reanalysis of the global atmosphere and surface conditions in 1957-2002

GCM – General Circulation Model

HadAM3P – Third Hadley centre Atmosphere Model version P; an updated version of HadAM3H, described in Gordon et al. (2000) and Pope et al. (2000)

HadCM3 – Third Hadley centre Coupled Model; a coupled ocean-atmosphere GCM

HadRM3P – Third Hadley Centre Regional Model version P; an updated version of HadRM3H, described in Jones et al. (2004)

IPCC – Intergovernmental Panel on Climate Change

IPCC SRES – IPCC Special Report on Emission Scenarios

NCEP – National Center for Environmental Prediction

NCAR – National Center for Atmospheric Research

PRECIS – Providing REgional Climates for Impact Studies; a RCM based on HadRM3P

RCM – Regional Climate Model

SEA – Southeast Asia

TMD – Thai Meteorology Department

UKMO – United Kingdom Met office

Abstract

The climate of Thailand has not been studied in as much depth as in other parts of continental Southeast Asia. The baseline climate of Thailand during 1961-1990 is first analysed using **daily** observational data from five surface stations, each representing a different region of Thailand, supplemented by the high resolution 0.5° **monthly** gridded observational dataset, CRUTS2.1. The latter leads to a deeper understanding of the spatial variation in seasonal cycles of key climate variables in Thailand. Also revealed is an increase in the number of tropical depressions crossing Thailand during La Niña years. It was found that there is a statistically significant intensification (reduction) of precipitation during La Niña (El Niño) years at Surat Thani (Chiang Mai) in southern (northern) Thailand during ON (JJAS). This work facilitates the Regional Climate Model validation work which follows.

The Providing REgional Climates for Impact Studies regional climate model, PRECIS, was run for the first time over Southeast Asia to specifically study the climate of Thailand. The first phase is model validation during the 1961-1990 baseline period. An ensemble of RCM runs is undertaken to study the sensitivity to the driving GCM. The added value provided by PRECIS in comparison to the coarser driving models is discussed. The possible causes of model bias are investigated. The model projections for the end of this century are undertaken based on high (SRES-A2) and low (SRES-B2) emission scenarios which estimate the range of possible climate change in Thailand. These RCM simulations suggest trends in temperature that are broadly in line with those reported by IPCC. PRECIS A2 and B2 simulations mostly produce small precipitation increases in JJAS and small precipitation increases (decreases) during DJF under the A2 (B2) scenario. Wet season precipitation increases appear to be related to higher rain intensity on fewer rain days.

Chapter 1

Introduction and literature review

The changing composition of the atmosphere, resulting from anthropogenic emission of greenhouse gases (carbon dioxide (CO_2), methane (CH_4), nitrous oxide (N_2O), halocarbons and sulphur hexafluoride (SF_6)) and natural variations in volcanic and solar forcing, causes radiative forcing changes which affect the climate system. For example, the variable forcing is associated with trends in surface air temperature at global and subcontinental scales, changing ocean heat content, snow cover extent, season length, precipitation regime and mean sea level pressure patterns (Mitchell et al. (2001); Zwiers and Zhang (2003); Stott (2003); Braganza et al. (2004); Gillett et al. (2004); Zhang et al. (2006); Karoly and Wu (2005)). IPCC-AR4 (2007) showed that positive forcing by greenhouse gases is propagated almost equally between the hemispheres and varies with latitude; response to anthropogenic forcing is detected over all continents except Antarctica. Greenhouse gases modify the warm climate by reducing longwave radiation escaping to space. They are well mixed through the troposphere so their concentrations vary little. Global climate changes associated with anthropogenic forcing in the latter half of the 20th century include climate extremes, upper level ocean warming, declining sea ice extent, glacier retreat contributing to sea level rise, increasing land-ocean temperature contrast, increases in heavy precipitation and troposphere height increase with simultaneous tropospheric warming and stratospheric cooling (IPCC-AR4, 2007). Recent studies show that anthropogenic greenhouse gas emissions are expected to lead to more frequent and intense summer temperature extremes, not only due to the mean warming itself, but also due to changes in temperature variability (Fischer and Christoph, 2009). Interestingly, over tropical regions, anthropogenic forcing contributed to increases in the frequency of the most intense tropical cyclones since the 1970s (IPCC-AR4, 2007).

The radiative forcing is also related to the capacity of atmospheric sulphate aerosols to directly reflect solar radiation back into space and to produce brighter clouds through their action as cloud condensation nuclei, producing a cooling effect. The (negative) climate forcing by the aerosols has strong regional character, with the

greatest forcing over Northern Hemisphere land surfaces (Taylor and Penner, 1994). Anthropogenic sulphate aerosols contribute a globally averaged annual forcing of -0.3 Wm^{-2} as compared with +2.1 Wm^{-2} for greenhouse gases (IPCC, AR4, 2007). The magnitude of radiative forcing as a result of the sulphate effect is relatively low compared with that of the greenhouse gas effect and, with respect to their sulphur aerosol study over SEA, Siniarovina and Engardt (2005) concluded that the sulphur deposition is still relatively low (i.e. <0.5 g sulphur m^{-2} $year^{-1}$) in most of rural Malaysia.

Regional climate model simulations are now possible in every region of the world. However, while there is a considerable literature looking at global models and their description of current and possible future Southeast Asia (SEA; area of 24°N, 94°E to 15°S 154°E; Figure 1.1) climate, regional climate simulations in this area are only just beginning. Regional climate is an important issue in Southeast Asia because many countries in the region depend on agriculture. For example, in Thailand the proportion of the labour force in agriculture is 42.6% with GDP by sector of 11.4% (CIA, 2008). It is obvious that more study of current and future climate could benefit the agricultural economy of both the region and of Thailand in particular, helping them become more resilient. This thesis aims to extend knowledge regarding the current and future climate of Thailand by using both station and gridded observational data and through modelling of past and future regional climate in Southeast Asia.

Figure 1.1: Map of Continent of Southeast Asia. [Source: Central Intelligence Agency, USA].

1.1 The General Circulation of the tropics and the Southeast Asia monsoon

Study of the general circulation of the atmosphere requires consideration of air movement in three dimensions and is a prerequisite for understanding the global wind systems. The tropics commonly refer to the latitude region from 23.5^{o}S to 23.5^{o}N which covers more than 40% of the earth's surface. There are two large scale circulations associated with the tropical region, the meridional Hadley cell and the zonal Walker circulation. The Hadley circulations show seasonal variations because there is a larger equator-pole temperature gradient in the winter hemisphere (Newell et al., 1972) as show in Figure 1.2. The meridional Hadley cell dominates the tropical atmosphere with air rising at the inter-tropical convergence zone (ITCZ) and sinking

in the sub-tropics. The returning surface air flow near the equator is a prevailing pattern of easterly winds known as the trade winds. The trade winds in both the northern and southern hemisphere, laden with heat and moisture from surface evaporation and sensible heating, converge in the area known as the ITCZ. Seasonal shifts in the ITCZ relate to the shifts in the location of the overhead sun. The main characteristics of the ITCZ are increased mean convection, cloudiness and precipitation due to surface convergence (Waliser, 1993). There are seven non-overlapping ITCZ regions, including the Indian / Southeast Asia region as shown in Table 1.1.

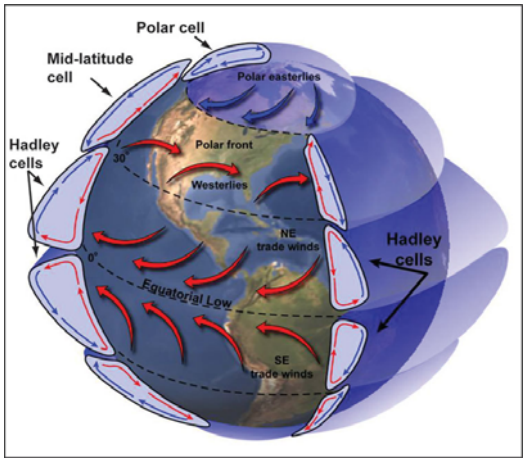

Figure 1.2: The Hadley Cell circulation illustrates how rising air in the superheated tropics descends in the subtropics. This creates high-pressure zones in subtropical regions. Source: Barbara Summey, NASA Goddard Visualization Analysis Lab. http://www.nasa.gov/

Table 1.1: Region and longitude limits for ITCZ domain analyzed. Latitude limits are 25 ^{o}S to 25 ^{o}N (Waliser and Gautier, 1993)

Region	Longitude limits
Africa	10^{o} - 40^{o}E
Indian	60^{o} - 100^{o}E
West Pacific	110^{o} - 150^{o}E
Central Pacific	160^{o}E- 160^{o}W
East Pacific	100^{o} - 140^{o}W
South America	45^{o} - 75^{o}W
Atlantic	10^{o} - 40^{o}W

Seasonal movement of the ITCZ near the equator induces large scale monsoonal wind regimes, known as the northeast and southwest monsoons. The tropical zonal circulation, the Walker circulation named after Sir Gilbert Walker, explains the distribution of tropical convection which is caused by the pressure gradient force that results form high pressure over the eastern Pacific and relatively low pressure over Indonesia, leading to ascending motion over Indonesia and the western tropical Pacific and descending motion over the eastern Pacific, with upper level westerly (low level easterly) winds (Bjerknes, 1969) as shown in Figure 1.3. This circulation is part of a more complex ocean–atmosphere coupled phenomenon called the El Niño/Southern Oscillation (ENSO), through the exchange of air between the eastern Indian Ocean/Indonesia and the south-eastern tropical Pacific. The low (warm) phase of the ENSO is accompanied by higher than normal sea level pressure (SLP) in the western tropical Pacific and lower than normal SLP in the southeastern tropical Pacific, positive sea surface temperature (SST) anomalies and weakened trade winds in the central and eastern equatorial Pacific (e.g. Rasmusson and Carpenter, 1982; Rasmusson and Arkin, 1985). These variables show nearly reversed anomaly patterns during the high (cold) phase of the ENSO (Kousky and Ropelewski, 1989). In the normal condition, the tropical western Pacific is warmer than the eastern Pacific. As a result air rises over the warm western Pacific and flows eastward in the upper troposphere to subside in the eastern Pacific high pressure system and equatorial winds in the surface layers are westward associated with the convection in the western Pacific and subsidence over the eastern Pacific. This circulation cell is known as Walker Circulation.

During El Niño episodes, weaker easterly trade winds in the lower atmosphere and weaker westerly winds in the upper atmosphere over the eastern half of the Pacific reflect a reduced equatorial Walker Circulation with enhanced suppression of convective precipitation across the region; the convection in the west is weaker and the convection in the eastern Pacific is stronger. Since the convection is suppressed in the western Pacific, El Niño causes drier conditions over Indonesia, the Philippines, Indonesia and southern Thailand during the boreal winter, DJF, while northern Thailand is mostly influenced by the dry and cold air mass from the northeast monsoon. There are some studies in the literature which discuss El Niño/La Niña impacts on precipitation variability over SEA. An El Niño event tends to be associated with droughts while a La Niña event is more likely to be associated with

excessive monsoon rain over SEA including Thailand (with relatively small effect compared with maritime countries, i.e., Indonesia and the Philippines). In other words, seasonal precipitation over SEA is known to be modulated but not dominated by the El Niño Southern Oscillation (ENSO) phenomenon, with ENSO warm (cold) events contributing to drought (excessive precipitation) in many areas. Manton et al. (2001) reported that annual total precipitation in SEA and the number of rain days generally decreased between 1961 and 1998 and that this was associated with a predominance of El Niño events since the mid-1970s. Roy (2000) showed that El Niño events in 1972 and 1976 had lead to a 10% reduction in precipitation amount in Myanmar. During one of the strongest El Niño events in 1997, Bell and Halpert (1998) mentioned that most of the Southeast Asian countries experienced relatively lower precipitation than average; 50% in Indonesia during March to December, drought and wild fires in Sumatra and Borneo during July and August. Singapore, Malaysia, Brunei, Philippines, Thailand and Vietnam were also faced with prolonged drought during May to September. Indonesia is expected to be influenced by the Indian Ocean Dipole, IOD, a coupled ocean-atmosphere phenomenon in the Indian Ocean. Positive IOD is associated with anomalously warm SSTs in the western Indian Ocean and colder than normal SSTs in the east associated with surface winds which reverse from a westerly to an easterly direction over the central equatorial Indian Ocean; atmospheric convection normally situated over the eastern Indian Ocean shifts to the west and was related to severe dry conditions over Indonesia in 1997. Krishnan et al. (2000) indicated that suppressed convection over Burma, Vietnam, Thailand, the Philippines, and Indonesia is in phase with that over the Indian subcontinent. The 1997 El Niño year led to a reduction in cash crops, rice, and sugar over the next eight months; an 8% cut from expected in 1997/98 sugar cane yields; 38% reduction in 1998 second rice crop (from 1997 yields) and reduced agricultural exports in Thailand (http://enso.unl.edu/ndmc/enigma/elnino.htm). Singhrattna et al. (2005) found that ENSO has a negative relationship with the summer monsoon precipitation over Thailand in the post 1980 period, i.e. El Niño events tend to reduce equatorial Walker circulation over the Thailand-Indonesian region, as a result of significant convection reduction and reducing precipitation over Thailand. Dry years can be associated with ENSO events (Boochabun, 2004).

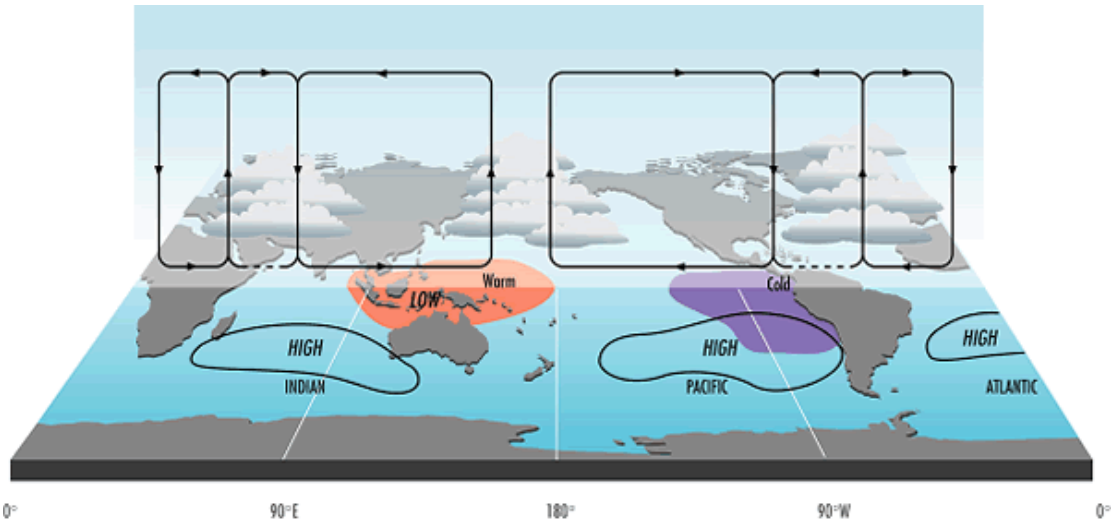

Figure 1.3: The east-west Walker Circulation of the tropics. Source: Bureau of Meteorology, Australian Government. http://www.bom.gov.au

The Asian monsoon, one of the most important components of the global climate system, plays a significant role in large-scale climate variability over much of the globe, affecting the Southeast Asia region. The term 'monsoon' generally refers to the seasonal winds and precipitation. Heat capacity differences between land and sea are the key driving force maintaining the Asian summer monsoon cycle. The onset, progression and retreat of the SEA can be diagnosed through the behaviour of deep convection and the atmospheric circulations. Ramage (1971) defined the monsoon as a resultant wind direction shift which exceeds 3 ms^{-1} by at least 120^{o} between January and July. Nicholls et al (1982) define the monsoon onset as a precipitation amount greater than or equal to 15% of the mean annual. Davidson et al (1983) define the monsoon onset by using infrared satellite imagery to identify the first large-scale development of tropical convection spanning the region for several days. Others define the recognised characteristics of the Southeast Asia summer monsoon onset to be strong deep convection, a threshold of 5 mm precipitation per day and a south westerly wind over the Indo-china Peninsula and the South China Sea at low level (Tanaka, 1992; Murakami and Matsumoto, 1994). Sangwaldach (2006) suggested that the southwest monsoon onset criteria should require that (i) there are three consecutive rainy days in a five day period (pentad analysis), (ii) the consecutive rainy days must have not less than 5 mm each day, (iii) the accumulated rain of the five rainy days must not be less than 25 mm, (iv) the low level wind direction must

change to westerly or southwesterly and (v) the upper level wind must change to easterly.

Traditionally, the Asian monsoon is considered to consist of two subsystems; the Indian and East Asia monsoons. The Southeast Asia monsoon circulation is a part of the Indian monsoon. There are two seasonal monsoons over Southeast Asia; (i) the north-east monsoon, (ii) the south-west monsoon. Nieuwolt (1981) points out that January (July) can be considered to represent the typical climate of the north-east (south-west) monsoon period as shown for the surface wind system in Figure 1.3.

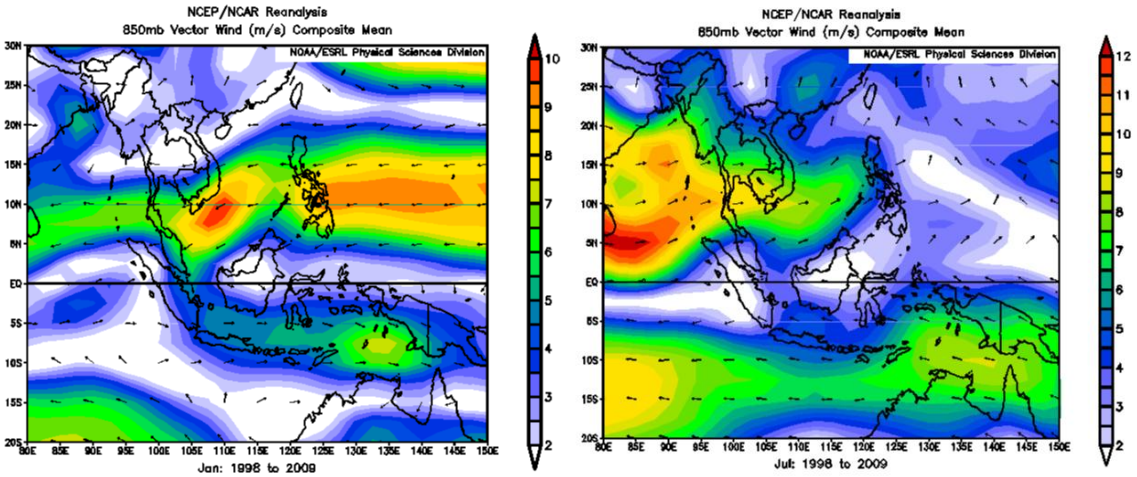

Figure 1.4: Average NCEP Reanalysis 850 mb winds (ms^{-1}) for January (left) and July (right) in 1998-2009 over SEA.

1.1.1 The Northeast monsoon

The northeast monsoon, also known as the winter monsoon, occurs between November and February when the ITCZ moves southwards. The Northeast monsoon brings two air masses which are (i) a very cold, dry and stable (polar-continental) air mass from Siberia and Mongolia and (ii) a generally very warm and moist (tropical/equatorial maritime) air mass from the Pacific Ocean, north of the equator, carried by trade winds (Nieuwolt, 1981). During the north-east monsoon, the cold air mass emanates from a region of high pressure and travels across Korea, Japan, southern China, Indochina and the western Pacific resulting in relatively dry conditions (Chang and Lau, 1982). Occasionally, typhoon activity over the South China Sea decreases in this north-east monsoon period (Lau and Yang, 1996). As the air associated with the northeast monsoon traverses the South of China it is

transformed to a warm and tropical air mass as it moves along the east coast of peninsular Thailand and maritime SEA, resulting in convective activity and a relatively wet period during November to March (Houze et al, 1981; Webster et al, 1998). In the November-December period equatorial westerlies converge with the advancing northeast monsoon resulting in ascent and a considerable increase in precipitation where the centre of convection is located over Indonesia (Nieuwolt, 1981). Sudden increases in wind speed are usually stronger during the early northeast monsoon period and progressively weaker during the latter half of the northeast monsoon. Over the northern South China Sea winds can increase from 4-6 ms^{-1} to over 30 ms^{-1}. In the latter period of the northeast monsoon, the low level jet flows across the equator and this marks the beginning of the northwest Australia monsoon. Convective activity increases over Borneo, the Indochina coast and the Philippines (Kemball and Wang, 2001).

1.1.2 The Southwest monsoon

The Southwest monsoon, also known as the summer monsoon, occurs form June to September. There are two main origins of the air mass of the Southwest monsoon. First, the southeasterly trade winds from Australia and the South Pacific bring stable air to the equatorial area (Nieuwolt, 1981; He et al., 1987; Murakami, 1994; Lau, 1997; Ding 2004). The air then flows westward over the warm seas and islands of Indonesia so that when it reaches continental Southeast Asia it is very humid and has become unstable (Nieuwolt, 1981; Qian and Lee, 2000; Wang 2002). Second, the other important air masses come from the Indian Ocean (Nieuwolt, 1981). The main feature of this period is deep convection. In the meantime, convection and low-level winds from the equatorial Indian Ocean move northward to the Bay of Bengal (Joseph, 2007). Lau and Yang (1996) found that the Asian summer monsoon onset is a demonstration of northward progression of convection in early May. An Easterly jet from the South China Sea across India can produce precipitation over northern Southeast Asia (Hasternrath, 1991, Matsumoto, 1997; Zang and Gottschalck, 2002). The rain's progress moves toward northwestern and northern India during June (McGregor and Nieuwolt, 1998).

1.1.3 The Inter-monsoon

There are two transitional periods in between the Northeast and Southwest monsoons and these are known as inter-monsoons which are characterised by light winds, overcast skies and squally weather over the South China Sea.

In the inter-monsoon period of April and May, the continental high pressure area over Siberia and Mongolia has declined and the trade winds with lower speed are mainly from the North Pacific. During April, the general circulation over SEA is relatively weak. May is part of the Southwest monsoon period over southern Thailand, Malaysia and Indonesia. but is still a month of transition over the northern part while the other parts, such as Indonesia, Brunei, east Malaysia, Papua New Guinea and Philippines, are much more influenced by equatorial winds.

In the Inter-monsoon period of October, the Southwest monsoon is weakened while at the same time the Northeast monsoon still mainly consists of trade winds from the northern Pacific. The wind velocities are generally very low. November sees the complete retreat of the southwest monsoon and the influence of the northeast monsoon which brings moisture from the South China Sea to the peninsula.

1.2 The Climate of Southeast Asia and Thailand

Southeast Asia can be divided into two geographic regions: (i) the Indochina consists of Cambodia, Laos, Myanmar, Thailand, Vietnam, Peninsular Malaysia, and (ii) maritime sections consist of Brunei, East Malaysia, East Timor, Indonesia, the Philippines and Singapore. The region covers an approximate latitude range from 10°S to 25°N (Figure 1.1). Thailand is located between latitudes of 5.4˚N and 20.3˚N and longitudes of 97.7˚E and 105.45˚E. Its estimated land area, 513,115 km^2, can be divided into four distinct topographic regions: (i) The peninsular region begins from the head of the Gulf of Thailand and consists of several ridges parallel to the coast; (ii) The elevation along the border with Myanmar reaches 1300-1800 m, (iii) the remaining ridges are generally below 300-600 m; (iv) The northern and eastern regions of the plateau are separated from Laos by the Mekong River.

The four Thai topographic regions are influenced by the southwest monsoon; a strong monsoon system would appear to be very beneficial. A weak summer monsoon with lower than mean precipitation may lead to lower crop yields while a strong summer monsoon is likely to produce higher crop yields. Rice is the chief crop of SEA; rubber, tea, spices and coconuts are also important since the 1960s For example, in Thailand, Rice is grown on approximately 66% of the land area (source: the Office of Agricultural Economics, Thailand, 2002). The rice cultivation season begins in May or June with the onset of the monsoon showers in northern Thailand while the first crop is grown in central Thailand in March-October. Too much precipitation can result in flooding and associated problems. Obviously, better understanding of the monsoon variability could lead to improvements in seasonal forecasting and climate modelling which could assist agriculture and society.

The first rains occur over Myanmar and Thailand in mid-May associated with the development of a lower tropospheric trough over the Bay of Bengal (Slingo, 1999). In May the whole of Thailand receives well over 100 mm of precipitation, and the west coast of the peninsula, i.e. areas on the windward side of the mountain ranges facing the south-westerly air-stream, receives more than 200 mm. Some portions in this region even receive 500 mm of rain based on station data over 1961-1980 (Kripalani et. al, 1995). In Thailand, during May to October, the weather is dominated by the Southwest monsoon blowing from the Indian Ocean bringing a warm, humid air mass and much cloud. Precipitation during this period is not only caused by the Southwest monsoon but also by orographic precipitation enhancement, the Inter Tropical Convergence Zone (ITCZ) and tropical cyclones. The ITCZ first arrives in the southern part of Thailand in May and then moves rapidly northwards and generally lies across southern China during June to early July leading to a dry spell over northern parts of Thailand. Precipitation on the west coast of peninsular Thailand, in the southeastern region, over a large part of the continental highlands, and in the eastern section of the northeastern region is typically over 200 mm, but dry portions can be found on the leeward side of the mountain ranges. In the central valley and in some parts of the western region, precipitation remains below 100 mm (Kripalani et. al, 1995). The ITCZ moves southward once again, following the path of the overhead sun, to lie over the northern and northeastern parts of Thailand in August and later over the central and southern parts in September and October respectively.

Interestingly, the variation in timing of the beginning and end of the rainy season in Thailand is quite large from place to place with precipitation peaking first in the east, northeast, central and then north of Thailand (Chokngamwong and Chiu, 2006). Wang (2002) proposed that the summer monsoon cycle spans from the middle of May to early September. Matsumoto (1997) indicated that the onset passes over the Indochina peninsula, i.e., Laos, Vietnam, Cambodia, Myanmar, Thailand, in pentad 25 (6 to 10 May) and 26 (11 to 15 May). Takahashi and Yasunari (2006) found that the monsoon season extends from pentad 26-60. The first monsoon rains occur over Myanmar and Thailand in approximately mid-May and subsequently extend to the northwest.

With respect to the summer monsoon, Zhang et al. (2004), using NCEP reanalysis data, confirmed the mechanism of summer monsoon onset over the Indochina peninsula as being triggered by active convection and precipitation resulting from the convergence of southwesterly flow from the Bay of Bengal vortex and easterly winds associated with the subtropical anticyclone over the South China Sea in early May, although the atmosphere over the Indochina peninsula has already become quite thermally unstable since early April. By April, the whole of Thailand, except for a small portion in the northwestern region, receives over 50 mm, and the peninsula receives over 100 mm of precipitation (Kripalani et. al, 1995).

Kripalani and Kulkarni (1997) analysed station precipitation data during 1970-2000 and did not find systematic climate change in the Southeast Asia region. Similarly, Zveryaev and Aleksandrova (2004) indicated that there is no significant precipitation trend in the South China Sea precipitation during January and February based on CRU05 0.5°lat/lon gridded monthly climate data for 1949–98. They also showed that decadal-scale JJAS precipitation changes over Southeast Asia become more pronounced during 1979-1998 with predominantly dry conditions from 1984 to 1990 and anomalously wet conditions in 1993–97. Pai (2007) found that monsoon onset at the surface is recognised as a rapid, substantial and sustained increase in precipitation. The monsoon onset in each year in Thailand, located in the central part of the Indochina Peninsula, was defined by Zhang et al (2004) using the daily area-averaged precipitation from 30 stations over the region from 1951-1996. The trend in overall precipitation over Thailand, both temporal and spatial, has not changed significantly over 1980-1999. McGregor (1998) found that precipitation during the summer

monsoon over the South China Sea (SCS) is associated with the ITCZ returning southward, reaching 15°N during July-August when moist air from the Indian Ocean helps enhance convection.

Chokngamwong and Chiu (2008), using Thailand gauges over the period 1993-2002, show two distinct seasons, dry and rainy with the latter starting in May and progressing southeast to northwest. The wettest month occurs in August for the north and northeast Thailand, in September for the central and east regions and in November for the southern region with the retreat of precipitation following ITCZ movement from north to south, bringing extremely intense precipitation. The reason for this peak in precipitation is a significant increase of westerly wind components at 850mb while westerly winds are being slowly replaced by easterlies, of anticyclonic origin, in the upper parts of the troposphere. The boundary between these two airstreams, at around 19˚N latitude, is associated with the zone of the doldrums with light wind velocity and changeable wind direction; strong upward motions and convection are promoted from the associated atmospheric instability (Ding, 1994; Zhu and Houghton, 1996, Kripalani and Kulkarni, 1997a) This situation persists until it becomes cooler over the land and until Sea Surface Temperature (SST) attains a sufficient level to affect the horizontal pressure gradient and thereby reduce the moist inflow from the sea, marking the end of the monsoon season.

In addition to the ITCZ and the South-west Monsoon, cyclonic disturbances make an important contribution to the seasonality of precipitation in some parts of Thailand. A Tropical cyclone is a synoptic-scale low pressure system occurring over regions of Tropical Ocean with latitude greater than 5^{o} and with SST greater than 26.5^{o}C and limited vertical wind shear in order to facilitate thunderstorm development (Hasternrath, 1991 and McGregor and Nieuwolt, 1998). Observation tracks indicate that more tropical storms develop in the South China Sea than in the Indian Ocean. According to records of cyclonic disturbances moving across Thailand, the most active months are in September, October and November, respectively (Table 1.2). The highest record of cyclonic disturbance parts in September is moving easterly toward Vietnam followed by upper NE and lower northern Thailand, including Phitsanuloke site. This cyclonic disturbance related to the high surface water temperatures over the

South China Sea, often occur near Vietnam and may also reach Thailand during June to September developed from the South China Sea or the northwest Pacific Ocean (Takahashi and Arakawa 1981). And during October and November, the record shows favourite path of the disturbance moving to southern Thailand. It is implied that the cyclonic disturbance path is related to ITCZ movement.

Table 1.2: Record of cyclonic disturbances moving across Thailand provided by Thai Meteorology Office.

Year/month	Jan	Feb	Mar	Apr	May	Jun	Jul	Aug	Sep	Oct	Nov	Dec	Total
1961				1	2			1		2			6
1962							1		1	1	1		4
1963							1		2	1	1		5
1964									2	4	2	1	9
1965								2	6			1	9
1966						1				2	2	1	6
1967									1	3	1		5
1968								2		1	1		4
1969						1	1		2	1	1		6
1970								1	2	2	2		7
1971							2		1	1			4
1972						1			2	1		1	5
1973							1	1	1	1	2		6
1974								1		1	1	1	4
1975					1				2				3
1976													0
1977									1		1		2
1978							1	1	2		1		5
1979								1	1				2
1980					1				2		1		4
1981										1			1
1982					1				1				2
1983						1				3	1		5
1984						1				1	1		3

Table 1.2 (continued)

Year/month	Jan	Feb	Mar	Apr	May	Jun	Jul	Aug	Sep	Oct	Nov	Dec	Total
1985									1	2			3
1986									1	1			2
1987								1					1
1988									1				1
1989					1				2	1			4
1990													0
total				1	6	5	7	11	34	30	19	5	118

With respect to upper tropospheric winds, the tropical easterly jet, TEJ was found to be responsible for the large high-cloud amount in the Asian monsoon region cooling this region by spreading the cloud tops and increasing the high-cloud amount. Sathiyamoorthy et al. (2004) suggest that apart from the TEJ, other meteorological (e.g. shifts in the position of convective clouds between excess and deficient monsoon years) and cloud microphysical properties (water/ice particle size, shape, etc.) may also affect the cloud radiative forcing in the Asian monsoon region. It is noted that large data gaps are present in the radiative flux data over the Indian and SEA region.

With respect to teleconnections, Ye and Bao (2001) used long-term historical synoptic observational records and recently available remote sensing observations during 1936–1990 to demonstrate that teleconnections exist between Eurasian winter snow and Southeast Asian summer monsoon precipitation (for example snow volume has a more significant connection to summer monsoon precipitation than snow coverage). The earliest snow onsets over northeastern Siberia significantly affect warm season monsoon strength, i.e. precipitation, moisture fluxes and wind vectors, over Southeast Asia (Ye, et al., 2005). They implied that snow depth over the northern Ural Mountains may have some influence on June precipitation over Southeast Asia. Many studies have also found that snow volume has a larger impact on monsoon precipitation than spatial snow coverage (e.g. Barnett *et al*., 1988, 1989; Douville and Royer, 1996; Dong and Valdes, 1998). The variation of snow depth over western rather than eastern Eurasia seems to have a significant influence on summer monsoon

precipitation over Southeast Asia. The monsoons over SEA are sensitive to uplift over the Tibetan Plateau and positively correlated with the snow cover (and hence the surface albedo) over the Tibetan Plateau (Liu and Chen, 2000). With respect to El Niño events, it is directly related to the onsets of the Southeast Asian monsoon rather than the withdrawal dates (Fasullo and Webster, 2003) and it tends to overwhelm the connections of the snow-monsoon relationship (Fasullo, 2004).

In summary, the known climate of Thailand based on analysing precipitation data reveals a climate which is governed by monsoonal air flow and ITCZ movement. In this study, additional observational data are deployed to generate derived variables such as, for example, number of wet days and diurnal temperature range, in order to gain a more comprehensive understanding of the climate of Thailand.

1.3 Climate Change in SEA

It is well known that the global temperature has increased in recent times. The IPCC Third Assessment Report states that the average global surface temperature over the 20th century has increased by about 0.6±0.2 °C (Houghton 2001) while the IPCC Fourth report (AR4) updated the 100 year observed linear trend (1906-2005) indicating that the average global surface temperature over the 20th century has increased by 0.74°C with the range 0.56°C to 0.92 °C and the linear warming trend over the last 50 years is 0.13°C per decade. Griffiths et al. (2005) found that there is spatial coherence in daily maximum and minimum temperatures, extremes and variance across the Asia-Pacific region based on station observations during the period 1961-2003. The majority of stations exhibit significant trends, with increases in mean, maximum and minimum temperature, decreases in cold nights and cool days and increases in warm nights. Correlations between mean temperature and the frequency of extreme temperatures were strongest in the tropical Pacific Ocean from French Polynesia to Papua New Guinea, Malaysia, the Philippines, Thailand and southern Japan. The annual mean temperature during the period 1976-1990 over Bangladesh, the Bay of Bengal, northern Thailand, Malaysia and Sri Lanka significantly increased by 0.04 °C/year (Quadir et al. 2004). Moreover, the region over northeastern India and its east coast and over southern Thailand has shown a considerable decrease in temperature standard deviation so a reduction in variability

(Shrestha et al. 2004). Two out of five surface monitoring stations in Thailand, Supun Buri and Chanthaburi showed a considerable increase in minimum temperature during the period 1961-2003 with larger decreases in minimum temperature variability, significant at the 5% level, than at the other stations, Nan, Udon Thani and Prachuap Khiri Khan (Griffith et al. 2005). Normally, seasonal temperature variability is especially small in the lowest latitudes. However, in the north of Thailand the variability of temperature is larger due to mountainous topography.

With respect to temperature projection, IPCC-AR4 (2007) projects that annual warming for SEA is 2.5°C by the end of the 21st century, with little seasonal variation under the A1B scenario and a stronger warming tendency was found over Indochina. IPCC-TAR (2001) indicated the change in global average annual surface air temperature by the end of the century is 3.0°C (with a range of 1.3 to 4.5°C) for the A2 scenario and 2.2°C (with a range of 0.9 to 3.4°C) for the B2 scenario (the warming over SEA is greater than the average annual warming in DJF and JJAS in both A2 and B2). The warming over Thailand is lower than the SE Asia average in all seasons. Some studies project that the temperature will be in the range 1-2 ◦C higher during the rainy season in upper Thailand and in the range 0.5-3 ◦C warmer all year round in southern Thailand according to the A2 projection (2010-2029). Weaker increases of the mean precipitation in Southeast Asia are suggested due to increased concentrations of sulfate aerosols in the future (Roeckner et al., 1999).

With respect to precipitation projection, the change, over the current century, in global average annual precipitation is +3.9% (with a range of 1.3 to 6.8%) for the A2 scenario and +3.3% (with a range of 1.2 to 6.1%) for the B2 scenario (IPCC-TAR, 2001). Average precipitation change over SEA, of between -5 and 5%, is categorised as "no change", in DJF for both A2 and B2 as well as JJA for A2, however, there was disagreement in JJA for B2. The B2 scenario, which is consistent with a lower rate of increased atmospheric GHG emissions. IPCC-AR4 (2007) shows simulations with the A1B scenario over SEA with 7% annual precipitation change by 2080-2099. The strongest precipitation increases widely follow the ITCZ, occurring over northern Indonesia and Indochina in JJA, and over southern Indonesia and Papua New Guinea in DJF.

1.4 General Circulation Models over Southeast Asia

In the Southeast Asia (SEA) region, the first detailed climate scenarios were developed by the Climate Impact Group (1992) using four general circulation models (GCMs), namely the Canadian Climate Centre model (CCCJ1), the United Kingdom Meteorological Office model (UKMO), the Geophysical Fluid Dynamics Laboratory model (GFDL), and the Australian CSIRO9 model (IPCC, 1997). Based on these models under a doubled CO_2 level assumption, the temperature in most of the SEA region was projected to increase by 0.4–3.0°C by the year 2070, which is well below the global average largely because polar regions were expected to warm more due to albedo changes. For the same future years, the precipitation was projected to fluctuate between -5% and +15% during the northeast monsoon, and between 0 to +10% during the southwest monsoon. In further global modelling studies in the region by Hulme et al. (1999), using the HadCM3 global model under the influence of IS92a emission scenarios, the radiative forcing was projected to increase by about 20% (1.0 Wm^{-2}) by the year 2100 with economic growth averages of 2.3% $year^{-1}$ from 1990. In the same studies, doubling the GHGs such as CO_2 with no aerosol forcing caused a projected global temperature and precipitation increase of 3.0°C and 3.2% respectively in the 30 year averages from the present (1961−1990) to the future (2070–2099) periods. Using the same model, Hulme et al. (1999) also projected that at regional scales, SEA would experience a fairly uniform progression of warming and larger precipitation by the year 2050.

Another modelling study using the same model, the coupled atmosphere-ocean model HadCM3, found that the simulated 30 year averages (from 2069−2099) for temperature over Southeast Asia under the A2 and A1F1 emission scenarios of IPCC (1994) were 3.4°C and 4.1°C respectively, which are higher than the projected global average temperature increase of 3.2°C (Johns et al., 2003), as shown in Figure 1.5. In terms of precipitation, four emission scenario experiments (B1, B2, A2, and A1F1) for the 30 year averages also showed a clear and significant signal in both monsoon seasons, where conditions were projected to be drier during the NE monsoon and wetter during the SW monsoon. Corresponding with the SW monsoon period (JJA), the mean precipitation signals were found to be higher than the global average of 0.8

mm/day, namely 0.9 mm/day (B2), 1.1 mm/day (A2), and 1.8 mm/day (A1F1) (Johns et al., 2003), as shown in Figure 1.6.

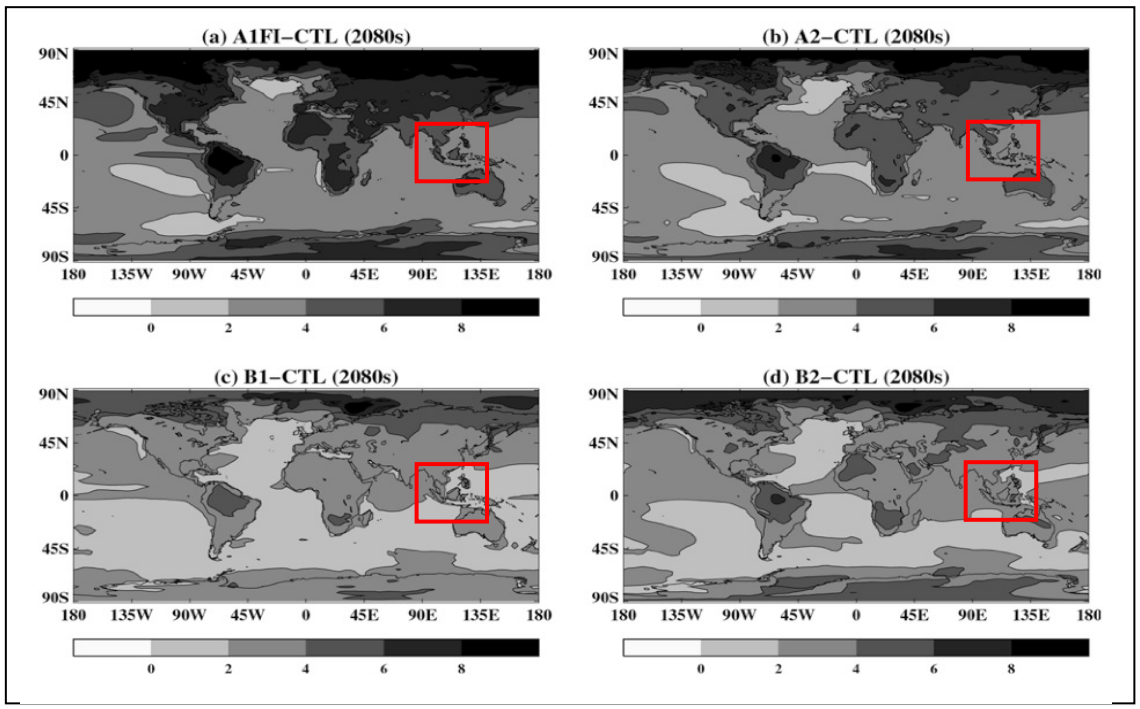

Figure 1.5: Annual mean changes in surface air temperature (°C) averaged over years 2070-2099) for A1F1, A2, B1 and B2 emission scenarios (adapted from Johns et al., 2003).

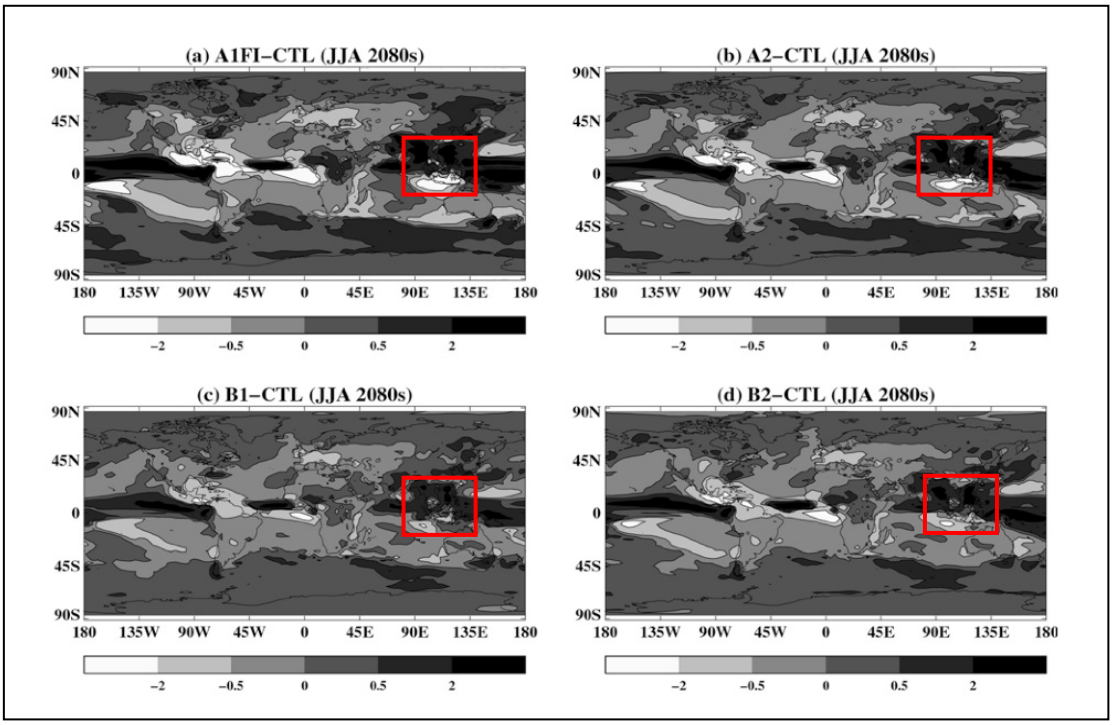

Figure 1.6: JJA changes in precipitation (mm/day) averaged over years 2070-2099) for A1F1, A2, B1 and B2 emission scenarios (adapted from Johns et al., 2003).

More recent studies by Hori and Ueda (2006) and Ueda et al. (2006) on the impact of global warming in the region of SEA using a composite of nine coupled GCMs have revealed that the region may experience drier and warmer conditions during the northeast monsoon, coinciding with the winter monsoon in East Asia that spans from December to early March during the current century. The average surface temperature in SEA (90°–140° E, 30° N–5° S) during both monsoons was projected to increase between 2.2°C to 2.8°C by the period 2081–2100 (30 year averages) (pers. communication with Matasake E. Hori). Meanwhile, the precipitation was also projected to fluctuate between -2.4% to 6% depending upon season with 6% precipitation increase during JJA.

There is a general agreement from the global climate modelling results that there will be an increase in temperature and notable significant changes in precipitation in response to the increase in climatically active gases and aerosols in the atmosphere,

though there is less agreement about the possible regional climate changes such as in SEA, even if the forcing and the global-mean sensitivity are the same. The disagreement about prospects for the SEA has been well documented (Hulme et al., 1999), and the fundamental differences in model design (Hulme et al., 1999), which in turn are a function of incomplete understanding of important physical processes and feedback (e.g. the treatment of the interactions between the atmosphere and the oceans and of cloud formation) have been identified as one of the attribution factors. These differences may also be attributed to different climate sensitivities and climate system unpredictability (Hulme et al., 1999).

The RGOALS-g.10 GCM, created by China, focuses upon ENSO and SST anomalies over the North Pacific and Indian Ocean (Saji and Xie 2006; Zhou and Yu et al. 2006). The RGOALS-g10 successfully simulates several major El Niño events in the east mode and La Niña events in the west mode similar to the observations, although the region of difference between the two modes at the 95% significant level extends to the whole equatorial Pacific (Zhou, Yu et al. 2006). Moreover, the model simulates the realistic convergence zone near 30°N and the spatial distributions of precipitation anomalies in parts of the Yangtze River Valley, South Japan, and the Korean Peninsula with only a small difference from the observations. Dai (2006) indicates that the MRI-CGCM2.3.2, Japanese GCM, has the most realistic precipitation pattern at low latitudes among the models with data submitted to the Program for Climate Model Diagnosis and Inter comparison (PCMDI). The MRI-CGCM2.3.2 also reproduces the broad patterns of the daily precipitation frequency and intensity over the Asia monsoon region. Among GCMs in PCMDI without flux corrections, HadCM3 produces relatively realistic patterns of tropical precipitation and the horseshoe-shaped ENSO-related precipitation pattern originating from the Indonesia region and extending northeast- and southeast-ward (Dai 2006). This is a good reason for selecting HadCM3/HadAM3 as the global model used in this research.

1.5 Regional Climate Modelling

A regional climate model (RCM) is a higher resolution model that covers a limited area of the globe. RCMs are comprehensive physical models which include the

atmosphere and land surface components of the climate system, as well as the representation of the important processes within the climate system. In RCMs the physical processes that take place on much smaller spatial scales than the GCM model grid are either resolved or calculated using parameterizations (Jones et al., 2004). By using boundary and initial conditions from a GCM, RCMs produce high resolution simulations for an interest region which are consistent with the large-scale simulations from that GCM. The whole process is a form of dynamical downscaling. There are a number of reasons to consider why a RCM is necessary as a tool in the investigation of regional climate change at a higher resolution (Jones et al., 2004). A RCM has the capability to simulate current climate more realistically particular in mountainous areas and closer to the coastline on scales of 100 km or less. A finer spatial scale is clearly more apparent in such areas with RCM simulations than from a GCM (Figure 1.7). RCMs are also able to represent smaller islands in change simulations, in which the RCM can resolve the difference in terms of thermal inertia between land and ocean (Figure 1.8). Another interesting feature of RCMs is their capability to better simulate extreme changes of weather such as heavy precipitation events than GCMs. RCMs could also resolve greater detail associated with features such as cyclones and hurricanes, which may be absent in the driving GCM (Figure 1.9).

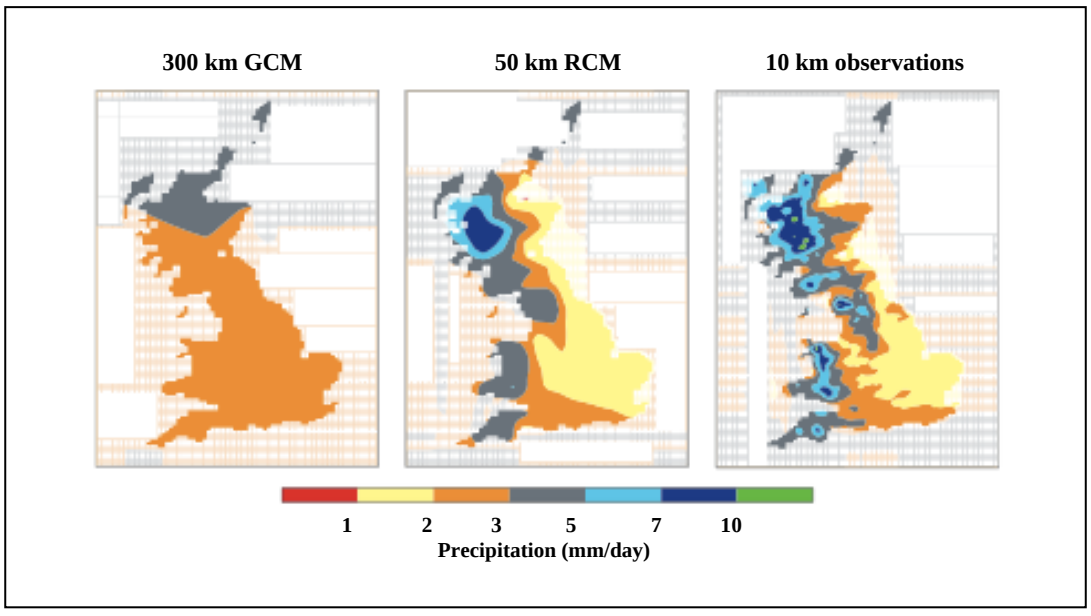

Figure 1.7: A more realistic simulation by a RCM of enhanced precipitation (mm/day) over the mountains of western Great Britain in winter (adapted from Hulme et al., 2002)

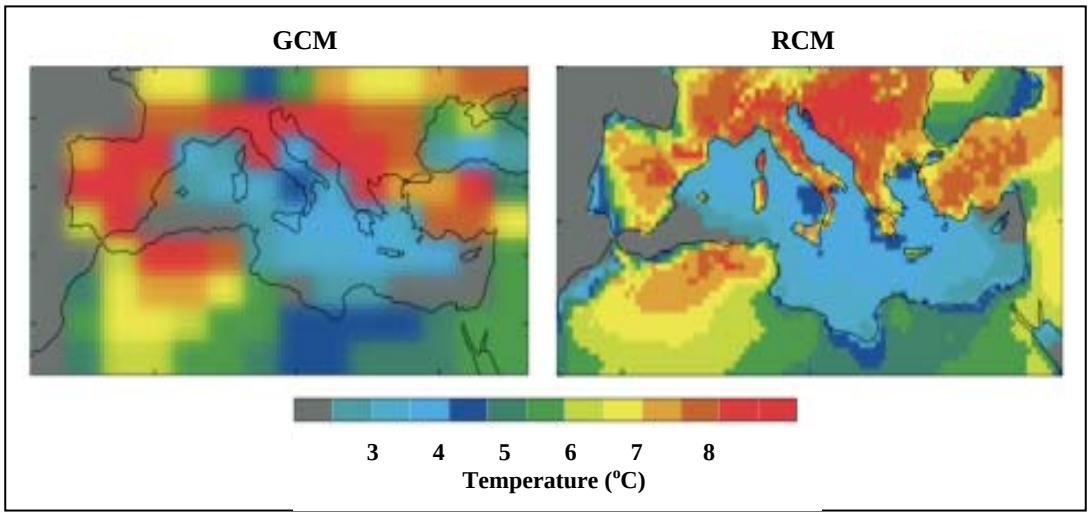

Figure 1.8: A temperature simulation by a RCM in summer over southern Europe showing the details of the simulation over islands in the Mediterranean (e.g. Corsica, Sardinia and Sicily) in comparison with a GCM simulation (adapted from Jones et al., 2004).

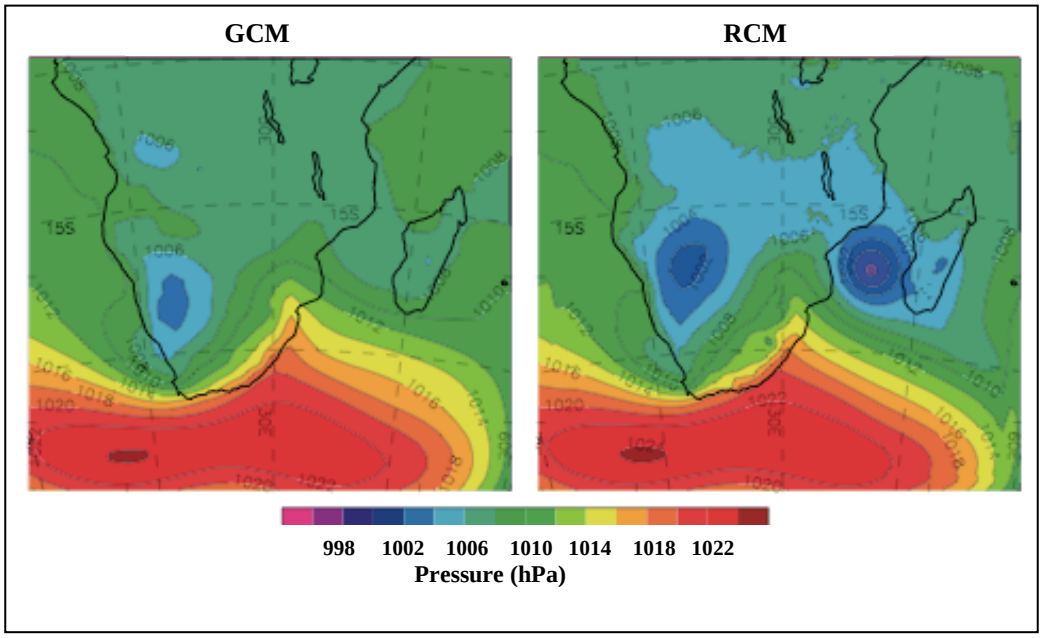

Figure 1.9: Mesoscale pressure patterns indicating a cyclone in the Mozambique Channel, clearly illustrated in the RCM but absent in the driving GCM (adapted from Hudson and Jones, 2002).

RCMs are nested into a GCM in either a 'one way' or 'two way' configuration, but to date nested regional climate modelling techniques tend to consist of using initial conditions, time-dependant lateral meteorological conditions and surface boundary conditions to drive RCMs in a 'one-way' only mode (Giorgi et al., 2001). The one-way nesting technique doesn't allow feedback from the RCM's simulation to the driving GCM. Theoretically, the one-way nesting technique could impose limitations such as the effects of systematic errors in the driving fields provided by GCMs. Also the lack of two-way interactions between RCM and GCM does not allow feedback effects from fine scales to coarse scales whereas in the real atmosphere, feedbacks derive from different regions and interact with each other (Giorgi et al., 2001). Despite the setbacks in terms of dependency on input from the GCM driving model, the lack of two-way nesting with its driving model, as well as the computationally expensive costs, RCMs are still developing rapidly and are widely used in climate change investigations as they are capable of providing higher spatial and temporal resolution information for a number of climatic variables while still providing better representation than the GCM for some weather extremes.

The Climate High Resolution Model (CHRM) is another regional climate model that has been used in a number of climate studies in Europe for example by Lüthi et al. (1996) and Vidale et al. (2003). Lüthi et al. (1996) using CHRM driven by ECMWF 6-hourly resolution analyses to simulate interannual variability, found that the model captures wintertime changes but does not satisfactorily simulate summertime precipitation totals. They suggested the shortcomings are related to (i) larger model bias in dynamical fields for summer than winter because summertime interannual variability is associated with weaker effects in dynamical fields and (ii) summertime precipitation distribution being affected by small-scale moist convection and surface hydrological processes.

The regional climate model REMO is based on the Europamodell, the former numerical weather prediction model of the German Weather Service. Jacob (2001) indicated that the capability of REMO driven by ECHAM4 to realistically simulate the water budget over the Baltic Sea covering a time period of 1979-1988 was good when compared against observations. The coupled regional climate model system, the Rossby Centre Atmosphere Ocean model RCAO, has also been used as a tool for

climate studies in northern Europe. For example Döscher et al. (2002), using RCAO driven by ERA15 over northern Europe, found that the coupled sea surface temperatures agree well with observations while overestimation of ice, due to negative bias of longwave radiation, was found.

The HIRHAM model is a state-of-the-art RCM that has already been successfully applied for European regions (Christensen and Christensen, 2007), for the Arctic (Rinke and Dethloff, 2008) as well as for Antarctica (Dethloff et al.,2010). Moreover, HIRHAM has recently been applied to simulate the Indian monsoon circulation driven by ERA40 for the period from 1958 to 2001 with a resolution of 50 km and successfully reproduced the summer monsoon climatology and its variability concerning temperature and precipitation (Polanski et al., 2010).

One of the earliest RCMs which has been developed is the NCAR Regional Climate Model (RegCM), initially built upon the PSU/NCAR Mesoscale Model version 4 (MM4) by the National Center for Atmospheric Research (NCAR) and nested into the NCAR Community Climate Model (CCM) (Dickinson et al., 1989; Giorgi and Bates, 1989). Since then, the model has been updated and improved with new modules added for use in chemistry-climate interaction studies (Giorgi et al., 1993; 1999: 2002).

Table 1.3 General Information of some RCMs

Model Institution and model origin	Resolution	Nudging Zone (number of points)	Vertical levels	Convection	Micro-physics	Land surface	Radiation
CHRM Swiss Federal Institute of Technology, Zurich, Switzerland (ETHZ)	0.5 deg (55 km)	8, Davies (1976)	20	Mass flux, Tiedtke, (1989)	Kessler (1969), Lin et al. (1983)	4 thermal and 3 moisture layers, Dickinson (1984), Jacobsen and Heise (1982)	Ritter and Geleyn (1992)
RCAO Swedish Meteorological and Hydrological Institute, Sweden (SMHI)	0.44 deg (50 km)	8	24-60	Mass flux, Kain & Fritach, 1990	Rasch and Kristjansson, 1998	2 soil thermal and 2 moisture layers Bringfelt et al., 2001	Savijarvi, 1990 Sass et. al., 1994
RegCM3 National Center for Atmospheric Research (NCAR)	50 km	11	16	mass flux (3 options) Anthes-Kuo scheme/ the Grell scheme / the Massachusetts Institute of Technology (MIT) scheme	Pal et al. (2000)	Force-restore soil thermal layers, 3 soil moisture layer Dickinson et al. (1993)	Kiehl et al. 1996, Giorgi et al., 1999

Table 1.3 (continued)

Model Institution and model origin	Resolution	Nudging Zone (number of points)	Vertical levels	Convection	Micro-physics	Land surface	Radiation
REMO Max-Planck-Institute for Meteorology, Germany (MPI)	0.5 deg (55 km)	8, Davies (1976)	20	Mass flux, Tiedtke (1989), Nordeng (1994) for CAPE closure	Sundqvist (1988)	5 thermal layer, 1 moisture bucket, Du¨menil and Todini (1992)	Morcrette (1991), Giorgetta and Wild (1995)
HIRHAM Danish Meteorological Institute, Denmark (DMI)	0.44 deg (50 km)	10 (no vertical dependence), Davies (1976)	19	Mass flux, Tiedtke (1989), Nordeng (1994)	Sundqvist (1988)	5 thermal layer, 1 moisture bucket, Du¨menil and Todini (1992)	Morcrette (1991), Giorgetta and Wild (1995)
PRECIS Hadley Centre, UK Meteorological Office	0.44 deg (50 km),	4	19	Mass flux, Gregory and Rowntree (1990), Gregory and Allen (1991)	Smith (1990), Jones et al. (1995)	4 thermal and 4 moisture layers, Cox et al. (1999)	Edwards and Slingo (1996)

Frei et al. (2006) undertook an intercomparison of precipitation extremes as simulated by six European RCMs: HIREM, CHRM, HadRM3H/HadRM3P, REMO, GKSS and SMHI, driven by the atmosphere-only GCM of the Hadley Centre at the UKMO, HADAM3H, for 1961-1990 and for 2071-2100 covering the European continent from the Mediterranean to Scandinavia. They found that in the wettest season, autumn, all RCMs are capable of representing mesoscale spatial patterns in precipitation, however model biases are large in some cases, in particular in summer. HadRM3P (PRECIS) tended to overestimate topographic enhancement at the southern rim but

underestimate values in the Po valley while CHRM, HIRHAM, SMHI and REMO all show an overall underestimate. The simulation of dryness occurrence in RCMs, particularly in summer, reveals model biases in soil moisture and in other components of surface water and energy budgets. In terms of wet day analysis, all models overestimate wet day frequency in the northern Alps from autumn to spring which is possibly due to errors in the driving GCM since similar bias was not found in RCMs driven by reanalysis data. Clearly, comparison of the RCM results to those of their driving GCM reveals the benefit from the higher model resolution, moreover, Frei et al. (2003) implied that errors inherited from the forcing GCM were small and did not change the RCM specific error characteristics. With respect to simulated future changes, all six RCM simulations are very consistent, with precipitation increasing by 0–11% in central Europe and by 10–22% in southern Scandinavia. However, in summer changes in the magnitude of precipitation vary considerably between models (-13% to +21% over central Europe and +2 to +34% over southern Scandinavia). The authors mentioned that the differences are explained by differences in the change of average precipitation events as represented by wet day intensity and frequency.

RCMs developed by the Hadley Centre, which include PRECIS, the latest version RCM (third-generation), have been used in a number of climate change impact studies worldwide, and these are briefly highlighted in the following sections (the full detail is in Chapter 3). It is possible to widely apply PRECIS to any part of the globe, with the boundary conditions of the model's domain needing to be specified. The model is forced at the lateral boundaries by a high resolution GCM, HadAM3, with horizontal resolution of 150km x 150km. HadAM3 is an atmosphere-only GCM derived from the atmospheric component of HadCM3. The observed SST and sea-ice are used as lower boundary conditions.

1.5.1 RCMs over SEA.

In the last 15 years, RCMs have been recognised as an excellent tool in a number of climate studies in smaller geographical regions such as in climate impact studies (Jones et al., 1997; Bhaskaran et al., 1998; Hudson and Jones, 2002; Huntingford et al., 2003), temperature extremes (Hennessy et al., 1998; Mearns, 2004), water resources (Wang et al., 1999; Stone et al., 2001, 2003; Wilby et al., 1997), agriculture

(Erda et al., 2005; Challinor et al., 2005, 2007), energy demand, paleoclimate studies, atmospheric chemistry studies and forest fires. Feser (2008), using an atmospheric regional climate model, the Climate version of the Lokal Model (CLM), simulated a typhoon track, Winnie, similar to the observations. Kreasuwun et.al (2009) using the MM5 Regional Climate Model driven by CCSM3 found that simulated temperatures are not very different from the station observations during the rainy season (May-September) but are about 2-5 ◦C underestimated during the dry season (ONDJFM) over the period 1970-1999. Torsri (2009) using RegCM3 driven by ERA40 during 1961-2000 indicated that the model systematically underestimates near surface temperature in dry and wet seasons compared with selected station observational data from the Thai Meteorology Department, with smallest biases in southern Thailand. Liu et al. (2006) suggested that the reduced moisture transport to the South China Sea, SCS, simulated in the model results in underestimated precipitation over the SCS. Satomura (2000), using a two dimensional, nonhydrostatic, and cloud-resolving numerical model indicated that diurnal variation of precipitation is as follows: convection is activated at the lee-side foot of two mountainous regions located in western and central Thailand in the late afternoon, forming squall lines which propagate eastward and which produce night maxima of precipitation in inland areas far eastward of the high ground.

Chotamonsak et al. (2011) applied the WRF RCM at 60 km resolution forced by ECHAM5 and SRES A1B emissions to simulate temperature and precipitation over SEA during 1990–1999 and 2045–2054. They found a cold bias for maximum temperatures and a warm bias for minimum temperatures and projected warming varies from <0.1 to 3 °C while precipitation slightly increases for all seasons in the overall region with local decreases in the dry season. McGregor (1998) using the fine resolution (44 km) Division of Atmospheric Research Limited Area Model (DARLAM) predicts small increase in precipitation over land in SEA with larger increase over the oceans and Sulawesi and temperature increases of around 1.5°C for most countries in the region after 100 years with little change in diurnal range compared with 1990.

1.5.2 Use of the PRECIS model around the world

Asia – South Asia

Bhaskaran et al. (1998) used an early version of the RCM developed by the Hadley Centre to study the intra-seasonal variability of the oscillation circulation and precipitation anomalies in South Asia. The study found that the HadRM3 captured the intra-season variability more realistically than the driving GCM. Further investigations by Hassell and Jones (1999) for the same area concluded that a nested RCM captured observed precipitation anomalies in the active break phases of the monsoon that were not detected by the driving GCM.

A study in India by Kumar et al. (2006) used PRECIS to develop high-resolution climate change scenarios for the 21st century for various surface and upper air parameters. This study concluded that PRECIS has the capability to resolve features at a higher resolution than GCMs do, particularly in projecting the spatial patterns of summer monsoon precipitation along the windward side of the Western Ghats. With respect to island and coastal areas, the PRECIS simulation was able to clearly distinguish climate over land and surrounding oceans, for example the land surface has less heat capacity than the oceans and warms faster. Notable quantitative biases (overestimates, both in terms of mean and extreme amount) were identified, particularly in precipitation over some regions of the Indian sub-continents. The authors indicated that the overestimation of precipitation has been inherited from the bias of the driving GCM in representing the large-scale features. Interestingly, some apparent cold bias in the model throughout the year, particularly in the seasons other than spring, could be partly due to the limited network of stations and interpolation due to the gridding algorithm used to derive the observed patterns. The authors showed that model simulations by PRECIS under scenarios of increasing GHG concentrations and sulphate aerosols in this study have indicate marked increases in both precipitation and temperature towards the end of the 21st century.

In Bangladesh, a study was carried out to validate the performance of PRECIS against the surface observational data of precipitation and temperature at 26 observational sites from 1961-1990 (Islam and Mannan, 2005). Results indicated that PRECIS

revealed positive biases for precipitation and temperature in the region, though in some locations it provides better performance. Islam et al. (2007) reported that PRECIS simulated an overestimate of precipitation between the dry month of December and the monsoon month of June, underestimates of precipitation during July to September and accurate estimates in the post monsoon months of October and November in Bangladesh, when compared with the Tropical Precipitation Measuring Mission (TRMM). It is mentioned that there are seasonal changes in the characteristics of precipitation in this region and it is suggested that the same selected cloud parameterization cannot accurately represent this seasonality. Comparing the model grid to a gridded observation analysis method produced similar precipitation patterns with a few exceptions. They reported that this may be partly attributed to the lack of observational data sites throughout the country and may also have resulted from the inherent uncertainties of the model. Islam et al. (2007) indicated that temperature variation (i.e. cold bias in the dry season and hot bias in the rainy season) may be due to the decrease and increase of latent heat flux for the two seasons respectively, which may not be well simulated by the model.

Saeed et al. (2006) applied PRECIS forced by reanalysis data, ERA15, to study physical processes responsible for the extreme precipitation event of September, 1992 that caused severe flooding in the River Jhelum, South Asia and found that the model reproduced well the temporal pattern of area averaged precipitation, the monthly mean spatial precipitation pattern and the daily precipitation intensity distribution. The model realistically simulated the trends and fluctuations in the area averaged daily maximum and minimum temperature except for a warm bias (less then 2°C) in the daily maximum temperature in June and minimum temperature in June and August and a cold bias (0.8°C-3.5°C) in both maximum and minimum temperature in the later months. They suggested that the maximum bias is in June and then reduced in the later months, probably because the land surface processes and the associated forcings are better resolved in the later months. The model captured not only the moisture transport from the Arabian Sea and Bay of Bengal but also the intense westerly wave over the north of Pakistan which generated the high amount of moisture in the circulation and orographic uplifting producing precipitation intensification.

Asia - Far East

In China, PRECIS was used by Erda et al. (2005) to investigate the future climate and to develop climate change scenarios for China. The results from this study concluded that at the end of the 21st century, depending on the level of future emissions, the average annual temperature was projected to increase between 3-4°C. Meteorological output data from PRECIS was also used to drive regional crop models to investigate possible changes in yields of the main crops in China such as rice, maize, and wheat. It was found that the projected climate change without carbon dioxide (CO_2) fertilization could potentially reduce the production yields by up to 37% in the next 20-80 years. Wang and Shallcross (2005) also used PRECIS to simulate Taiwan's current climate, with particular focus on time-slices between 1979-1981. The simulation results have been compared against observed data, reanalysis data, and other global climate models. The PRECIS simulation was found to reproduce well the spatial patterns of surface precipitation as well as the inter-annual variability of precipitation. PRECIS was also found to demonstrate good capability in simulating the spatial distribution of surface temperature over the whole selected region, particularly over Taiwan's Central Mountain Range.

Europe

The regional climate model, HadRM3P, which is also the model used in the regional modelling system PRECIS, was used by Moberg and Jones (2004) to evaluate the simulations of daily maximum and minimum near-surface temperatures across Europe by comparison with the observational data for the same period. The performance of the model for surface temperature is generally good over the United Kingdom, and elsewhere between latitudes 50 and 55°N, with biases within ±0.5K. However, in other regions within the domain of study, seasonal biases were found to be higher and even biases in climatological averages were as high as ±15K at the Icelandic coast and in northern Sweden. These authors mentioned that significant positive summer temperature biases in southern Europe have been observed in several RCM simulations and the possible reasons are circulation biases, deficiencies in convective parameterization, parameterization of cloud, clear-sky radiation errors and errors in precipitation frequency distribution. The main cause for the problem is that warm bias in summer associated with too little precipitation and too dry soils in RCMs (Moberg

and Jones, 2004). PRECIS was also used to investigate the regional climate model performance against the observed data obtained from radiosondes in Cyprus (Hadjinicolaou et al., 2006). This study also concluded that the PRECIS simulation over the selected region could satisfactorily reproduce the temporal evolution of temperature and other meteorological parameters. Lalas et al. (2005) also used PRECIS in Greece to evaluate the regional climate change impact on the energy system in Greece. Based on annual analysis, results have indicated that climate change in the region has caused the electrical energy demand to increase approximately 5% solely due to the change in meteorological conditions.

North America and South America

PRECIS has also been tested over North America by Martineu (2005) to investigate climate changes in the region. In terms of performance, PRECIS has the capability to reproduce regional climates quite satisfactory, particularly over the Rocky mountains, the Cordillera, and the Caribbean islands. The spatial patterns of precipitation and temperature of the selected domains are coherent with the observational datasets, though some biases (overestimates of up to 6°C) exist, particularly on seasonal datasets over the central US in the summer of 1980. Preliminary results of the PRECIS application in Brazil under the SRES A2 scenario have shown a large warming in 2070-2100 for southern Amazonia (up to 6^{o}C) (Marengo and Ambrizzi, 2006). In terms of precipitation, the simulation has indicated a drier phenomenon occurring in Eastern Amazonia and North East Brazil, and precipitation reduction in Southern Brazil and parts of Western Amazonia along the Andes. For comparison, the precipitation projection in Amazonia using the GFDL, RCM, was also found to show some reduction in individual locations, but the evaluation of the performance of the model in this region was not that satisfactory (Fowell, 2006). A PRECIS experiment over Bolivia by Seiler (2009) shows underestimation of temperature and overestimation of precipitation in highland regions. It was commented that the lateral boundary conditions did not appear to be the main error and the failure may be related to an inaccurate representation of the topography and/or to the parameterization schemes.

Marengo *et al*. (2009) stated that PRECIS realistically reproduces the spatial and temporal patterns of precipitation and temperature in tropical and subtropical South America during 1961-1990. Nevertheless systematic negative precipitation biases were detected during the warm rainy season and a systematic cold bias existed throughout the year compared to the CRU temperature climatology. It was suggested that the parameterization of radiation or land-surface processes may be related to precipitation underestimation and a possible effect of local dynamic forcings for example dry or wet soil may be dominant over the large-scale SST forcing. Meanwhile the cold bias, which is not large, could be the result of too few observing stations contributing to the CRU data set.

Soares and Marengo (2009) affirmed that the ability of PRECIS forced by HadAM3P to accurately represent specific humidity fields over South America is the same order of magnitude as that of reanalyses. Some systematic positive or negative biases in some regions could also be due to the meridional shifts of bands of high specific humidity during the annual cycle, or to the parameterization of the Andes in PRECIS. They found that the RCM underestimated the zonal wind intensity in the tropical region as compared to the reanalyses, by about 3 ms^{-1} and underestimated pressure over a large part of South America. Larger pressure differences are observed over northern Argentina, perhaps due to an overestimation (more intense) of the thermal low pressure in this region by the model.

Alves and Marengo (2009) indicated that PRECIS underestimates the surface temperature by 2°C over South America which may be due largely to some misrepresentation in land-surface processes and interactions associated with changes in surface energy and water balances, therefore, leading to cooling through long wave radiation reduction. Another possible problem is the observed temperature interpolated from too few stations over tropical South America.

Africa

A number of studies have used PRECIS to investigate climate changes in the African continent. In one of the recent studies by Beraki (2005) over the Eritrean domain, the PRECIS simulation has indicated satisfactory performance in terms of spatial patterns against the observed data (the correlation with the observed data was 0.88 to 0.89).

Future climate scenario simulations over this region in terms of temperature were found to increase in both SRES A2 and B2 scenarios at the end of this century. Meanwhile, for precipitation, mixed signals were found, though it was expected to increase in most of the Eritrean region. Earlier studies have been carried out by Arnell et al. (2003) using the regional climate model, HadRM3H with spatial resolution of 0.44 × 0.44° with two other global models (HadCM3 and HadAM3H) to investigate the macroscale river runoff in southern Africa. Jones and Hudson (2002) have also used the Hadley Centre RCM, HadRM3H, to investigate the climate change scenario over southern Africa. The results have shown that the RCM is capable of resolving features on fine scales, which includes extreme events such as tropical cyclones, though there are indications of positive biases in precipitation and negative biases in surface temperature over most of southern Africa in summer.

Druyan et al. (2009), studying the domain 20°S–35°N and 35°W–35°E commented that PRECIS uses initial soil moisture and soil temperature fields at four vertical levels spun up from a multi-year integration driven by the reanalysis so it did not detect any significant sensitivity to the specification of initial soil moisture. Moreover, PRECIS favours a double ITCZ over the West African monsoon region during June creating the early onset of Sahel precipitation, accompanied by light rain during the onset of the South African monsoon onset, with the precipitation band encroaching too far northward. PRECIS was found to underestimate orographic precipitation in regions of inland orographic enhancement maxima along the southwest African coast by at least 5 mm day^{-1} and the Cameroon Highland effects imply a model deficiency rather than the negative influence of unrealistic boundary data. With respect to precipitation, PRECIS scores a near perfect spatial correlation against observations over the eastern Sahel and a small positive bias over the central region. With respect to moisture, PRECIS shows a local reduction in the meridional moisture advection in the lee of the Guinean Highlands, which is likely a real feature that reflects their higher resolution of topography. They suggested that some of the PRECIS precipitation deficit could derive from inhibitions in triggering moist convection since P-E is not underestimated. With respect to zonal winds, downscaling with PRECIS produces no discernable impact on the cross-section of zonal winds which closely resemble the solution of the driving data, despite the increased horizontal and vertical resolutions of the regional model – this is thought to be due to the similarity of the

physics in the driving GCM, HadAM3 and PRECIS. Lastly, PRECIS was found to better resolve lower tropospheric meridional moisture advection in West African, through higher resolution topography, than HadAM3.

Moufouma-Okia and Rowell (2010) indicated that PRECIS underestimates the orographic precipitation maxima by 3–4 mm/day, overestimates precipitation over the Sahel, and likely produces too much precipitation over the oceanic areas adjacent to the coast occurring in May–June and September–October when the ITCZ lies in the Gulf of Guinea. They also suggest a possible deficiency in triggering moist convection along the coastal regions.

Table 1.4: Limitations and biases with PRECIS which have been reported in the literature.

Limitations and biases with PRECIS	Effects and Possible causes of biases
Any errors in the driving GCM, HadCM3/HadAM3, may be carried through to the RCM	- shortcomings in the ability to accurately reproduce larger scale circulation features (Kumar et al., 2006). - excessive soil drying in the GCM (Moberg and Jones, 2004). - cloud and radiation parameterization schemes (Randall, 1989).
Internal model physics error	- excess of thick cloud producing incident surface shortwave radiation deficit (Hudson and Jones, 2002). - Increased evaporation contributing to increased moisture convergence into the ITCZ over the tropics (Hudson and Jones, 2002). - unsuitable selected cloud precipitation for region (Islam, 2007).
Error in soil moisture input	- insufficient sensitivity of soil moisture (Druyan et al., 2009, Hudson and Jones, 2002). - too dry soil affecting low evaporation and land surface warm too rapidly (Moberg and Jones, 2004).

Table 1.4 (continued)

Limitations and biases with PRECIS	Effects and Possible causes of biases
positive precipitation biases in mountainous region	- an inaccurate representation of the topography and/or sub-optimal parameterization schemes (Saeed et al., 2009). - incorrect balance between the effect of radiation or land-surface process parameterizations and the effect of local dynamic forcings. (Marengo *et al*., 2009). - failure in simulating convective precipitation (Alves and Marengo, 2009, Shahgedanova et al., 2010). - overestimation (more intense) of thermal low pressure systems (Marengo *et al*., 2009, Soares and Marengo, 2009). - Possible deficiency in triggering moist convection along the coastal regions (Okia and Rowell, 2010). - underestimation of the zonal wind intensity and pressure in the tropical region (Marengo *et al*., 2009, Soares and Marengo, 2009).
Cold biases	- misrepresentation in the land-surface processes and interactions associated with changes in the surface energy and water balance (Alves and Marengo, 2009). - too small a latent heat flux in the dry season (Islam et al., 2007; Uchiyama et al. 2006). - circulation and soil moisture errors. (Moberg and Jones, 2004). - inaccurate topography and parameterization in highland region (Seiler, 2009)
hot bias	- too little precipitation and artificially enhanced drying of soils in summer. - circulation biases. - deficiencies in convective parametrization. - errors in precipitation frequency distribution. - errors in clear-sky radiation and clouds, and parameterization of land-surface schemes (Islam et al., 2007; Moberg and Jones, 2004).

1.5.3 Motivation for RCM use over SEA.

Most studies of Southeast Asia climate use GCMs which can provide the overall climate regimes. SEA has complex topography, including the Indochina peninsula and the surrounding maritime continent in the Indian and Pacific Oceans. It is clearly shown that there is a lack of regional modelling studies in Southeast Asia, especially in Thailand, compared with the other parts of Asia, for example, South Asia, China, Japan. Most of the studies investigate ENSO, SST anomalies, the Indian Ocean, the North Pacific and the monsoon cycle over India. So, to address this deficiency, in this study a RCM is used as a tool to investigate regional climate over SEA.

1.6 Structure of Thesis Content

This chapter has, through a literature review, provided background to the issues which are relevant to this research. The remaining chapters are structured as follows.

Chapter two

Description of the project design, including the aims and objectives of this project followed by details of the methodology, including the model climate simulation experiments.

Chapter three

In this chapter, detail is given of the regional climate model system, the Providing REgional Climates for Impact Studies (PRECIS) model. Also discussed are the observational datasets used in this thesis.

Chapter four

Station and gridded observational data are used to present analyses and fill gaps in understanding of the current climate of Southeast Asia and, specifically, of Thailand.

Chapter five

Before using the PRECIS model to simulate future possible SEA climate, the model is verified against current climate. The results of the first known RCM simulation over Southeast Asia are presented in this chapter. Model validation is undertaken using key climate variables such as temperature and precipitation, using high resolution gridded observational data sets and station data. The sensitivity of the model to incorporating a realistic sulphur cycle and to different initial conditions are also investigated. Possible causes of model bias are discussed and compared with the findings in the literature.

Chapter six

This chapter contains an ensemble approach for the possible climate regimes in SEA at the end of the current century. The future simulations of RCM and GCMs are used to gain an indication of the nature of possible future changes to the main climate features in Thailand, for example the trend of heavy precipitation.

Chapter seven

This chapter provides the conclusions leading from this research. The strengths and weaknesses of the approaches are discussed. Finally, recommendations for possible future work to extend this study are proposed.

Chapter 2
Project Design and Methods

2.1 Introduction

One of the most stringent tests of a climate model is its ability to simulate a realistic climate regime. The literature discussing model simulations of tropical climate, either of mean climate or its variability, was summarized in chapter 1. One of the major components of the tropical circulation is the monsoon system. Many general circulation models, GCMs, have produced a reasonably good monsoon simulation in terms of both circulation and precipitation, however the latter is rather overestimated and the onset is slightly early in comparison with observations. GCMs with global coverage have been the primary tools used in climate studies. The current resolution GCMs (200–500 km) are generally capable of simulating the broad global climate. However, due to their low resolution, the simulated results for regional climate tend to produce apparent errors of as much as $\pm 5^{o}$C in annual temperature, and -40% to +60% in annual precipitation (IPCC, 2001; Leung et al., 2003; Fowell, 2006). In order to provide a more realistic response of regional climate changes to radiative forcings, particularly in areas with complex orography, coastline, and landuse patterns, it has been suggested that higher resolution regional climate models should be considered (IPCC, 2001). RCMs developed by the Hadley Centre, which include PRECIS, the latest version RCM (third-generation), have been used in a number of climate change impact studies worldwide and they have been discussed in Chapter 1. Chapter 3 describes the PRECIS setup in detail. There are some publications paying attention to using Thai station observational data (Chokngamwong and Chiu, 2006; Matsumoto, 1997; Kripalani et. al, 1995; Zhang et al., 2004; Chokngamwong and Chiu, 2008; Takahashi and Arakawa 1981; Henson 2002) and limited published information about Thai climate, based on gridded observations.

2.2 Aims

The overall aim of this study is to understand current climate and possible future climate change over Southeast Asia and, in particular, over Thailand by using station and gridded observational data and PRECIS as a regional climate modelling tool.

The following specific questions will be addressed in the study:

- How much can be understood about the recent climate of Thailand from the limited observational data?
- How well does the regional climate model, PRECIS, capture main regimes in SEA for current climate? How does this performance compare with other published PRECIS studies and with RCMs in general?
- What are the strengths and weaknesses in the output of PRECIS and the driving GCMs: HadAM3 and ECHAM4?
- Does the RCM add value to the GCM?
- What range of climate changes are anticipated in SEA by the end of century according to ensemble experiments based on different emission scenarios and assumptions?
- Does the model reveal any apparent trend in extreme events by the end of the century, such as in heavy precipitation?
- Do RCMs capture realistic inter-annual and/or inter-decadal variability of the Southeast Asia Monsoon system?

2.3 Project Design

The manner in which the above aims will be addressed is now considered in detail.

How much can be understood about the climate of Thailand from the limited observational data?

There is very little published in the literature on the current climate of Thailand. Those studies that do exist also used the surface station dataset provided by the Thai Meteorology Department (TMD) over mainland Thailand. A few of them have

investigated the current climate over the peninsula of Thailand; due to complex topography in the Thai peninsula, the area was previously ignored in studying Thai climate, i.e. Takahshi and Yasunari (2006) used 27 stations to validate the monsoon onset over Thailand. Another recent publication indicated that ENSO events are an important source of inter-annual/inter-decadal variability in Thailand air surface temperature (Limsakul, 2008). So the inter-annual variability in precipitation during El Niño and La Niña years should be considered. Thai surface station data over the period 1961-1990 and the gridded observation dataset CRUTS2.1 (full detail found in section 3.1.2) for the period 1960 to 1990 are used. 5 station observational timeseries of precipitation data will be analysed as pentad mean time series of precipitation to evaluate monsoon onset and to identify any trends. The gridded data set is analysed seasonally to identify temporal and spatial climate features, for example daily precipitation, wet day frequency, surface temperature and diurnal temperature range as well as specific El Niño/ La Niña impacts over Thailand.

How well does the regional climate model capture main regimes for current climate?

There was no evidence that RCMs were being used in application to SEA just 5 years ago (2006). This project is the first one to study both current and future climate in Thailand by using a RCM. First of all, the model validation for the current climate needed to be studied in terms of building more confidence for investigating future climate projections. The CRUTS2.1 high resolution gridded dataset, which has a comparable resolution to that of the RCM and which is based on 36 station observations would be more useful for model evaluation than individual station observations. Nevertheless, the gridded data set has monthly resolution so daily station data is also needed to address this question.

Does the RCM add value to the GCM?

One of the purposes of an RCM is clearly to add detail to the GCM, through dynamical downscaling capturing the climate regime at a finer scale. An RCM is one-way nesting dynamical downscaling so the RCM simulation does not allow feedback to the driving GCM. It is a key research question as to how much the RCM, PRECIS, adds value to the driving GCM, in this case HadAM3P. This leads to the question of

justifying if the RCM is necessary to study Thai climate. The answer to the question "what are the strengths and weaknesses in the RCM and GCM output" is also needed in terms of applications.

To meet these objectives, a three-phase simulation experiment is carried out.

(i) Three 30-year RCM simulations (1961-1990) driven by HadAM3H (with different initial conditions -more detail found in section 2.3.2), by ECHAM4 and by ERA40.

(ii) Three simulations for the A2 future scenario (2071-2100), one for the B2 future scenario driven by HadAM3P.

(iii) Simulations for the A2 and B2 future emission scenarios (2071-2100) driven by ECHAM4

More detail on the models and emission scenarios is found in Chapter 3.

Regarding the numerical experiments, collaboration with other centres is helpful in terms of an 'ensemble' approach. The participants in a SEA PRECIS workshop (2006) agreed to run the experiment with the same domain. With PRECIS centre support, I was a consortium member able to share the model output. The experiments run by the consortium are shown in Table 2.1.

Table 2.1: Experiment designs with consortium. UEA; University of East Anglia, LANCS; Lancaster University, UKM; University Kebangsaan Malaysia, MMD; Malaysia Meteorology Department.

Experiment	Source	
	Run without Sulphur cycle	Run with Sulphur cycle
1. control experiment		
HadAM3P(baseline1)	UEA	MMD
HadAM3P(baseline2)	LANCS	LANCS
HadAM3P(baseline3)	UEA	UEA
ECHAM4	UEA	-
ERA40	UKM	UKM
2. A2 scenario experiment		
HadAM3P-A2(future1)	UEA	MMD
HadAM3P-A2(future2)	LANCS	LANCS
HadAM3P-A2(future3)	UEA	UEA
B2 scenario experiment	UEA	MMD
3. ECHAM4 scenario experiment		
A2 echja	UKM	-
B2 echjd	UKM	-

It should be noted that the ECHAM4 forced runs are without sulphur cycle only but the other experiments were designed to run PRECIS both with and without the sulphur cycle. However, in this study, the runs without sulphur cycle are used for climate analysis in terms of investigating the impact of using different forcing GCMs. It is shown that there is no marked change in the simulations either in terms of precipitation or surface air temperature when comparing between the simulations performed with and without sulphur cycle switched on in PRECIS (Kumar, 2006). sulphate aerosol particles tend to give a surface cooling because more solar radiation reflects back to space resulting from the particles themselves scattering incoming solar radiation and increasing planetary albedo. As the driving GCM already has the sulphate aerosols included, the regional sulphur cycle considered by the model therefore has no major impact on the scenarios derived. With respect to investigation of differences between the runs with and without the sulphur cycle, Islam et al. (2006) ran three experiments with different initial conditions and undertook validation of an RCM applying a grid to grid method and point to point method over Bangladesh.

These authors produced a seasonal cycle of precipitation and temperature and undertook time series analysis in comparison with observations to investigate model bias. The simulations from runs with and without sulphur cycle show insignificant differences while they found that among 3 experiments with different initial conditions (IC), the run with first type of IC produced results closest to observations (Islam et al., 2006).

This research focuses more on the sensitivity of the results to the driving GCMs than to either the sensitivity to different initial conditions or to the presence or not of a sulphur cycle in the RCM; Table 2.2 supersedes Table 2.1. Nevertheless, comparing the differences between the mean and standard deviation of precipitation, maximum and minimum surface temperature shows insignificant difference between runs with/without sulphur cycle and between the runs involving different initial conditions (Tables 5.1 and 5.2). The two-tailed t-test is applied to precipitation and maximum and minimum surface temperature to evaluate the statistical differences between the runs with and without a sulphur cycle. After doing the primary analysis, the p-level reported with a t-test represented the probability of error involved in accepting no difference between the with/without sulphur cycle runs. Theoretically, there were no significant differences found at the 95% confidence level so the selected experiment outputs are from the experiment running without sulphur cycle.

Table 2.2: Experiment designs and abbreviations in this study.

Experiment	Named
Control experiment Baseline ERA40 ECHAM4	 PRECIS-HadAM3P PRECIS-ERA40 PRECIS-ECHAM4
A2 scenario experiment B2 scenario experiment	PRECIS-A2 PRECIS-B2
ECHAM4 scenario experiment A2 B2	 PRECIS-ECHAM4-A2 PRECIS-ECHAM4-B2

2.3.1 Modelling domain

PRECIS has been configured for a domain extending from 30°N to 15°S and 90°E to 140°E in the Southeast Asian region with a horizontal resolution of 0.44° x 0.44° (Figure 2.1). The selected domain is large enough so that the RCM can develop its own internal regional-scale circulations, but not too large that the climate of the RCM differs significantly from the GCM in the centre of the domain. This is the first regional climate experiment over the region so that the choice of running the model with 50km resolution instead of 25 km resolution over the region is applied as a first step towards scientific understanding. The choice of running the model with higher resolution would indeed add detail over complex terrain, however, it does not necessarily lead to quantitatively accurate values of those variables. If the choice of running the model with 50 km resolution reveals “added value” over this geographical area, then it may also be worth undertaking 25km resolution simulations. In terms of the computer simulation time, 50 km resolution runs take up to 4 months over the area of interest using the IT facilities available while the 25km run takes twice as long. The original aim of this study is to address if the RCM, PRECIS, adds value to the driving GCM, HadAM3P which leads to the question of justifying if the RCM is necessary to study Thai climate. Moreover, increasing resolution without tuning the model physics increases model bias, such that if, for example, the model simulation is already too wet, the bias may simply be even larger at higher resolution. Rauscher et. el. (2010) noted that spatial disaggregation at high resolution without any improved representation of processes or topography, will lead to increased temporal variability of local precipitation at 25 km.

The land-sea mask and surface topography have been developed by the PRECIS Malaysia workshop based on the US Navy 10-minute resolution dataset. Land mask and surface topography changes, relative to the US Navy dataset, are shown as orange grid cells in Figure 2.1 based on additional reliable datasets provided by, for example, the Philippines and Malaysia governments. The changes include terrain height, vegetation and soil type. Surely, the effect of land-use change on RCM run has to be through physical land-atmosphere inter-action. The selected domain is large enough that the regional model can develop its own regional scale circulations driven by the

application of the boundary conditions, and small enough that the climate of the RCM does not deviate significantly from the GCM and that a simulation can be completed in a reasonable amount of time (Wanner et al., 1997; Kumar, 2006). The selected domain should not be too large that the generated climate of the RCM is significantly different from the GCM in the centre of domain (Kumar, 2006). The selected domain might, arguably, be extended further north, given the role of Eurasia and the Tibetan plateau, but the area would fall within the maritime continent, where the latent heating is considered one of the important energy sources of the global circulation. However, there is a risk of extending the domain further north in terms of insufficient boundary conditions from the driving GCM in the complex topography of the Himalaya mountain range. The computational expense and length of experiment would also be extended.

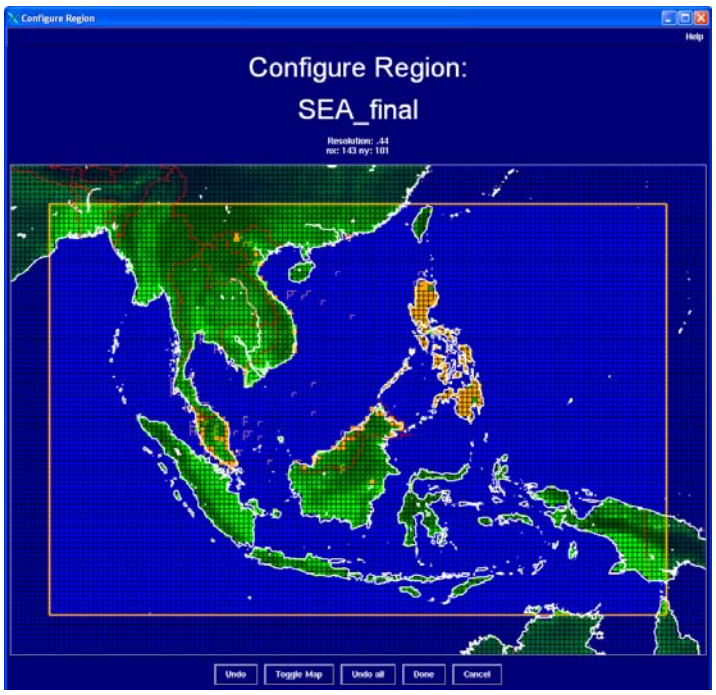

Figure 2.1: PRECIS domain for model simulation over SEA, showing cells in orange with updated land data relative to the US Navy 10' dataset.

2.3.2 Model Experiments

The second part of the project involves model validation for the 'current' climate, taken to be 1960-1990 for the purposes of this study, including comparisons with both station and gridded observational dataset (full detail in section 3.3). The second

section studies model projections for the end of the century. PRECIS and the driving GCM model (HadAM3P) use emission scenarios developed by IPCC (2000). The climate of the recent past, which is assumed as belonging to the present-day climate, is used as a climatological baseline or control. Good quality climatological data is required in order to characterise the present-day climate in the SEA region for a given baseline period. The baseline period of 30 years, from 1961 to 1990, is defined by the World Meteorological Organisation (WMO) as the normal period and fulfils the criteria set by the IPCC (1994) – it has therefore been used in this study as the climatological baseline. The following section is a listing of climatological simulation scenarios used in this study, which are simulated by PRECIS and defined in terms of the source of the boundary data and the relevant emissions data.

Baseline scenario (HadAM3P: 1961-1990)

Data for this scenario is derived from three 31-year (1960-1990) integrations of HadAMP3P (atmosphere only GCM; full details in section 3.3) with 150 km resolution (Wilson et al., 2005). That is, this scenario is an ensemble of three realisations or simulations of lateral boundary conditions, known as addfa, addfb and addfc in PRECIS, each spanning from 1st January 1960 to 1st January 1991, which have been integrated using different initial conditions in terms of testing model sensitivities (but all using a common observed time series of HadISST sea-surface temperatures and sea ice for the same period (Moberg and Jones, 2004)). The current climate simulation is important for the evaluation of the performance of the PRECIS regional climate model and as a baseline for the climate change investigation. The other SEA consortium partners also use the baseline simulation in terms of comparison with future projections.

ERA40 (1957-2001)

ERA40 reanalysis data are gridded data (2.5° x 2.5°), derived from ECMWF (European Centre for Medium-Range Weather Forecasting) Re-Analyses (ERA) through data assimilation over the period 1957-2001, combining observations with simulated data from a single, consistent numerical model. ERA40 is a second-

generation reanalysis carried out by the ECMWF after ERA15, with the objective of producing the best analysis with the availability of enhanced observational and computational resources (Uppala et al., 2005). In comparison with ERA15, ERA40 is produced with an improved NWP model wherein the assimilation, sea surface temperature (SSTs), and sea ice fractions are taken from a combination of the HadISST and NCEP observed datasets. Also, ERA40 uses the observed values of various greenhouse gases for this period to provide relevant information on atmospheric composition, compared to ERA15, which used only the average values (Jones et al., 2004). In comparison with ERA15, ERA40 can provide fields with higher horizontal and vertical resolutions in the planetary boundary layer and stratosphere (Uppala et al., 2005). The RCM output, using large quantities of reanalysis datasets as an input, is useful in describing the climatological baseline, for example in examining the relationship between reanalyses of upper air fields and surface variables to produce regional climate scenarios downscaled from GCM outputs (Kaas and Frich, 1995). This methodology helps with the diagnosis of model errors since model outputs can be compared directly with observational data for specific events.

Future climate scenario (HadAM3P: 2070-2100)

The simulation study consists of an ensemble of three simulations based on the SRES A2 emission scenario, known as addja, addje and addjf in PRECIS, and one realisation for scenario SRES B2, known as addjd, running for the period 2070-2100. The running of the ensemble (particularly SRES A2) is important for addressing sensitivity to initial conditions.

Emission scenarios

The Intergovernmental Panel on Climate Change (IPCC, 2000) has produced four emission scenario families with their coherent narrative part storylines, namely SRES A1, SRES A2, SRES B1, and SRES B2 (Table 2.3) for future emissions reflecting different possible human future activities that yield different levels of greenhouse gas emissions. These scenarios were constructed to reflect the possible future developments in environmental or economic perspectives, and reflecting either global or regional development. Each storyline describes a demographic, social, economic,

technological, environmental, and policy future. For future climate simulations in SEA, a time slice from 2070-2100 was selected from 240-year transient simulations (1860-2100) with HadCM3. Within this time slice, two emissions scenarios were selected, namely SRES A2 and SRES B2, For general comparison between the two selected scenarios, SRES A2 was assumed to have a higher population growth, slower per capita economic growth rates, and technological change, resulting in higher emissions of CO_2 and larger emissions of other GHGs such as methane, nitrous oxides and hydrofluorocarbons (HFCs) (IPCC, 2000).

Table 2.3: Emission scenario storylines; source IPCC (2000)

Scenarios	Storyline Descriptions
A1	Describes a future world of very rapid economic growth, global population that peaks in mid-century and declines thereafter, and the rapid introduction of new and more efficient technologies. Major underlying themes are convergence among regions, capacity building, and increased cultural and social interactions, with a substantial reduction in regional differences in per capita income. The population increases to 8.7 billion by 2050 and declines toward 7 billion by 2100 which combines low fertility with low mortality. The total CO2 emission range of the A1 family scenarios is so wide from 4.3 to 37 GtC in 2100. The total cumulative carbon emission of the A1 family scenarios from around 1000 GtC to more than 2500 GtC.
A2	Describes a very heterogeneous world. The underlying theme is self-reliance and preservation of local identities. Fertility patterns across regions converge very slowly, resulting in a continuously-increasing population. Economic development is primarily regionally-oriented, and per capita economic growth and technological change is more fragmented and slower than other storylines. The A2 scenario family is based on a high population growth scenario of 15 billion by 2100 assuming a significant decline in fertility for most regions and stabilization at above replacement levels. Total cumulative carbon emissions in the A2 scenario group range between 1710 and 1860 GtC by 2100.

Table 2.3 (continued)

Scenarios	Storyline Descriptions
B1	Describes a convergent world with the same global population that peaks in mid-century and declines thereafter, as in the A1 storyline, but with rapid change in economic structures toward a service and information economy, with reductions in material intensity and the introduction of clean and resource-efficient technologies. The emphasis is on global solutions to economic, social, and environmental sustainability, including improved equity, but without additional climate initiatives. The B1 population statistic is the same rate as the A1 scenario. Carbon Emissions peak around 2040 at 12 GtC, twice the 1990 level, and by 2100 the emissions fall below the base-year level to 5 GtC. Total cumulative carbon emissions in the B1 scenario amount to 983 GtC by 2100.
B2	Describes a world in which the emphasis is on local solutions to economic, social, and environmental sustainability. It is a world with continuously increasing global population at a rate lower than A2, intermediate levels of economic development, and less rapid and more diverse technological change than in B1 and A1 storylines. While the scenario is also oriented towards environmental protection and social equity, it focuses on local and regional levels. The B2 scenario indicates population projection of 10.4 billion by 2100. A steady increase of CO_2 emissions emerges in the B2. By 2050 emissions reach 11 GtC and by 2100 they reach 14 GtC and total cumulative CO_2 emissions in the B2 marker scenario amount to 1160 GtC by 2100.

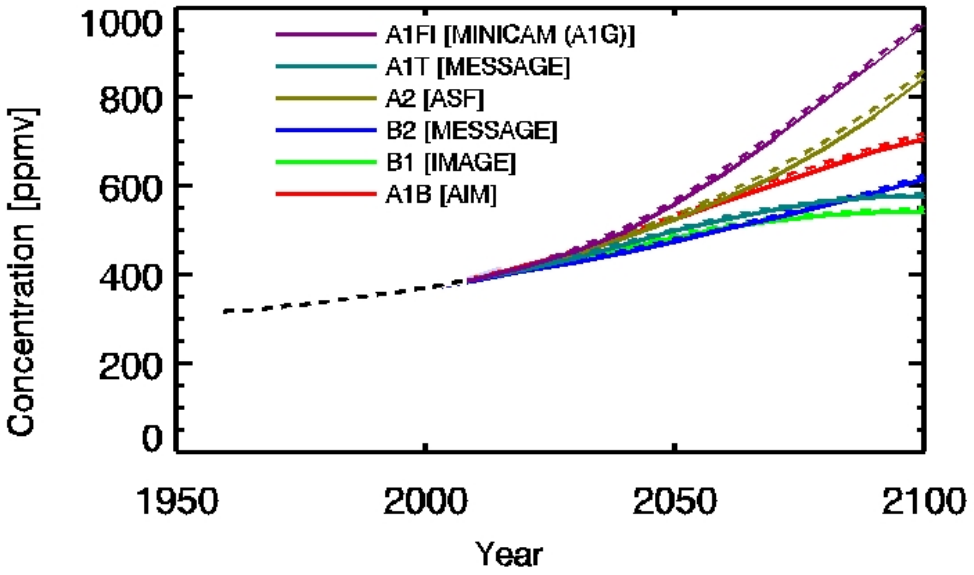

Figure 2.2: Atmospheric CO2 concentrations as observed at Mauna Loa from 1958 to 2008 (black dashed line) and projected under the 6 SRES marker and illustrative scenarios. (IPCC, 2001)

2.4 Model spin-up and simulation duration

2.4.1 Initial conditions (Spin-up)

Land, ocean, and sea ice contribute significantly to surface forcing in regional climate simulations (see Giorgi et al., 1996; Pielke et al., 1999; Maslanik et al., 2000; Rummukainen et al., 2001), and therefore, at the beginning of the RCM modelling experiment, the initialisation of surface variables, particularly soil moisture and temperature are not in equilibrium conditions. Since the atmosphere within the RCM domain takes a few model days to achieve equilibrium with its lateral boundary conditions, and while the temperature and moisture in the deep soil levels take many months to reach equilibrium, it is therefore necessary to allow the atmosphere and land surface to adjust or "spin-up" to a mutual equilibrium state prior to the commencement of climate simulation. In PRECIS, the spin-up period of 12 months is applied and during this period the RCM climate will experience some drift (Jones et al., 2004). The output during this spin-up period was not used as input to analyses undertaken in this project.

2.4.2 Length of simulation

For regional climate investigations in SEA, the simulation length for the current climate (1960-1990) and future climate (2070-2100) has been set for 30 years, although the minimum length requirement is at least 10 years. This length is chosen in order to provide a reasonable idea of the mean climate change and to better determine changes in higher order statistics, particularly for the analysis of climate variability (McGregor et al., 1999; Kato et al., 2001; Jones et al., 2004). Longer periods of simulation (i.e. 30 years) were found to capture about 75% of the variance of the true climate change signals, compared to 50% for 10-year simulations (Jones et al., 1997). Another study by Huntingford et al. (2003) has shown that statistically significant changes in extreme precipitation can be obtained using 20-30 year simulations.

2.4.3 Boundary conditions

Normally, RCMs are driven with either observed boundary conditions, which are derived from Numerical Weather Prediction (NWP) analyses, or with GCM boundary conditions (Gibson et al., 1997; Kalnay et al., 1996). For PRECIS-RCM, the boundary conditions consist of the surface and lateral boundary conditions. Surface boundary conditions are only required over the ocean and inland water points, where time series of surface temperature and ice extent are provided and are updated daily. Meanwhile, the lateral boundary conditions provide information on atmospheric dynamics and thermodynamics at the latitudinal and longitudinal edges of the model domain such as surface pressure, winds, temperature, humidity, and sulphur variables (if sulphur cycle is chosen) and are updated every 6 hours (Jones et al., 2004). Due to the improved aspects of internal physics and dynamics, as well as the incorporation of better large-scale boundary condition fields, regional biases have been reduced in RCMs as shown in a number of previous studies in Europe (Noguer et al., 1998; Jones et al., 1999), South East Asia (McGregor et al., 1998), East Asia (Kato et al., 2001), and the US (Giorgi et al., 1998).

For the simulation study, the boundary data are obtained from the four 30 year integrations of the HadAM3P (atmosphere-only) GCM. For the two selected future scenarios (A2 and B2), the sea-surface boundary conditions are derived by combining changes in sea-surface temperature (SST) and sea ice simulated in integrations of

HadCM3 (ocean-atmosphere GCM) with the HadISST (observed time-dependent fields of SST and sea ice), which has been detailed by Moberg and Jones (2004). Meanwhile, the evolution of greenhouse gases (GHGs) and sulphur dioxide (from anthropogenic and natural sources) concentrations prescribed in the regional model over the simulated period are the same as in the corresponding HadCM3 experiment, which were calculated offline from the SRES emission scenarios data (Jones et al., 2004).

2.4.4 Post-Processing and Visualisation of PRECIS Data

Once the modelling run was completed, all PRECIS output data were saved under the $ARCHIVEDIR/RUNID directory. All the PRECIS output data were generated in the pp format, which is a default file format. The pp format is a record-based binary format, a UK Met Office proprietary format, mainly associated with Met Office products. One of the advantages of this format is that the data format can be converted to other data formats such as GRIB and NetCDF (network Common Data Form) at any time for post-processing (Wilson et al., 2005). In this study, the output file is manipulated in pp format using the utility package and then it is converted to NetCDF format (nc). The PRECIS output data with a fine resolution of 50 km x 50 km (0.44°) were then re-interpolated to a slightly coarser resolution (0.5^{o}), the same resolution as the CRUTS2.1 datasets, in order to facilitate model validation in Chapter 5 but the output remains the original resolution for analysis in Chapter 6. In this study, the PRECIS output is visualised using GrADS (Grid Analysis and Display System; http://www.iges.org/grads/gadoc/users.html).

2.5 Statistical methods

In the investigation of climate change using RCMs, there are a number of uncertainties that need to be taken into consideration when discussing the simulation results. This section provides brief insights of uncertainties in climate modelling (regional or global) resulting from the development of climate scenarios or from the model itself, and how these uncertainties were addressed using PRECIS. Future emission uncertainty has been one of the most clearly identified major causes of

uncertainty in future climate projection (Jones et al., 2004) and has been well documented (Morita et al., 2001). This is due to the inherent uncertainties in key assumptions and relationships about future population, socio-economic development, and technology changes that are the basis of the IPCC SRES Scenarios (Morita et al, 2001). In PRECIS, the future emissions uncertainties have been addressed by running the Hadley Centre GCM with a range of emission scenarios (SRES A1F1, A2, B2, and B1 emissions) (Jones et al., 2004). In this project we consider only A2 and B2 emission scenarios because these projections represent the possible worst and central estimates, producing a range of results which are useful to policy makers for agreeing climate adaptation and mitigation decisions.

Another important uncertainty that has been identified in the use of RCMs is the future concentration of atmospheric pollutants, due to the incomplete understanding of the processes and feedbacks in the carbon cycle and chemical reactions in the atmosphere that affect the emissions-to-concentration relationships. So far, this uncertainty has not yet been addressed in the current PRECIS-RCM, but in the near future this uncertainty will be reflected in climate scenarios by using atmosphere-ocean general circulation models (AOGCMs) that explicitly simulate the carbon cycle and chemistry of all relevant species (Jones et al., 2004).

Incomplete description of the key processes and feedbacks in the climate models has also contributed to the uncertainty in the response of climate systems (Jones et al. 2004). The current GCMs, which contain different representations of the climate system, project different patterns and magnitudes of climate change for the same period and same concentration scenarios (Cubasch et al., 2001). In climate impact studies, this uncertainty can be addressed by using a number of different GCMs, though this approach is still under development by the Hadley Centre (Jones et al., 2004).

The exhibition of internal variability in RCM simulations, due to linear internal dynamics not associated with the boundary forcing, has been identified as another factor of uncertainty in RCM simulations (Ji and Vernekar, 1997; Giorgi and Bi, 2000; Christensen et al., 2001). Uncertainty in the model simulation is reflected by annual and decadal climate variability. This uncertainty can be quantified, and

therefore can be addressed by running ensembles of climate projections. In PRECIS-RCM, an ensemble of three experiments or realisations for both Baseline (Control) Scenario and SRES A2 and one experiment for SRES B2 are provided (see Section 3.3.2), which used the same model and same emission scenarios but initiated from a different starting point (Jones et al., 2004).

Regionalisation techniques have been developed allowing fine scale information to be derived from the GCM output and applying to a wide range of climate-change problem. The approaches can be divided into statistical and dynamical technique. Applying regionalization, it is necessary to fully understand the assumptions and potential and limitations. In applying dynamical technique, i.e., RCM, uncertainties also arise from the regionalisation of climate change models from the driving GCM fields, as any errors from the GCMs are carried with them during this process. The inherent effect of systematic errors from the driving large-scale fields provided by the GCM have been observed and described in previous studies (Pan et al., 2001; Mearns et al., 2001). The differences in regionalisation techniques not only resulted in different projections, but even the use of the same regionalisation techniques on the same GCM projection can also give different projections. For example, using different RCMs with the same driving GCM, each RCM provides different simulations. This uncertainty issue can be addressed by using other RCMs or by carrying out statistical downscaling in parallel with PRECIS (Jones et al., 2004).

2.5.1 RCM validation

Mearns et al. (2003) stressed that any regional climate model for climate change studies should be capable of reproducing the present day climate of the studied region with reasonable error bounds. Since the signals of GCM and RCM are often different, either at the regional or sub-regional scale, it is therefore important that the RCM simulations are validated and the performance of the simulation is verified to ensure that the model errors are identified, quantified, and understood, as these can help in the interpretation of the climate change simulations. The RCM validation is essential for a number of reasons, primarily because most of the PRECIS runs are over new areas where the model performance is untested, and also as an indicator of how much

credibility the RCM results have and how the model should be used in impact studies (Wilson et al., 2005). Furthermore, in assessing the model, the discrepancies between GCM, RCM and the real observations can be addressed by identifying any systematic model bias, spatial sampling issues (differences in resolution of model and observations) and observational errors (gridding issues, instrument-dependent errors). In this study, the validation of PRECIS is undertaken as follows: PRECIS-CRUTS2.1, PRECIS-ERA and PRECIS-GCM.

2.5.2 Future Climate Projection

In this study, the climate projections of PRECIS are analysed by comparing PRECIS-future with PRECIS-baseline and PRECIS & GCM. The comparison of GCM-future and GCM-baseline is also analysed. The correlation, or the correlation coefficient, is a normalised measure of how well the simulated and observed data co-vary. The bias of a series of observations and their corresponding simulations can be interpreted as a systematic error for a given variable. If the bias is less than zero then the model is under-predicting the mean, and if the bias is larger than zero then the model is overestimating the mean. The typical difference between observations and model predictions can be estimated by using the Mean Square Error (MSE). The MSE will have the value zero for a perfect forecast. However, it is sensitive to only a few large differences between observations and predictions due to the squaring of the difference. A variant of the MSE is the Root Mean Square Error, which can be interpreted as the expected error of the simulations. Another variant is the Normalised Mean Square Error (NMSE) that obtains a value between 0 and 1, which can be practical when comparing the relative efficiency between observations and simulation. A two-sided student t-test was also used to measure the statistical significance of the difference between averages of two series of datasets.

Chapter 3

Data and Tools

3.1 Introduction

In this chapter, detail is given of the regional climate model system utilised in this thesis, the Providing REgional Climates for Impact Studies (PRECIS) model. Also discussed are the observational datasets used in this research for establishing a climatology of Thailand and for model verification.

3.2 Observational Dataset

To address the aims of this project, there is a desire for long, high resolution, continuous observational datasets over the region of SEA. This section describes the detail of those datasets.

3.2.1 Thai surface station observational dataset

There are currently 87 surface measurement weather stations unevenly spread over the whole area of Thailand, data for which are provided by the Thai Meteorology Department (TMD) (Figure 3.1(a)). The meteorological data are available at monthly and daily temporal resolution, three hourly at some sites. A charge is made in response to data requests, even for education purposes, of approximately 1 penny per kilobyte. The data volume for one single site would be approximately 8.5 Mb, costing £85, so the dataset for the complete Thai network would cost around £7,000. Written requests were made asking for the fees to be waived. Over a period of twelve months, free access to an essential subset of the station network was negotiated; stations were selected which broadly encompassed the range of climatic environments across Thailand. The period which the data covers in this study is 1961-1990 because this is the period over which the model climate simulations are being evaluated.

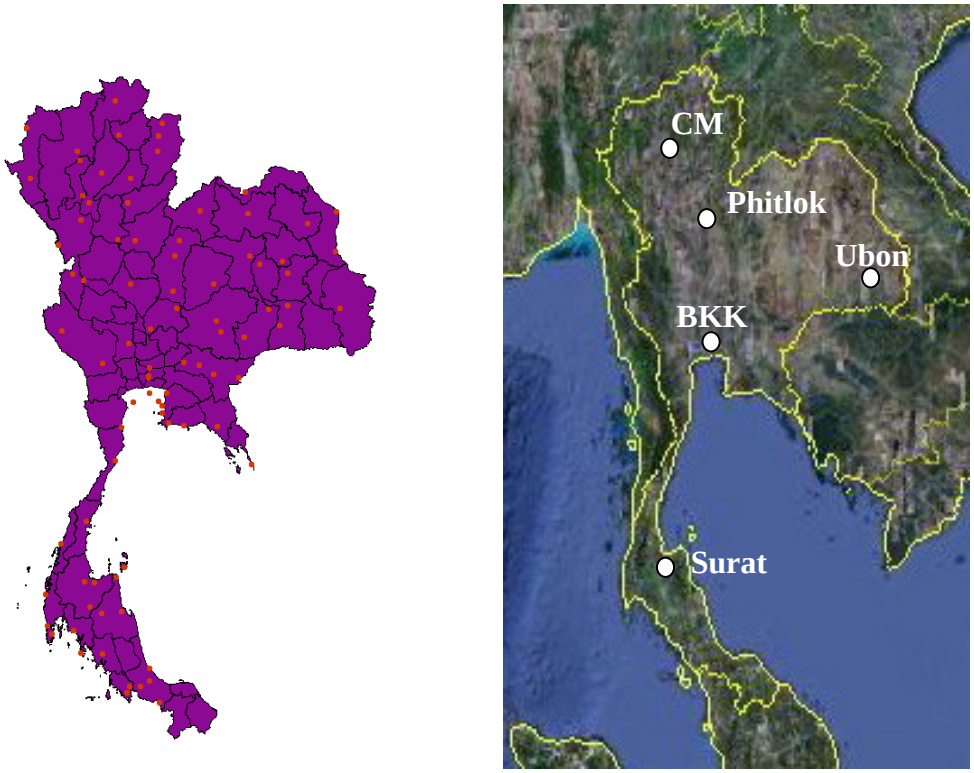

Figure 3.1. : (a) Locations of the 87 stations over Thailand (b) Location of 5 selected stations in Thailand (source: www.googleearth.com).

The TMD classified the climate of Thailand into four geographic regions. The northern part is mountainous with the highest peak 2,565 m above sea level. The northeastern part consists of Plateau with average altitude of 140-200 m above sea level while the centre of Thailand is very flat. Eastern areas consist of a mixture of mountainous and plain areas. Southern Thailand is a peninsula with the Gulf of Thailand and part of the South China and Andaman Seas. The 87 surface measurement stations spread over Thailand are categorized into these four regions; each station located in the same region has a similar mean air surface temperature seasonal cycle. Chiang Mai, Phitsanulok, Ubon Ratchathani, Surat Thani and Bangkok were carefully chosen as study sites because they characterise the range of topographies in Thailand located in northern, lower northern or upper central, northeastern, southern areas and in the capital of Thailand. The correlation coefficients between station pairs of mean monthly surface temperature and precipitation over the available period 1970-1990, as shown in Tables 3.1 and 3.2, indicated that these chosen stations reasonably represent regional climate.

Table 3.1: Correlation coefficient of mean monthly surface temperature (1970-1990) between the selected station and nine nearest stations in the same region.

Nearby stations	Chiang Mai (North)	Phitsanulok (lower North)	Bangkok (Center)	Ubon Ratchathani (Northeast)	Surat Thani (South)
1	0.992	0.985	0.985	0.986	0.969
2	0.983	0.996	0.990	0.998	0.968
3	0.981	0.980	0.985	0.987	0.956
4	0.992	0.993	0.982	0.987	0.931
5	0.995	0.989	0.983	0.995	0.962
6	0.993	0.993	0.996	0.991	0.922
7	0.996	0.984	0.987	0.983	0.957
8	0.989	0.987	0.998	0.986	0.920
9	0.972	0.992	0.982	0.974	0.922

Table 3.2: Correlation coefficient of mean monthly precipitation (1970-1990) between the selected station and nine nearest stations in the same region.

Nearby stations	Chiang Mai	Phitsanulok	Bangkok	Ubon Ratchathani	Surat Thani
1	0.972	0.973	0.988	0.955	0.902
2	0.962	0.968	0.971	0.991	0.945
3	0.974	0.967	0.986	0.965	0.965
4	0.99	0.939	0.984	0.93	0.924
5	0.97	0.943	0.953	0.982	0.917
6	0.979	0.973	0.948	0.981	0.937
7	0.954	0.924	0.995	0.978	0.913
8	0.921	0.936	0.976	0.922	0.898
9	0.976	0.947	0.996	0.987	0.905

These stations (Figure 3.1) also have long and reliable records (Table 3.3). In terms of recording time scale, these five stations have 30 year daily records covering the

baseline 1961-1990 period to support the subsequent modelling work. The data consists of daily surface measurements of precipitation amount, minimum/maximum/mean temperature, cloud fraction and mean pressure along with rawinsonde data, i.e. vertical profiles of wind, temperature and humidity.

Table 3.3: Percentage of missing surface meteorological data during the period 1961-1990

Station	Daily precipitation	Daily temperature	Daily wind profile
CM	1.78	0	1.78
Phitlok	1.60	0	1.60
BKK	2.52	0	2.52
Ubon	1.79	0	1.79
Surat	3.15	0	3.15

The Chiang Mai (CM) site, 312m above sea level, is nearby the area of highest terrain in Thailand which extends from the Himalaya range to the north. Chiang Mai province, the 2nd largest province in Thailand, divides into two contrasting geographical areas (i) 80% mountainous over northern and western watershed areas and not suitable for cultivation (ii) basin plain and flat area between valleys. The typical altitude in northern Thailand is about 250-400 m above sea level.

The Phitsanulok site, hereafter called Phitlok, is 45m above sea level and was chosen because it was likely to be affected by tropical depressions more than the other stations among nearby stations approaching from the South China Sea. Phitsanulok province has generally high terrain in the northern region, and basin plains in central and southern areas.

The Ubon Ratchathani site, hereafter called Ubon, is located 123m above sea level. General plateaus average 68m above sea level sloping to the east to the river Mekong and the southern border of the province is hilly.

The Surat Thani site, hereafter called Surat, is located on the Thai peninsula. Surat Thani Province is located on the east coast of southern Thailand with varied topography; hilly, mountainous, coast of the Gulf of Thailand. The province is

typically rainy during the northeast monsoon flow with moisture from the South China Sea and Bay of Thailand as mentioned in chapter 1.

The Bangkok (BKK) site, 3m above sea level, is also a challenging location for representation by models. As capital of Thailand it is the most crowded and polluted urbanised area in Thailand, and the main river basin for flow from central Thailand. This station might be particularly affected by an urban heat island phenomenon that would be difficult for an RCM to fully account for. The temperature difference between urban and rural areas is known as the Urban Heat Island (UHI) and this is greatest under clear-sky, low-wind situations which often occur during wintertime at higher latitude locations globally. Stations located in urbanized areas typically show large increases in mean maximum/minimum surface temperature (Voogt and Oke, 2003) due to the storage and later release of solar energy by the urban fabric and exacerbated also by city anthropogenic heat sources. Bangkok city is expanding its borders and population due to increased industrialization and urbanization. This can lead to increases in temperature in the urban area (moderated however by the coastal location) and create an urban heat island which can affect human comfort and air pollution concentration and lead to higher energy consumption for air conditioning. Tran et al (2006) revealed large highest day time surface UHI intensity values using satellite measurements in most Asian megacities in the period 2001-2003 , such as in Tokyo (12 °C), Bangkok (8 °C), and Shanghai (7 °C). Tonsuwonnont (2006) also mentioned that the maximum intensity of around 6-7°C is detected during clear and calm nights in the dry season (when excess energy is more likely to contribute to sensible heat transfer rather than for evaporating water). Moreover, she found that the mean annual air temperature in Bangkok city is higher by 0.8°C than outside the city by using hourly air temperature data from ten automatic stations around Bangkok, one in rural site and nine in urban sites during 2000-2004. The magnitude of observed surface UHIs are positively correlated with urban growth and the population density of that area and inversely proportional to wind, clouds, and precipitation. An inverse relationship between green area and surface temperature is found and the difference between urban parks and built-up areas can be 6-8°C (Tonsuwonnont, 2006). A decrease in urban vegetation and the extension of the built-up area can enhance the magnitude of the UHI. The location of Bangkok monitoring station is within the city environment, located about 30 km north of the Gulf of Thailand. There is no published evidence that the other selected stations here are affected by an UHI.

Table 3.4: Location and Elevation of surface monitoring stations in the study area and average of four nearest model grid cells

Station name	Location		Elevation (m)	
	Station	Model grid cell	Station	Model grid cell
Chiangmai	18.78°N, 98.98°E	18.83°N, 98.82°E	312	606.1
Phitsanulok	16.78°N, 100.27°E	16.99°N,100.08°E	45	317
Bangkok	13.73°N, 100.57°E	13.85°N, 100.74°E	3	5
Ubon Ratchathani	15.25°N, 104.87°E	15.34°N, 104.85°E	123	122.4
Surat Thani	9.12°N, 99.35°E	9.12°N, 99.07°E	5	140.7

It is clear in Table 3.4 that PRECIS is using a terrain field over northern Thailand where the nearest gridcells are higher than the stations adopted here for model verification – these altitude differences will need to be accounted for in the analyses.

The TMD considered geographies and divided the climate of Thailand into 4 sectors which are covered by the stations selected.

(i) North (CM and Phitlok); mostly north-south mountainous terrain

(ii) Northeast (Ubon); hilly and sloping southeastward

(iii) Central (BKK); plains sloping down to the Gulf of Thailand

(iv) Southern (Surat); Peninsula situated between the Andaman Sea to the west and the Gulf of Thailand in the east.

Peel et al. (2007) produced a global map of climate using the Koppen-Geiger system based on a large global data set of long-term monthly precipitation and temperature station time series. Figure 3.2 shows climate types for SEA. A description of Koppen climate types is shown in Table 3.5.

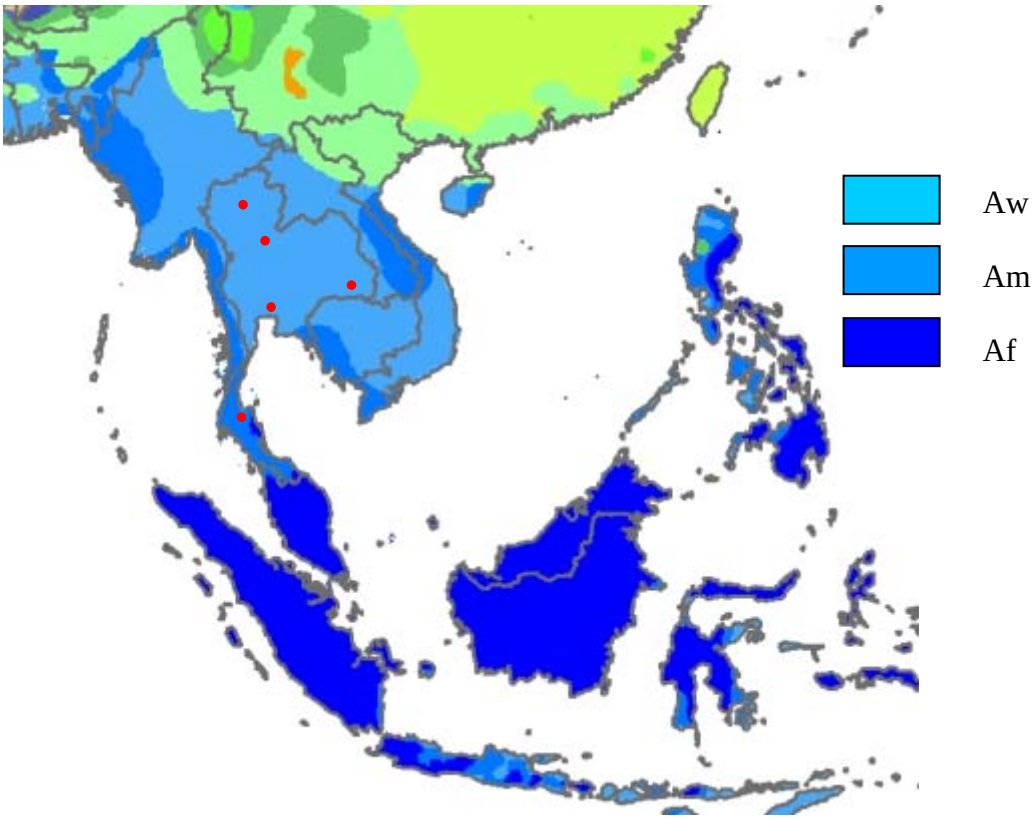

Figure 3.2: The map of Koppen-Geiger climate type over SEA (Peel et al., 2008) [Noted that the red point in the map representing 5 selected station; i.e., CM, Phitlok, Ubon, BKK and Surat]

Tabel 3.5: A description of the Koppen climate symbol (Peel et al., 2007)

T_{cold} =Temperature of the coldest month

P_{dry} =Precipitation of the driest month

MAP=mean annual precipitation

1st	2nd	Description	Criteria
A		Tropical	$T_{cold} \geq 18\ ^{o}C$
	f	- Rainforest	$P_{dry} \geq 60$
	m	- Monsoon	Not (Af) & $P_{dry} \geq 100 - MAP/25$
	w	- Savannah	Not (Af) & $P_{dry} < 100 - MAP/25$

SEA is classified as having a tropical moist climate which means that average surface temperature each month is higher than 18°C and total precipitation is higher than 150 cm per year. The maximum mean temperature difference between daytime and nighttime is up to 10°C.

Based on the Koppen climate classification, the regions of north, northeast and central Thailand are considered as Aw (Savannah Climate) and southern Thailand as Am (Tropical Monsoon). Therefore, Chaing Mai, Phitsanulok, Bangkok and Ubon Ratchathani stations are considered in the same Koppen classification, Aw, while the southern station, Surat Thani, is considered as Am.

These sets of daily station data are used (i) to underpin the analysis of climate including the study of the mesoscale southeast monsoon onset and the effect of El Niño and La Niña events in chapter 4 and (ii) to compare and validate grid point model output in chapter 5.

It is worth recalling that systematic errors can appear in point precipitation measurements. Such errors could occur due to the following reasons: (i) Aerodynamic effects; (ii) wetting of the internal walls of the gauge; (iii) evaporation of water in the gauge; (iv) surrounding afforestation and (v) splashing of raindrops away from or into the gauge.

Aerodynamic effects have the most influence on the accuracy of raingauge measurements. These effects cause greater systematic errors if rain gauges are set above the ground surface. The systematic error range in measurements of precipitation varies from 10% to 30 % and depends on wind velocity and precipitation type. Wind is the most dominant environmental variable affecting the gauge collection efficiency, for example, with wind speeds exceeding 3 ms^{-1}, the wind caused losses may be above 5% (Goodison et al., 1998).

Wetting loss is another cumulative systematic loss from manual gauges which depends on precipitation type and gauge type and the frequency with which the gauge is emptied. Average wetting loss for some gauges can be up to 0.3mm per observation. Countries using manual gauges for precipitation measurement have

determined the average wetting loss for their National gauge. At synoptic stations where precipitation is frequent and measured every six hours, this can become a very significant amount, for example, wetting loss was calculated to be 15-20 percent of the measured winter precipitation at some Canadian stations (Goodison et al., 1998).

Evaporation from manual gauges can significantly lead to the systematic under-measurement of precipitation. Aaltonen et al. (1993) reported on the comprehensive assessment in Finland of evaporation loss. Average daily losses varied by gauge type and time of year, for example, evaporation loss was a problem in the late spring; evaporative losses from the gauge in April of over 0.8 mm/day were measured. Losses during winter were much less than that recorded during comparable spring and summer comparisons, and ranged from 0.1-0.2 mm/day. These losses, however, are cumulative. Many gauges install a funnel for summer (precipitation) measurements, helping to reduce potential evaporation loss.

Increase of collected precipitation amounts from the exposed gauge site will appear a few years after any surrounding afforestation, when the height of growing trees reaches above the level of the gauge opening.

3.2.2 Gridded Observational Data

The high resolution half degree resolution monthly surface climatology of the global land area for the period 1901-2002, CRUTS2.1 (Mitchell and Jones, 2005), comprises nine variables: cloud cover, diurnal temperature range, frost day frequency, precipitation, mean temperature, minimum temperature, maximum temperature, vapour pressure and wet day frequency. Primary variables, such as precipitation, mean temperature, and diurnal temperature range, were interpolated directly from station observations. Secondary variables were interpolated from merged datasets comprising station observations and, in regions where there were no station data, synthetic data estimated using predictive relationships with the primary variables. In this study the relevant modelling period is the period 1961-1990. The data are in large ASCII formats which are in 360x720 grid cells so the data is converted to netcdf format by using Climate Data Analysis Tools, CDAT. The sources of station data

contributing to CRUTS2.1 are the World Meteorological Organisation (WMO), National meteorological agencies, CRU global datasets of station time series, the Centro Internacional de Africultura Tropical South American database, published sources and the U.S. Air Force Climatological Data Volume. Data from the WMO collection were comprehensively analysed to quality control (QC) checks, for example, data failing QC were flagged by the National Climate Data Center and were removed from interpolation for CRUTS2.1. All data from the other sources were subjected to a two stage QC process; (i) internal consistency checks and between variable consistency tests and (ii) interpolation of station data with identification of station months with large residuals. Data failing QC were removed, however, the data could be replaced with data from the CRU monthly station time series. The accuracy of the monthly grids for temperature is most reliably interpolated from the available station data while precipitation reliability is lower. The less reliable variables have poor data coverage and complex topography particularly Greenland, the Himalaya-Tibetan region and SEA during the active monsoon season. Some errors in station location were not identified in the interpolation process. However, comparing CRU precipitation to other climatological data sets, for example, Legates and Willmott (YEARLEG), Leemans and Cramer (YEARCRA), CRU grids are more accurate in high elevation regions. Uncertainties in primary variables, such as temperature, may be caused by poor measurements, uncertainties in the station data, sampling uncertainties caused by the limited number of measurements available, and large-scale biases such as urbanisation.

The data are interpolated by using a distance weighting which has a number of variants in both the selection of stations that contribute to a grid point estimate and the form of the distance weighting function. The eight nearest stations are used, regardless of direction or distance, in estimating each grid point value. All stations are first weighted by distance from the grid point. The limitation of this gridded data set is that interpolation over SEA as a function of latitude and longitude ignores the influence of elevation. However, interpolation of mean temperature and diurnal temperature range as a function of only latitude and longitude is adequate. The stations used in the interpolation in the SEA region are shown in Figure 3.3. More detail is available in Mitchell and Jones (2005). The data are available from the Climatic Research Unit via http://www.cru.uea.ac.uk/cru/data/hrg/cru_ts_2.10.

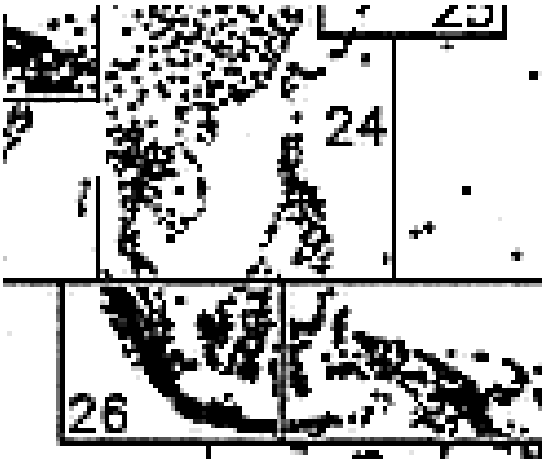

Figure 3.3: Location of stations used in the CRUTS2.1 interpolation over SEA. (New et.al, 1998)

The purpose of using the surface station observational dataset in this study is to build a climatology and validate the model performance at individual points at the daily timescale while the objective of using the monthly gridded data is to analyse spatial variation and directly compare with the spatial model output. [Note that the CRU dataset has resolution of 0.5x0.5 degree while the RCM downscales to 0.44x0.44 degree so, in this study the RCM outputs are re-gridded to the coarser CRUTS2.1 resolution.]

Tables 3.6 and 3.7 show comparisons between station data and the nearest CRUTS2.1 grid cell data. The station sites are located at the centre of the 9 surrounding grid cells.

Table 3.6: Correlation coefficient of mean monthly surface temperature (1970-1990) between surface stations and the respective nearest grid cell data.

Nearby grid cell	Chiang Mai	Phitsanulok	Bangkok	Ubon Ratchathani	Surat Thani
1	0.99	0.995	0.985	0.992	0.968
2	0.996	0.997	0.991	0.987	0.972
3	0.991	0.986	0.986	0.983	0.981
4	0.992	0.991	0.984	0.972	0.988
5	0.986	0.987	0.982	0.985	0.963
6	0.991	0.989	0.995	0.991	0.985
7	0.993	0.993	0.993	0.978	0.977
8	0.989	0.992	0.984	0.981	0.97
9	0.987	0.982	0.986	0.995	0.959

Table 3.7: Correlation coefficient of mean monthly precipitation (1970-1990) between surface stations and the respective nearest grid cell data

Nearby grid cell	Chiang Mai	Phitsanulok	Bangkok	Ubon Ratchathani	Surat Thani
1	0.979	0.978	0.977	0.965	0.914
2	0.972	0.979	0.985	0.981	0.962
3	0.988	0.951	0.976	0.953	0.973
4	0.975	0.95	0.984	0.94	0.933
5	0.977	0.941	0.993	0.991	0.939
6	0.941	0.951	0.971	0.986	0.945
7	0.963	0.966	0.985	0.988	0.921
8	0.943	0.951	0.964	0.934	0.914
9	0.985	0.988	0.976	0.987	0.912

The CRUTS2.1 dataset was created by calculating a mean climate for 1961–1990, and then calculatingting anomalies for that period and adding them to the mean to create the full field (New et al. 1999, 2000). The station data were interpolated to the grid using thin plate splines considering latitude, longitude, and elevation as parameters.

No corrections for rain gauge type, wind conditions, or anthropogenic disturbances were applied. The uncertainties in the gridded data depend on effects of the station uncertainties, on the density of stations and on sampling error.

It is of course also instructive to compare the relative degree to which ERA40 data and CRUTS2.1 correlate with the station data used in this project In comparison with the station observations CRUTS2.1 best matches annual precipitation, while ERA-40 reports less precipitation than the observations. With regard to the amplitude of the inter-annual variations, CRU is better than the reanalyses in representing the corresponding observations. The amplitude in CRUTS2.1 is almost the same as TMD over northern and southern Thailand but that of ERA-40 is higher and lower than the observations in northern Thailand and the other three parts of Thailand, respectively. ERA-40 has a less obvious inter-annual variability than CRUTS2.1 and TMD in the mainland of Thailand. The results also suggest that the magnitude of the precipitation difference between ERA-40 and the station observations is larger than that between CRUTS2.1 and the observations.

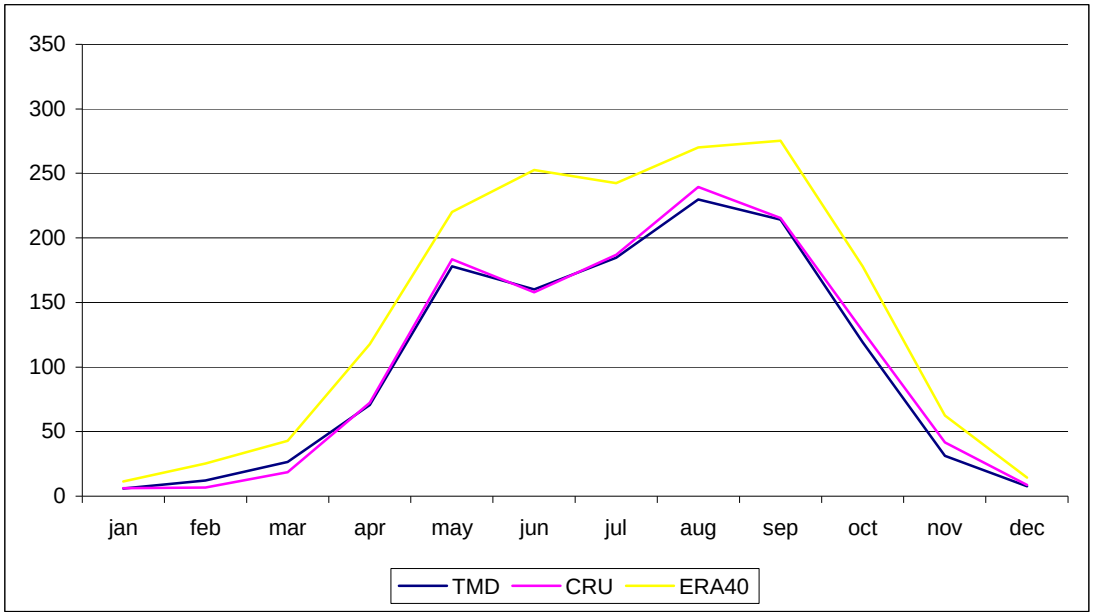

(a)

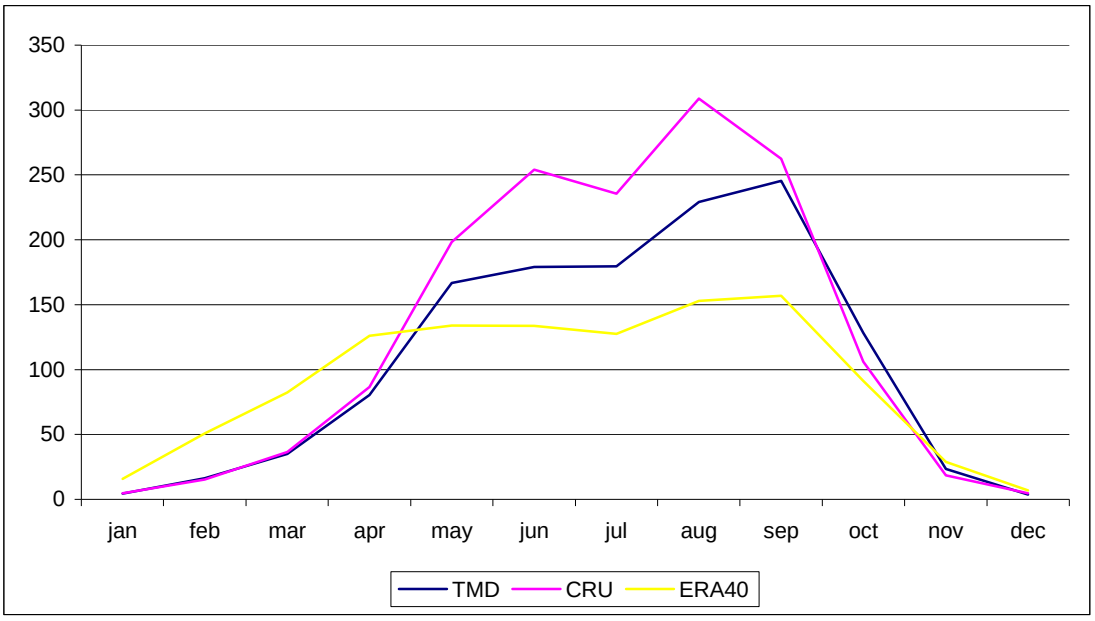
350
300
250
200
150
100
50
0
jan
feb
mar
apr
may
jun
jul
aug
sep
oct
nov
dec
TMD
CRU
ERA40

(b)

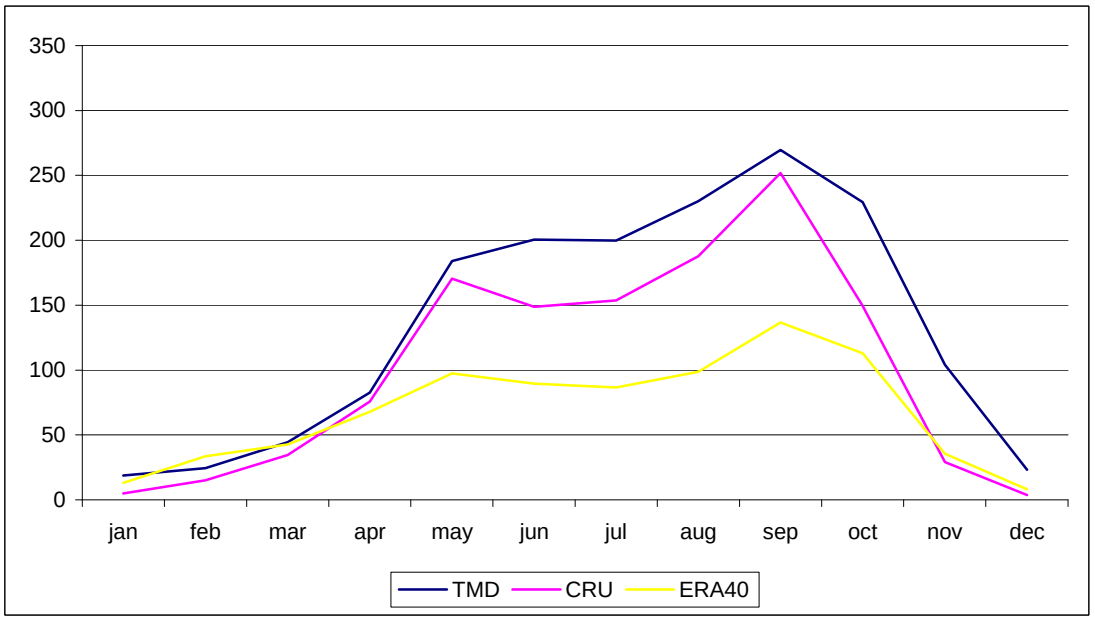
350
300
250
200
150
100
50
0
jan
feb
mar
apr
may
jun
jul
aug
sep
oct
nov
dec
TMD
CRU
ERA40

(c)

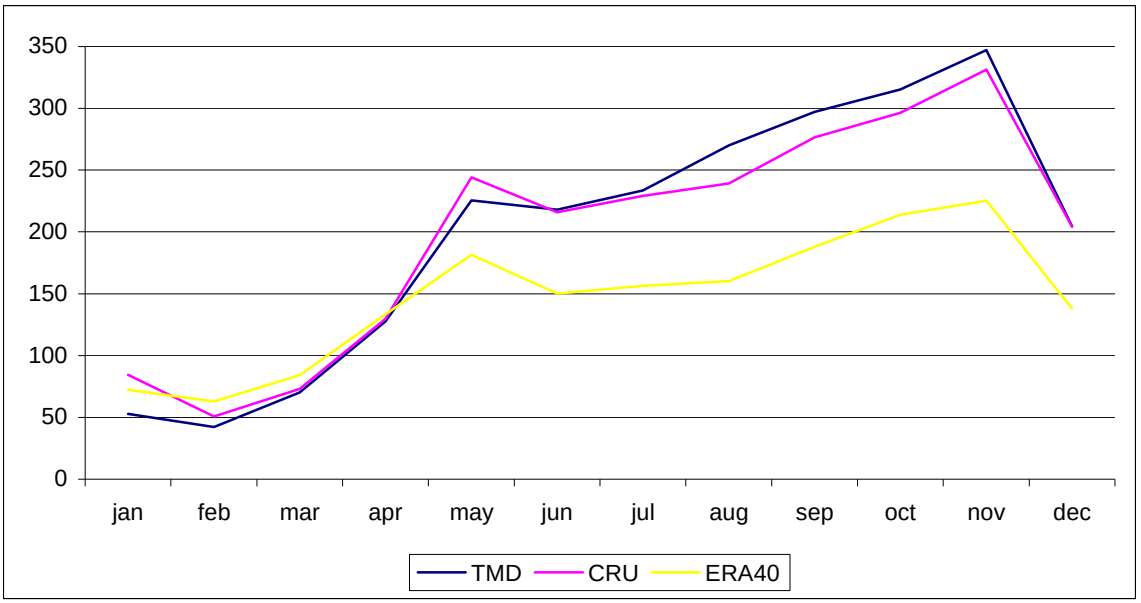

(d)

Figure 3.4: Area average annual mean total precipitation (mm) from 1961-1990 comparing ERA40 data, CRUTS2.1 and station data (using monthly averages for 89 stations). (a) Northern Thailand (b) Northeastern Thailand (c) Central Thailand (d) Southern Thailand

3.2.3 TRMM satellite data

The main goal of the Tropical Precipitation Measuring Mission (TRMM), a joint scientific initiative between NASA and NASDA, the National Space Development Agency of Japan, (ex-organization of JAXA, Japan Aerospace Exploration Agency) is to provide accurate estimates of global tropical precipitation (Simpson et al. 1996). TRMM's sensors, including the precipitation radar and the TRMM Microwave Imager, have provided information about precipitation in the Tropics since 1997. TRMM's orbit which allows for coverage of the tropics taking about 91 minutes for one orbit around the earth is circular which ranges between 35°N and 35°S of the equator at an attitude of 350km. Information on monthly precipitation is important for the evaluation of regional model simulations, especially where other forms of observational datasets are lacking. Satellite observations are also important for contributing to a better understanding of the global water cycle. However, satellite data sometimes have large biases and need to be compared with and adjusted to site observations. It was shown that the TRMM 3B42 data is useful for estimating the average values of precipitation over Bangladesh (Islam and Uyeda, 2006). They

compared daily precipitation measured by TRMM 3B42 to that of rain-gauge values from pre-monsoon to post-monsoon months (March–November) and found that spatial and temporal averages of precipitation revealed good estimations of precipitation: during March to November; the V5 3B42- and rain gauge-estimated daily average precipitation were 8.12 and 8.34 mm, respectively. The average percentage of rainy days determined by V5 3B42 data with respect to the rain-gauge value was 96%.

As in Bangladesh, the SEA climate is also influenced by the movement of the ITCZ. In this thesis, the 3-hourly TRMM product 3B42 (Adler et al. 2000) data are used to describe the general precipitation patterns within the wet and dry spells associated with monsoon intra-seasonal variability. All TRMM datasets are distributed by the Goddard Distributed Active Archive Center (see online at lake.nascom.nasa.gov/data/dataset/TRMM/). The 3-hourly TRMM data are an optimal combination of different high-quality microwave products to adjust infrared estimates from high-frequency geostationary observations (see online at http://trmm.gsfc.nasa.gov/3b42.html). Therefore, the dataset does not have issues arising from satellite sampling issues and it provides a reasonably good idea of the convective activity throughout the day. The spatial resolution of this dataset is 0.25° with data available from January 1998 to the present. The average precipitation, as shown in Figure 4.1 in the following chapter, are from the available period of January to August 2009. In this study, TRMM satellite is used to contribute to the understanding of ITCZ movement and for the purpose of model validation. One of the uncertainties in the TRMM satellite data set compared to surface precipitation observations is that gauges give a near-point precipitation rate while radar estimates correspond to a volume-averaged precipitation rate. Stephen (2009) indicated that variability of a factor of 2–10 inches (50-250mm) is common in actual annual precipitation totals over spatial scales of several to tens of kilometers in steep topography. Franklin (2002) highlighted that TRMM is the first satellite to carry both active and passive sensors for measuring precipitation with associated uncertainties; passive estimates are a less direct measure of precipitation.

3.2.4 NCEP–NCAR reanalysis

Average monthly zonal and meridional wind components were obtained from the National Centers for Environmental Prediction–National Center for Atmospheric Research (NCEP–NCAR) reanalysis product archived on a 2.5° grid for use in describing the general climate of Thailand (www.esrl.noaa.gov/psd/data/gridded/data.ncep.reanalysis.html).

3.3 Model boundary and initial condition data

3.3.1 Hadley Centre Atmospheric Model version 3 with higher resolution (HadAM3P)

The HadAM3P is an atmosphere-only GCM with a spatial resolution of 1.24° latitude × 1.88° longitude (~150 x 150 km) and a timestep of 15 minutes (Pope, 2000). The output from this model is provided by the UK Meteorological Office. HadAM3P is UKMO's GCM which is used extensively in the IPCC 4th Assessment. The initial atmospheric and land surface conditions in HadAM3P are interpolated from the atmosphere model, HadAM3, with a lower-resolution of 3.75° latitude x 2.5° longitude (~300 km). The HadAM3 is based on the previous version of the climate model HadAM2b, described by Stratton (1999), with some major improvements (not shown here, see Pope, 2000). In terms of the output used in this study, the tropical cold bias is reduced by 0.3°C in the annual mean in HadAM3 when compared to HadAM2b and there is less precipitation over most regions in the tropics. There are increases in precipitation over the Indonesian region. These show improvement in simulation over the region.

3.3.2 ECMWF Reanalysis Data (1951-2001); ERA40

The ERA40 spans the period of September 1957 to August 2002. The data set consists of 6 hourly analyses with a resolution of TL159 (2.5° x 2.5° regular latitude/longitude grid). The data during 1957-1972 is known as "pre-satellite" with old observation

types only while the data during 1972-1988 incorporates the assimilation of some satellite observation types and the data during 1988-2002 incorporate the assimilation of other latest observation types. ERA40 produces surface wind analyses and surface turbulent exchanges more realistically than ERA15. A revised and more accurate surface orography description has been used in the ERA-40. The most serious problem diagnosed in the ERA-40 analyses is excessive tropical oceanic precipitation since 1991 (note that in this study, the baseline period is 1961-1990). Chan and Nigam (2009) indicated that ERA-40 tropical heating and divergent circulations were found to be stronger in the tropics (especially in the summer, July) than in NCEP-NCAR reanalyses, which is consistent with the stronger Hadley Circulation. Moreover, ERA-40 reanalyses show a significantly stronger ITCZ than NCEP-NCAR Reanalysis. Challinor et al. (2005) mentioned that ERA-40 overestimates the frequency of light rains, and underestimates heavy rains over India. Simmons et al. (2004) noted that gaps in the availability of synoptic surface data contribute to relatively poor performance of ERA-40 prior to 1967, leading to a warm bias.

3.4 PRECIS modelling

3.4.1 Introduction

The PRECIS model (Providing Regional Climates for Impact Studies), which was used in the research was developed by the UKMO Hadley Centre with a resolution of 50km x 50km, is capable of producing a high resolution climate with reasonable computational requirements (Jones et al., 2004) and has been used in a number of climate change impact studies in South Asia (Bhaskaran et al., 1998; Hassel and Jones, 1999; Islam and Mannan, 2005; Challinor et al., 2006; Kumar et al., 2006), East Asia (Erda et al., 2005; Wang and Shallcross, 2005), Europe (Moberg and Jones, 2004; Lalas et al., 2005), Africa (Hudson and Jones, 2002; Arnell et al., 2003; Beraki, 2005), and North America and South America (Martineu, 2005; Marengo and Ambrizzi, 2006). Further details of these studies are given in Chapter 1.

PRECIS, also know as HadRM3P, is the latest Hadley Centre model based on the atmospheric component of the HadCM3 climate model (Gordon et al., 2000), which differs from earlier versions mainly in the representation of dynamic and convective clouds and thresholds associated with the formation of precipitation. The model

employs one-way nesting. The nesting ensures that the RCM results are consistent with the driving model GCM projection; the additional detail due to the increase in resolution facilitates interpretation of climate responses and impacts (Hudson and Jones, 2002; Arnell et al., 2003; Wang et al., 2004). Using this approach, the GCM is used to simulate the response of the global circulation to large-scale forcing, while the RCM is used to account for sub-GCM grid scale forcing in a physical way (orography, land cover, etc.), and to enhance the simulation of atmospheric circulation and climatic variables at fine spatial scales (Mearns et al., 2003). PRECIS is an atmospheric and land surface model of a limited area with a horizontal resolution of 0.44° x 0.44° (50 x 50 km) or 0.22° x 0.22° (25 x 25 km) on its own rotated latitude-longitude grid and has a timestep of 5 minutes.

PRECIS is embedded in the atmosphere-only GCM (HadAM3P) which has spatial resolution of 1.24° latitude × 1.88° longitude (~150 x 150 km) and a timestep of 15 minutes. The sea surface boundary conditions are derived by the observed time series of HadISST and sea-ice for 1960-1990 for the baseline period and by combining changes in SST and sea-ice simulated in integrations of the HadCM3 coupled model with the HadISST for the future scenarios. The initial atmospheric and land surface conditions in HadAM3P are interpolated from the lower-resolution (3.75° latitude x 2.5° longitude, ~300 km) coupled ocean-atmosphere model (HadCM3) (Gordon et al., 2000). Both HadAM3P and HadRM3P (PRECIS) have 19 levels in the atmosphere; from approximately 50 m up to the 0.5 hPa pressure level and four levels in the soil (Hudson and Jones, 2002).

3.4.2 Model description

Numerical models such as PRECIS are used to obtain an objective simulation of future climates by solving a set of equations that describe the evolution of atmospheric variables such as temperature, wind speed, humidity, and pressure. The numerical modelling process involves the analysis of the observation data and assimilation of those observations in the model in order to generate and obtain the best estimate of the current true state of the atmosphere. All numerical models of the atmosphere are based upon the same set of governing equations as described in the following sections, but differ in the approximations and assumptions made in the

application of these equations, how they are solved, and also in the representation of physical processes. A numerical model of the atmosphere consists of several components such as atmospheric dynamics, physical parameterisations, and sulphur cycles (Jones et al., 2004).

Atmospheric dynamics

The atmospheric component of the PRECIS is a hydrostatic version of the full primitive equations and uses a regular latitude-longitude grid, in the horizontal, and a hybrid vertical coordinate. All the governing equations of the model are solved numerically on a discrete 3-D grid spanning the area of the model domain and the depth of the atmosphere. The model simulates values at discrete and evenly spaced points in time with a 5-minute timestep to maintain numerical stability. The evolution of atmospheric dynamics of pressure, wind, temperature, and moisture are governed by three fundamental principles: conservation of momentum, conservation of mass, and conservation of energy.

Physical parameterisations

Physical processes in the atmosphere such as clouds and precipitation, radiation, convection and boundary layer exchanges, and gravity wave drag have been represented numerically in the PRECIS. Due to computational constraints as well as shortcomings due to lack of understanding of the processes involved, assumptions are required for the parameterisation of these physical processes (Jones et al., 2004). The following sections briefly describe the parameterisation principles of the important physical components of the atmosphere in the model.

Radiation

The atmosphere is driven by solar radiation, which can be divided into short-wave (incoming radiation) and long-wave (outgoing radiation) components. The amounts of short-wave (sunlight) and long-wave (terrestrial heat) radiation that are absorbed, emitted and reflected depend on the properties of the atmosphere such as temperature, water vapour, concentration of chemically reactive gases (such as GHG, trace gases, etc.), the surface (land cover types, etc.) and the frequency of the radiation. In PRECIS, the spectrum of radiation is split into six short-wave bands and eight long-

waves bands, where each band has different strengths of interaction with atmospheric constituents such as GHGs (Jones et al., 2004). Short-wave fluxes depend principally on the solar zenith angle (varying according to latitude, season, and time of day), clouds and the albedo of the surface, while long-wave fluxes depend upon the amount and temperature of the emitting medium and its emissivity (Edwards and Slingo, 1996). For full radiation calculations, both schemes require more computational expense than any other physical process, and thus longer timesteps of about three hours (Ingram et al., 1997).

Surface exchange and sub-surface processes

In PRECIS, the soil and vegetation types that characterise the land points are considered in the calculation of the heat, moisture, and momentum fluxes at each land grid point. The land cover type was used in the calculations to determine the surface albedo, surface roughness length, and hydraulic properties of the roots and the vegetated canopy. The HadAM3P component of PRECIS simulates the global atmospheric and land surface processes at a horizontal resolution of 2.5º x 3.75º using the Radiative Transfer Scheme (Edwards and Slingo, 1996) and Meteorological Office Surface Exchange Scheme (MOSES) (Cox et al., 1999). Depending on the local land cover types, the parameters representing "snow-free albedo" and "maximum deep-snow albedo" in each grid box were assigned with appropriate values.For example the albedo parameter was assigned a higher value for open land (e.g grassland, pasture and cropland) and lower values for woodland and forests (Cox et al., 1999; Betts, 2000). Within the model, the radiative forcing due to surface albedo change can be calculated by performing additional sets of calculations of surface albedo and the shortwave radiation budget on a model timestep. In the tropics, surface albedo change due to land cover changes may affect the climate via evapotranspiration, where the rate of evapotranspiration and the fluxes of sensible and latent heat are dependant on the parameters of rooting depth, aerodynamic roughness length and canopy water holding capacity (Betts et al., 1997).

In the MOSES simulation, all these parameters are assigned with an appropriate value in each grid box, where values are comparatively lower for open land compared to forested areas (Cox et al., 1999). In the SEA region, which consists of mostly forested

areas, a cooling influence is anticipated as a result of the greater flux of moisture to the atmosphere and the larger ratio of latent to sensible heat fluxes. In PRECIS, the global datasets of the vegetation parameter values were derived from Wilson and Henderson-Sellers (1985) at a resolution of 1º x 1º grid. The land cover dataset has specified 53 land cover classes, which includes 11 crop classes, 7 pasture/grazing classes, and 1 urban class. In PRECIS, the land cover dataset allows two classes of land cover for each grid, namely the primary land cover class if the coverage of the grid box is between 50-100%, and the secondary land cover class if the coverage is between 25-50%. These vegetation covers, which are represented in the HadAM3 surface parameter, are then bi-linearly interpolated to the GCM resolution. Meanwhile for the soil, a multilayer scheme (4-layer scheme) is used to model the heat transport through the soil (Smith, 1993), which also includes the effects of soil water phase change and the influence of water and ice on the thermal and hydraulic properties of the soil (Jones et al., 2004).

In PRECIS, the soil properties dataset provided by Wilson and Henderson-Sellers (1985) was used in the parameterisation of the soil scheme. In MOSES, the thickness of the soil layers from the top are 0.1, 0.25, 0.65, and 2.0 metres, which are specifically designed to resolve the diurnal and seasonal cycles with minimal distortion. The 4-layer scheme with appropriate values of parameters was found to provide good amplitude and phase response for periods of surface forcing between half a day and a year; the details of the multilayer soil thermodynamics model can be found in Smith (1996). This project assumed no change in surface characteristics in the future.

Clouds and precipitation

The representation of clouds and precipitation in PRECIS is very important as clouds interact strongly with solar and infrared radiation, which may affect the occurrence of precipitation. The release of latent heat during this process also plays a critical role in the movement of air in the atmosphere. Layer cloud cover and cloud water content in each grid box of the model are calculated from a saturation variable (q_c), which is defined as the difference between total water (q_τ) and the saturation of vapour pressure (see Smith, 1990). The formation of layer cloud is assumed to occur at any

level of the 19 levels of the atmosphere, except at the 19^{th} level (top of the stratosphere). In PRECIS, an assumption is made that the cloud water is in liquid form above 0°C, frozen below -9°C, and a mixture in between (Smith, 1990; Smith et al., 1998).

The large-scale formation of precipitation is assumed to occur when the threshold values of cloud liquid water reach 1.0×10^{-3} (kg/kg) over land and 2.0×10^{-3} (kg/kg) over sea (Smith 1990). Large-scale formation of precipitation is dependent on cloud water content, with a greater efficiency of precipitation when the cloud is glaciated, and assumed to fall on 75% of the land surface within a grid box in the model regardless of layer cloud fraction (Jones et al., 2004). The large-scale cloud and precipitation scheme of the model has considered the water transfer between clouds and precipitation as a result of cloud physics processes, the free fall of ice and rain downwards to the earth surface, and the calculation of fractional coverage of cloud in each grid box of the model.

The cloud physics processes that are represented in the scheme are condensation of water vapour to cloud droplets and the evaporation of these droplets, deposition of water vapour to ice crystals or aggregates and the evaporation of these particles, the riming of supercooled cloud droplets by ice particles, melting of ice particles to produce raindrops, evaporation of raindrops, accretion ("sweep-out") of cloud droplets by raindrops, the collision/coalescence mechanism to form raindrops from cloud droplets, and the downward fall of ice particles and raindrops (Wilson and Ballard, 1999). This model is also able to account for the convective precipitation (occurring on a local scale), which represents the convection of cumulus and cumulonimbus clouds. A single cloud model is used to represent a number of convective plumes within the grid box, and the convective precipitation is diagnosed within that grid box if the cloud liquid/ice content exceeds a critical amount and the cloud depth exceeds a critical value. The threshold values of cloud liquid water for convective precipitation are higher than for the large-scale clouds and precipitation of 2 g/kg over land and 0.4 g/kg over sea. This value is set to 1.5 km over the sea and 4 km over land. However, for cloud depth, if the cloud-top temperature is less than -10°C, the critical depth is reduced to 1 km over land or sea. Similar to large-scale

precipitation, the convection scheme also allows for evaporation and melting of precipitation. In each grid box, it is assumed that the convective precipitation falls on 65% of the land surface, regardless of the convective cloud fraction (Jones et al., 2004).

Gravity wave and orographic drag

In the free atmosphere, the gravity wave drag scheme parameterises the effect of the mountain ranges on scales between 5 km and the model grid scale, which acts as a sink for the momentum. Depending on the conditions of atmospheric stability and wind shear, air passing over the mountains may create lee waves, which could result in eddies over and to the lee of the mountains and deprive momentum over a considerable depth (Palmer et al., 1986). The fundamental elements of this scheme are the determination of surface stress, and the distribution of this stress through the atmospheric column, which is dependent on the wind speed, density, and static stability of the low-level flow, where the low-level flow is the layer of air that intersects the sub-grid scale orography (McIntyre, 1980). Closer to the earth's surface, the orographic drag scheme parameterises the effect on the boundary layer of sub-grid scales of about 5 km or less, where the wind speed decreases due to interaction with the roughness of the earth surface. The orographic drag is determined in terms of a constant drag coefficient and linearly depends on the silhouette area of orography, which is a measure of the slopes within a grid box (Jones et al., 2004). The calculation also uses an effective roughness length, which is a combination of the effects of the topography and vegetation within a grid box (see Gregory et al., 1998) but does not take into account the wave reflection or trapping as well as the gravity waves generated by other means such as convective storms (Wilson and Swinbank, 1996).

Chapter 4

The Climate of Thailand based on Observational Data

4.1 Introduction

This chapter examines Thailand climatology using the station and gridded observational datasets described in Chapter 3. The year-to-year and seasonal variability along with the spatial patterns in the period 1961-1990 are analysed, supported by satellite and model data from more recent years. The estimated southwest monsoon onset date is also investigated. The impact of tropical cyclones and the effect of El Niño and La Niña events on climate variability are discussed.

4.2 The mean climate of Thailand

4.2.1 Precipitation

The Intertropical Convergence Zone (ITCZ) is recognised as a band of relatively intense convective precipitation, associated with surface moisture, which moves seasonally. Figure 4.1 shows the seasonal migration of the ITCZ, a narrow latitude zone of wind convergence and precipitation, associated with the onset and duration of precipitation in tropical areas.

Figure 4.1(a) shows the average precipitation (1998-2009) from TRMM (left) and the average wind (right) over the same period from NCEP/NCAR reanalysis data during December, January and February, respectively. The northeast monsoon is active during DJF, the winter season in the northern hemisphere. During December (Figure 4.1(a) top), the ITCZ fully retreats back to the southern hemisphere. Precipitation is found over Indonesia, peninsular Indochina, Borneo and the Philippines. The wettest areas are peninsular Malaysia and eastern Philippines with the prevalence of northeasterly/easterly winds. The wind brings moisture from the northwest Pacific Ocean and the South China Sea. Some precipitation is also found over southern Thailand. During January, the ITCZ is located in the southern hemisphere. Thailand,

Indochina and other regions in the northern hemisphere are not affected by the ITCZ at this time and they are under the influence of the northeasterly trade winds (northeast monsoon) as show in Figure 4.1(a) (middle). The ITCZ gradually moves further northward but is still located in the Southern hemisphere with consistent northeastery trade winds in February as shown in Figure 4.1(a) (bottom).

Figure 4.1(b) shows the average precipitation (1998-2009) from TRMM (left) and the average wind over the same period from NCEP/NCAR reanalysis data during March, April and May respectively. The ITCZ gradually moves further northward across the equator covering the Thai peninsula, the Bay of Bengal and the nearby area. The winds turn from northeasterly to southwesterly in this region. This is the trigger for the southwest monsoon. The heaviest precipitation can be found in the Bay of Bengal.

Figure 4.1 (c), representing the northern hemisphere summer season, shows that the ITCZ rapidly propagates further northward, moving to the area of northern Thailand. Heaviest precipitation can be found on the west coast of peninsular Thailand and in eastern Thailand near the Gulf of Thailand. During the period of August and September, the southwest monsoon is at its maximum strength. The southward movement of the ITCZ, first over northern Thailand and in September over central Thailand, brings extremely intense precipitation. Heavy precipitation over the south China Sea was also identified during this period by Cheang (1993) and McGregor (1998) who found that precipitation during the summer monsoon over the South China Sea is associated with the ITCZ returning southward, reaching 15°N during July-August when moist air from the Indian Ocean helps enhance convection. As noted in earlier chapters, the seasonal variation of monsoon precipitation involves the Hadley Circulation, the zonal mean meridional overturning mass flow between the tropics and subtropics involving the ITCZ and the Walker Circulation, the latter being the zonal east-west overturning.

Figure 4.1 (d) shows the average precipitation (1998-2008) from TRMM (left) and the average wind over the same period from NCEP/NCAR reanalysis data during the months of October and November (ON). October is already a dry month in the north

and northeast of Thailand but still wet in the central plains and in the Thai peninsula. The wind direction changes to northeasterly across the region.

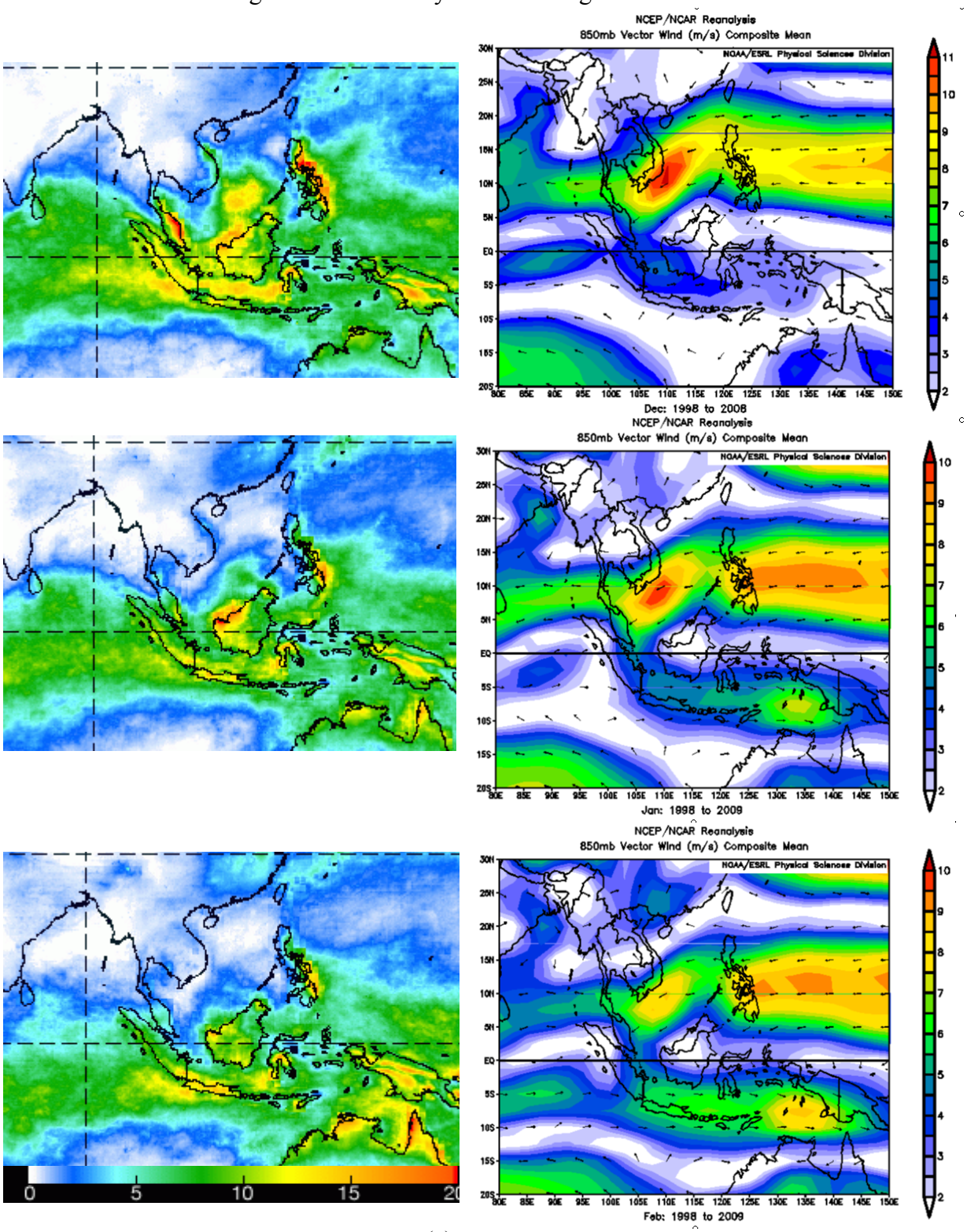

(a)

Figure 4.1: Average SE Asia monthly precipitation (mm) from TRMM during 1998-2008 (left) and wind vectors (right) based on NCEP/NCAR reanalysis data, 1998-2008; the colour bar shows wind speed (m/s). (a) DJF (b) MAM (c) JJAS (d) ON

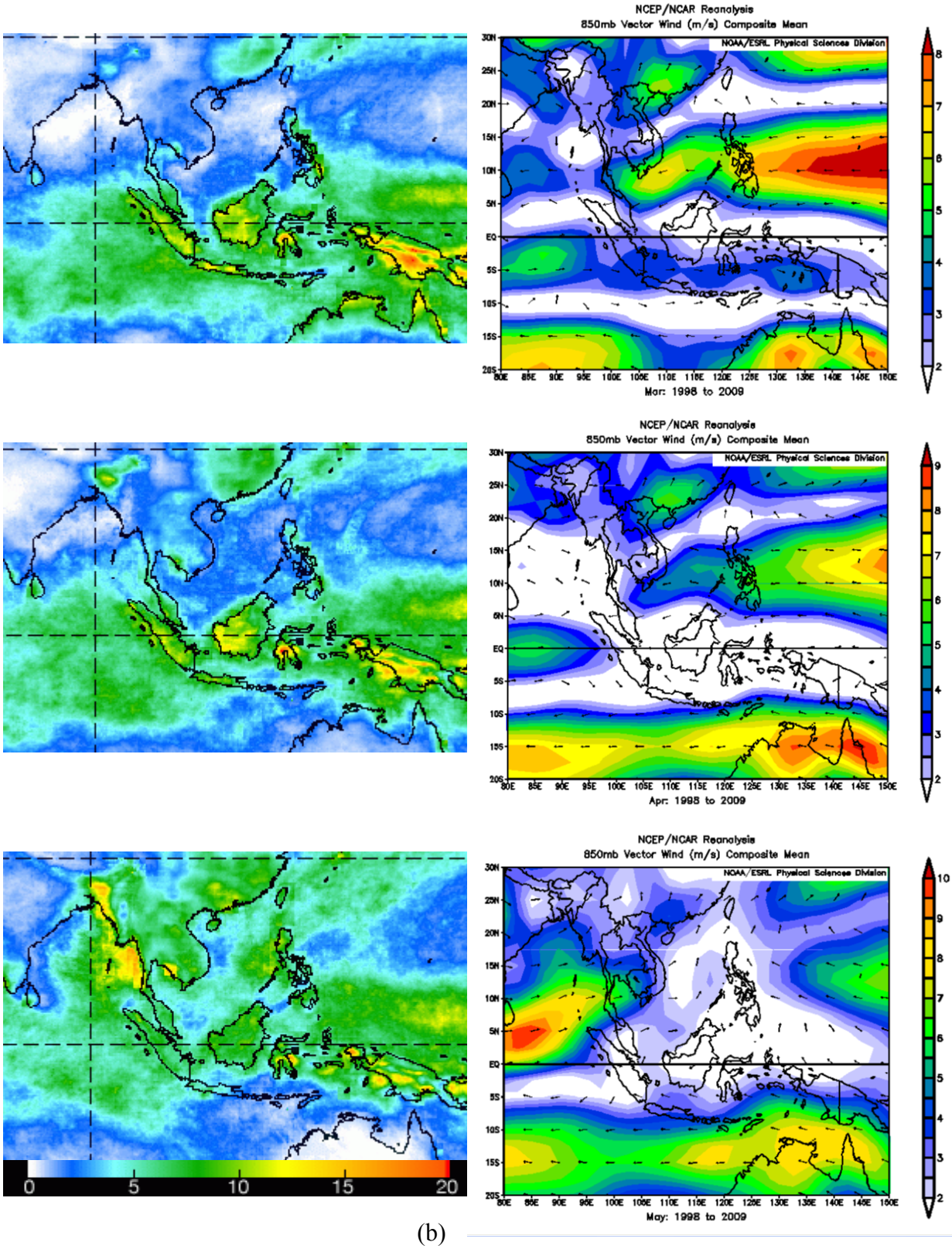

(b)

Figure 4.1(continued)

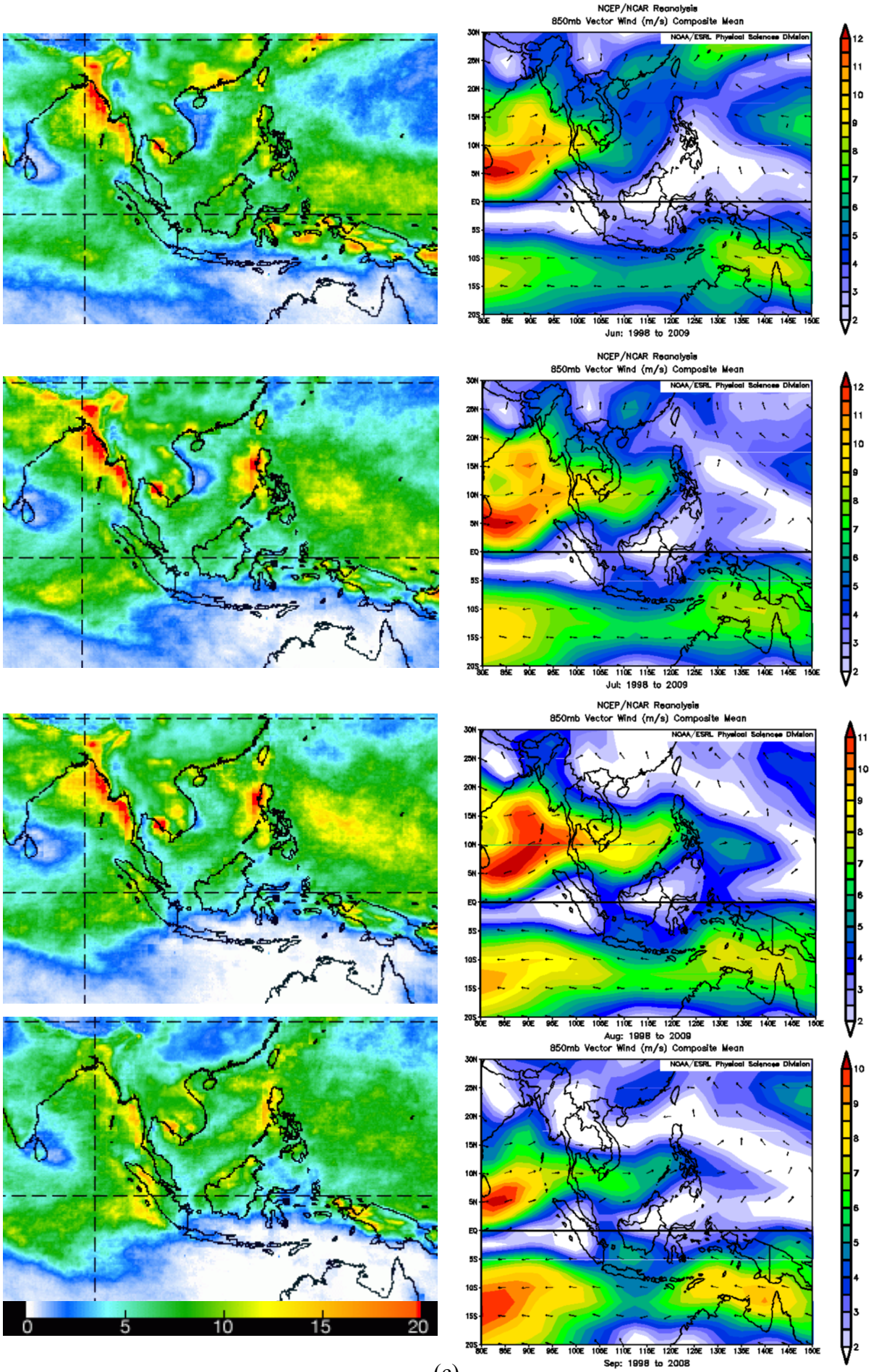

(c)

Figure 4.1 (continued)

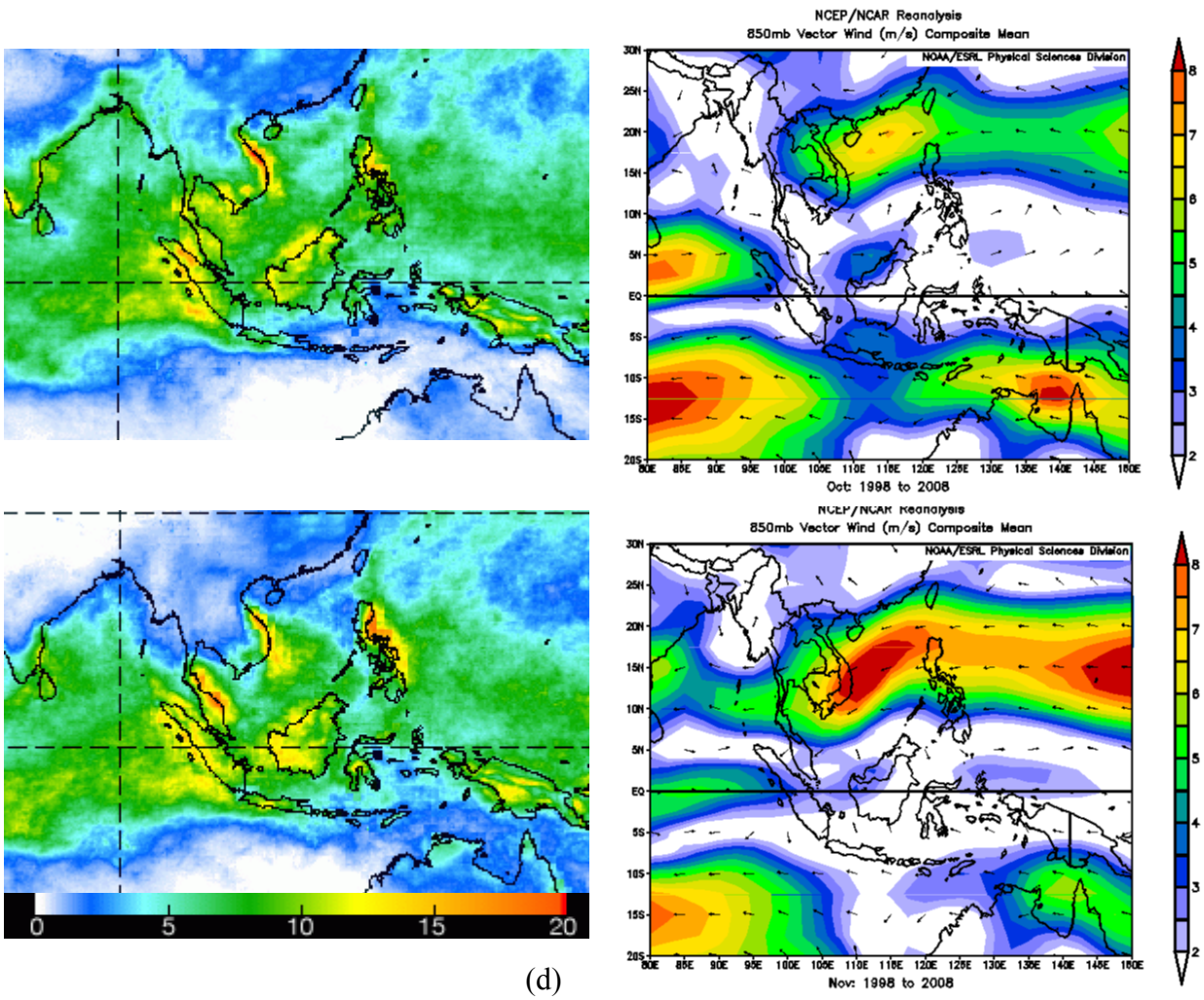

(d)

Figure 4.1 (continued): Average SE Asia monthly precipitation from TRMM during 1998-2008 (left) and wind vectors (right) based on NCEP/NCAR reanalysis data, 1998-2008; the colour bar shows wind speed. (a) DJF (b) MAM (c) JJAS (d) ON

As discussed in chapter 3, there are two sets of TMD station data, monthly during 1970-2000 and daily mean during 1961-1990. The station average of annual precipitation total in the period 1970-2000 based on TMD monthly datasets from 87 stations is 1543 mm. This can be broken down into four different topographic regions with 23, 17, 22 and 25 stations contributing to the northern, northeastern, central and southern areas respectively. The wettest part is southern Thailand (2158mm) and where 1398mm, 1379mm and 1218mm represent the 30-year average precipitations in central, northeastern and northern regions, respectively. The average number of rain days (days with rain exceeding 1 mm) for the whole year in southern, central, northeastern and northern Thailand are 161, 120, 116 and 121 days, respectively. Figure 4.2 shows that northern and northeastern Thailand have very similar seasonal

precipitation regimes, the highest peak tending to be in August (September in the central region). However, the Thai peninsula behaves somewhat differently with maximum rain in November. The possible cause of the later November peak is the complete retreat of the southwest monsoon and the influence of the northeast monsoon which brings moisture from the South China Sea to the peninsula as discussed in section 1.1.3.

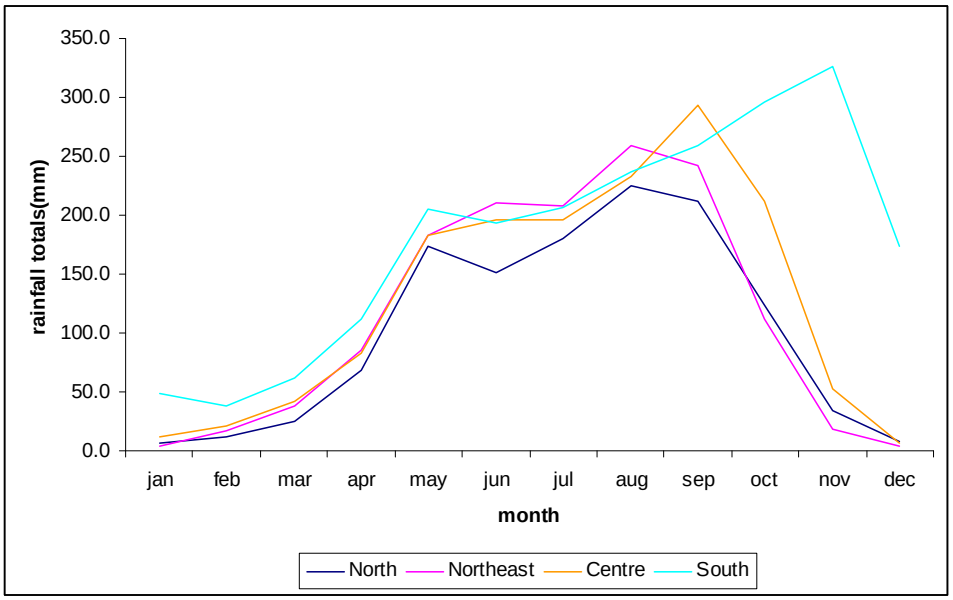

Figure 4.2: Seasonal cycle of 30-year (1970-2000) average monthly precipitation (mm) divided into four topographic regions and based on 87 stations

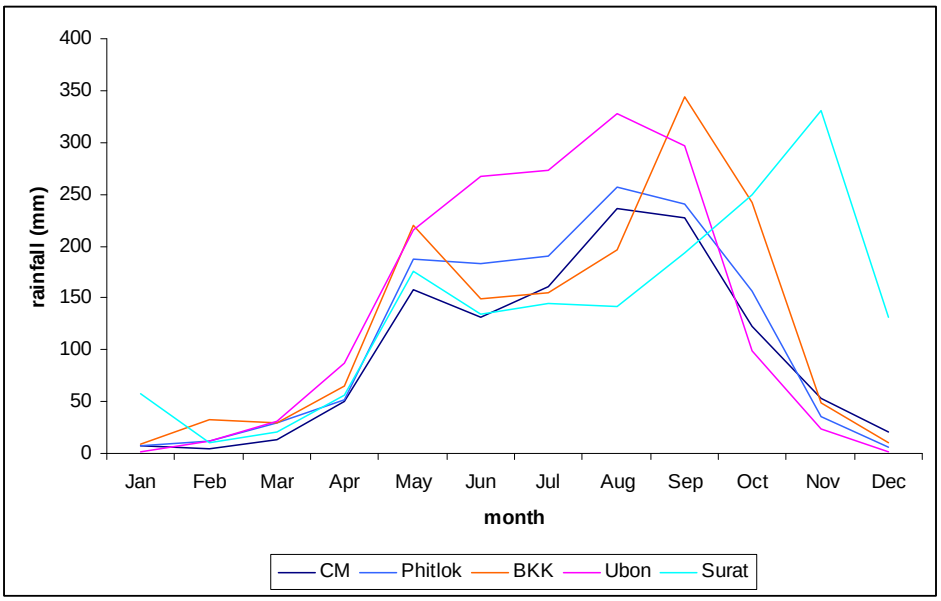

Figure 4.3: Seasonal cycle of 30 year (1961-1990) average monthly precipitation for the five representative daily reporting stations across Thailand.

Figure 4.3, in comparison with Figure 4.2, shows that the five selected daily reporting stations chosen for this research can be seen to be representative of the regions. Chiang Mai and Phitsanulok are located in northern Thailand and Bangkok, Ubon Ratchthani and Surat Thani are representative of central, northeastern and southern Thiland, respectively.

The correlations between the seasonal cycle of monthly precipitation at individual stations and the corresponding region are 0.98 (Chiang Mai and north), 0.99 (Phitsanulok and north), 0.95 (Bangkok and centre), 0.98 (Ubonratcha Thani and northeast) and 0.95 (Surat Thani and south). In this study, the meanings of correlation value are defined as (i) 0.95-1.00 means very strong positive correlation (ii) 0.8-0.94 means strong positive correlation (iii) 0.5-0.79 means weak positive correlation, (iv) -0.49-0.49 means no correlation. Therefore, reduction in station numbers to 5 does not show a significant impact on validation. It is noted that Phitsanulok is an extra chosen station in northern Thailand because it is more likely to be in the tropical cyclonic track. Each station and its corresponding region has a very strong positive linear relationship so the reduction in station numbers to five does not impact detrimentally upon the climatological results nor on the model validation presented later. Correlations among stations located in northern, northeastern and central Thailand (CM, Phitlok, Ubon and BKK) are between 0.87-0.99 while correlations between those stations and southern Thailand are between 0.47-0.62. This suggests that CM, Phitlok, Ubon and BKK can be summarized by a single averaged mainland station which is quite distinct from conditions in the south. This is consistent with the Koppen-Geiger climate type (Figure 3.2).

Precipitation peaks first in May and a secondary peak occurs in August/September over the mainland and then in November in the south of the peninsula, consistent with ITCZ movement. Seasonal precipitation variation shows two significant peaks in the climatological annual cycle over Thailand, the first rainy peak occurs during pentad 29 and the second rainy peak occurs during pentad 50 while the monsoon break occurs during pentad 34-36 (Figure 4.4) consistent with may studies. For example, Wang (2002) proposed two views of the summer monsoon cycle; (i) running from the middle of May to early July with a precipitation peak in mid-June and (ii) from late July to early September with a precipitation peak in late August. Takahashi and

Yasunari (2006) found that there is a similarity of average precipitation during 1951-2000 over mainland Thailand based on using 32 sites distributed randomly over the region, finding that the first peak occurs from pentad 28-30 and the second peak occurs from pentad 49-51. A possible cause of the monsoon break during July is that the monsoon wind changes direction from southwesterly to westerly in association with the trough over the Bay of Bengal (Figure 4.1(c)) and a strong ridge is formed over western Indochina.

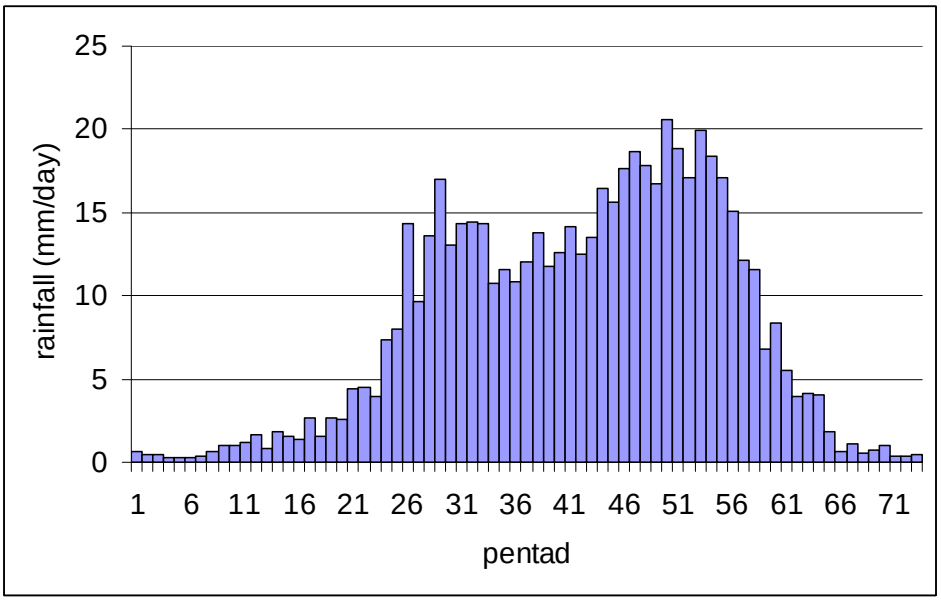

Figure 4.4: Climatological pentad mean time series of precipitation (1961-1990) in units of mm/day. The index is averaged precipitation at the mainland stations [CM, Phitlok, BKK and Ubon].

Considerable differences between the stations can be observed regarding absolute values, variations and temporal trends. The analysis of the 30 year records of TMD from 1961 to 1990for the four individual stations at CM, Phitlok, BKK and Ubon in Thailand reveals no significant trend in annual precipitation (not shown here); instead the precipitation time series for the mainland as a whole and for the Surat site are presented (Figure 4.5). The precipitation variability over the Surat site is higher in comparison with the mainland in all seasons. It can be observed that year-to-year time series precipitation trends at both mainland sites and at Surat reveal decreases at both the annual and seasonal scales (excluding ON on the mainland and MAM at Surat which show positive trends). . At Surat, a 95% statistically significant decreasing

trend can be detected for ON and DJF when the absolute precipitation totals are still relatively high (about 40% of annual totals) while the precipitation trend during JJAS (40% of annual precipitation total) also shows a negative sign (Table 4.1); a positive precipitation trend in MAM at Surat is insufficient to overcome the negative overall annual trend (Table 4.1). Meanwhile, JJAS, with about 60-70 % of annual precipitation totals over the mainland, clearly shows the existence of negative trends over the mainland region. The corresponding regression lines are also plotted. The inter-annual precipitation variability around the mean value (118 mm/month over the mainland and 137 mm/month over the Surat site) reveals a declining trend given the slope of the regression line; the slopes are -0.1331 and -0.6622 mm/month-year giving an estimated decrease of about 1.6 mm/year and 7.9 mm/ year over mainland and Surat sites, respectively. However, these trends are not statistically significant. During JJAS, the slope reveals that precipitation decreases about 9.13 mm/year and 3.42 mm/year over the mainland and Surat sites respectively (Table 4.1).

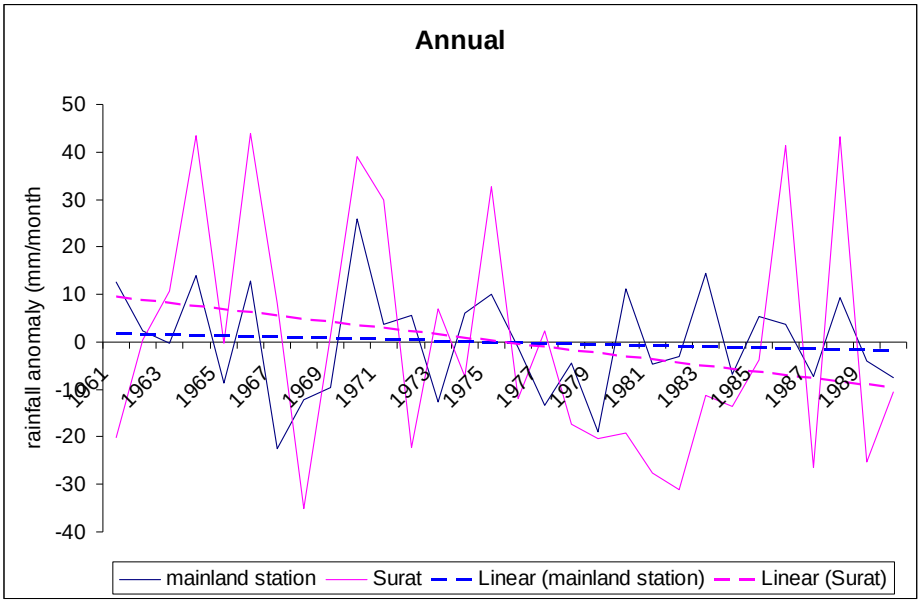

(a)

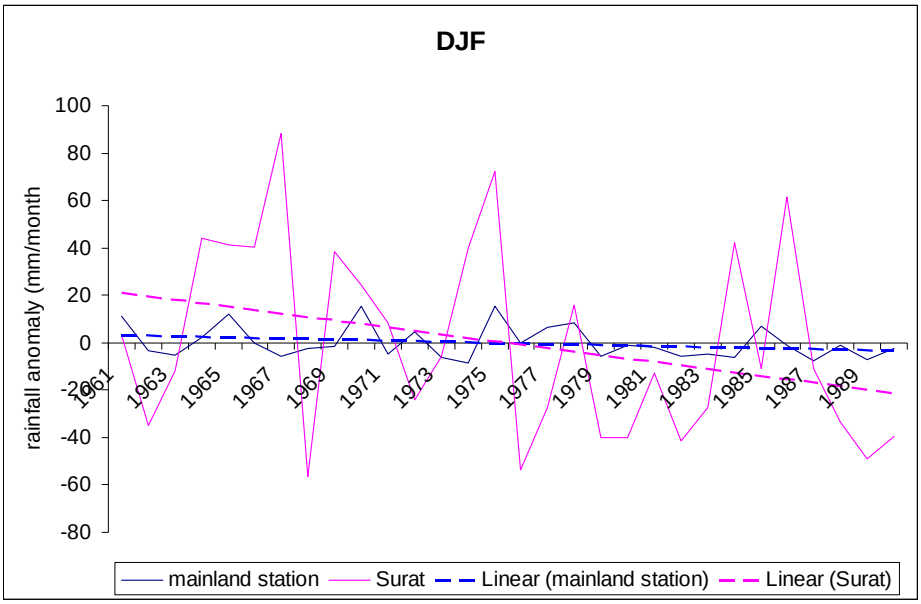
DJF
rainfall anomaly (mm/month
100
80
60
40
20
0
-20
-40
-60
-80
1961
1963
1965
1967
1969
1971
1973
1975
1977
1979
1981
1983
1985
1987
1989
mainland station
Surat
Linear (mainland station)
Linear (Surat)

(b)

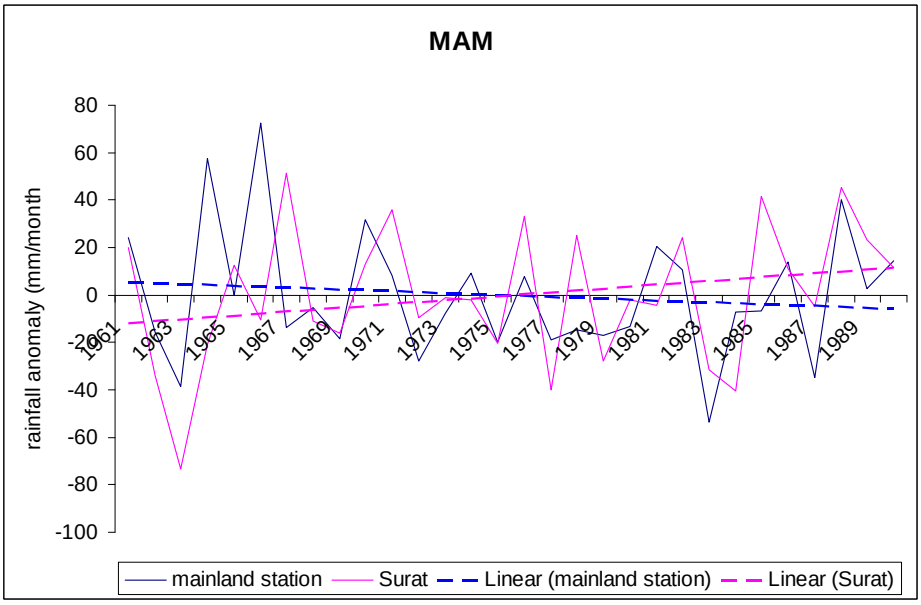
MAM
rainfall anomaly (mm/month
80
60
40
20
0
-20
-40
-60
-80
-100
1961
1963
1965
1967
1969
1971
1973
1975
1977
1979
1981
1983
1985
1987
1989
mainland station
Surat
Linear (mainland station)
Linear (Surat)

(c)

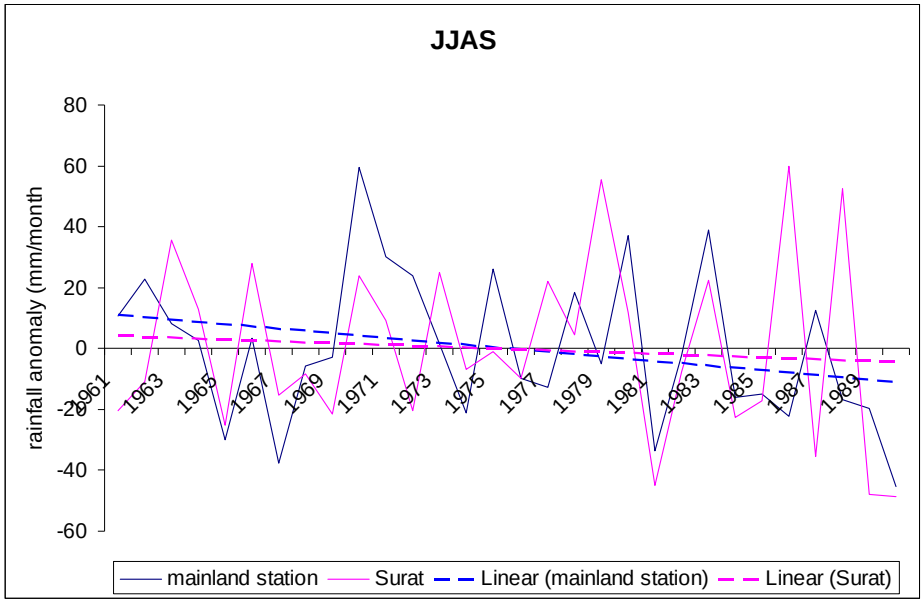

(d)

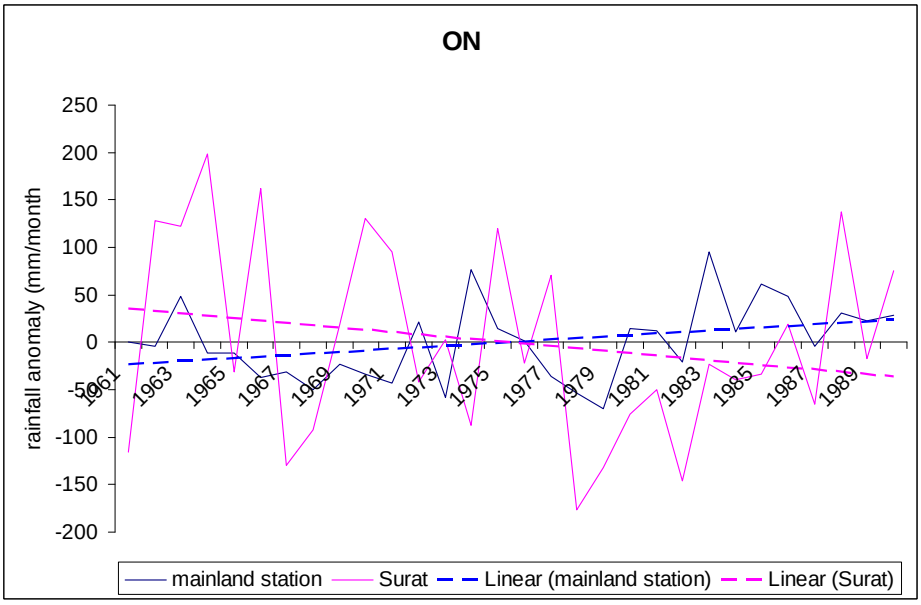

(e)

Figure 4.5: Precipitation time series for mainland (average of CM, Phitlok, Ubon, BKK) and Surat site expressed as anomalies from 1960-1990 (a) annual (b) DJF (c) MAM (d) JJAS (e) ON

Table 4.1 Variance and Linear Trend of anomaly precipitation in 1961-1990 over mainland (average of CM, Phitlok, Ubon and BKK) and Surat site.

Station	Variance(R^2)	Slope (mm/month-year)
Mainland		
Annual	0.0111	-0.1331
DJF	0.0780	-0.2205
MAM	0.0153	-0.3833
JJAS	0.0734	-0.7613
ON	0.1230	1.6297
Surat		
Annual	0.0546	-0.6622
DJF	0.0988	-1.4498
MAM	0.0601	0.8113
JJAS	0.0072	-0.2850
ON	0.0444	-2.4454

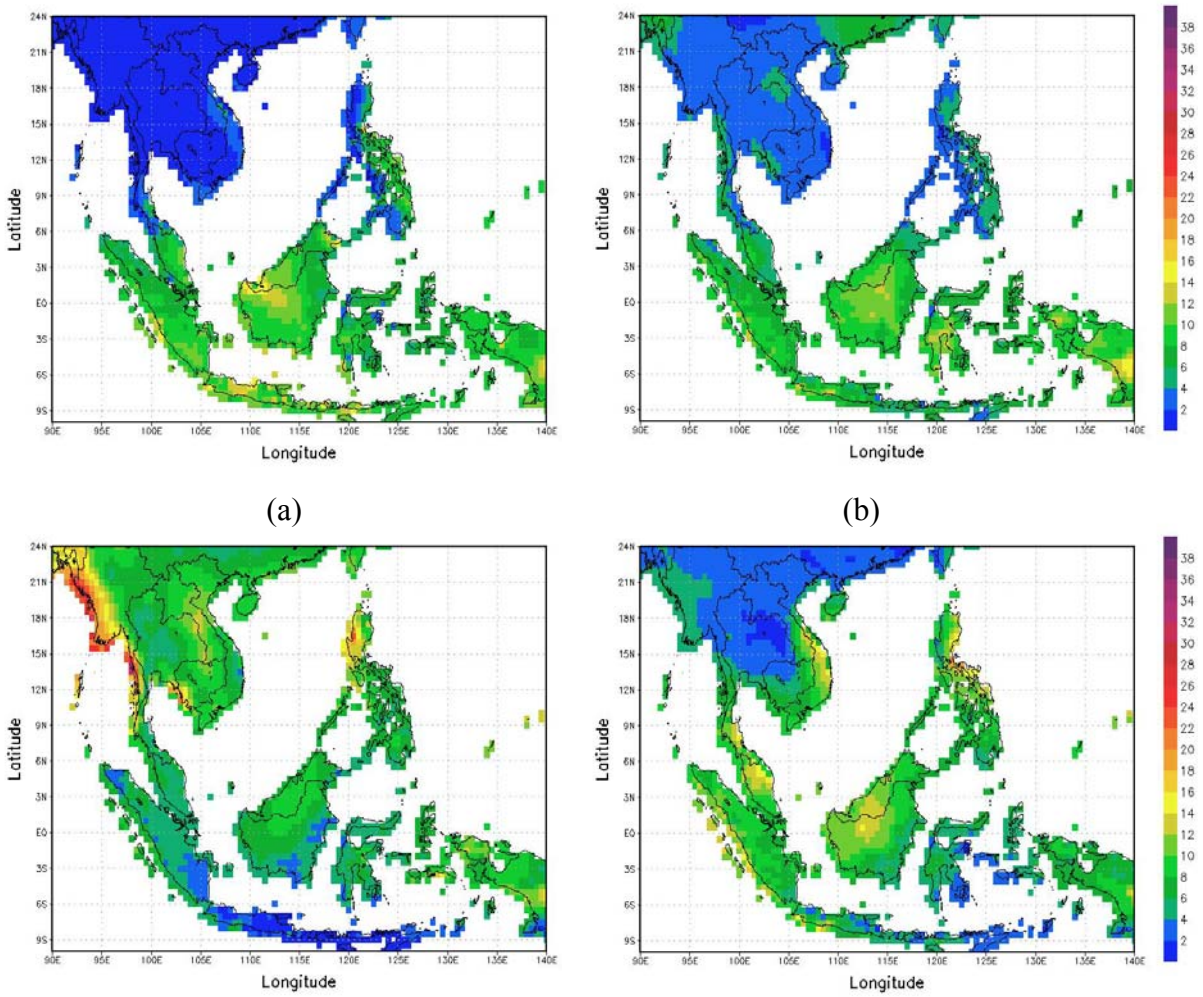

Figure 4.6: Spatial distribution of average precipitation (mm/day) in the period of 1961-1990 from CRUTS2.1 during (a) DJF (b) MAM (c) JJAS (d) ON

The gridded CRUTS2.1 data set is useful for visualising spatial patterns and in extending the station analysis, even though it is based upon the surface station network, and seasonal patterns are shown in Figure 4.6. The precipitation over the mainland of SEA is relatively low during the winter monsoon because of the influence of the Siberian High which contributes to mild and dry weather conditions (as shown in the PRECIS simulation in Chapter 5). During ON and DJF the equatorial region of SEA experiences more precipitation when compared to the summer monsoon, in particular over the maritime continent; the centre of deep convection is located over Indonesia (Webster and Yang, 1992).

The pre-summer monsoon, MAM, sees a notable decrease of precipitation over the maritime region of SEA while over Indochina, the South China Sea precipitation starts to appear before the full trigger of the summer monsoon around mid May. During the pre-winter monsoon, precipitation activity starts to increase over the marine continent and conversely for the mainland of SEA. Major cloud movement switches from a northeastward direction in the Indian Ocean to a northwestward direction over the western North Pacific. The air flow from the Indian Ocean and northern Australia arrives in SEA however during JJAS the Indochina peninsula is predominantly influenced by the southwesterly wind flow which comes from the South Asian monsoon region (Ding, 1994) and the other parts of SEA are much more influenced by northern Australia (Kripalani, 1998).

Table 4.2: Seasonal total precipitation over Thailand for the 1961-1990 based on CRUTS2.1.

Precipitation(mm)	DJF	MAM	JJAS	ON	Annual
North	22	288	785	165	1261
Northeast	24	321	1061	124	1532
Centre	24	281	742	179	1225
South	339	447	961	628	2375

The mean 1961-1990 precipitation over Thailand (Table 4.2) shows the maxima in the annual total is in the south, followed by the north-east, central Thailand and, finally, the northern region. There is a remarkable contrast between rainy season and winter precipitation totals in the mainland of Thailand with some sections featuring up to 1000mm during the rainy season and only 25 mm during DJF. The peninsula precipitation is significantly enhanced during both JJAS and ON which is in agreement with the station data where November is the wettest month in this region [recall that the gridded dataset is based on station data].

The precipitation during JJAS in peninsular Thailand is about 40% of the annual total while the contribution of this season over the Thai mainland is about 64% of the annual. The precipitation fractions during ON and DJF in peninsular Thailand are

about 26% and 14% respectively of the annual total while the equivalent amounts over mainland Thailand are about 12% and 2% of the annual.

4.2.2 Wet days

To be consistent, the definition of a wet day in this study is a day with at least 1 mm of rain as defined in CRUTS2.1 over the tropical region. As mentioned in section 4.2.1, 40-60% of total precipitation occurs during JJAS, according to location, so in this section, the frequency of wet days is focused upon in this summer season. Figure 4.7 shows that the frequency of wet days during JJAS lies mostly in the range 50-70 days. The annual total precipitation decreased between 1961 and 1990 as shown earlier in 4.2.1 and this is associated with decreases in the number of monsoon season wet days at a rate of 10 days per 30 years (Figure 4.8). The corresponding regression lines over the mainland and Surat sites are also shown in Figure 4.8; decreases in wet day frequency are shown over both areas with the respective slopes of the time series being about 2.8 days/10 years and 3 days/10 years. The r-squared value is 0.25 and 0.01 over the mainland and Surat sites, respectively. It is clear that the number of wet days in 1987 and 1990 is anomalously low during the wet season at Surat (Figures 4.5(d) and 4.8). In 1987 (1990), there are 34 (33) out of a possible 122 days with precipitation over 1 mm corresponding to precipitation anomalies of -35 (-48) mm/month giving an estimated decrease of about 140 (192) mm during JJAS. While at Surat in the wettest year, 1973, the number of wet days is 70 with a positive precipitation anomaly of 25 mm/month, or about 100 mm over the four month summer season. Menton et al. (2001) show that the number of days with greater than 2mm of rain has decreased significantly throughout most of Southeast Asia over 1961-1998.

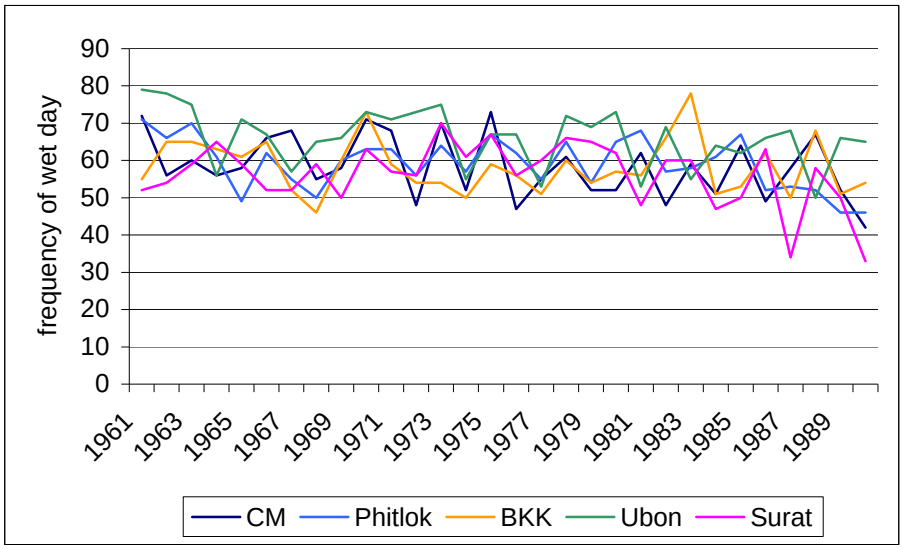

Figure 4.7: Time series of the number of wet days for the five stations for the active southwest monsoon season (JJAS)

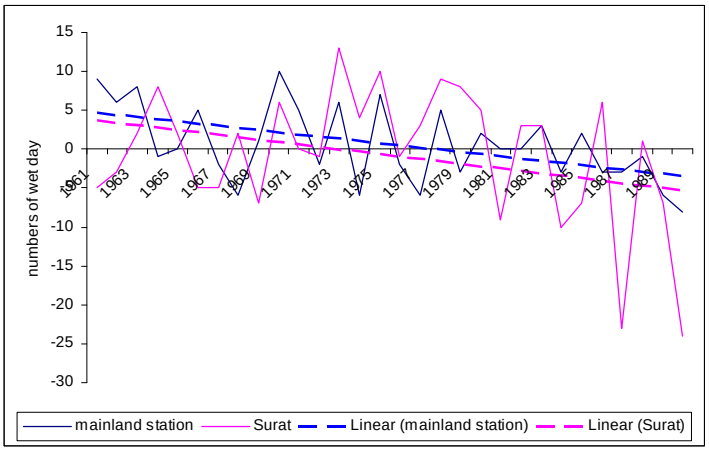

Figure 4.8: Time series of the number of wet days (≥1mm) for mainland (CM, Phitlok, Ubon, BKK) and Surat site expressed as anomalies from the 1961-90 average for the active southwest monsoon season (JJAS)

The relationship between the number of wet days and precipitation amount for all five sites is a simple linear function as shown in Figure 4.9 which implies that if the model correctly simulates the number of wet days, then the possibility of accurately simulating total precipitation is increased; the r-squared value is 0.45 in both data sets which means that the linear trend explains 45% of the variability.

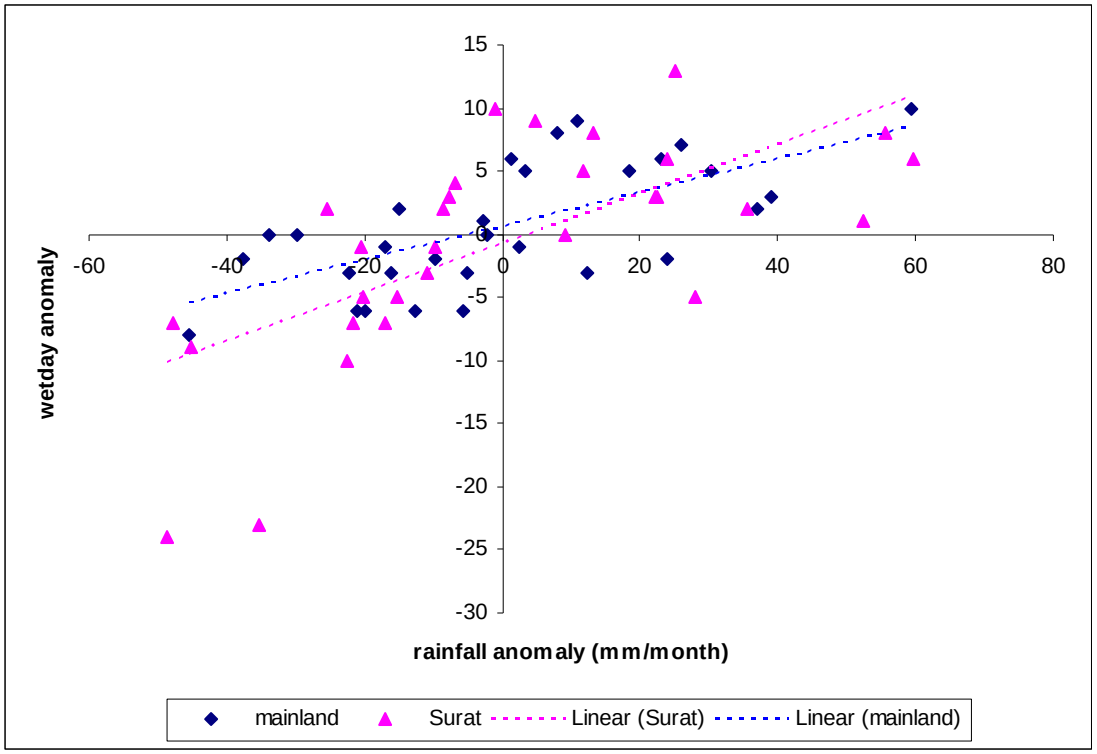

Figure 4.9 Linear relationships between wet day anomalies and precipitation total anomalies for JJAS (1961-1990)

4.2.3 Tropical Depressions

Tropical cyclones in this study region are called typhoons. Tropical cyclones moving into Thailand mostly weaken into depressions. The statistics for 1961-1990 show a single record of a tropical typhoon over Thailand, Typhoon Gay, during 1-10 November, 1989, six tropical storms and 114 tropical depressions (Figure 4.10).

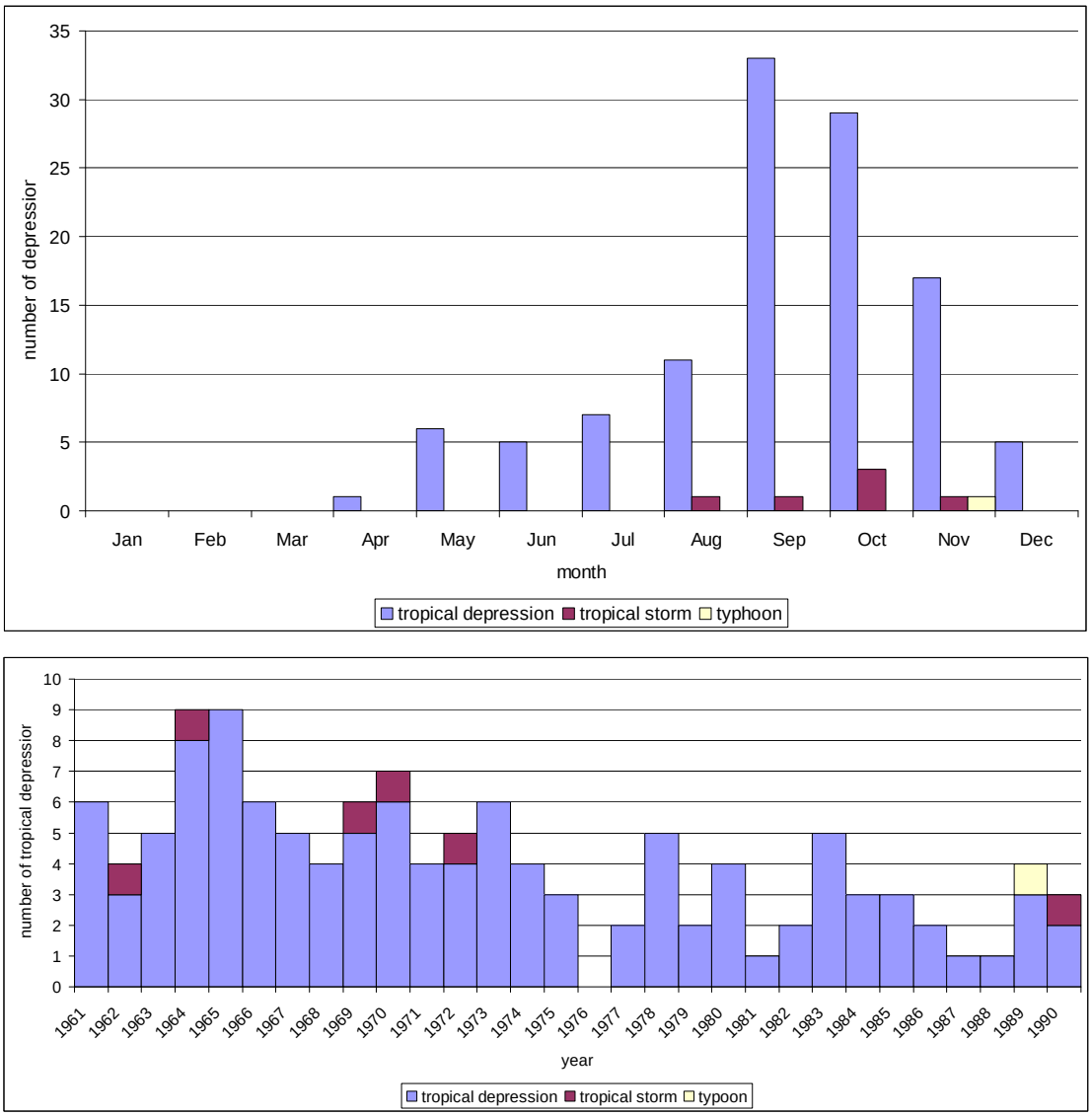

Figure 4.10: Record of all cyclonic disturbances from tropical depressions upwards moving across Thailand (1961-1990) based on Thai Meteorology Department records.

It can be seen in Figure 4.11 that the precipitation ranges in September at all stations in the mainland region are 65.9 to 499.3mm in years with no depressions, 148.3mm to 351.6mm in years with 1 depression moving across those stations, 194.7mm to 529.6mm in years with 2 depressions and 553.5mm in the year with 3 depressions. The precipitation ranges in November at the Surat station (noting that tropical depression tracks only move across the peninsula during this month) are 146.5 mm to 1333.6 mm in years with no depression, 73.4 mm to 507.8 mm in years with 1 depression moving across those stations and 315.9 mm to 844.5 mm in years with 2 depressions (Figure 4.12). There is a weak positive link between the number of cyclonic disturbances and monthly precipitation.

Analysing precipitation on the individual days when depressions pass the corresponding station revealed a statistically significant difference at the 95% confident level in precipitation between individual days with and without cyclonic disturbances activities (Table 4.3). Therefore, depressions statistically significantly increase precipitation, consistent with several studies. Tropical cyclones have an important effect on total precipitation over ocean basins. They have the potential to lead to extreme precipitation totals which may lead to flood risk and may also generate coastal flooding due to sea surge area Shepherd et al. (2007) indicated that over the southeastern U.S., days with tropical cyclones active are more likely to produce wet days than days without them and more intense tropical cyclones, for example category 3–5 hurricane days, contribute extreme precipitation days while tropical depression days make important contributions (8-17%) to cumulative seasonal precipitation. Rappaport (2000) showed that a hurricane can typically produce 5-12 inches of precipitation and the amounts of precipitation greatly depend on storm speed and size. Therefore, the impact of strong tropical cyclones on precipitation totals may be apparent in extreme daily events while weaker cyclones may critically affect trends in cumulative seasonal precipitation. Trends in precipitation associated with tropical cyclones may be apparent if the number of storms is changing over time; Figure 4.10 suggests fewer tropical cyclones have affected Thailand in the second half of the 1961-90 period. It is therefore desirable that RCMs should be able to simulate tropical depressions reasonably well.

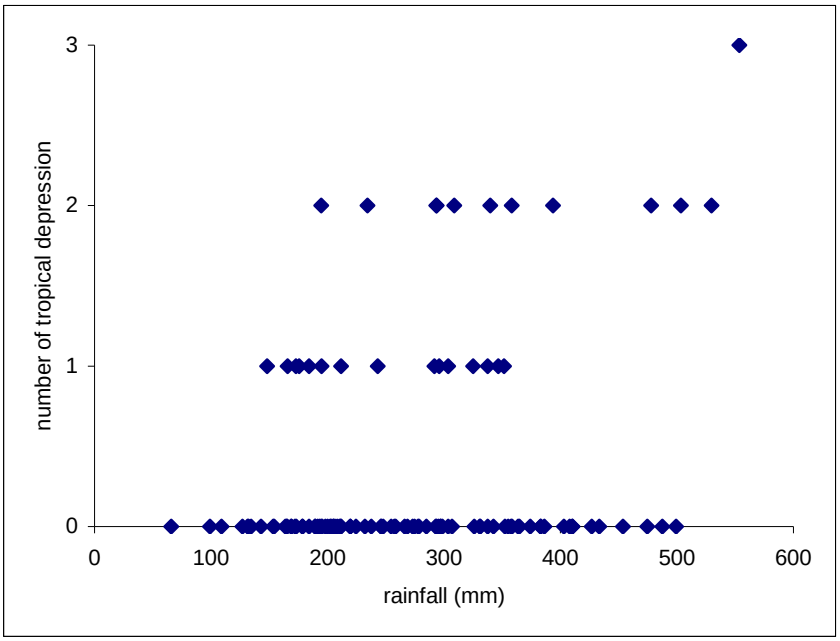

Figure 4.11: Number of cyclonic disturbances (from tropical depressions upwards) moving across Thailand (1961-1990) considered by cyclone track against total precipitation in September over all stations located on the mainland.

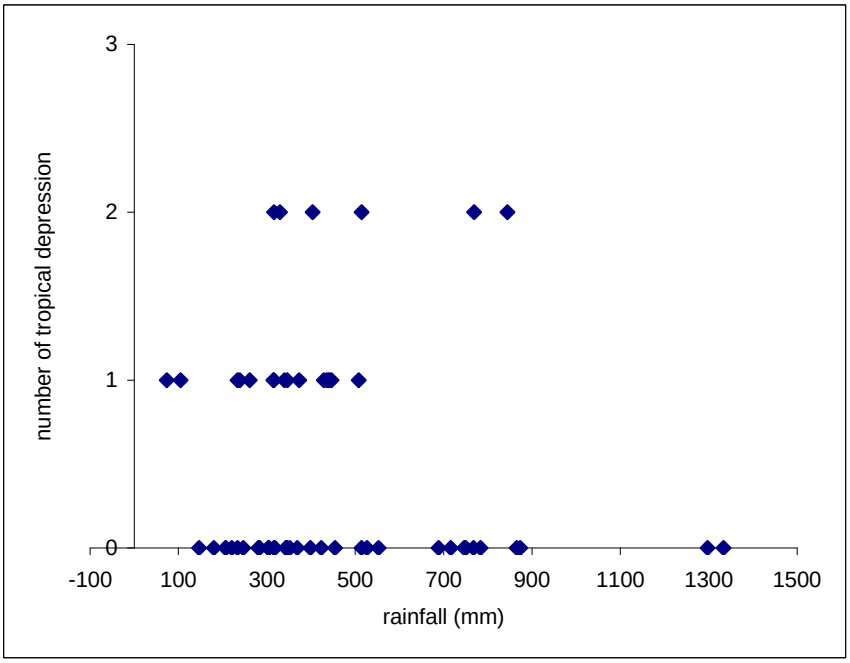

Figure 4.12: Number of cyclonic disturbances (from tropical depressions upwards) moving across Thailand (1961-1990) considered by cyclone track against total precipitation in November at Surat.

Table 4.3: Analysis of the influence of cyclonic disturbances on individual station precipitation during 1961-1990. (noted that mean precipitation with depression is determined by averaging individual station precipitation and mean precipitation with no depression is determined by averaging daily precipitation in the month with depression excluding the day with depression.)

Station	Mean Precipitation (mm)		Standard daviation		p-value
	With depression	With no depression	With depression	With no depression	
Chiang Mai	47.1	6.2	26.4	11.5	2.14×10^{-6}
Phitsanulok	42.6	9.4	16.9	22.6	0.003
Bangkok	64.2	9.9	31.4	17.6	0.004
Ubon	62.7	4.7	47.0	10.4	8.04×10^{-4}
Surat Thani	78.4	7.8	40.7	14.4	0.0002

4.2.4 El Niño and La Niña

An El Niño event is associated with droughts while a La Niña event is more likely to be associated with excessive monsoon rain over Indochina (section 1.1). This section further investigates whether ENSO is specifically associated with the climate of Thailand. The El Niño and La Niña data were obtained from http://www.cpc.ncep.noaa.gov/. The criteria used to classify the year as El Niño and La Niña is sea surface temperature anomaly over the equatorial Pacific Ocean, warm (cold) SSTs relating to El Niño (La Niña). During the occurrence of an El Niño event, the easterly trade winds relax over central and western Pacific which leads to the thermocline descending in the eastern Pacific and ascending in the western Pacific.

During the 1961-90 period, El Niño/La Niña events occurred as follows:
El Niño years (1961-1990): 1963, 1965, 1969, 1972, 1976, 1982, 1986
La Niña years (1961-1990): 1964, 1970, 1973, 1975, 1984, 1988

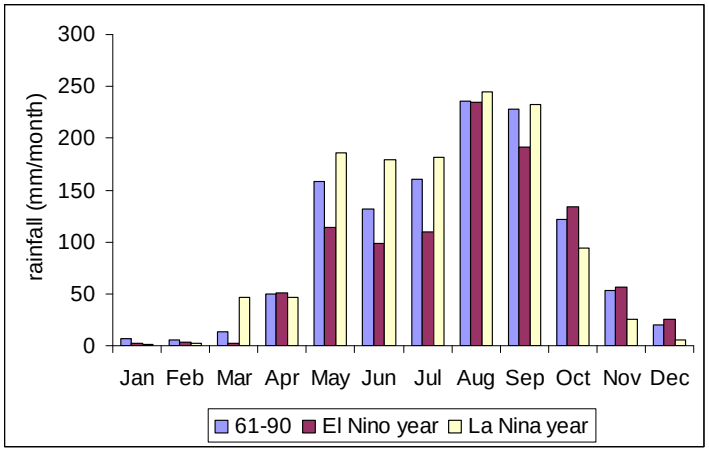
300
250
200
150
100
50
0
rainfall (mm/month)
Jan Feb Mar Apr May Jun Jul Aug Sep Oct Nov Dec
61-90 El Nino year La Nina year

(a)

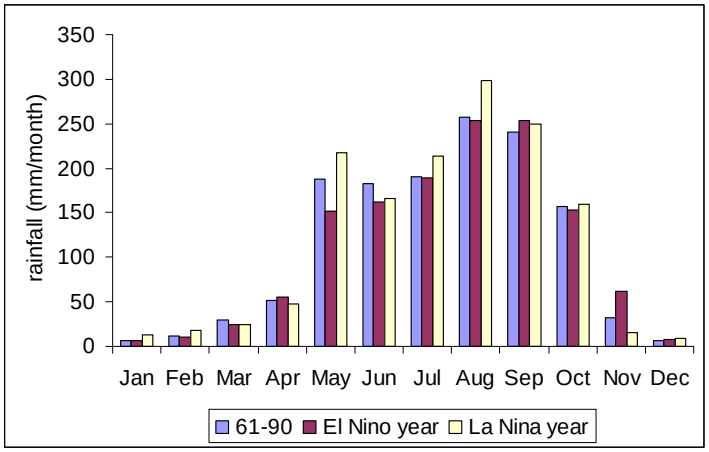
350
300
250
200
150
100
50
0
rainfall (mm/month)
Jan Feb Mar Apr May Jun Jul Aug Sep Oct Nov Dec
61-90 El Nino year La Nina year

(b)

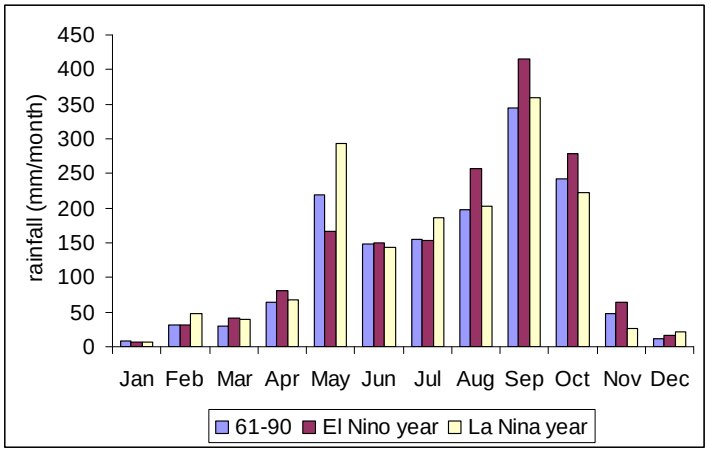
450
400
350
300
250
200
150
100
50
0
rainfall (mm/month)
Jan Feb Mar Apr May Jun Jul Aug Sep Oct Nov Dec
61-90 El Nino year La Nina year

(c)

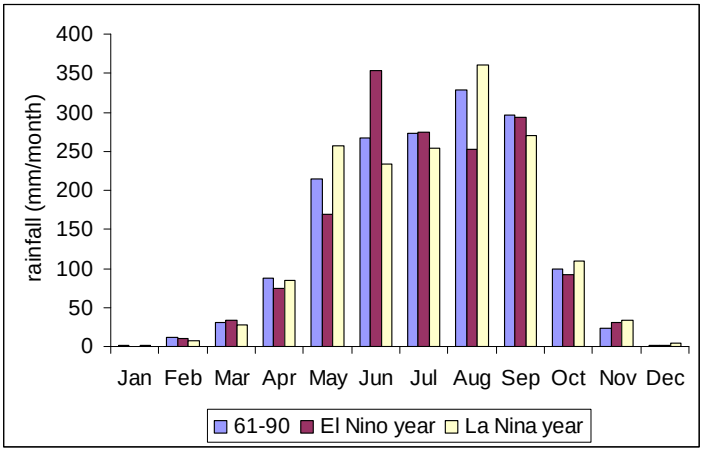

(d)

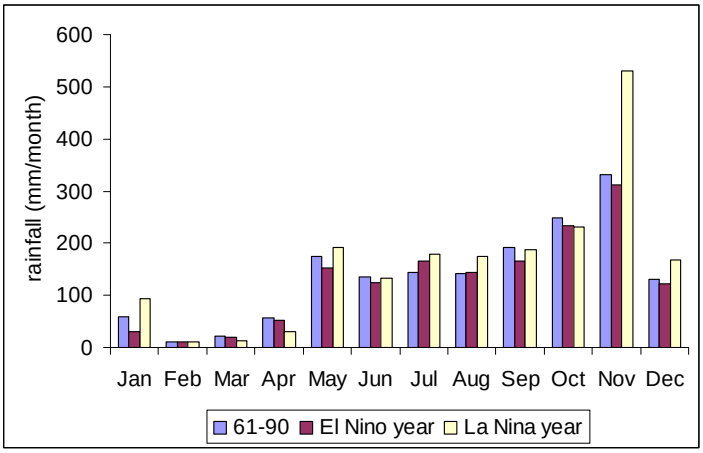

(e)

Figure 4.13: Average monthly precipitation totals during 1961-1990 in El Niño and La Niña years at (a) CM (b) Phitlok (c) BKK (d) Ubon (e) Surat

Table 4.4: Average precipitation anomaly (%) during the JJAS season in El Niño years and La Niña years, relative to 1961-90 averages.

Site	Precipiation anomaly during JJAS (%)			
	JJAS		ON	
	El Niño	La Niña	El Niño	La Niña
CM	-23	+11	+9	-13
Phitlok	-1	+13	+13	-8
BKK	+22	+10	+10	-14
Ubon	+3	-12	+12	+24
Surat	-3	+11	+3	+22

Figure 4.13 and Table 4.4 show that during El Niño years, a reduction in precipitation is found at the CM site (in JJAS), a intensification at the BKK site and no sign of precipitation change at the Phitlok, Ubon and Surat sites. Meanwhile during La Niña years, modest precipitation increases were found at the CM, Phitlok, BKK and Surat sites and a small precipitation decrease at the Ubon site. Due to the relatively small number of events and the inter-station variability, it is not possible to draw strong conclusions from these results. Table 4.5 summarizes the results of the p value at the 95% confidence level from two tailed t-test of the differences in precipitation in DJF, MAM, JJAS and ON for the 5 stations between El Niño and La Niña, El Niño and neutral, and La Niña and neutral events as defined on page 103. For DJF and MAM seasons, no statistically significant differences in rainfall are found between any pair of these ENSO events. This indicates that the rainfall during the DJF and MAM seasons is not influenced by the ENSO phenomenon. Differences in JJAS precipitation between the El Niño and La Niña events, as well as, between El Niño and neutral years can be found at CM, located at northern Thailand (Table 4.5). Moreover, Differences in ON precipitation between the El Niño and La Niña events, as well as, between La Niña and neutral years can be found at Surat, located at southern Thailand. Therefore, El Niño (La Niña) events can be lead to statistical significant precipitation decrease (increase) during JJAS (ON) at CM (Surat) site (table 4.4 and 4.5).

Table 4.5: Analysis of the influence of ENSO on precipitation in season at selected stations in Thailand and *t* -tests of the difference in precipitation between El Niño, La Niña and normal years.

Station	p value		
	El Niño-La Niña	El Niño-Normal	La Niña -Normal
DJF			
CM	0.98	0.96	0.95
Phitlok	0.39	0.40	0.20
BKK	0.78	0.66	0.57
Ubon	0.97	0.73	0.61
Surat	0.35	0.60	0.10
MAM			
CM	0.16	0.07	0.54
Phitlok	0.21	0.26	0.77
BKK	0.66	0.32	0.12

Table 4.5: continued

Station	p value		
	El Niño-La Niña	El Niño-Normal	La Niña -Normal
JJAS			
CM	0.04	0.01	0.46
Phitlok	0.42	0.78	0.36
BKK	0.93	0.26	0.35
Ubon	0.72	0.91	0.60
Surat	0.42	0.61	0.12
ON			
CM	0.43	0.65	0.61
Phitlok	0.40	0.57	0.73
BKK	0.21	0.57	0.49
Ubon	0.78	0.66	0.57
Surat	0.04	0.68	0.02

Seasonal precipitation in the Philippines is known to be modulated by the El Niño Southern Oscillation (ENSO) phenomenon, with ENSO warm (cold) events frequently contributing to drought (excessive precipitation) in many areas of the Philippines. Based on bridging the gap between seasonal climate forecasts and decision makers in agriculture, a project in the Philippines preliminarily found that tropical cyclone frequency was about 6.5 in neutral years, 6.7 in La Niña years and 4.4 during El Niño years during October-December 1948-2005. It could be concluded that El Niño events have a negative effect on tropical cyclone frequency in the Philippines. Analysis of the average number of tropical depressions in Thailand from July to November showed that there are about 3.11 in neutral years, 3.57 in El Niño years and 4.8 in La Niña years. Tropical depression activity during neutral years and El Niño years is approximately equal for the JASON period, however it can be seen that during La Niña years, the number of depressions in Thailand is generally above average.

A case study of El Niño in 1982

Based on El Niño records during the baseline 1961-1990 period from the El Niño 3.4 region (5^{o}N-5^{o}S, 120^{o}-170^{o}W), a major event occurred in 1982. The associated SST anomaly over the Pacific Ocean began increasing above 0.5^{o}C from May 1982 to July

1983 as shown in Table 4.6 (This highlights the important point that El Niños can run across years).

Table 4.6: SST anomalies (°C) over the Pacific Ocean El Niño 3.4 region bounded by 120°W-170°W and 5°S- 5°N during 1982-1983 (source: http://www.cpc.ncep.noaa.gov/).

Year	DJF	JFM	FMA	MAM	AMJ	MJJ	JJA	JAS	ASO	SON	OND	NDJ
1982	0.0	0.1	0.1	0.3	**0.6**	**0.7**	**0.7**	**1.0**	**1.5**	**1.9**	**2.2**	**2.3**
1983	**2.3**	**2.0**	**1.5**	**1.2**	**1.0**	**0.6**	0.2	-0.2	-0.6	-0.8	-0.9	-0.7

La Niña is associated with cooler than normal water temperatures in the Equatorial Pacific Ocean, unlike El Niño which is associated with warmer than normal water.

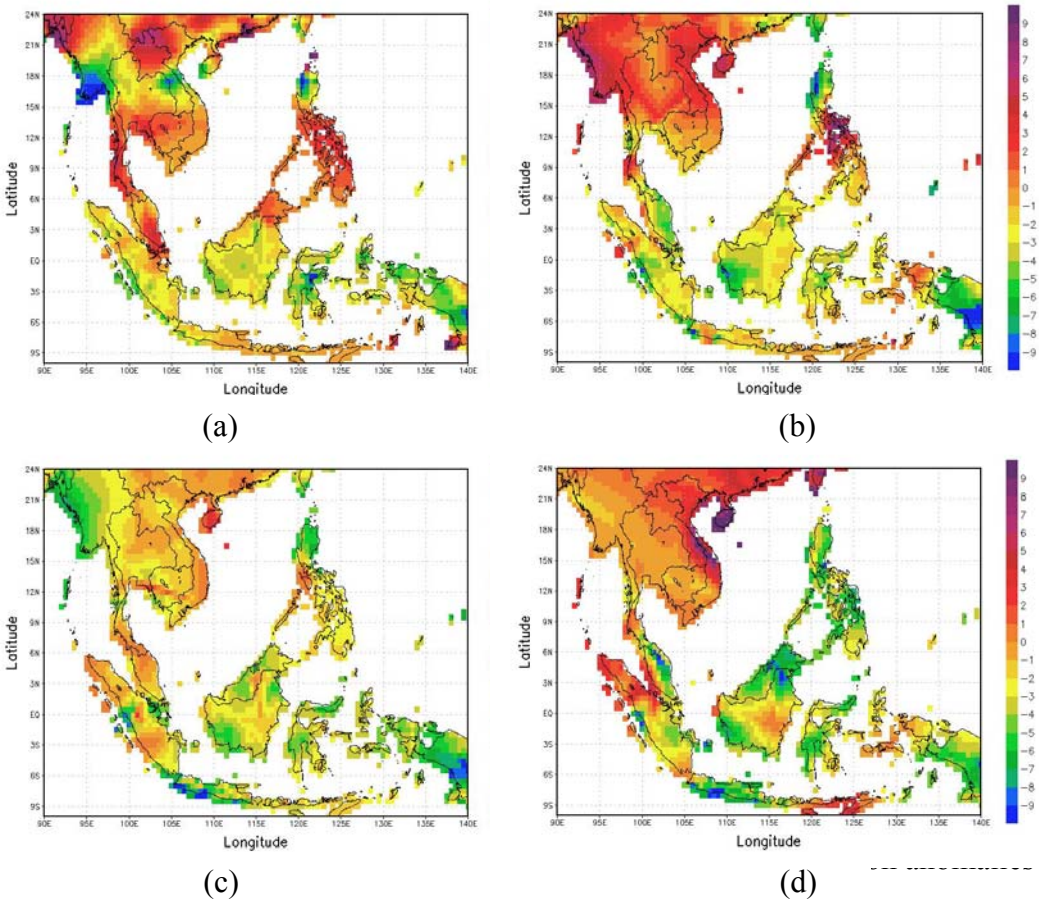

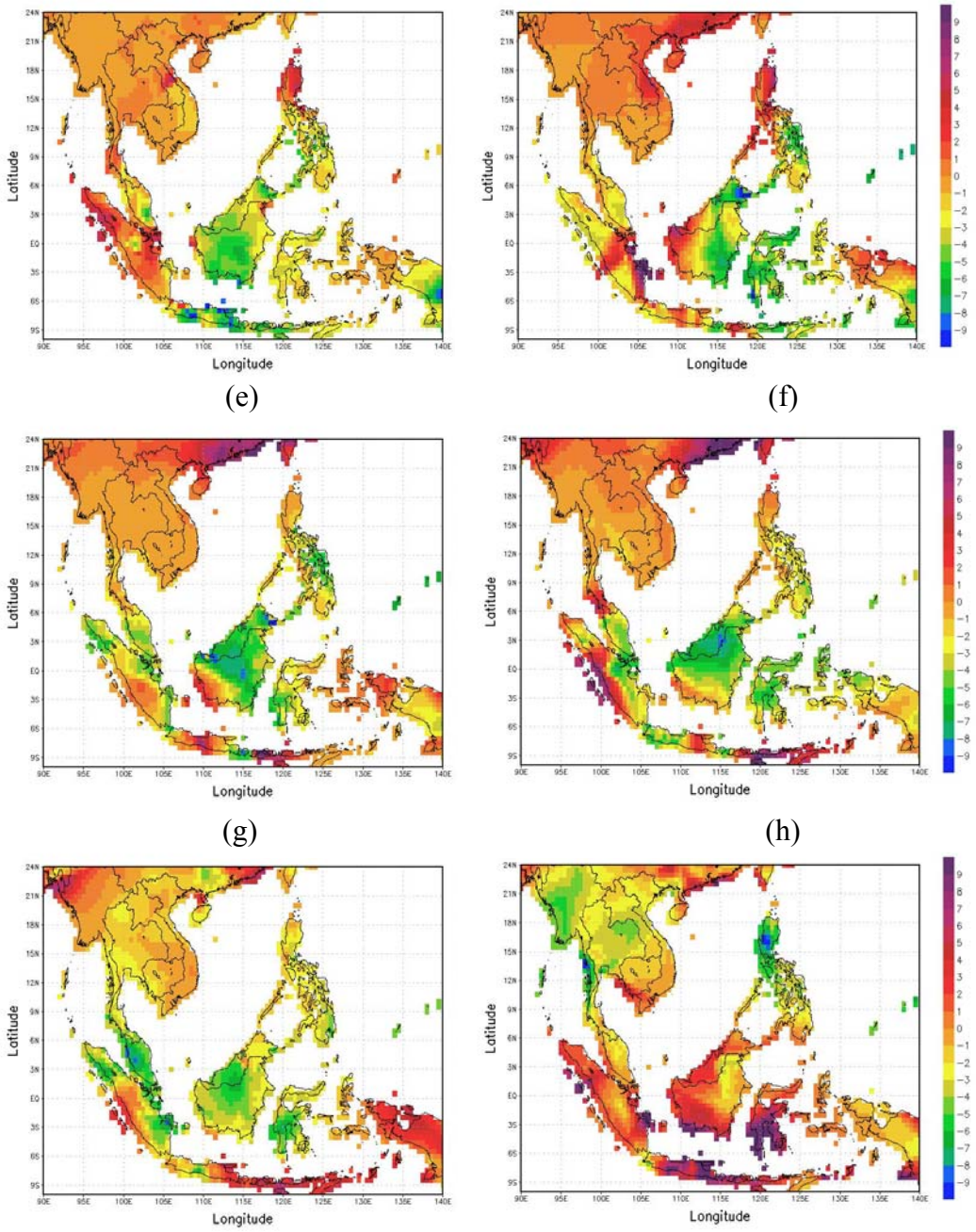

Figure 4.14: Precipitation anomalies (mm/day) during active El Niño in 1982-83 relative to a 1961-1990 baseline for (a) August (b) September (c) October (d) November (e) December (f) January (g) February (h) March (i) April (j) May

Due to the late arrival in August of the southwest monsoon in 1982 a negative precipitation anomaly occurred in the region north of 15°N in Thailand and a significant negative precipitation anomaly along the Bay of Bengal and over

Indonesia (Figure 4.14a) while the rest of Thailand recorded a positive precipitation anomaly and in September (Fig 4.14b) a positive precipitation anomaly occurred over the whole land region north of 13°N and over some parts of the western coast of Thailand. During the peak in precipitation normally experienced over peninsular Thailand in October and November, there is no significant precipitation anomaly. In summary, there is no significant overall precipitation anomaly in Thailand during this El Niño event.

A case study of La Niña in 1988

Based on La Niña records during the baseline period of 1961-1990, one of the recognised El Niño 3.4 events is in 1988-89, with the sea surface temperature over the Pacific Ocean increasing between May 1988 and May 1989 as shown in Table 4.7.

Table 4.7: SST anomalies over the Pacific Ocean El Niño 3.4 region, 1988-89.

Year	DJF	JFM	FMA	MAM	AMJ	MJJ	JJA	JAS	ASO	SON	OND	NDJ
1988	**0.7**	**0.5**	0.1	-0.2	**-0.7**	**-1.2**	**-1.3**	**-1.2**	**-1.3**	**-1.6**	**-1.9**	**-1.9**
1989	**-1.7**	**-1.5**	**-1.1**	**-0.8**	**-0.6**	-0.4	-0.3	-0.3	-0.3	-0.3	-0.2	-0.1

La Niña is associated with cooler than normal water temperatures in the Equatorial Pacific Ocean, unlike El Niño which is associated with warmer than normal water.

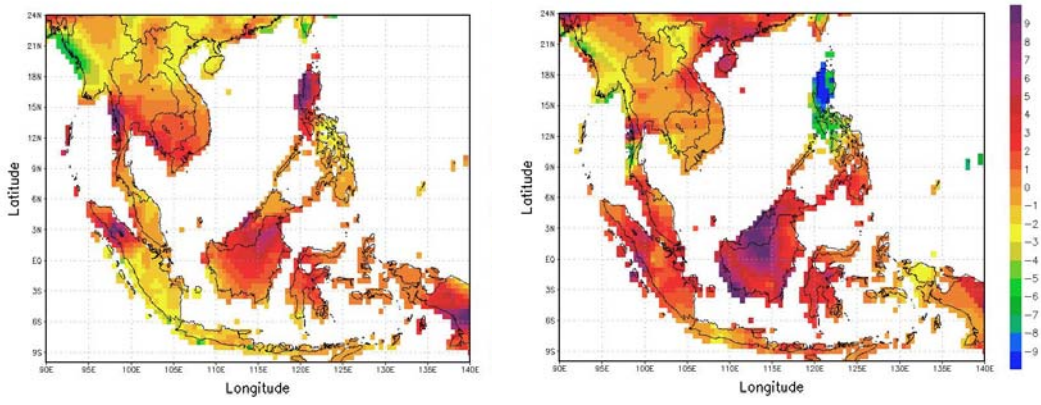
Latitude
Longitude

(a) (b)

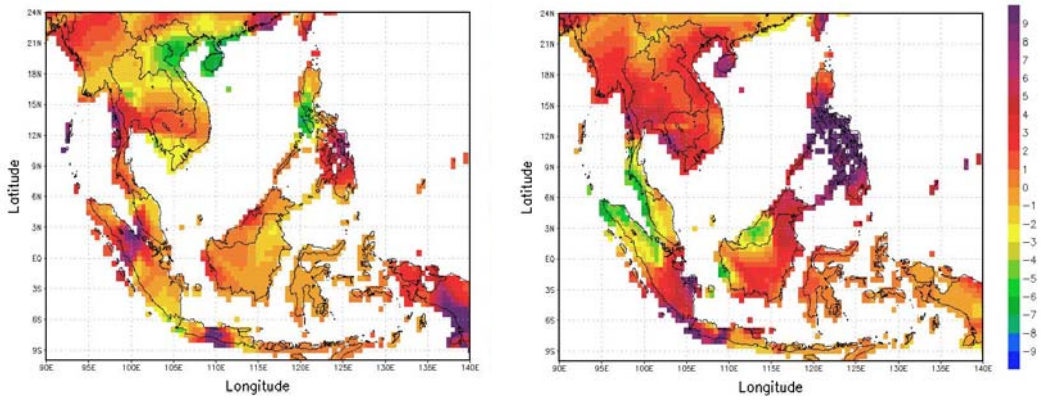
Latitude
Longitude

(c) (d)

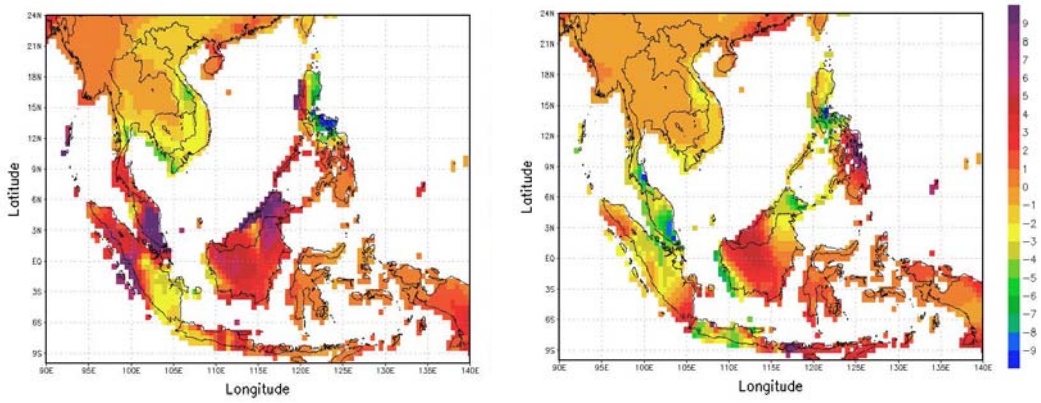
Latitude
Longitude

(e) (f)

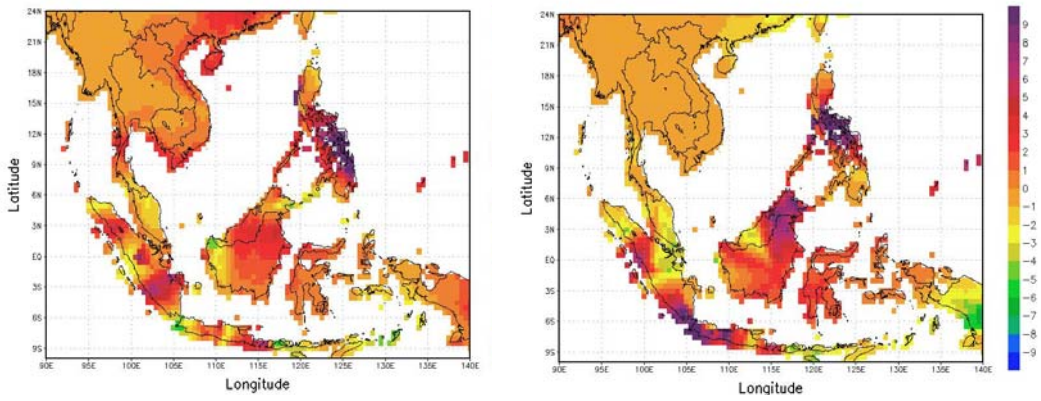

(g) (h)

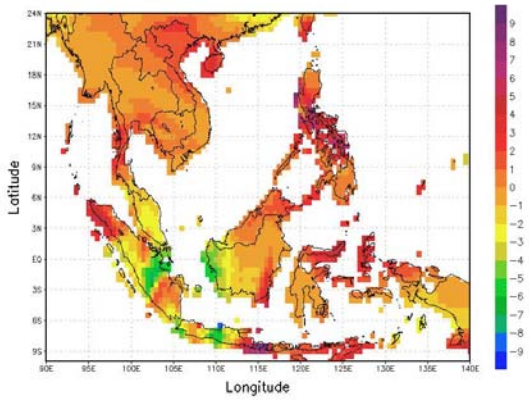

(i)

Figure 4.15: Spatial precipitation anomaly (mm/day) during the active La Niña in 1988-89 based on a 1961-1990 baseline for (a) July (b) August (c) September (d) October (e) November (f) December (g) January (h) February (i) March

In July 1988, early in the event, there are positive precipitation anomalies around western Thailand, Burma and along the Andaman Sea coast, northern Philippines, northern Sumatra and Borneo (Figure 4.15a). In August 1988, the precipitation anomaly increases over most areas of Indonesia and the southern Philippines and, interestingly, the northern Philippines sees a rapid decrease in precipitation totals (Figure 4.15b). In November 1988, there was an increase in precipitation amount over mainland Thailand and a decrease in precipitation over the peninsula. It is seen that there is no significant change in Thailand in the other months during this La Niña event (Figure 4.15e). In summary, there is no significant overall precipitation anomaly in Thailand during this El Niño/ La Niña event.

4.2.5 Temperature

Figure 4.16 shows that the seasonal cycle in mean temperature over Thailand exhibits a similar pattern at all the mainland sites; a peak in April and a trough in January. The TMD defines 3 seasons in Thailand, namely summer (mid February to mid May), the rainy season (mid May to mid October) and the cool season (mid October to mid February). In contrast, we also observe that the peninsula, represented by the Surat station, exhibits very little seasonality in terms of mean temperature, a feature typical of maritime equatorial latitudes. Around the peninsula the surrounding waters are warm all through the year and daily solar heating establishes local circulations with warm moist air from the sea converging inland and triggering deep atmospheric convection and precipitation in the afternoon.

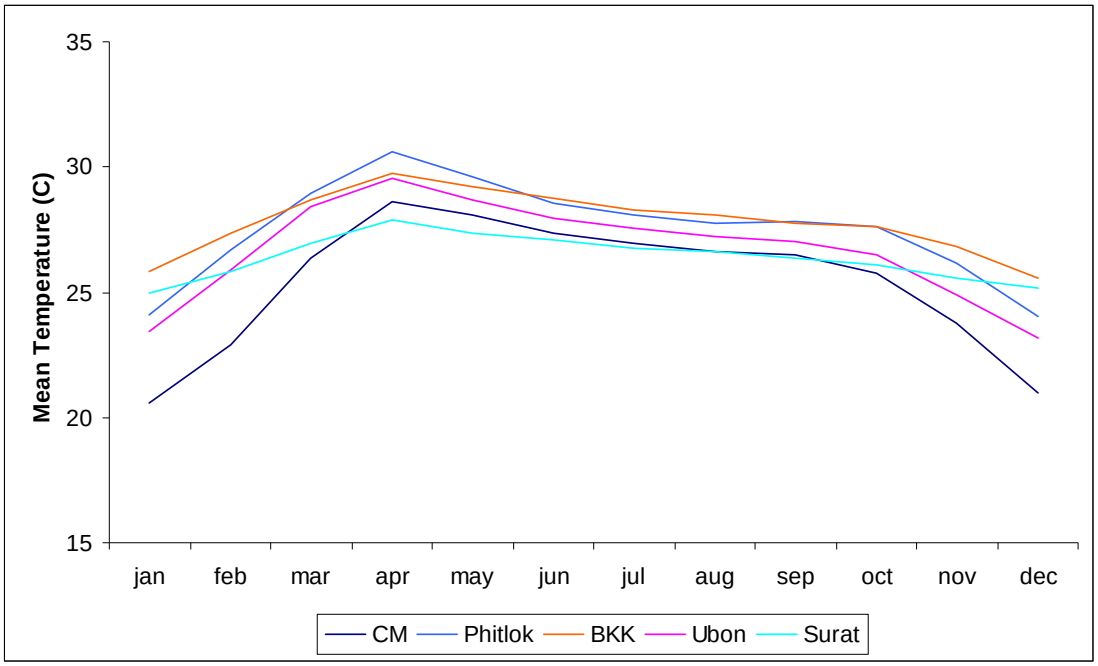

Figure 4.16: Average 30 year (1961-1990) mean temperature (deg C) seasonal cycle for five stations over Thailand

A positive trend over time of both maximum and minimum temperature is detected at both mainland sites and at Surat for MAM and DJF (Figures 4.17 and 4.18). The slope of the yearly maximum temperature time series is approximately +0.16 °C /10 years during MAM over both regions. The minimum temperature shows a warming rate of +0.36°C/10 years and +0.26°C/10 years over the mainland and Surat sites

respectively during MAM. However the warming trends are not statistically significant. The largest maximum temperature anomalies during MAM occur in 1966, 1969, 1980, 1983 and 1989 when, in the years of 1966, 1969 and 1983, an El Niño event was underway.

During MAM, 1961-1990, maximum temperature has risen approximately 0.5 °C at both mainland sites and at Surat while during DJF, the maximum temperature has risen by approximately 1°C at the Surat site (but not significantly at the mainland sites). During MAM, 1961-1990, minimum temperature has risen approximately 1°C at mainland sites and by approximately 1.6°C at Surat while during DJF, the equivalent figures are 1.1°C at the mainland sites and about 0.8°C at Surat. Through reference to the CRUTS2.1 dataset, there is considerable spatial coherence in the sign of the maximum and minimum temperature increases. Figure 4.19 shows the number of grid cells exhibiting increases in the maximum temperature anomaly. Some of the grid cells showing warming occur over northern Thailand as well as over Sumatra and the Philippines. Figure 4.20 shows a noticeable number of grid cells with positive minimum temperature trends over the whole region, in particular, over Thailand, Burma, Laos, Cambodia and Vietnam. Most of the grid cells over SEA show warming. IPCC-AR4 (2008) indicated that the updated 100 year linear trend (1906-2005) for global surface temperature is 0.74°C with a range of 0.56°C to 0.92 °C and a linear warming trend over the last 50 years of 0.13°C per decade.

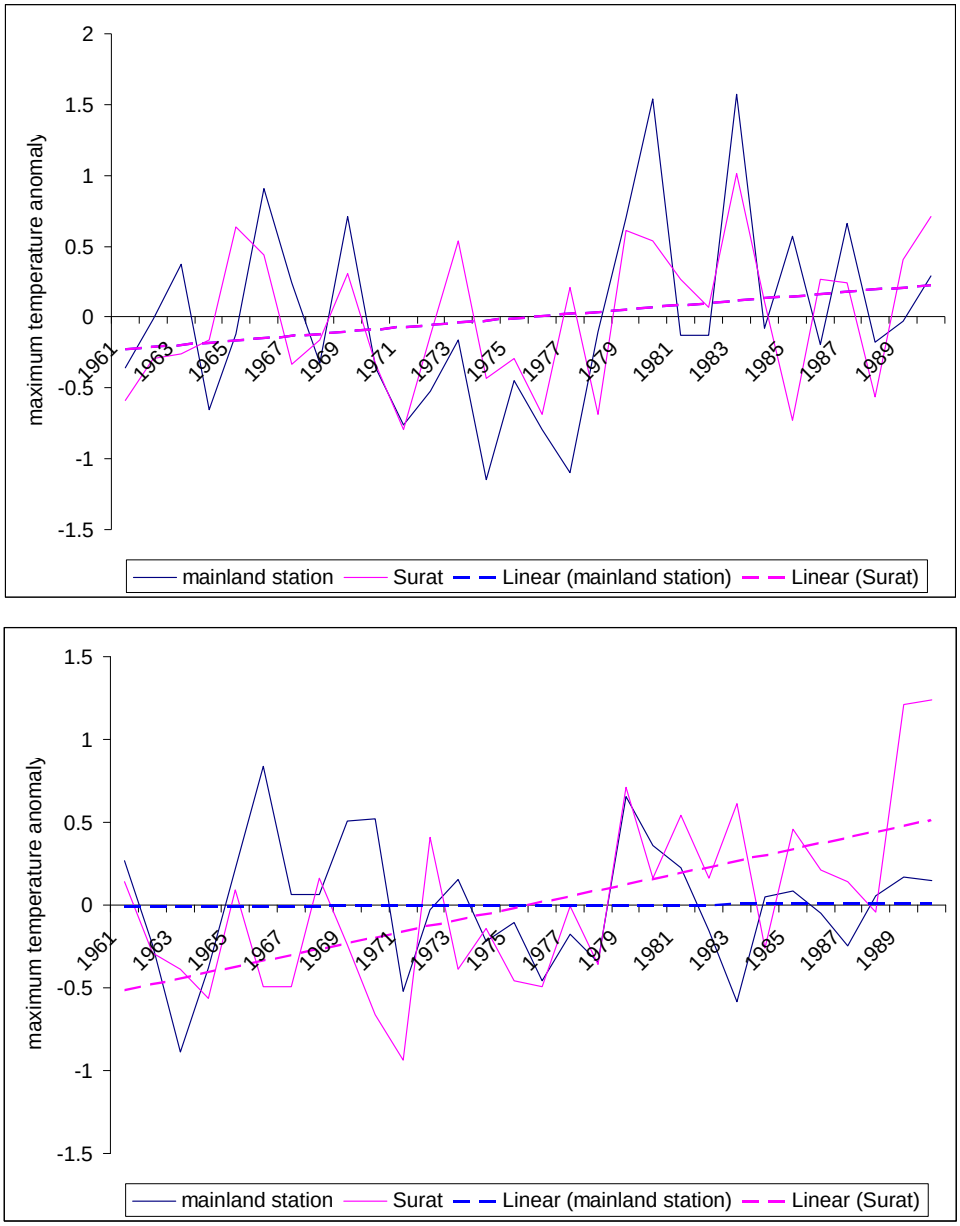

Figure 4.17: Mean maximum temperature (°C) time series for mainland (CM, Phitlok, Ubon, BKK) and Surat sites expressed as anomalies from 1960-1990 during MAM (top) and DJF (below)

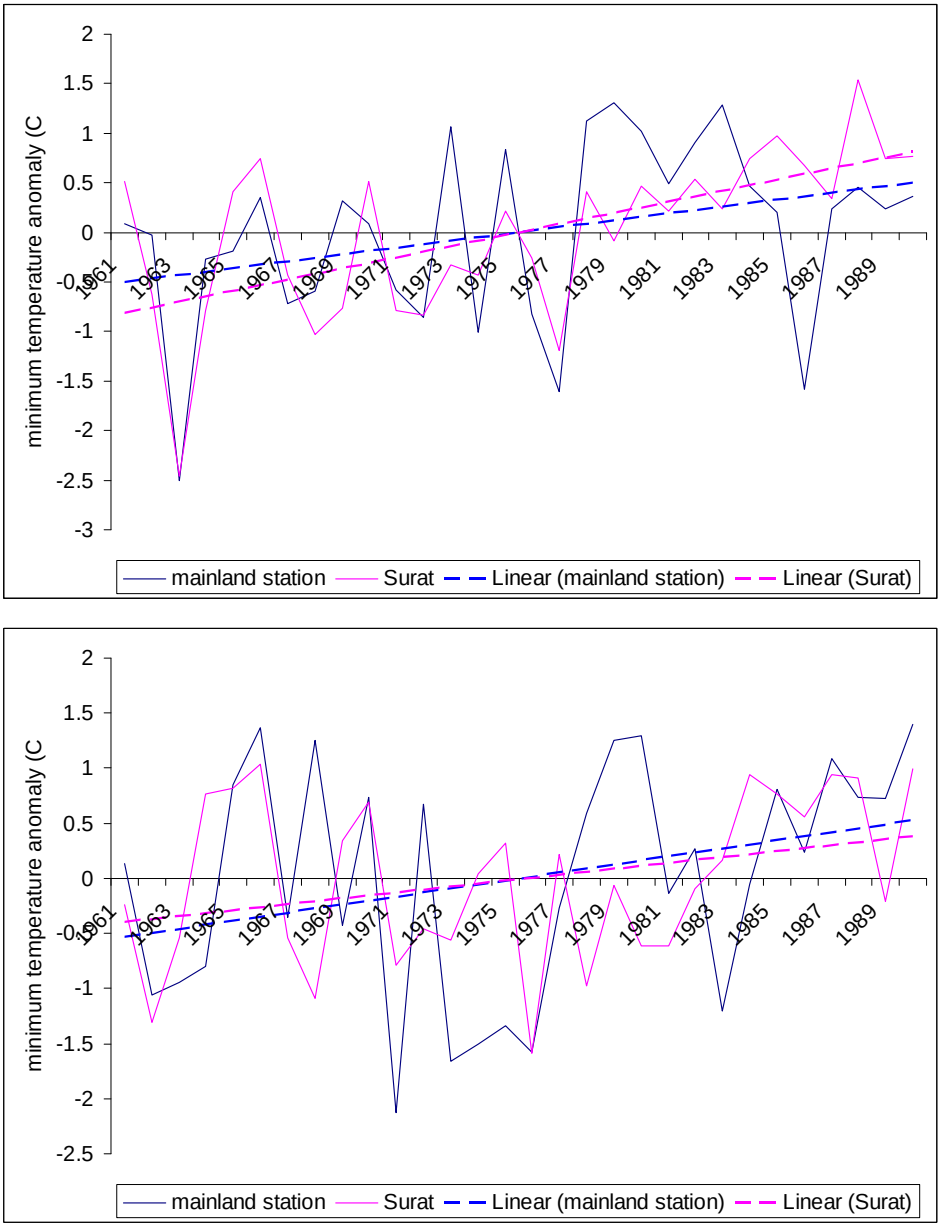

Figure 4.18: Mean minimum temperature (°C) time series for mainland (CM, Phitlok, Ubon, BKK) and Surat sites expressed as anomalies from 1960-1990 during MAM (top) and DJF (below)

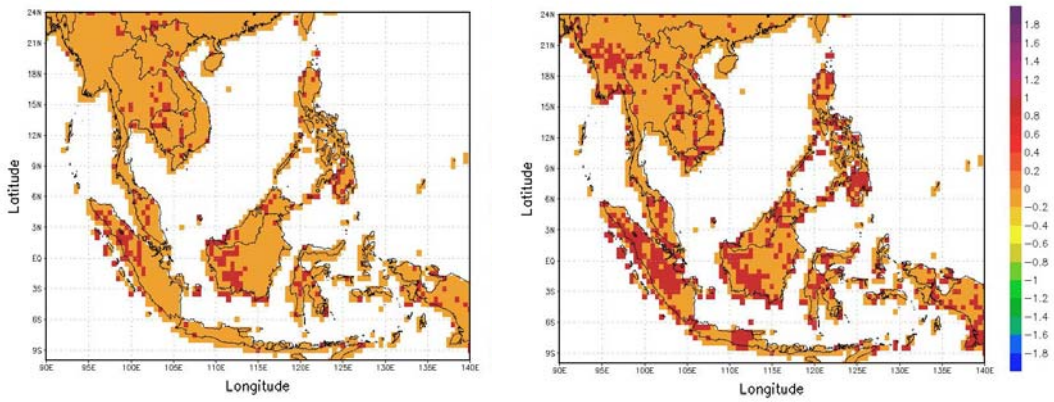

Figure 4.19: Spatial distribution of average maximum temperature (°C) from CRUTS2.1 during 1961-1970 (left) and 1981-1990 (right), expressed as an anomaly from the 1961-90 average.

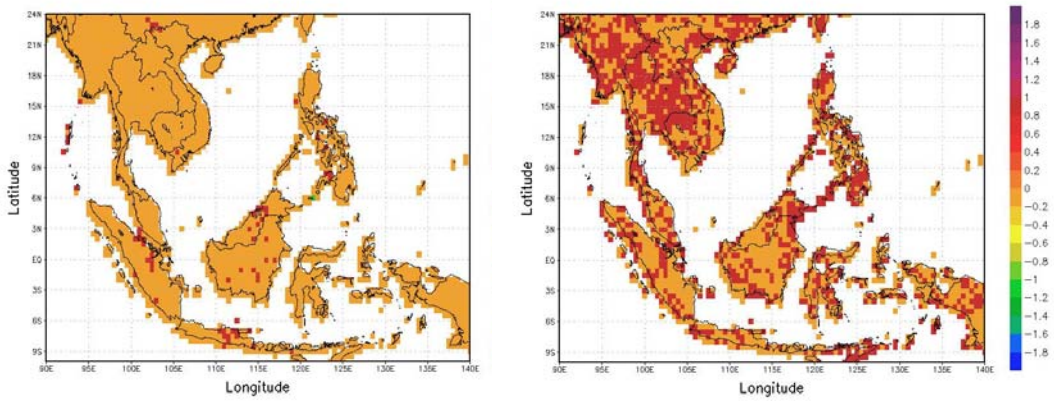

Figure 4.20: Spatial distribution of average minimum temperature (°C) from CRUTS2.1 during 1961-1970 (left) and 1981-1990 (right), expressed as an anomaly from the 1961-90 average.

Figures 4.21 and 4.22 show the SEA spatial patterns of absolute seasonal mean maximum and minimum temperature respectively, clearly revealing the TMD cool and hot seasons. Table 4.7 shows that, within a season, there is remarkably little temperature variation across Thailand.

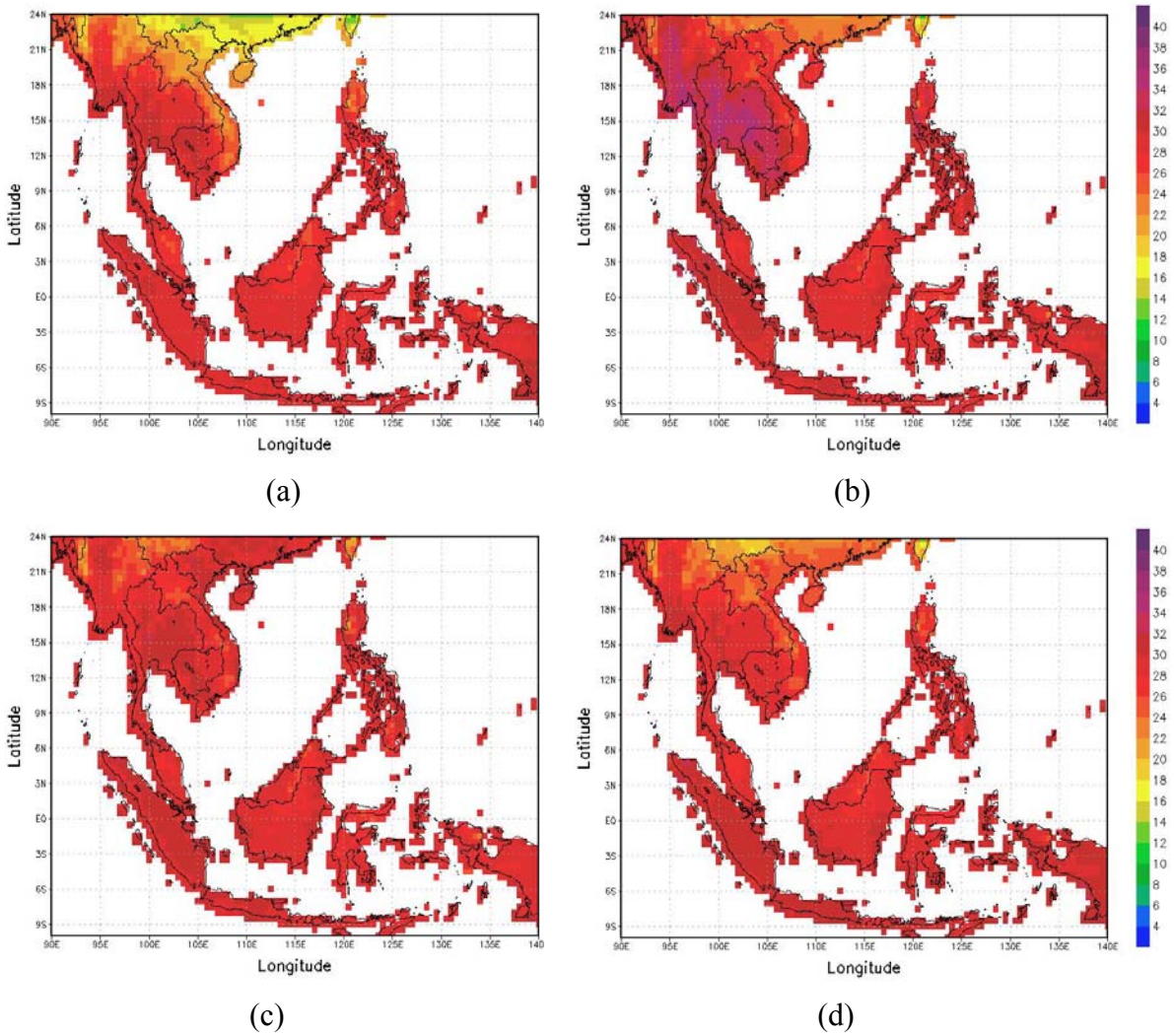

Figure 4.21: Spatial distribution of average maximum temperature (°C) in the period of 1961-1990 from CRUTS2.1 during (a) DJF (b) MAM (c) JJAS (d) ON

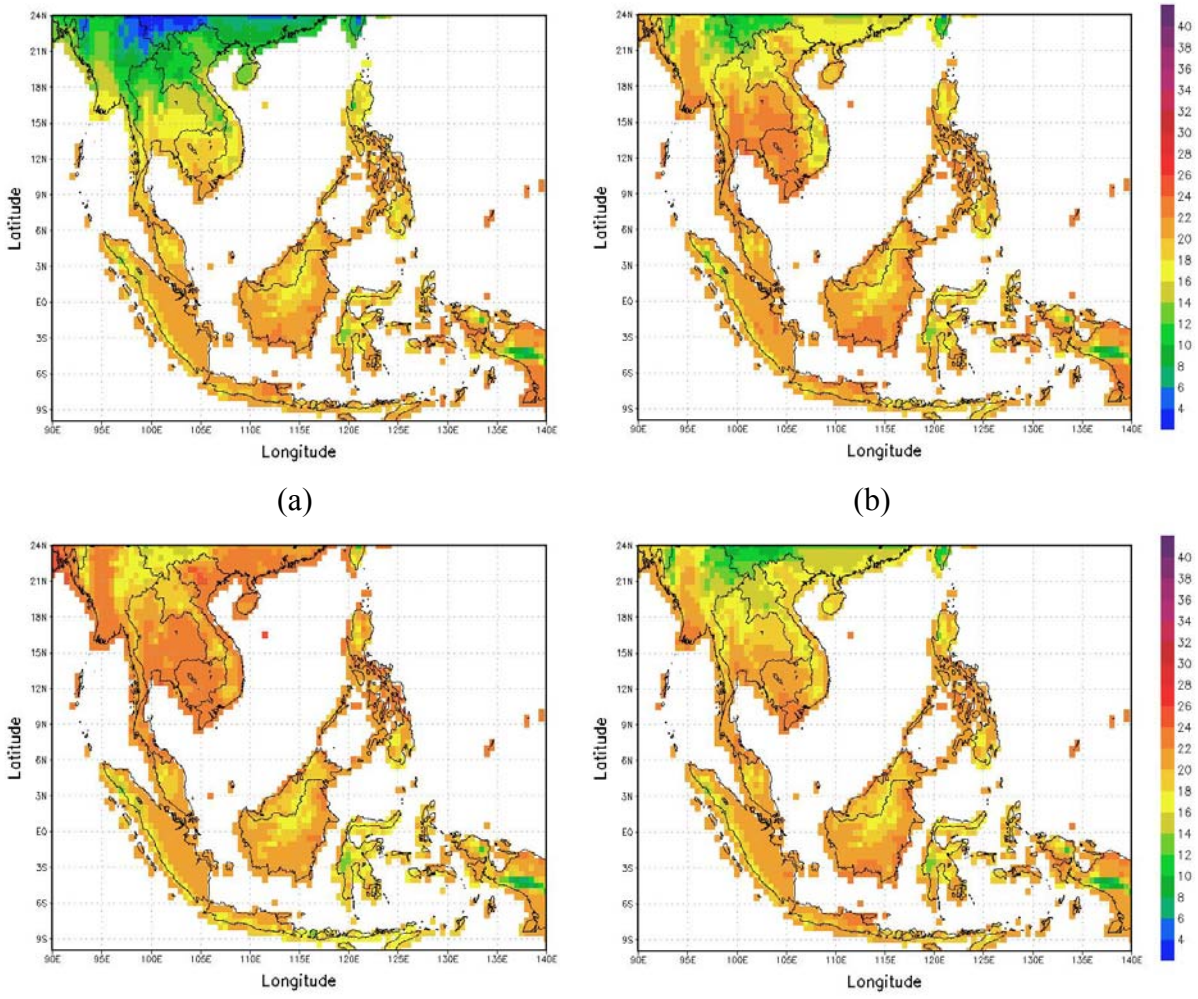

Figure 4.22: Spatial distribution of average minimum temperature (°C) in the period of 1961-1990 from CRUTS2.1 during (a) DJF (b) MAM (c) JJAS (d) ON

Table 4.8: Seasonal maximum and minimum temperatures (^{o}C) over Thailand based on CRUTS2.1

Maximum Temperature (^{o}C)	DJF	MAM	JJAS	ON	Annual
North	28.5	33.1	29.7	28.6	30.1
Northeast	29.5	33.8	31.1	29.8	31.2
Centre	31	34.8	31.4	30.2	32
South	29.9	31.9	30.5	29.6	30.6
Minimum Temperature (^{o}C)	DJF	MAM	JJAS	ON	Annual
North	12.5	19.3	21.5	18.2	18.2
Northeast	16.4	22.8	23.6	20.4	21.1
Centre	17	22.5	22.9	20.7	20.9
South	20.8	22.1	22.2	21.8	21.7

4.2.6 Diurnal temperature range (DTR)

The greatest DTR values occur during the cool season but the magnitude is seen to vary at the five stations (Figure 4.23). It is known that urbanized areas often show a smaller DTR than nearby rural areas, due to the overnight release of heat from the building fabric, and this is shown to be true at BKK. To be consistent, the five sites are once again divided into mainland sites and Surat for analysis. Since the DTR is the maximum temperature minus the minimum temperature, the DTR can decrease when the trend in the maximum or minimum temperature is positive, negative or unchanging. The section 4.2.5 showed a faster rise in minimum temperature over time than in maximum temperature, during MAM, resulting in a decrease in the DTR for both mainland sites and the Surat site while during DJF there is a decrease in the DTR at mainland sites but an increase at Surat (Figure 4.24). The slop of yearly DTR time series is approximately -0.19°C/10 years (-0.09°C/10 years) over mainland and -0.31°C/10 years (+0.08°C/10 years) at Surat during MAM (DJF).

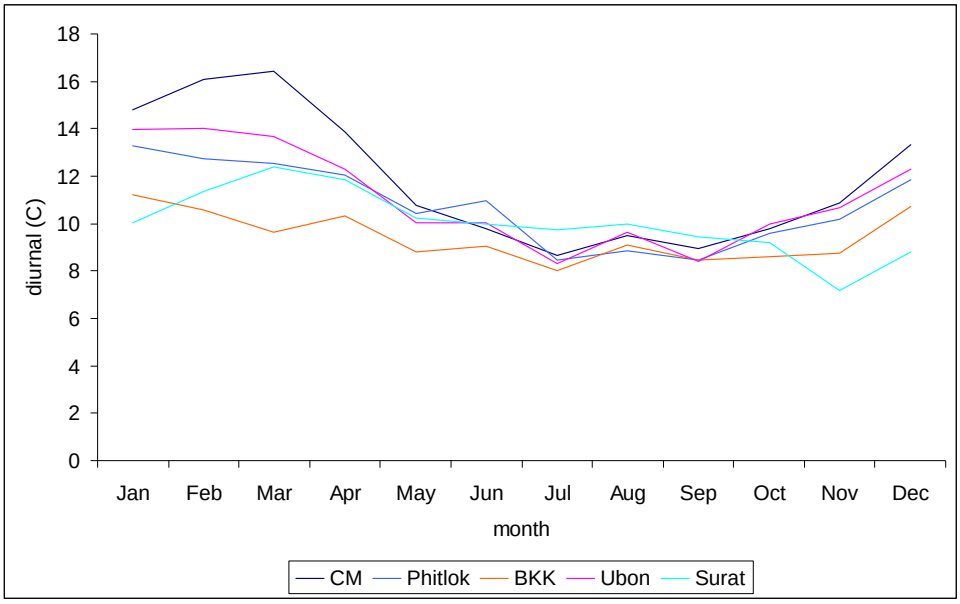

Figure 4.23: Average 30 year (1961-1990) seasonal cycle in DTR (°C) for five stations over Thailand

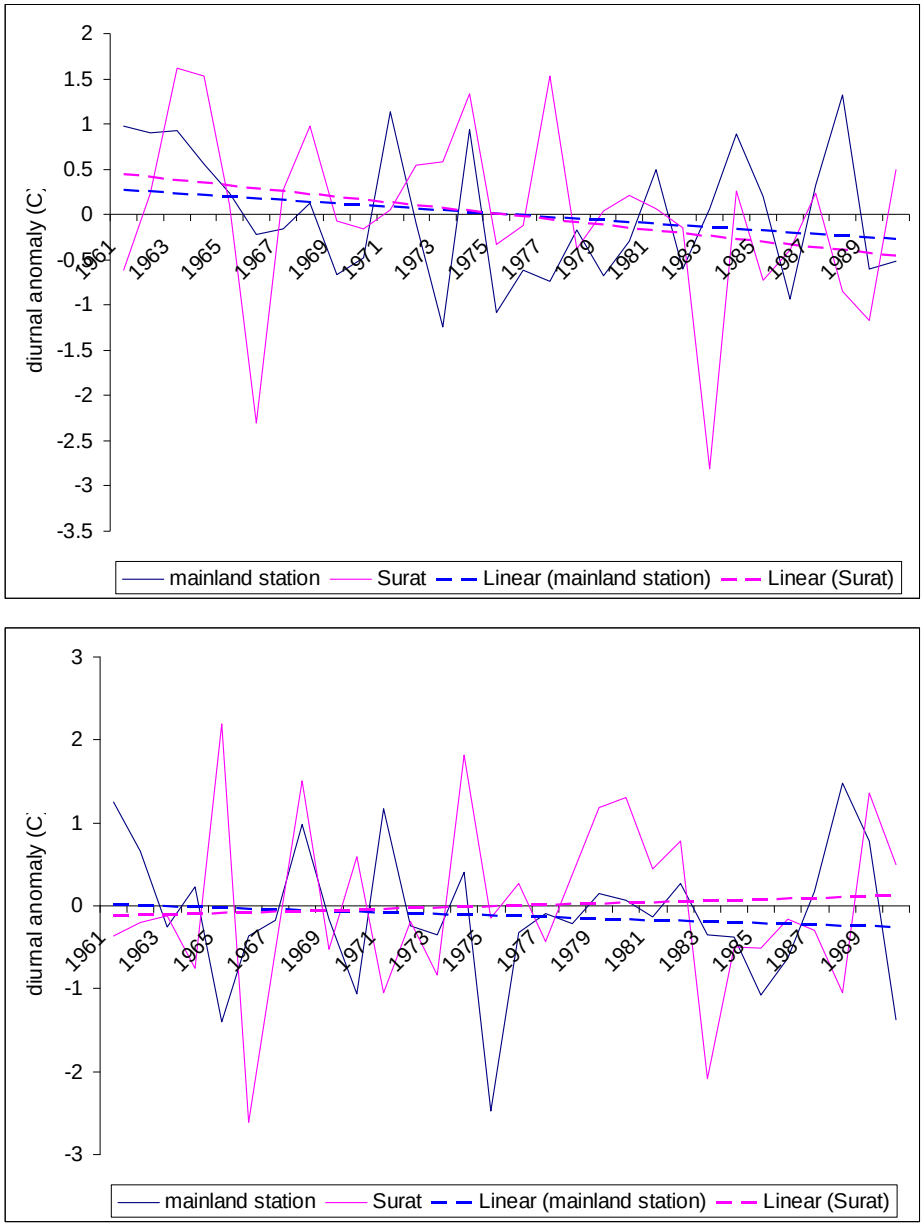

Figure 4.24: Annual DTR temperature time series for mainland (CM, Phitlok, Ubon, BKK) and Surat sites expressed as anomalies from 1960-1990 during MAM (top) DJF (below)

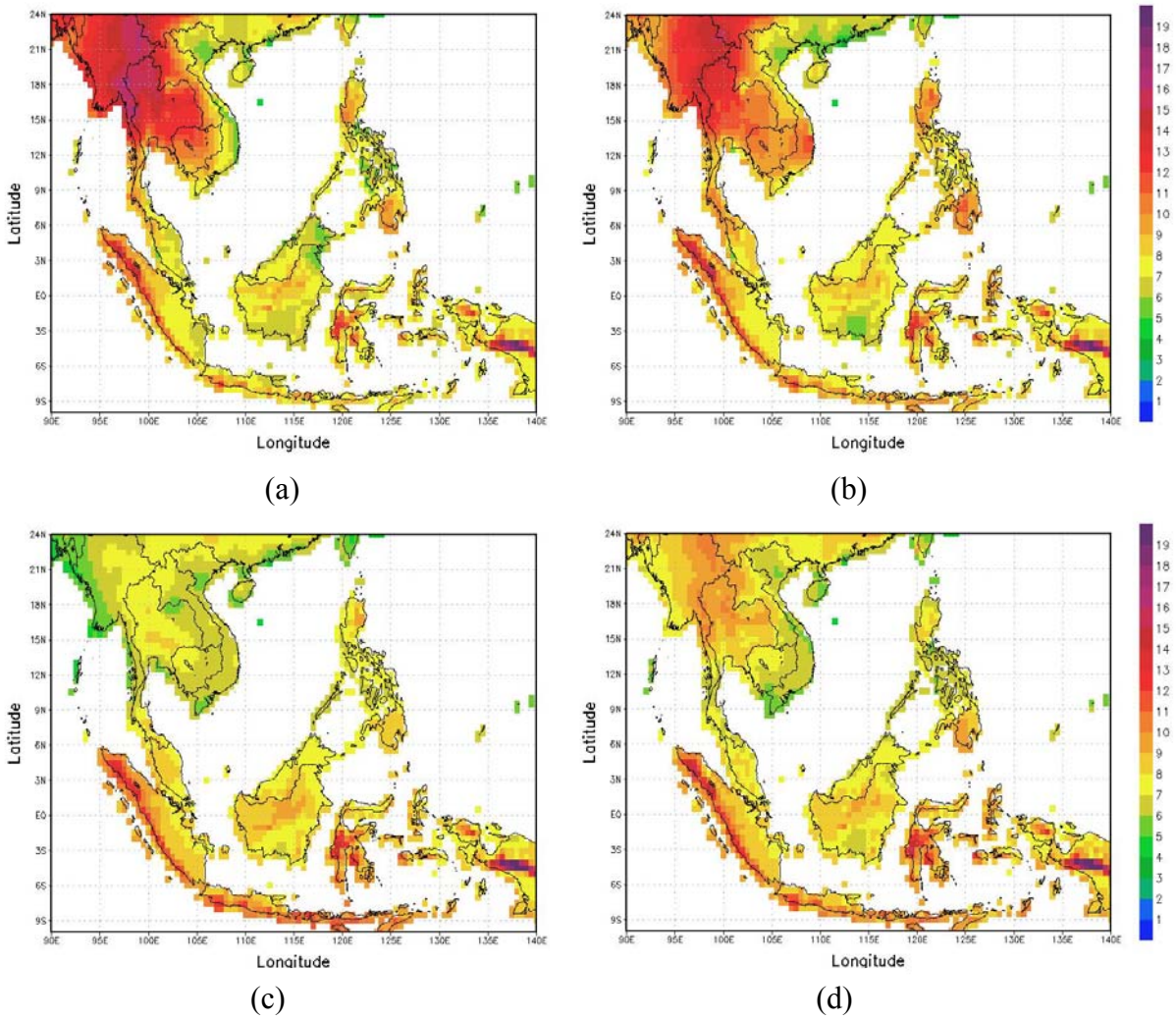

Figure 4.25: Spatial distribution of seasonal DTR (^{o}C) in the period of 1961-1990 from CRUTS2.1 during (a) DJF (b) MAM (c) JJAS (d) ON

Table 4.9 Seasonal DTR (^{o}C) over Thailand for 1961-1990 based on CRUTS2.1

Diurnal (^{o}C)	DJF	MAM	JJAS	ON	Annual
North	15.6	13.6	7.6	10.1	11.5
Northeast	12.5	10.4	7.0	8.9	9.6
Centre	13.5	11.8	8.0	9.2	10.5
South	8.7	9.4	8.0	7.5	8.4

The most DTR over mainland was found in DJF while DTR over southern Thailand has a small seasonal variation.

4.2.7 Monsoon onset

Definition of southwest monsoon onset

Several criteria for identifying the monsoon season onset have been applied to the monsoon regions of the world, for example based on precipitation (Nicholls et al. 1982), wind (Ramage, 1971) or cloudiness from satellite observations (Davidson et al. 1983). For Thailand, Sangwaldach (2006) suggested using five successive rainy days with more than 5mm each day accompanied by westerly or southwesterly low level winds and easterly upper level winds to determine the monsoon onset. This issue is discussed extensively in Chapter 1.

In this study, the onset of the southwest monsoon season over Thailand is defined as the occurrence of an 850-hPa westerly wind with minimum speed of 4 m/s and 250-hPa easterly wind along 100^{o}E in the band 5-20^{o}N together with precipitation greater than 6 mm/day each day for a consecutive five day period. Based on Thai Meteorology Department reports the onset of the rainy season in Thailand occurs around mid-May .

Approximated southwest monsoon onset date

Based on the above definitions of the onset of the monsoon and on TMD available daily precipitation and wind data, the approximate dates of monsoon onset at mainland sites and at Surat over the period 1961-90 are shown in Table 4.10.

Table 4.10: Approximated monsoon onset date (May) over 1961-1990 at mainland sites and at Surat

year	Mainland (CM+Phitlok+Ubon+BKK)	Peninsula (Surat)	Onset Timing difference (Mainland-Peninsula)
1961	6th	1st	5
1962	16th	14th	2
1963	18th	21st	-3
1964	3rd	3rd	0
1965	20th	18th	2
1966	2nd	6th	-4
1967	2nd	3rd	-1
1968	1st	1st	0
1969	5th	6th	-1
1970	10th	10th	0
1971	16th	15th	1
1972	9th	8th	1
1973	7th	8th	-1
1974	15th	11th	4
1975	6th	7th	-1
1976	4th	1st	3
1977	22nd	21st	1
1978	8th	9th	1
1979	19th	12th	7
1980	16th	17th	-1
1981	17th	17th	0
1982	19th	21st	-2
1983	24th	21st	3
1984	18th	12th	6
1985	11th	10th	1
1986	6th	6th	0
1987	1st	1st	0
1988	1st	1st	0
1989	6th	2nd	4
1990	14th	14th	0

From statistical analysis, the monsoon onset date averaged over the 1961-1990 period over the mainland is approximately 11th May and over the peninsula is the 10th May; there is no significant different at the 5% level. The 95% confidence interval is -0.11 to 1.78 day. Applying t-test, it found that monsoon onset over mainland is related the onset over the peninsula.

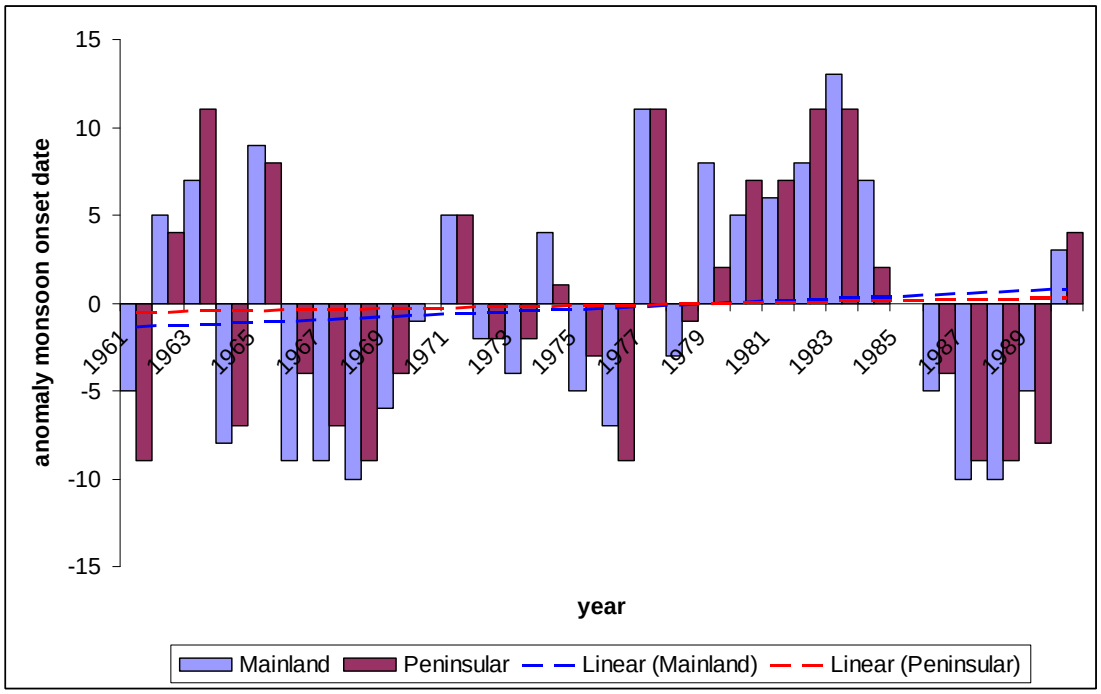

Figure 4.26: Inter-annual variation of the date of monsoon onset over Thailand during the period 1961-1990

Figure 4.26 shows a small delay in the arrival of the monsoon over Thailand, based on the selected criteria, of 3 days over the mainland and 1 day over the peninsula over the 30 year period, possibly occurs in association with SST anomaly. Based on an analysis of SST fields, Joseph *et al*. (1994) hypothesized that the delay of monsoon onset is due to warm anomalies over the equatorial central Pacific Ocean causing a delay in the shifting of convection from the equatorial western Pacific to the north Indian Ocean.

4.3 Summary

Based on the literature review, there are few publications about Thai climate, most of them using the station data over the Thai mainland to study current climate, ignoring the peninsular Thailand climate completely. Yet a gridded observational data set is available over SEA and Thailand. In this chapter, the limited observational data, i.e., station observation data from the Thai Meteorology Department (TMD) and the high resolution gridded dataset (CRUTS2.1) are studied to more fully quantify the Thai climate. It is demonstrated that the climate over peninsular Thailand can be clearly

distinguished from the climate over the Thai mainland. Furthermore, this work provides a valuable baseline against which the model climates, presented in the following two chapters, can be compared.

The average annual precipitation over the **mainland** region is shown to decrease marginally by about 4mm during 1961-1990; the dominant precipitation season is JJAS contributing 60-70 % of the annual rain, with the number of rain days (≥ 1 mm) decreasing by approximately 10 days during JJAS over the thirty year period. Minimum temperatures are shown to be increasing at a rate of 1^{o}C/30 years during MAM and DJF which is somewhat higher than the linear global warming trend over 1956-2005 of 0.13^{o}C per decade (IPCC-AR4, 2008) while maximum temperature are increase at a rate of 0.47^{o}C (0.02^{o}C)/30 years in MAM (DJF). The diurnal temperature range (DTR) is shown to decrease at a rate of 0.6 ℃/30 years in MAM and 0.3℃ /30 years in DJF. The decrease in DTR is caused by temperatures increasing faster at night than during the day. The average monsoon onset (1961-1990) is about the 11th May and the trend over this period is 1 day/30 year.

Annual precipitation over the **southern** region of Thailand decreased at a faster rate than over the mainland region, by 20 mm during the 1961-1990 period, and precipitation during the JJAS wet season is found to contribute 40 % of the annual rain, with the number of rain days during JJAS appearing to decline by approximately 10 days in thirty years.The maximum precipitation in southern Thailand is detected in November due to the influence of the northeast monsoon which brings moisture from the South China Sea to the peninsula. The minimum and maximum temperature over southern Thailand show relatively small changes through the year. The minimum and maximum temperatures are shown to be increasing at 1.6^{o}C (0.7^{o}C) /30 years and 0.46^{o}C (1^{o}C) /30 years in MAM (DJF) respectively. The DTR is shown to decrease at a rate of 0.9^{o}C /30 years in MAM and increase at a rate of about 0.25^{o}C /30 years in DJF. The average monsoon onset date (1961-1990) is the 10th May, one day earlier than the mainland region, with minimal change over the 1961-90 period.

In terms of tropical depressions, there is a statistically significant difference in precipitation over both the mainland and the peninsula. Therefore, depressions

statistically significantly increase precipitation, consistent with several studies (Shepherd et al., 2007; Rappaport, 2000). It is therefore desirable that RCMs should be able to simulate tropical depressions reasonably well. Trends in precipitation associated with tropical cyclones may be apparent if the number of storms is changing over time. It was found that fewer tropical cyclones have affected Thailand in the second half of the 1961-90 period.

Moreover, it was found that the relationship between the number of wet days and precipitation amount for all five sites is a simple linear function as shown in Figure 4.11-4.12. The decrease in the number of wet days is one of the factors to induce the precipitation decrease.

In this study, analyzing precipitation amounts at 5 representative stations over Thailand, it was found that there is an statistically intensification (reduction) of precipitation during La Niña (El Niño) years at Surat Thani (Chiang Mai) during ON (JJAS) and no statistically significant differences in rainfall are found between any pair of these ENSO events during DJF and MAM seasons over 1961-1990. Regarding the El Niño years, the tropical depression activity during neutral years and El Niño years is roughly equal for the JASON period and, during La Niña years, the number of depressions in Thailand is generally above average. Therefore, there is no significant change in both precipitation amount and number of tropical depressions during El Niño years and there is an intensification of precipitation and increased number of tropical depressions moving across Thailand during La Niña years.

Chapter 5

Current Climate and Model validation

5.1 Introduction

This chapter examines how well PRECIS captures the main current climatic regimes in Southeast Asia and the extent to which PRECIS adds fine scale value to that provided by GCMs. Uncertainties in regional climate simulations were discussed in detail in earlier chapters and these are also addressed here by forcing with different (i) initial conditions (ii) boundary conditions (iii) global climate models. To address one of the main aims of the thesis, the daily station and gridded CRUTS2.1 datasets, described in Chapters 3 and 4, are compared with the model results.

According to the experimental design detailed in chapter 2, both spatial and point model precipitation and temperature estimates show insignificant differences between climate simulations run with and without interactive sulphur cycle (Tables 5.1 and 5.2). Moreover, in terms of simulations driven from different initial conditions of HadAM3P, a 150 km resolution version of the Hadley Centre's global atmosphere-only model, using observed time series of HadISST SST and sea-ice for 1960-1990, there is also no significant difference in output. Therefore, this chapter focuses on the sensitivity of the model simulations to the use of reanalysis and 2 different Global Models for RCM boundary conditions: (i) ERA40, (ii) HadAM3 (iii) ECHAM4, assuming no sulphur cycle since the results seem not to be sensitive to the latter. The baseline experiments are hereafter known by the names PRECIS-ERA40, PRECIS-HadAM3P and PRECIS-ECHAM.

Table 5.1 Seasonal total precipitation statistics for land points over the domain 5-20.5°N and 97-105°E. Results show the area-averaged mean precipitation and spatial standard deviation (mm/day) for experiments running with sulphur cycle and without sulphur cycle (note that PRECIS-HadAM3P-IC 1 stands for PRECIS driven by HadAM3P and a different initial condition.)

Total precipitation (mm/day)	DJF	MAM	JJAS	ON
Mean:				
PRECIS-HadAM3P-IC 1- with sulphur cycle	0.90	3.68	8.90	4.47
PRECIS-HadAM3P-IC 1- without sulphur cycle	0.98	3.80	9.12	4.76
PRECIS-HadAM3P-IC 2- with sulphur cycle	0.88	3.74	8.67	4.34
PRECIS-HadAM3P-IC 2- without sulphur cycle	0.97	3.83	8.96	4.60
PRECIS-HadAM3P-IC 3- with sulphur cycle	0.87	3.45	8.38	4.19
PRECIS-HadAM3P-IC 3- without sulphur cycle	0.95	3.52	8.71	4.42
Standard deviation:				
PRECIS-HadAM3P-IC 1- with sulphur cycle	1.62	1.20	3.94	3.11
PRECIS-HadAM3P-IC 1- without sulphur cycle	1.47	0.98	3.09	3.03
PRECIS-HadAM3P-IC 2- with sulphur cycle	1.30	1.15	2.73	2.78
PRECIS-HadAM3P-IC 2- without sulphur cycle	1.56	1.07	2.51	2.82
PRECIS-HadAM3P-IC 3- with sulphur cycle	1.38	0.95	3.13	2.93
PRECIS-HadAM3P-IC 3- without sulphur cycle	1.65	1.36	2.82	2.74

Table 5.2 Seasonal 1.5m air temperature statistics for land points only over the domain 5-20.5°N and 97-105°E. Results show the area-averaged mean surface temperature and spatial standard deviation (°C) for experiments running with sulphur cycle and without sulphur cycle.

Maximum Temperature (°C)	DJF	MAM	JJAS	ON
Mean:				
PRECIS-HadAM3P-IC 1- with sulphur cycle	28.5	32.2	29.7	28.8
PRECIS-HadAM3P-IC 1- without sulphur cycle	28.8	32.4	29.7	28.9
PRECIS-HadAM3P-IC 2- with sulphur cycle	28.0	32.5	29.4	28.1
PRECIS-HadAM3P-IC 2- without sulphur cycle	28.1	32.7	29.5	28.1
PRECIS-HadAM3P-IC 3- with sulphur cycle	27.9	32.3	29.5	28.5
PRECIS-HadAM3P-IC 3- without sulphur cycle	28.0	32.5	29.6	28.7
Standard deviation:				
PRECIS-HadAM3P-IC 1- with sulphur cycle	2.7	2.2	1.8	1.4
PRECIS-HadAM3P-IC 1- without sulphur cycle	2.6	2.2	1.6	1.7
PRECIS-HadAM3P-IC 2- with sulphur cycle	2.5	2.9	1.9	1.5
PRECIS-HadAM3P-IC 2- without sulphur cycle	2.7	2.4	1.9	1.4
PRECIS-HadAM3P-IC 3- with sulphur cycle	2.1	2.8	1.4	1.9
PRECIS-HadAM3P-IC 3- without sulphur cycle	2.3	2.8	1.8	1.6

Table 5.2: (continued)

Minimum Temperature (°C)	DJF	MAM	JJAS	ON
Mean:				
PRECIS-HadAM3P-IC 1- with sulphur cycle	16.2	20.8	22.0	19.9
PRECIS-HadAM3P-IC 1- without sulphur cycle	16.4	21.0	22.1	19.9
PRECIS-HadAM3P-IC 2- with sulphur cycle	15.8	20.8	21.7	19.6
PRECIS-HadAM3P-IC 2- without sulphur cycle	16.1	20.9	21.8	19.7
PRECIS-HadAM3P-IC 3- with sulphur cycle	16.0	20.9	21.8	19.6
PRECIS-HadAM3P-IC 3- without sulphur cycle	16.2	21.1	21.9	19.8
Standard deviation:				
PRECIS-HadAM3P-IC 1- with sulphur cycle	3.2	2.6	1.6	2.6
PRECIS-HadAM3P-IC 1- without sulphur cycle	3.6	2.2	1.4	2.2
PRECIS-HadAM3P-IC 2- with sulphur cycle	3.4	2.5	1.3	2.5
PRECIS-HadAM3P-IC 2- without sulphur cycle	3.9	2.7	1.8	2.6
PRECIS-HadAM3P-IC 3- with sulphur cycle	3.3	2.4	1.3	2.2
PRECIS-HadAM3P-IC 3- without sulphur cycle	3.9	2.8	1.8	2.9

5.2 Model Validation

5.2.1 Total Precipitation

The model precipitation simulations produced by the GCM (HadAM3P) and the RCM (PRECIS-HadAM3P, PRECIS-ERA40, PRECIS-ECHAM)) are compared in Figure 5.1 with the observational gridded dataset, CRUTS2.1, for JJAS, the southwest monsoon season, during the period 1961-1990. In general, the model simulations, excluding PRECIS-ECHAM4, realistically simulate the heavy precipitation over the Bay of Bengal coast shown in CRUTS2.1. The area of intense precipitation of up to 26 mm/day extends into the Bay of Bengal coastline in Western Thailand in both the

GCM and RCM simulations. The wettest areas of Indochina are the three mountain ranges named the Rakhine Yoma along the western coast of Burma where orographic lifting frequently occurs. Meanwhile the rain shadow areas on the eastern sides of the mountains, such as over central Burma and Thailand, are also captured by HadAM3P, PRECIS-HadAM3P and PRECIS-ERA40. The RCM, except PRECIS-ECHAM, shows patterns over both land and ocean which are consistent with the GCM HadAM3P. With respect to Thailand, the average daily precipitation during JJAS over 1961-1990 simulated by the RCM adds more detail, in particular, over the coastline but is insignificant in adding further value over the southern region. The relatively high amount of precipitation over the Bay of Bengal, northwest Pacific Ocean and the South China Sea also show a similar pattern but with differing magnitude. Applying the grid-to-grid analysis method, the displayed spatial JJAS precipitation patterns are similar, with more detail provided by the PRECIS simulation compared with HadAM3P itself, but it is not clear if PRECIS produces a more realistic simulation. To aid the comparison, precipitation amounts from all model simulations are re-gridded and displayed at the same resolution as applied for the gridded CRUTS2.1 dataset, at 0.5x0.5°. Interestingly, precipitation over mainland Thailand and the surrounding area from the RCM and GCM simulations agree well with CRUTS2.1, excepting the PRECIS-ECHAM4 simulation, while over peninsular Indochina, Sumatra and Borneo, the GCM noticeably underestimates compared with the absolute rainfall measurements from the observations. The resolution of the GCM is 150x150 km and it is less able to distinguish between land and sea. The heat capacity of water is approximately three times higher than the heat capacity of land. In other words, raising the water temperature by 1 degree requires significantly more heat energy than raising the air temperature by 1 degree. When land and water gain the same amount of thermal energy, the land surface temperature rises higher than the water surface temperature so convection occurs more readily over the land than over the ocean. Moreover, the concept of convective parameterization in a GCM is based on a process that is of a smaller scale than the grid spacing itself and hence simulated precipitation could be representative of scales smaller than the models' grid spacing. This is also one likely reason for the GCM underestimate of precipitation over the peninsula.

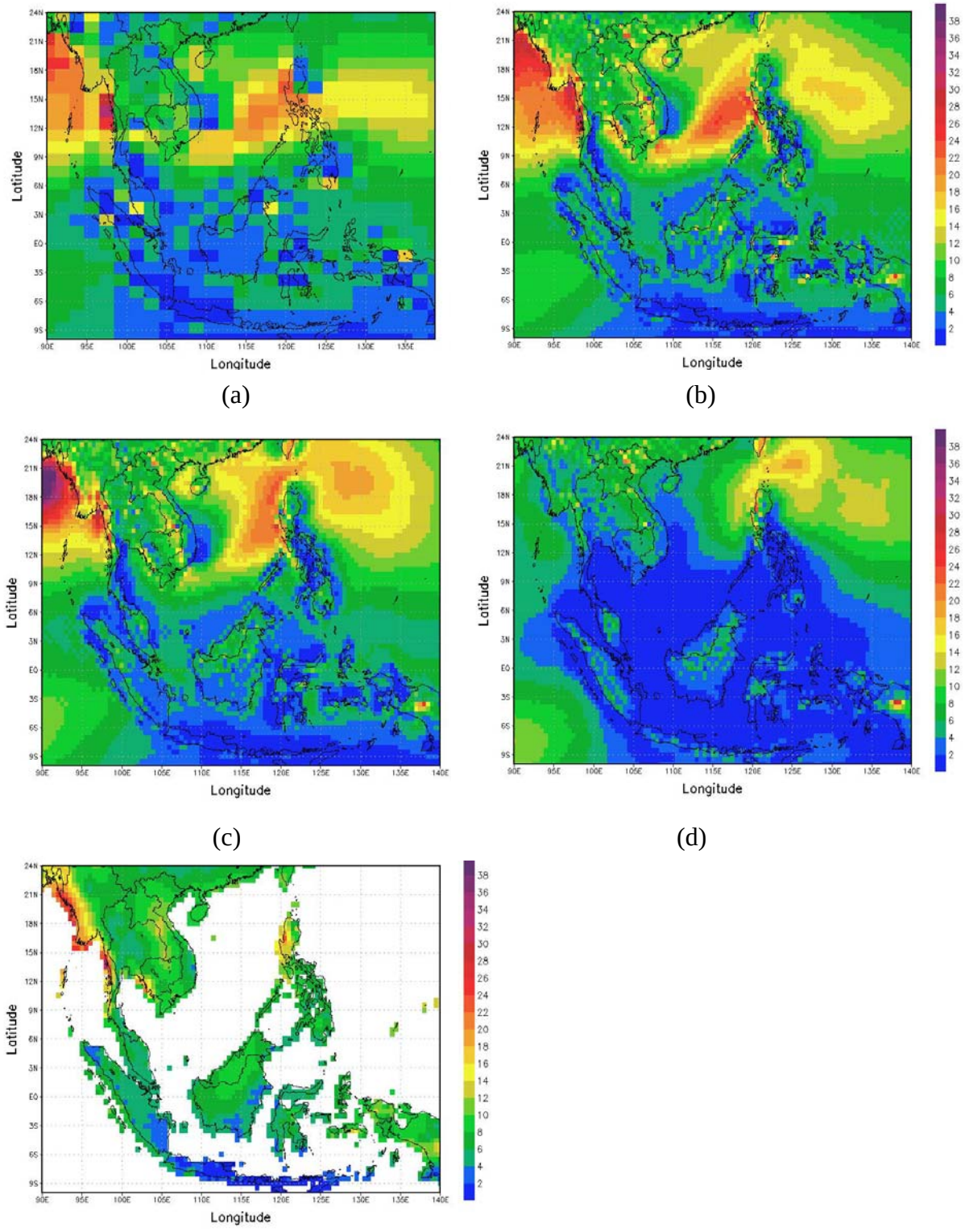

Figure 5.1: Spatial distribution of average precipitation (mm/day) in the period of 1961-1990 during JJAS (a) HadAM3 (b) PRECIS-HadAM3P (c) PRECIS-ERA40 (d) PRECIS-ECHAM4 (e) CRUTS2.1

Figures 5.2-5.5 show spatial distributions of seasonal precipitation difference (mm/day) between model and observations (CRUTS2.1) in the period 1961-1990. Over mainland Thailand and the surrounding area, the GCM and RCM, excepting PRECIS-ECHAM4, produce DJF precipitation amounts which are close to observations (Figure 5.2). An underestimate in precipitation was found in the Indochina peninsula and over Sumatra and Borneo. The GCM and PRECIS-ECHAM underestimate of precipitation over those regions is in the range of 6-9 mm/day which, is higher than the biases in the PRECIS-HadAM3P and PRECIS-ERA40 results over these regions (3-5 mm/day). Overestimates in precipitation produced by both the GCM and RCM in MAM were found in northern mainland Thailand and nearby areas, while the PRECIS-ECHAM underestimated precipitation in some areas in those regions (Figure 5.3). In contrast, the underestimated precipitations in MAM were found in the same region of underestimated precipitation in DJF. Figure 5.4 shows that all simulations excluding PRECIS-ECHAM4 reasonably reproduce precipitation in JJAS and PRECIS-HadAM3P adds more detail over Thailand. However, it is not possible to clearly see which simulations simulate precipitation amount over Thailand more consistently when compared with the observations and so this will be investigated later (section 5.2.1.1). The mixture of positive convective precipitation over mainland of Thailand may be due to increasing resolution of topography that may impact on local scale diurnal heating and airstream convergence. In general, underestimates in precipitation during ON were found across most of the domain (Figure 5.5). Interestingly, there is a striking difference in the sign of bias between the north and south of the domain, unlike other PRECIS studies over other part of the world, in which precipitation bias more likely depends on season, for example, underestimation (overestimation) during summer (winter) possibly responding to hydrostatic restriction as PRECIS fails to fully simulate convective precipitation (Hudson and Jones, 2002, Alves and Marengo, 2009, Shahgedanova et al., 2010). The bias over SEA more likely depends on geographical location. Therefore, the possible cause of the bias could be observation quality and/or RCM error. CRUTS2.1 is likely to be a reliable gridded observational precipitation dataset because the interpolated values depend on a number of surrounding station with large residuals are removed where they are defined as potentially in error (New et al., 2002). The interpolation methods assume relations between the variables latitude, longitude and surface elevation. The density of corresponding stations for interpolation over SEA was

provided by both GHCN and HadCRU and there are a few stations in each 0.5 x 0.5 resolution grid cell (http://www.appinsys.com/GlobalWarming/climapview.aspx) provided by both GHCN and HadCRU. The underestimate in both GCM and RCM for all season arounds the equator over marine continents implied that the convection scheme and/or the physical parameterization fail to faithfully reproduce precipitation over the region. Even with improved boundary conditions, the skill of dynamical downscaling was also controlled by the regional scale forcings which may include orography, land-sea contrast, vegetation cover, lake effects, or they may be anthropogenic for example air pollution, urban heat island, and land and water management.

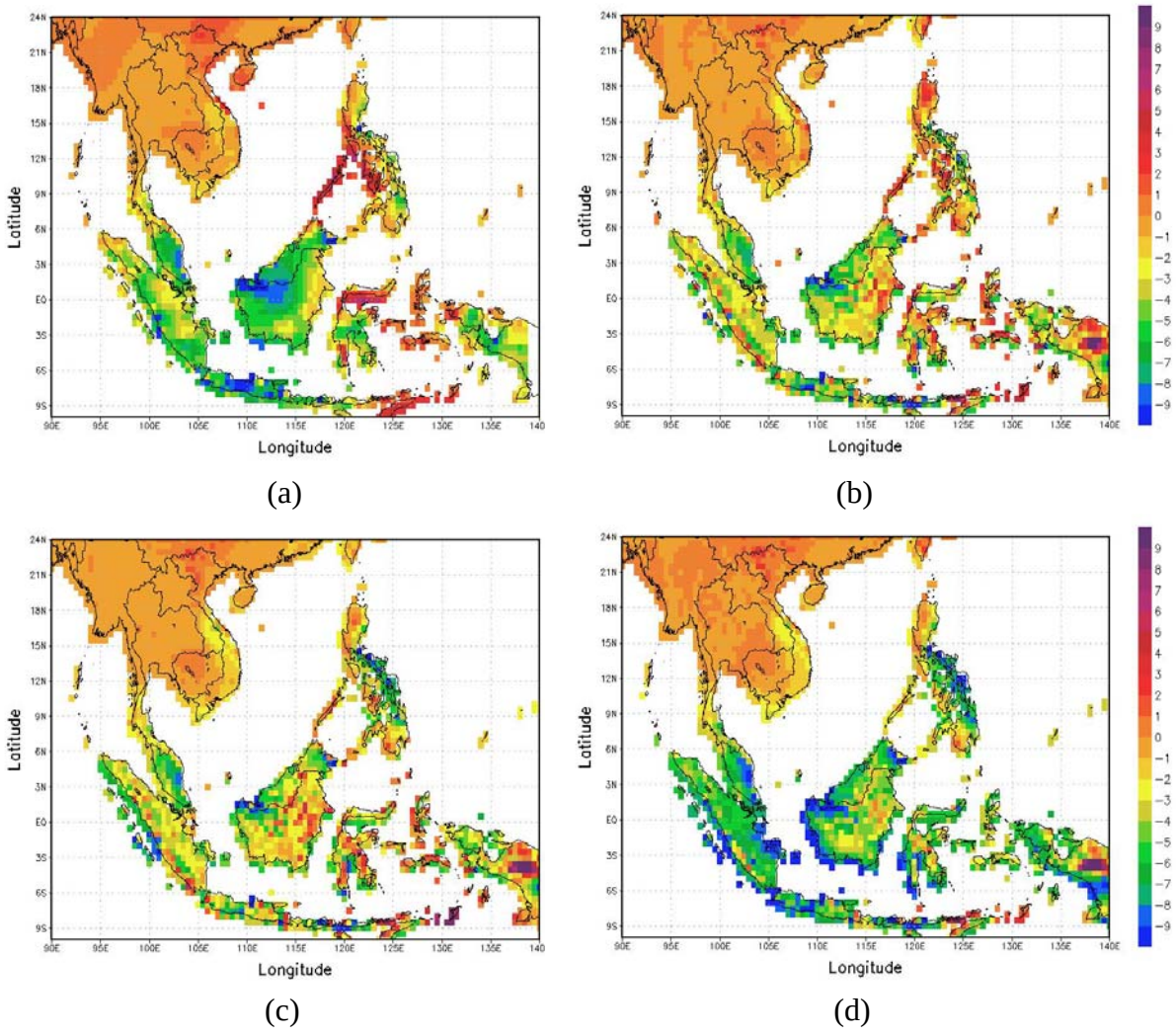

Figure 5.2 Difference between model and observations (CRUTS2.1) of average precipitation (mm/day) in the period of 1961-1990 during DJF (a) HadAM3P (b) PRECIS-HadAM3P (c) PRECIS-ERA40 (d) PRECIS-ECHAM4.

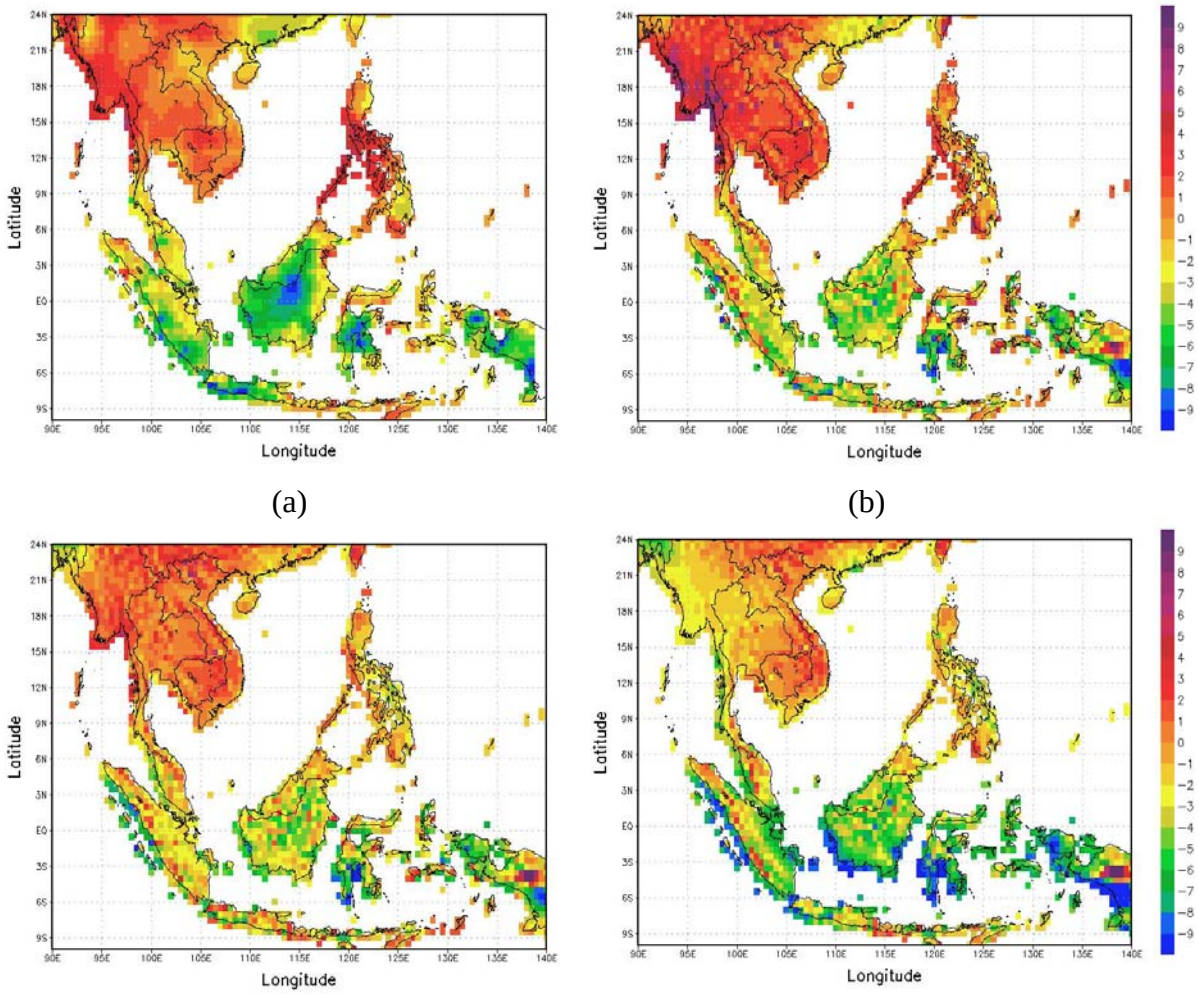

Figure 5.3: Difference between model and observations (CRUTS2.1) of average precipitation (mm/day) in the period of 1961-1990 during MAM (a) HadAM3P (b) PRECIS-HadAM3P (c) PRECIS-ERA40 (d) PRECIS-ECHAM4

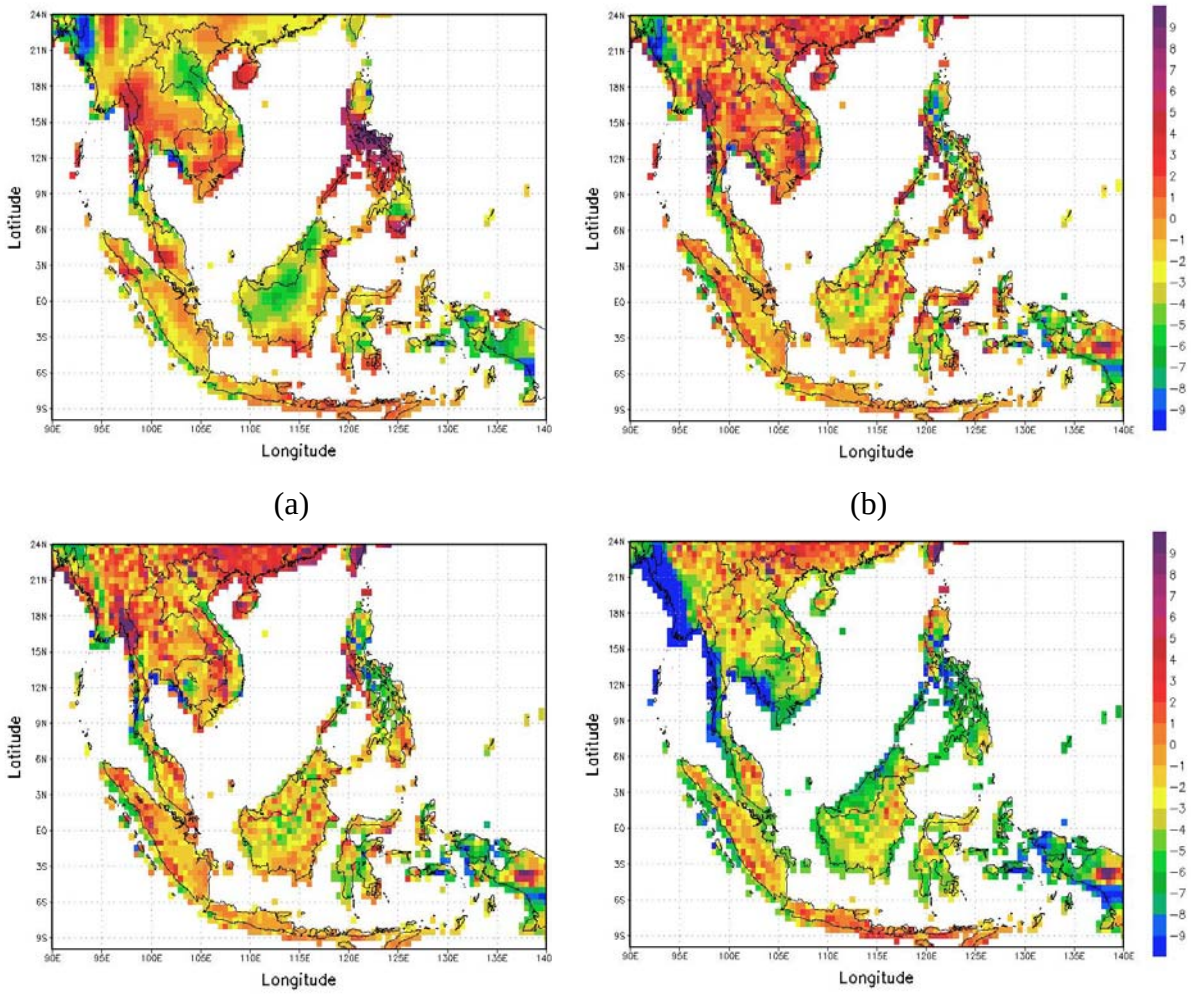

Figure 5.4: Difference between model and observations (CRUTS2.1) of average precipitation (mm/day) in the period of 1961-1990 during JJAS (a) HadAM3P (b) PRECIS-HadAM3P (c) PRECIS-ERA40 (d) PRECIS-ECHAM4.

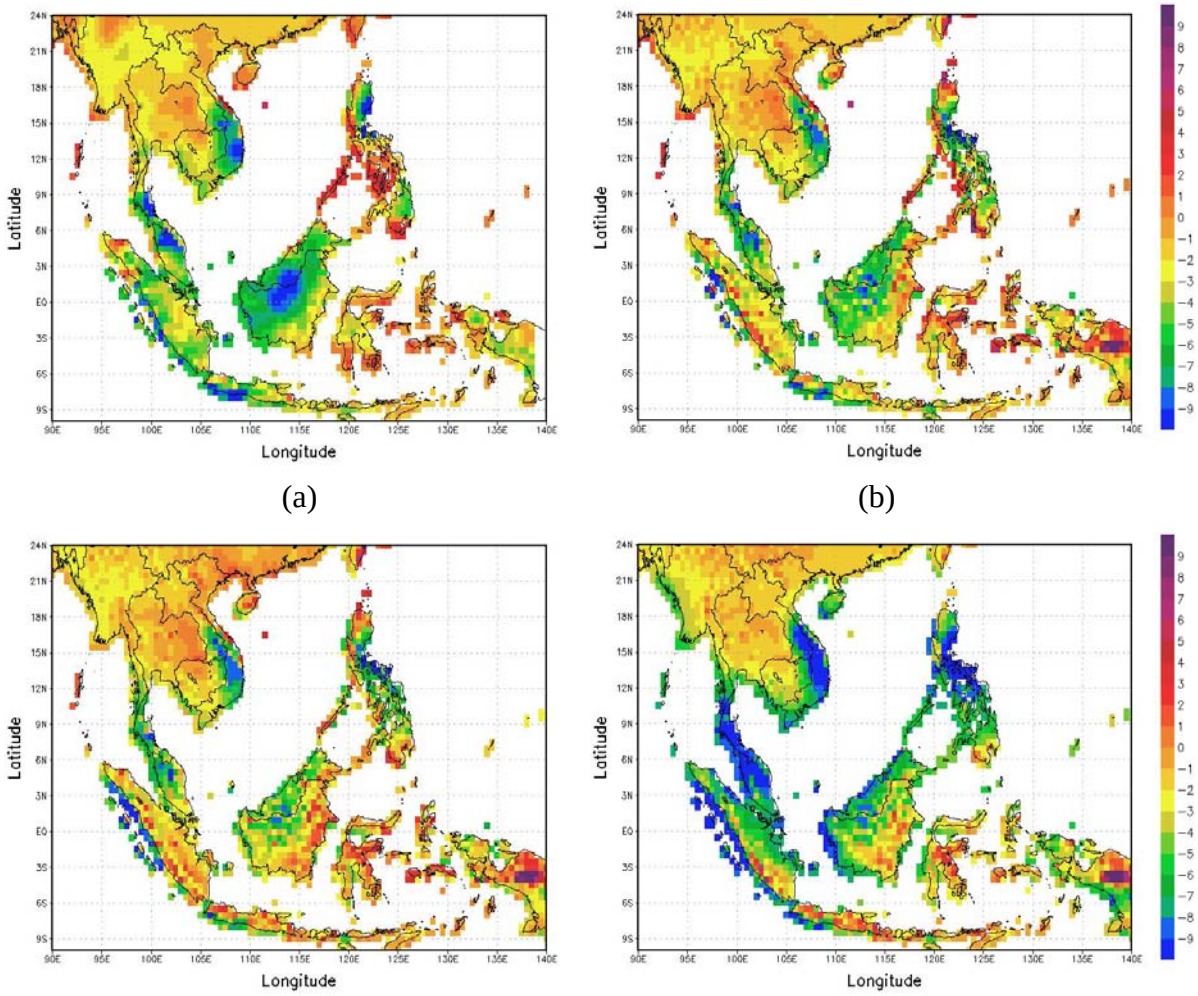

Figure 5.5: Difference between model and observations (CRUTS2.1) of average precipitation (mm/day) in the period of 1961-1990 during ON (a) HadAM3P (b) PRECIS-HadAM3P (c) PRECIS-ERA40 (d) PRECIS-ECHAM4

5.2.1.1 Comparison of GCM and RCM with gridded observation data

The Koppen-Geiger climate classification of Thailand divided the rainforest over mainland Thailand from the monsoon over the Thai peninsula as shown in chapter 3 and 4. As introduced in Chapter 3, Thailand is indeed divided by topography into 4 different regions, the north, northeast, centre and south of Thailand. The estimated precipitation totals over each topographic region from each simulation are shown in Figure 5.6.

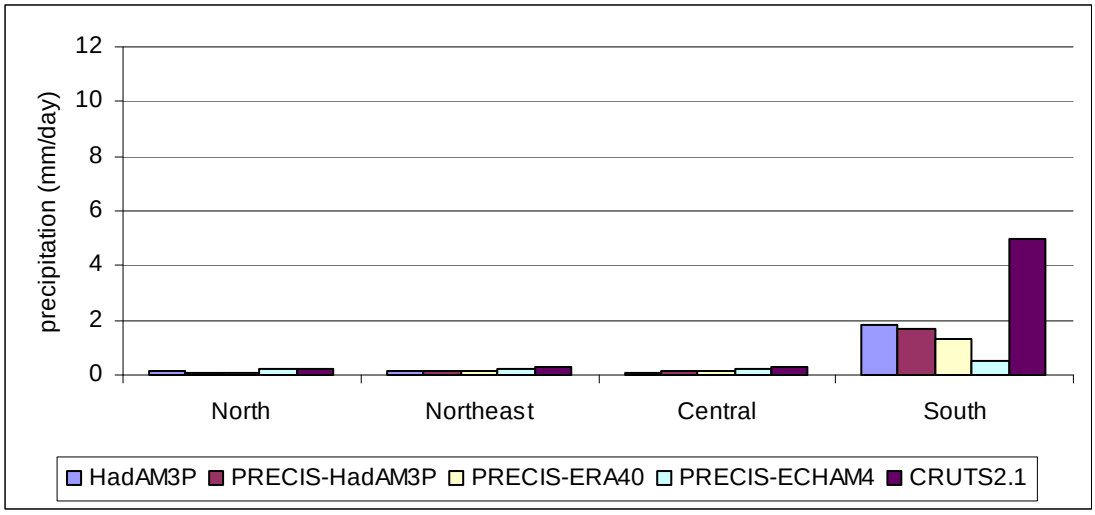
precipitation (mm/day)
12
10
8
6
4
2
0
North
Northeast
Central
South
HadAM3P
PRECIS-HadAM3P
PRECIS-ERA40
PRECIS-ECHAM4
CRUTS2.1

(a)

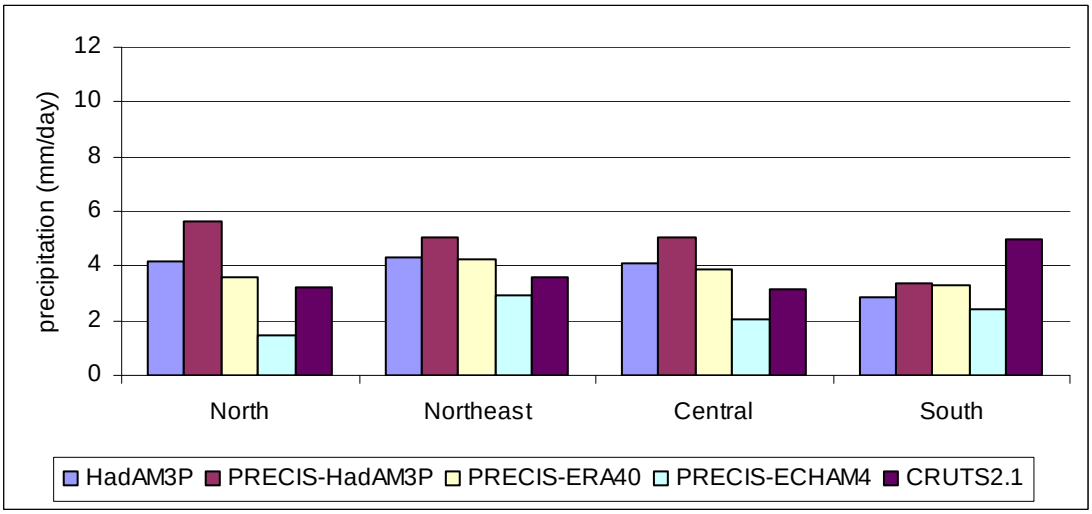
precipitation (mm/day)
12
10
8
6
4
2
0
North
Northeast
Central
South
HadAM3P
PRECIS-HadAM3P
PRECIS-ERA40
PRECIS-ECHAM4
CRUTS2.1

(b)

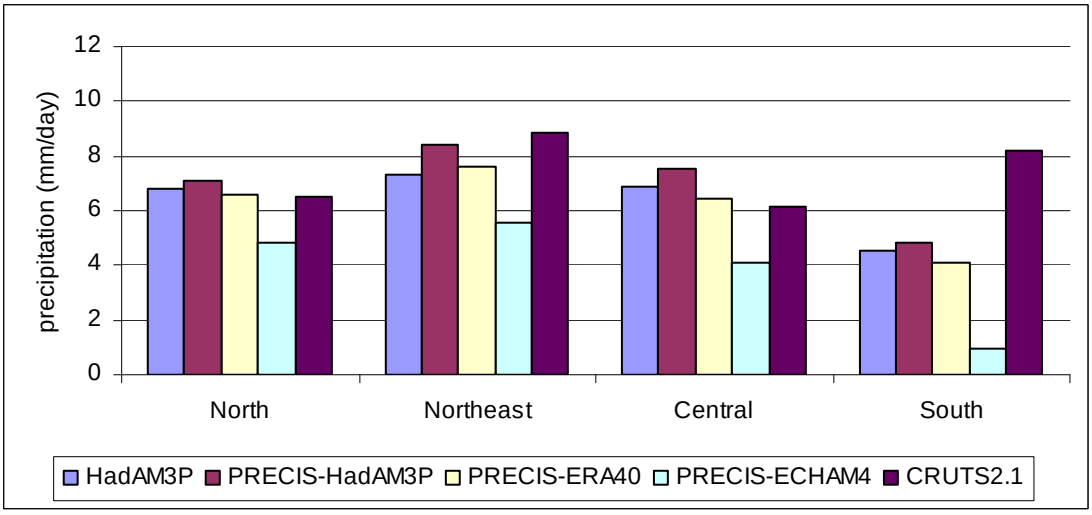
precipitation (mm/day)
12
10
8
6
4
2
0
North
Northeast
Central
South
HadAM3P
PRECIS-HadAM3P
PRECIS-ERA40
PRECIS-ECHAM4
CRUTS2.1

(c)

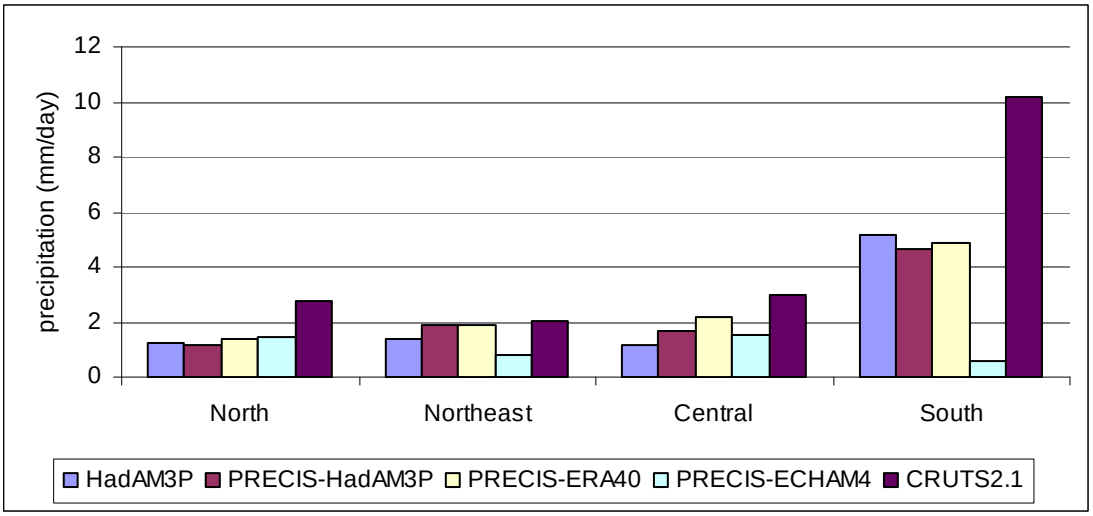

(d)

Figure 5.6: Mean seasonal precipitation (1961-1990) over land points divided into 4 topographic regions in Thailand from GCM and RCM simulations during (a) DJF (b) MAM (c) JJAS (d) ON.

The GCM and RCM data were interpolated to the 0.5x0.5° CRUTS2.1 grid and only land points used in the interpolation. In the cool season (DJF, Figure 5.6(a)), most of mainland Thailand records relatively low precipitation totals so it is difficult to achieve meaningful comparisons. Meanwhile, in the same season, the GCM, PRECIS-HadAM3P and PRECIS-ERA produce comparable amounts of precipitation and an underestimate in the order of 3 mm/day over the south region peninsula. During MAM (Figure 5.6b), all simulations excluding PRECIS-ECHAM slightly overestimated precipitation over mainland Thailand by 1-2mm/day. More specifically, the best estimated precipitation simulations are PRECIS-ERA over northern Thailand and the GCM, HadAM3P, and PRECIS-ERA are most accurate precipitation over northeast and central Thailand. The model simulations show the closest absolute precipitation totals to observations during JJAS are provided by PRECIS-ERA, PRECIS-HadAM3P, PRECIS-ERA and PRECIS-HadAM3P over north, northeast, central and south Thailand, respectively (Figure 5.6(c)), demonstrating a modest “added value” of using the RCM over the GCM. Figure 5.6(d) shows that all model simulations produced comparable precipitation during ON over northern Thailand, underestimating observations by approximately 50%. The PRECIS-HadAM3P and PRECIS-ERA show the closest absolute precipitation total compared with the observation. The PRECIS-ERA shows better skill in simulating precipitation over

northeast Thailand. All model simulations, excluding PRECIS-ECHAM4, estimated comparable precipitation totals over southern Thailand in ON representing approximately 50% of observed totals. The radiation scheme and/or land sea interaction may be related to precipitation underestimation in southern Thailand in particular. Marengo *et al*. (2009) mentioned that possible effects of local dynamic forcings, for example dry or wet soil, may be dominant over the large-scale SST forcing.

Table 5.3: p-value of precipitation produced from GCM and RCM compared with CRUTS2.1

Model simulation	P value				
	North	Northeast	Centre	Mainland	Peninsula
HadAM3P	0.878	0.472	0.910	0.538	0.010
PRECIS-HadAM3P	0.724	0.701	0.573	0.391	0.024
PRECIS-ERA40	0.534	0.594	0.939	0.442	0.016
PRECIS-ECHAM4	0.056	0.158	0.071	0.001	0.031

Results from a two-tailed t-test comparing model output with observations, CRUTS2.1, are shown in Table 5.3. The GCM and RCM excluding PRECIS-ECHAM4 are not significantly different at the 95% level of probability. Over the peninsula, the p-value is much less than 0.05 in all simulations so there are significant differences. This suggested that HADAM3P, PRECIS-HadAM3P and PRECIS-ERA40 are able to represent total precipitation over mainland Thailand.

5.2.1.2 Comparison of precipitation simulation between ERA40 and PRECIS-ERA40

Figures 5.7(a)–(c) show the value of PRECIS in its ability to realistically dynamically downscale. Over Central Thailand, the ERA40 total precipitation amount in July, August and September compared with the gridded observations reveals average relative errors underestimates of 45%, 52% and 60%, respectively, while the PRECIS-ERA40 simulates total precipitation amount in the same months with much lower

errors of 30%, 26% and 22%, respectively. This indicates that, in the summer monsoon season, the dynamical downscaling performed by PRECIS–ERA40 results in more accurately simulated precipitation amounts over this geographical area. The ERA40 strongly underestimated total precipitation mainly results from the coarse resolution, 2.5 x 2.5 degree, and may be related to (i) underestimation of atmospheric surface wind speed (ii) inaccurate cloud radiation and (iii) error of tropical deep convection cloud and low level cloud amount in particular over this geographic area which are improved with skill of PRECIS.

Over Southern Thailand, the ERA40 total precipitation amount in July, August and September underestimates the gridded observation with an average relative error of 34%, 31% and 30%, respectively, while the equivalent PRECIS-ERA40 underestimates are 54%, 56% and 50%, respectively (Figure 5.8a-c). This indicates that, in the more topographically complex peninsula area, the dynamical downscaling has not been able to add value during this summer monsoon season.

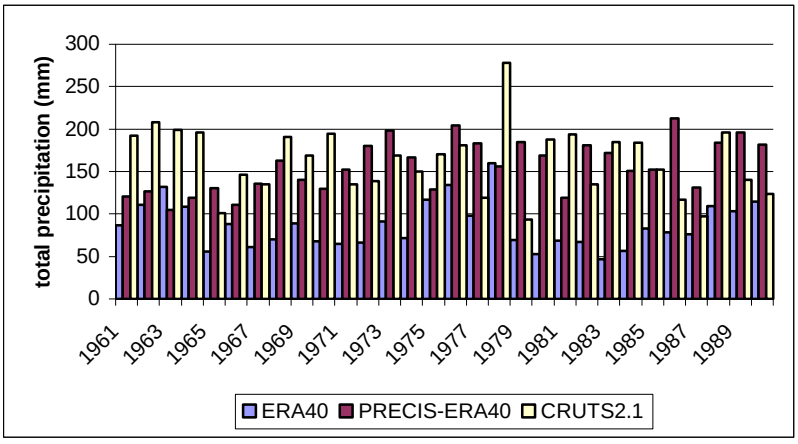

(a)

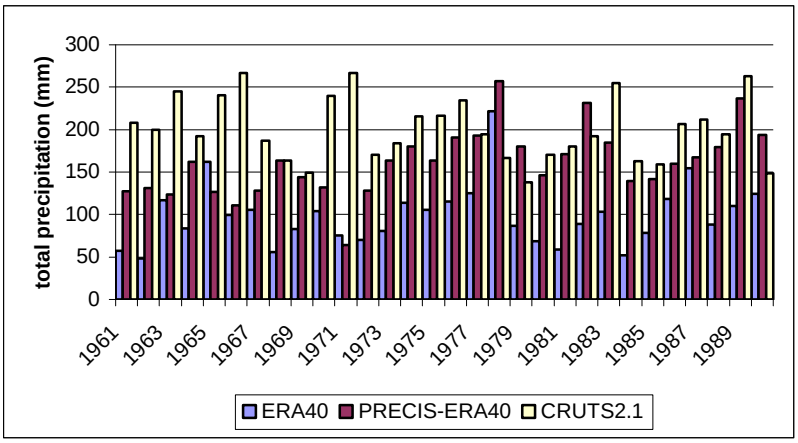

(b)

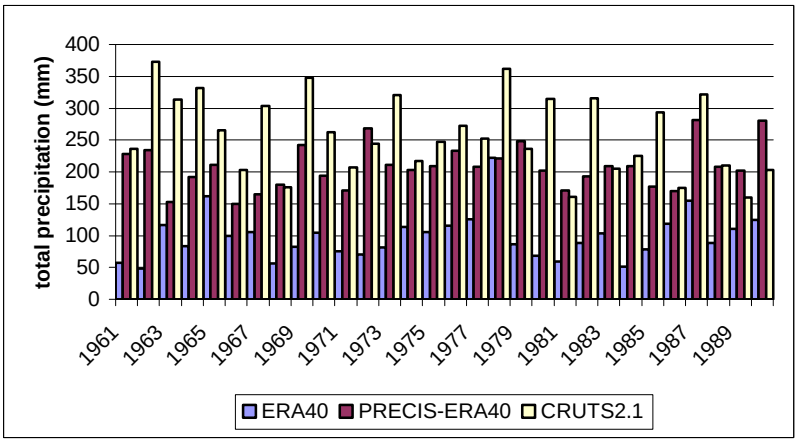

(c)

Figure 5.7: Total precipitation amount (mm) from ERA40, PRECIS-ERA40 and gridded observation during 1961-1990 over Central Thailand in (a) July (b) August (c) September

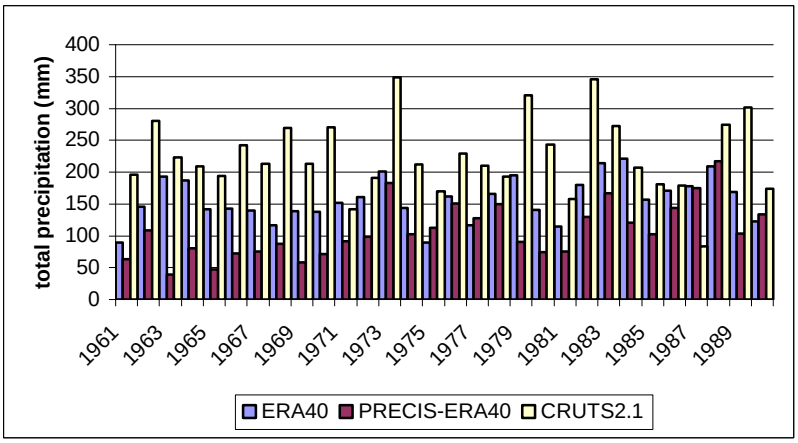

(a)

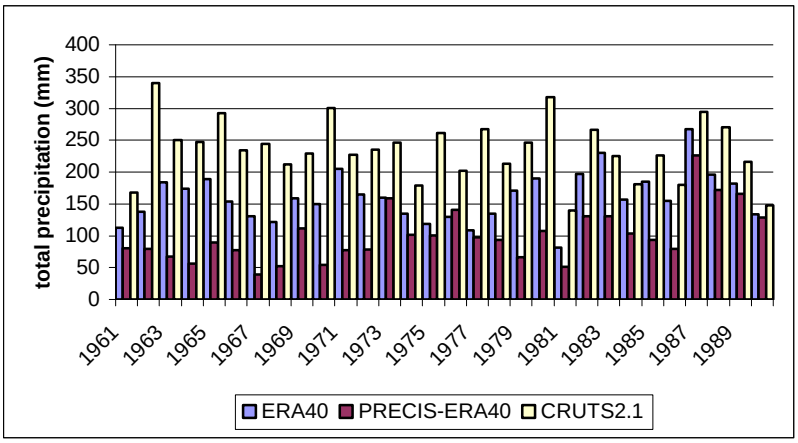

(b)

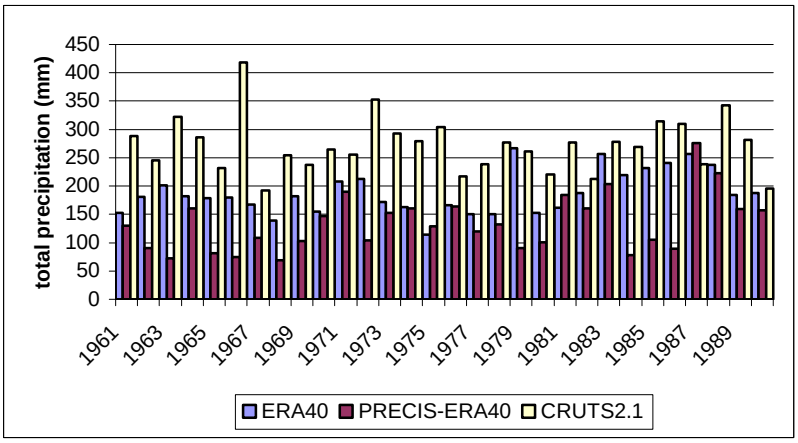

(c)

Figure 5.8: Total precipitation amount (mm) form ERA40, PRECIS-ERA40 and gridded observation during 1961-1990 over Southern Thailand in (a) July (b) August (c) September

5.2.1.3 Comparison of GCM and RCM with station observation data

Precipitation from station observations and from HadAM3P and PRECIS-HadAM3P simulations are compared using the point-to-point analysis method, comparison of a station and a nearest grid point, and shown in Figure 5.9. One nearest grid cell is appropriate enough to be compared with a station because the resolution of PRECIS in this study is 50 km so that using an average of four grid cells may be too wide to compare with a single site. PRECIS-HadAM3P and HadAM3P can be seen to be able to capture the two peaks of precipitation during the summer monsoon period. Takahashi and Yasunari (2006) demonstrated that the Indochina precipitation system

can be divided into two sub-systems in the vicinity of the climatological monsoon break; the former, secondary peak, is characterized as a monsoon southwesterly system in late May and the latter, primary peak, is characterized by tropical depression systems in September.

At the Chiang Mai site (Figure 5.9a), the GCM produces double the observed precipitation during mid May to late June and underestimates precipitation during mid July to October while the RCM produces too much precipitation in the first half of May, then produces realistic amounts during the monsoon break period (July) and also underestimates precipitation in the period mid July to October. At Phitsanulok (Figure 5.9b), the GCM produces too much precipitation for the whole period of mid March to October while the RCM simulates too much precipitation during mid May to June but is overall more realistic. In the southwest monsoon season, mountainous terrain over northern Thailand and the high plateau over north-eastern Thailand may provide up-slope heat and increased convection. Hudson (2002) concluded that PRECIS-HadAM3P over South Africa is too sensitive to the mesoscale variations in orography and the results presented here seem to concur to some degree.

The selected nearest GCM grid point to Bangkok is actually over the sea where the annual precipitation cycle is rather smooth, as can be seen in Figure 5.9(c) that means the GCM is not able to manage with the detail of coastline at this site and therefore not able to realistically simulate daily precipitation variability. Interestingly, the GCM and the RCM produce a reliable average seasonal precipitation cycle at the Ubon Ratchathani site located in northeastern Thailand. Meanwhile, the GCM produces an underestimate for precipitation over the whole year at Surat Thani and is not able to reproduce the observed maximum precipitation amount in November (Figure 5.9e). While the RCM produces too much precipitation during March and April but does a somewhat better job than the GCM through the remainder of the year. Of course it should be remembered that other types of error may be affecting the rain gauge data themselves, such as the reading practice and changes in the gauge location or local conditions near the station (urban area, vegetation) over the span of the measurements. Taking all the stations together, there is some evidence that the RCM adds some value to the GCM simulations in reproducing the station data.

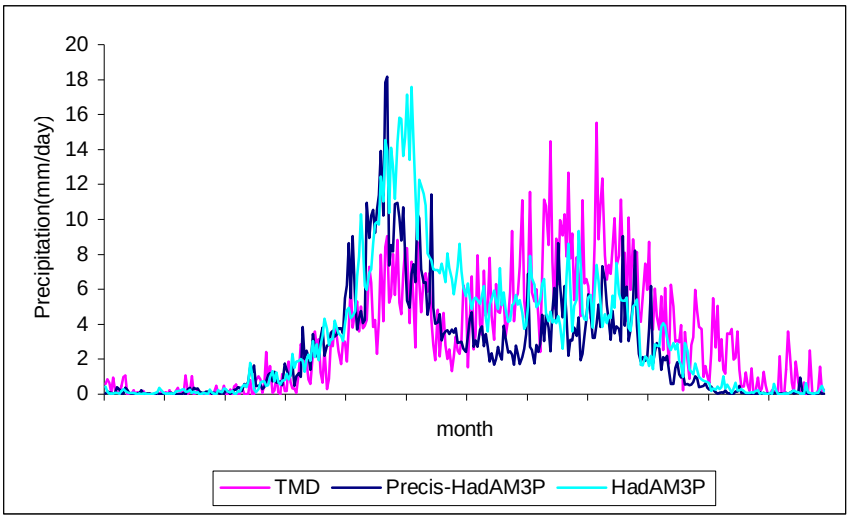
Precipitation(mm/day)
20
18
16
14
12
10
8
6
4
2
0
month
TMD
Precis-HadAM3P
HadAM3P

(a)

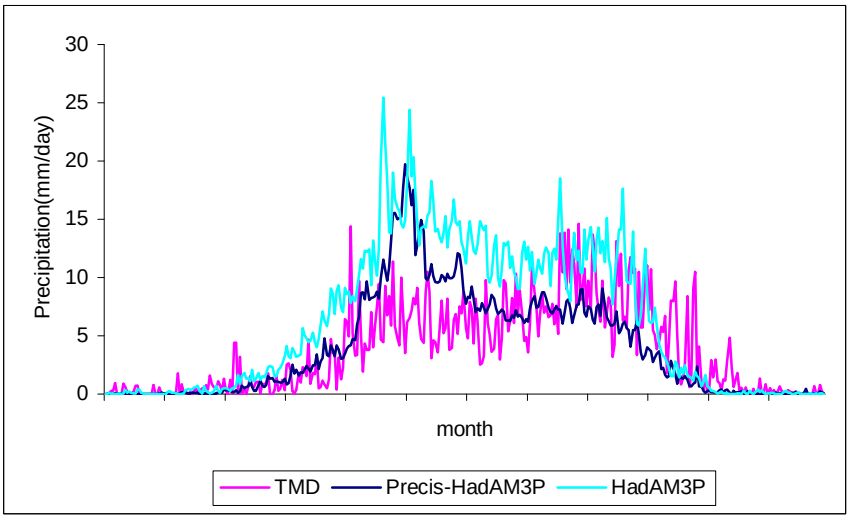
Precipitation(mm/day)
30
25
20
15
10
5
0
month
TMD
Precis-HadAM3P
HadAM3P

(b)

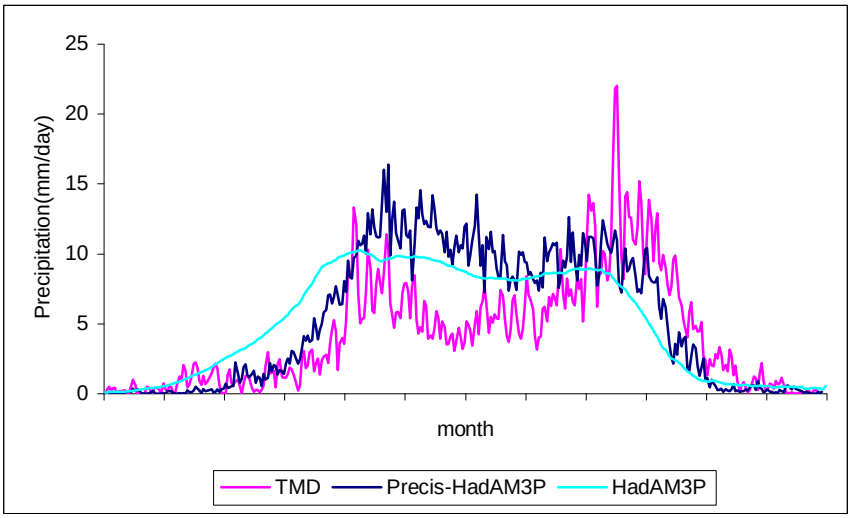
Precipitation(mm/day)
25
20
15
10
5
0
month
TMD
Precis-HadAM3P
HadAM3P

(c)

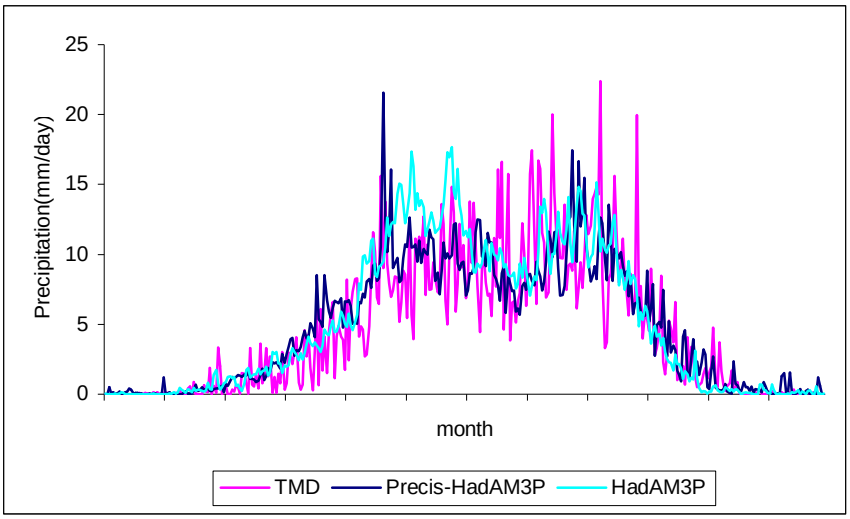

(d)

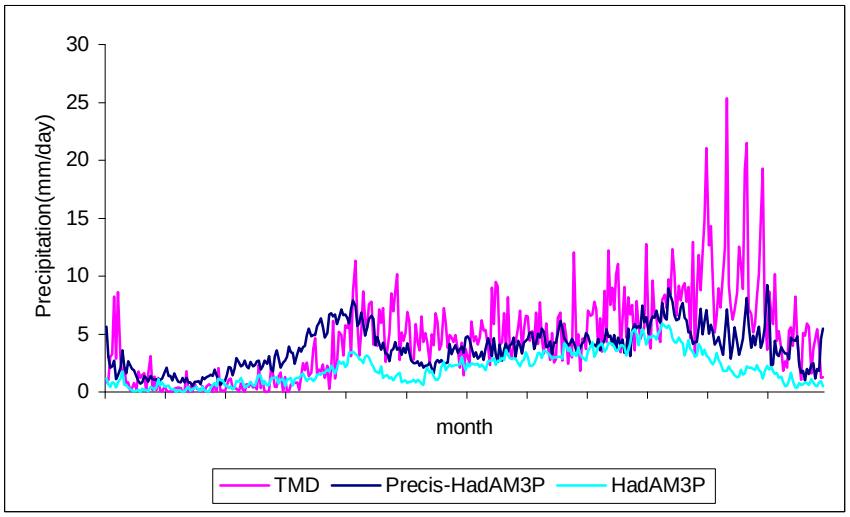

(e)

Figure 5.9: Observed and PRECIS-HadAM3P (nearest gridpoint) annual precipitation cycles for the 1961-90 period at station (a) Chiang Mai (CM) (b) Phitchanulok (Phitlok) (c) Bangkok (BKK) (d) Ubon Ratchathani (Ubon) (e) Surat Thani (Surat) [note that TMD means station observational data from Thai Meteorology Department.]

The frequency distributions of daily precipitation amounts from the PRECIS-HadAM3P RCM are compared with station observations in Figure 5.10. In general the model generates too many low precipitation events and insufficient high precipitation events. In other words, the number of extreme precipitation days in the model is lower than in observations, as shown in Table 5.4 below. Osborn and Hulme (1997) and Osborn (1997) evaluated daily precipitation characteristics of a GCM developed from

estimation in standard deviation and rain day frequency of grid-box mean. These authors applied a few stations in a GCM grid cell and they mentioned that reduction in variance as number station increases can be computed as $S_n^2 = \overline{s_i^2}\left[\frac{1+(n-1)\bar{r}}{n}\right]$ where $\overline{s_i^2}$ is the mean of station variances, S_n^2 is the variance of the combination of n station time series and $\bar{r}$ is the mean interstation correlation between all pairs of stations within the grid box considered. However, it is not possible to obtain an $\bar{r}$ value for grid boxes that have just one station in. In this thesis, with 50 km resolution RCM, each grid cell contains a single station. Therefore, standard deviations of daily precipitation time series give an indication of precipitation variability at a location (Table 5.4). A realistic model should produce a standard deviation similar to observation.

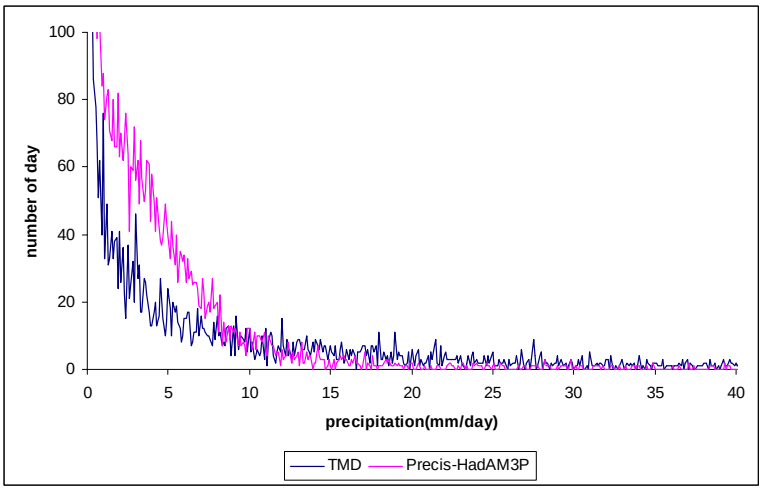

(a)

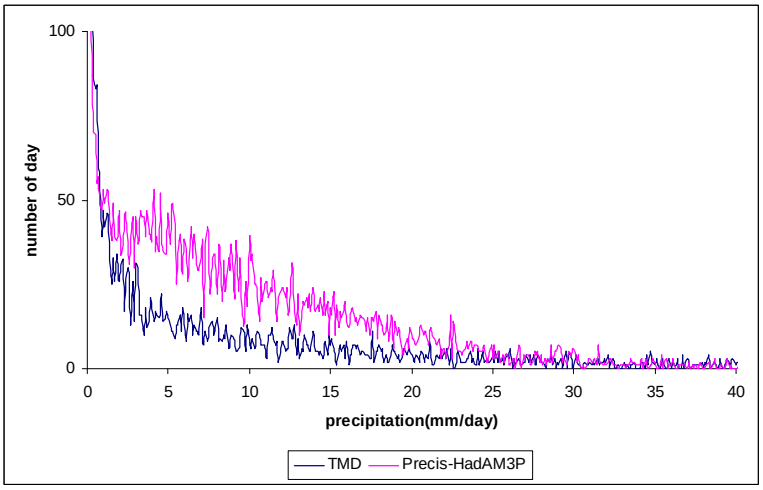

(b)

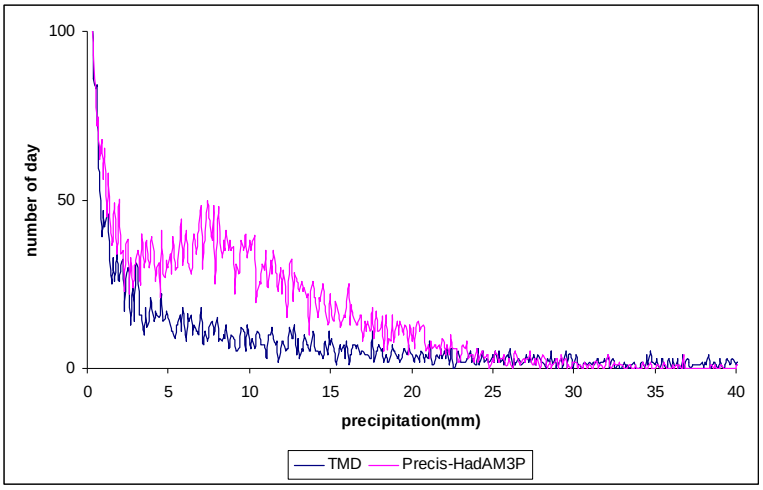

(c)

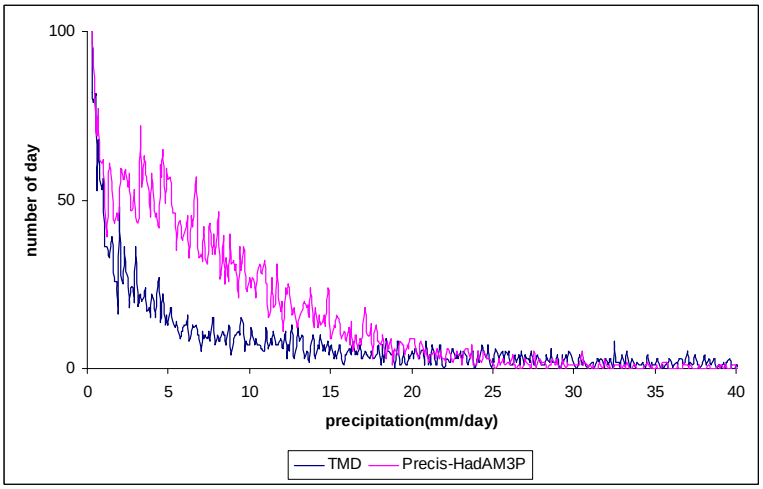

(d)

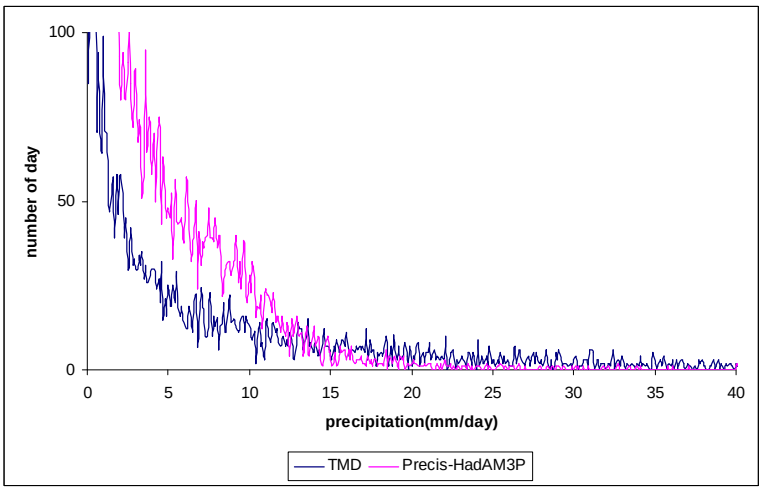

(e)

Figure 5.10: Observed and PRECIS-HadAM3P (nearest gridpoint) precipitation frequency distributions for the 1961-90 period at stations (a) CM (b) Phitlok (c) BKK (d) Ubon (e) Surat.

Table 5.4: Precipitation frequency using grid-to-grid analysis method at five stations over Thailand. In the table, TMD means the station observation data and Precis refers to the PRECIS-HadAM3P simulation.

Precipitation (per day)	Number of days (%)									
	CM		Phitlok		BKK		Ubon		Surat	
	Precis	TMD	Precis	TMD	Precis	TMD	Precis	TMD	Precis	TMD
≥0.1 mm	54.3	32.8	60.3	33.6	61.0	33.6	62.5	34.1	78.0	44.8
≥1mm	36.9	25.7	53.5	25.4	52.7	25.4	54.5	27.4	58.3	35.6
≥95th percentile of PRECIS	5.0	10.5	5.0	5.0	5.0	6.2	5.0	8.2	5.0	11.8
Standard deviation	8.4	7.9	10.9	11.1	6.4	11.4	7.8	13.0	4.7	13.2

5.2.2 Humidity fields

Over the oceans, the humidity is generally controlled by the SST for which PRECIS is forced by observation data. Vapour pressure is at a maximum near the equator and decreases polewards, largely as a function of the Clausius-Clapeyron equation; during DJF, MAM and ON, there are large differences over SEA between the land regions north and south of 16^{o}N. During JJAS the high humidity is simulated over the domain, in general, with moisture convergence prevailing over the equatorial regions in the area of the ITCZ, which is retreating and moving equatorward across Indochina. By compared with the CRUTS2.1 gridded observations, underestimations in vapour pressure were found in DJF, MAM and ON while overestimation was found in JJAS. Therefore, PRECIS-HadAM3P has a difficulty to accurately simulate humidity fields over this geographic area.

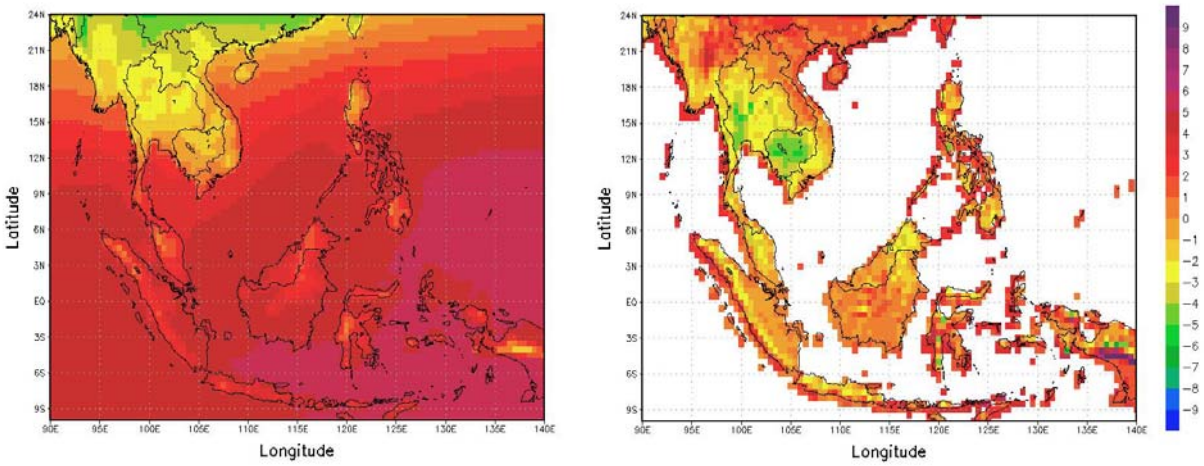
Latitude
Longitude
24N
21N
18N
15N
12N
9N
6N
3N
EQ
3S
6S
9S
90E
95E
100E
105E
110E
115E
120E
125E
130E
135E
140E
9
8
7
6
5
4
3
2
1
0
−1
−2
−3
−4
−5
−6
−7
−8
−9

(a)

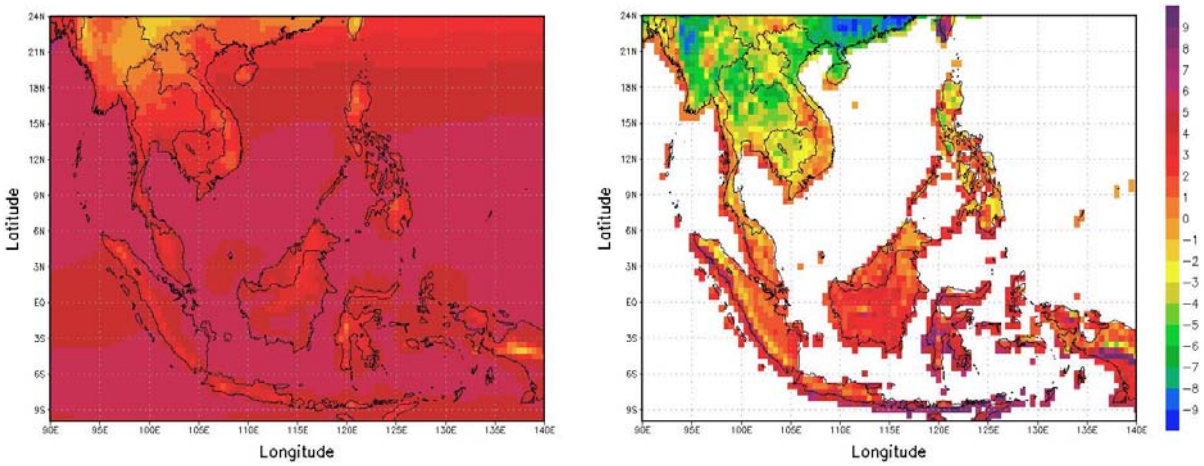
Latitude
Longitude
24N
21N
18N
15N
12N
9N
6N
3N
EQ
3S
6S
9S
90E
95E
100E
105E
110E
115E
120E
125E
130E
135E
140E
9
8
7
6
5
4
3
2
1
0
−1
−2
−3
−4
−5
−6
−7
−8
−9

(b)

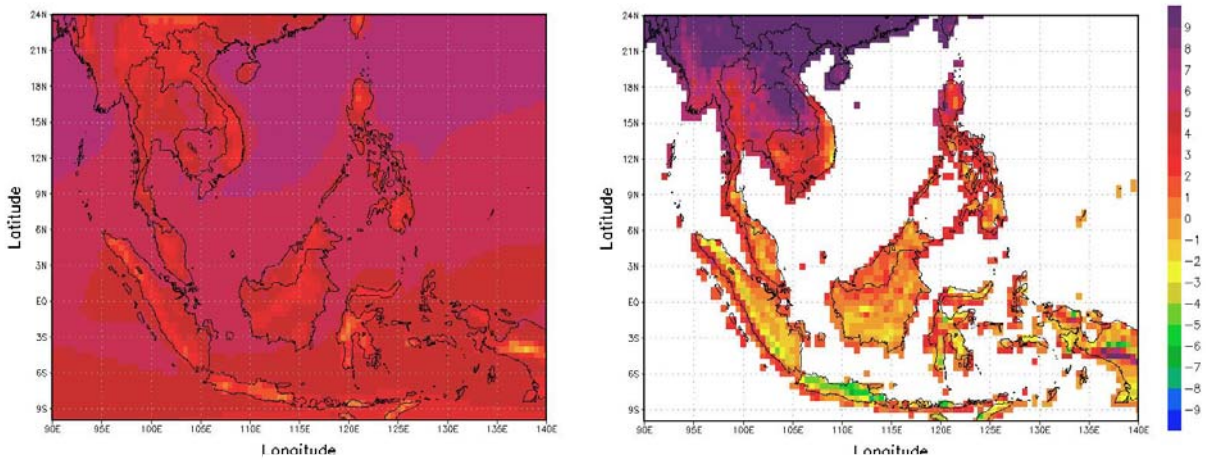

(c)

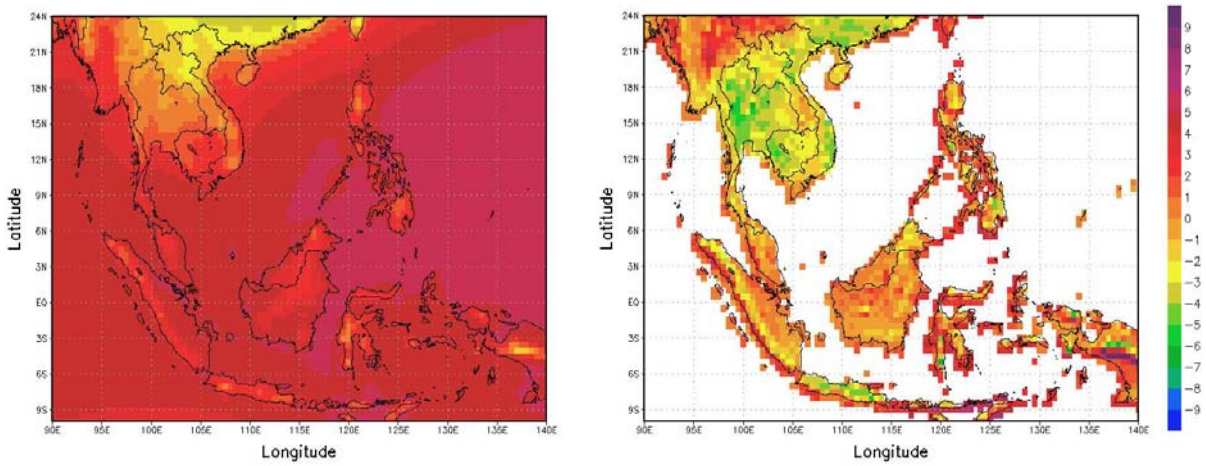

(d)

Figure 5.11: Vapour pressure fields (mb) (1961-1990) from PRECIS-HadAM3P (left) and PRECIS-HadAM3P compared with CRUTS2.1 (right) during (a) DJF (b) MAM (c) JJAS (d) ON

The IPCC AR4 report (IPCC, 2007) highlights that precipitation patterns are intimately linked to atmospheric humidity, evaporation, condensation and transport processes, therefore the model simulation of the seasonal cycle of vapour pressure is also compared with observational data in Figure 5.12

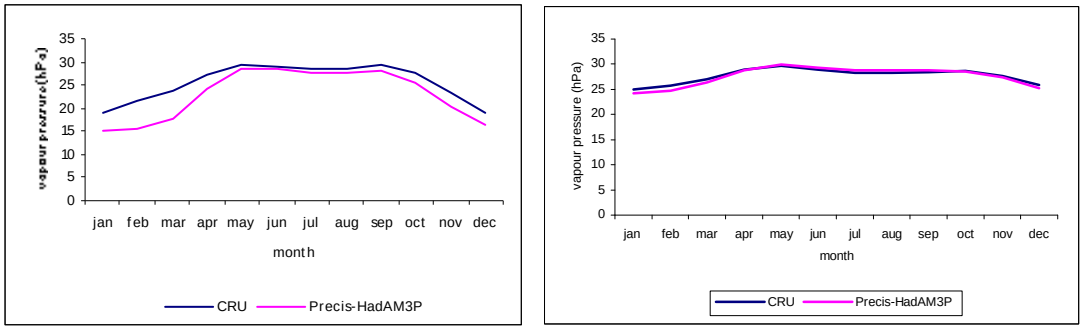

Figure 5.12: CRU and Precis-HadAM3P surface vapour pressure annual cycle (1961-1990) over central Thailand (left) and southern (peninsular) Thailand (right)

PRECIS-HadAM3P simulates too little humidity over central and northern Thailand, during the period December-April, and so this could be one of the possible causes for underestimated precipitation amount as shown in Figure 5.11. Meanwhile the model produced vapour pressure reasonably over the largely marine environment of the peninsula. This suggests a deficiency in the simulation of the water cycle, perhaps through land-atmosphere interactions, over more continental areas.

5.2.3 Wet days

Overall, the PRECIS simulations slightly overestimate the frequency of wet days, confirming the earlier analysis of frequency distributions and Figure 5.15. Considering the highest precipitation amounts during JJAS along Burma's west coast, as shown in Figure 5.1, and the spatial distribution of the number of wet days shown in Figure 5.13, the PRECIS model simulates total precipitation amount fairly accurately through an underestimate of precipitation intensity but an overestimate of wet day frequency. The same performances among PRECIS-HadAM3P, PRECIS-ERA40 and PRECIS-ECHAM4 also appear over central Thailand. The PRECIS-ECHAM4 number of wet days over the peninsula of Thailand is notably fewer than in the other model simulations, on top of the underestimate in precipitation intensity shown in Table 5.4.

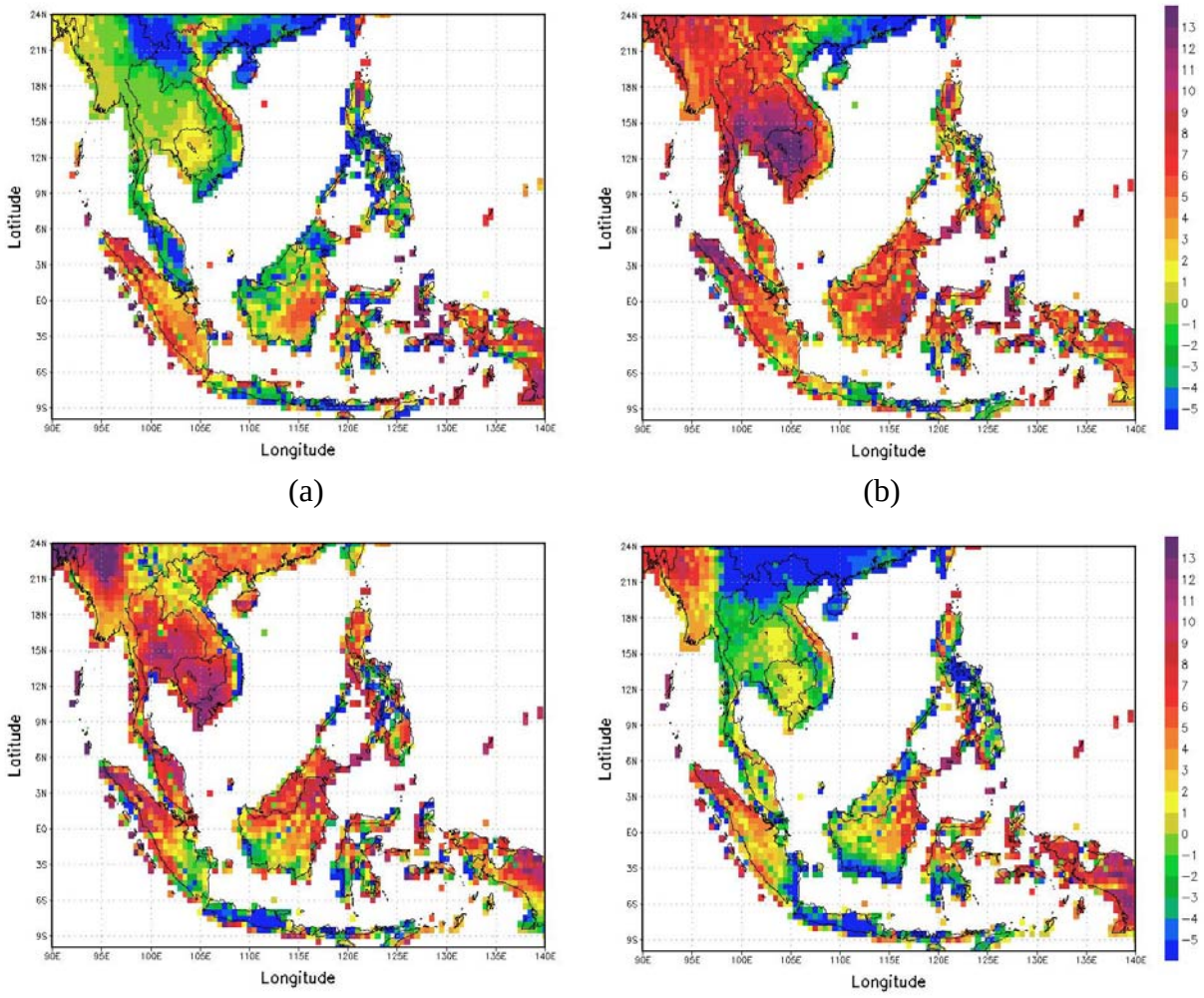

Figure 5.13: Difference between numbers of wet days (>1mm) (1961-1990) from PRECIS-HadAM3P compared with CRUTS2.1 during (a) DJF (b) MAM (c) JJAS (d) ON.

The annual precipitation cycle for 4 selected areas in Thailand is presented in Figure 5.14. The two precipitation peaks occur during the southwest monsoon period (mid May to mid September). The annual cycle test over the area of Peninsular Thailand simulated by ERA40 shows the closest pattern to CRUTS2.1, as would be expected given the nature of a reanalysis. However, over the other regions of the country, ERA40 strongly underestimates precipitation because the ERA 40 data during 1957-1972 represents the pre-satellite observation period. It is also reported that ERA40 underestimated the climatology of clear-sky outgoing longwave radiation by around 10 Wm^{-2} and clear-sky absorbed solar radiation by around 30 Wm^{-2} as well as cloud

fraction over tropical convection regions (Allan et al., 2004). Moreover, these same authors mentioned that ERA40 may underestimate humidity over tropical ocean regions. In general, the GCMs and RCM simulate that the first precipitation peak arrives in Peninsular Thailand in May, the same month as in central Thailand, because of the arrival of the southwest monsoon. During the month of May, the southwest monsoon gradually reaches the southern part of mainland Thailand but the northern part is in a transition period. The beginning of the monsoon in the northern part is more irregular, varying from May until June. Deep convection over the South China Sea (SCS) is detected. Cyclonic disturbances usually move with the monsoon air flow and can develop into typhoons. Convection is the key process for bringing precipitation especially at latitude 10^{o}N. Therefore the possible causes of overestimating precipitation during May could be (i) the earlier monsoon onset (ii) too much deep convection generated over the SCS and around the latitude of 10^{o}N. The later peak is observed in November in observations while PRECIS peaks one month earlier. Clearly, the PRECIS-ECHAM4 is not able to calculate either the first arrival of heavy precipitation in May or the later one.

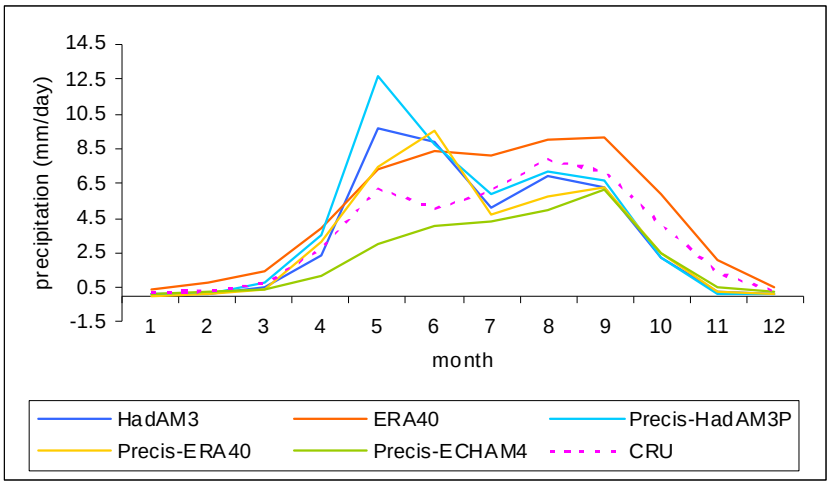

(a)

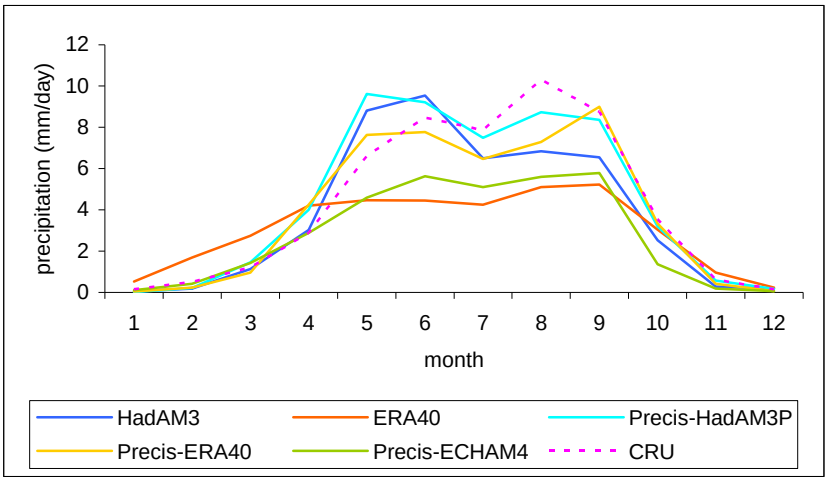

(b)

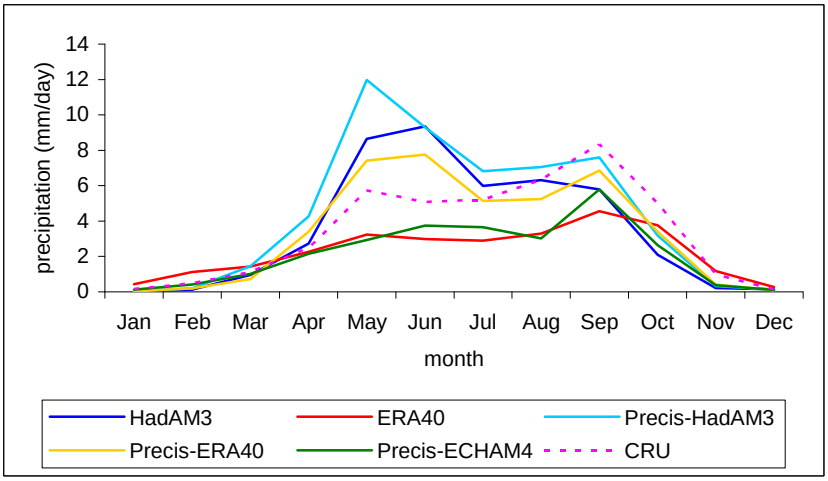

(c)

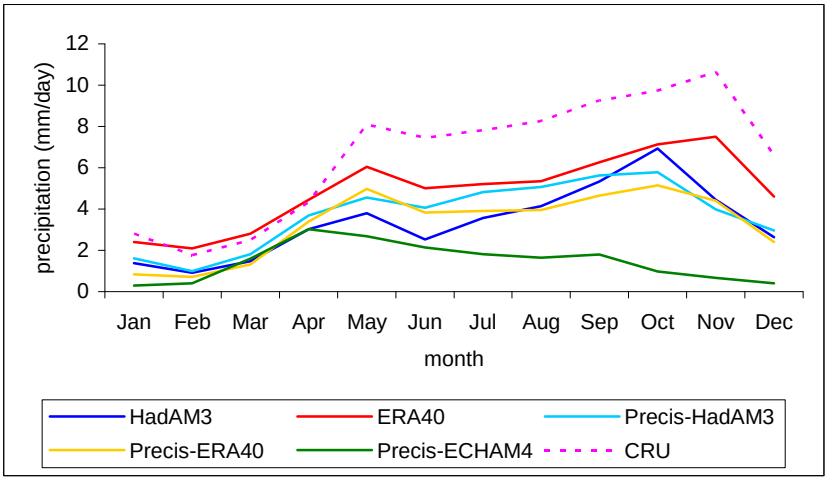

(d)

Figure 5.14: 30 year precipitation annual cycle (1961-1960) over (a) northern (b) northeastern (c) central (d) peninsular Thailand.

The PRECIS-ERA40 and PRECIS-ECHAM4 produce the first peak of precipitation in June while the ERA40 and PRECIS-HadAM3P produce the peak correctly in May. The PRECIS-HadAM3P and PRECIS-ERA40 overestimate precipitation by 58.6% and 30.8% in May. All RCM ensemble members and ERA40 perform correctly in simulating the timing of the secondary peak, although the magnitude of the latter is underestimated for PRECIS-HadAM3P, PRECIS-ERA40, PRECIS-ECHAM4 and ERA40 by about 10%, 15.1%, 30.9% and 74.8%, respectively. In some cases, HadAM3 is performing better than PRECIS, producing less precipitation than the RCM, for example, in the onset month of May in northern, northeastern and central Thailand. The RCM is likely to reproduce the convection which is activated at the lee-side foot of two mountainous regions located in western and central Thailand during the daytime and to extend that precipitation during the night time over inland regions far downwind from the mountains themselves. Generally, RCM simulations show more precipitation than driving GCM simulations because in the RCM there is more convective and large scale precipitation throughout the seasonal cycle as well as a more active hydrological cycle compared to the driving GCM (Hudson and Jone, 2002). However, during the southwest monsoon, the RCM performances are closer to the observations.

Interestingly, PRECIS-HadAM3 produced wetter conditions than other simulations from the warming month of March to the intermonsoon month of October over northern, northeastern and central Thailand, however, a significant positive bias in precipitation during May and June and a slight negative bias in the later active monsoon period, July-September, were detected (Figure 5.14 and 5.15) which is similar to the findings with the station analysis (Figure 5.9 and 5.10). The bias may be partially related to the tropical region where more optically thick clouds are simulated than are observed (Hudson and Jones, 2002) and Figure 5.16 shows total cloud fraction slightly in excess of observations. However, there is mix bias in precipitation during JJAS that implied that the systematic model error which could be error in the wind and pressure field through the lateral boundaries (Hudson and Jones, 2002). That possibly produced convergence condition at low level and divergence condition in upper level of the atmosphere which promoted strong updraft and positive precipitation over the region during the beginning of southwest monsoon active combined with orographic convection from the Bay of Bengal. In the other hand, all

model simulations produced negative bias in precipitation throughout the year with excessive of wet day during most of year and cloud fraction closed to observation during JJAS, this due to RCM calculated precipitation less than the actual condition which may related to the limitation of hygroscopic nuclei, which water vapour can condense, over the region surrounding with the ocean which could be one of recommendations for further study.

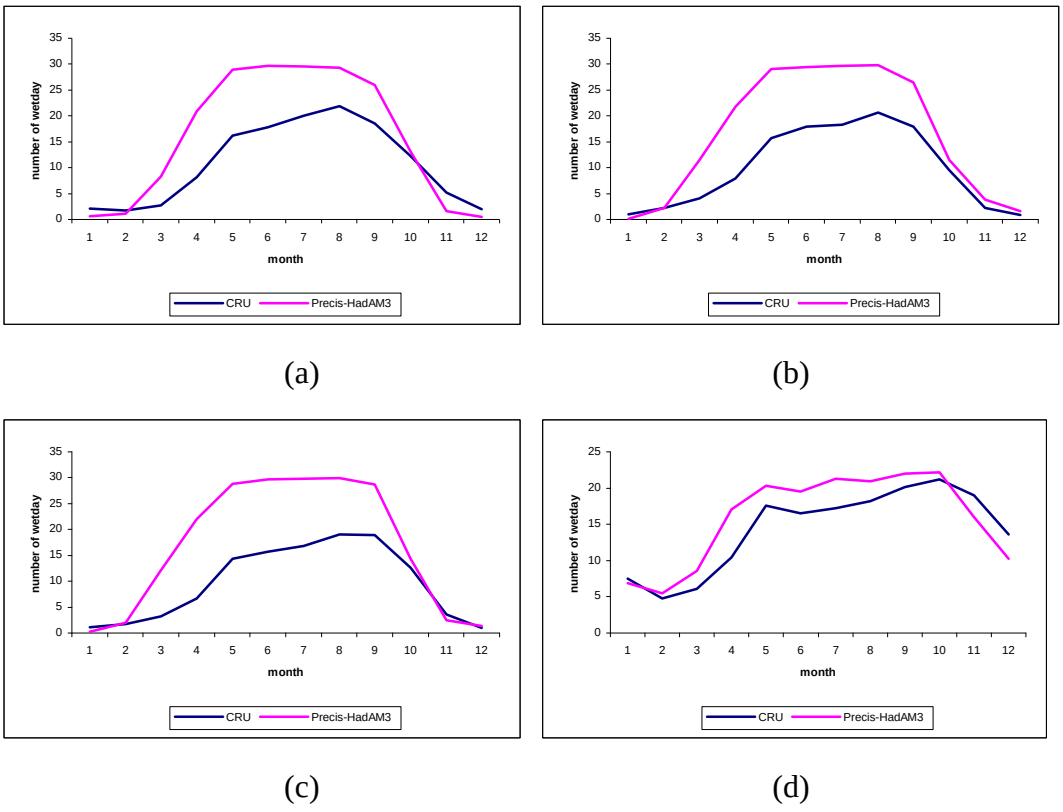

Figure 5.15: CRUTS2.1 and PRECIS-HadAM3 annual cycle in the average number of wet days (1961-1960) over (a) northern (b) northeastern (c) central (d) Peninsular Thailand

Since precipitation over the tropics is dominated by convection it is clearly relevant to consider model simulation of cloud amount (Figure 5.16). The modelled annual cycle of total cloud fraction in Central Thailand is fairly realistic (Figure 5.16).While the model looks acceptable in creating cloud over the peninsula during the active southwest monsoon period, it significantly underestimates total cloud amount during the northeast monsoon and this affects precipitation amount in November as shown in Figure 5.15.

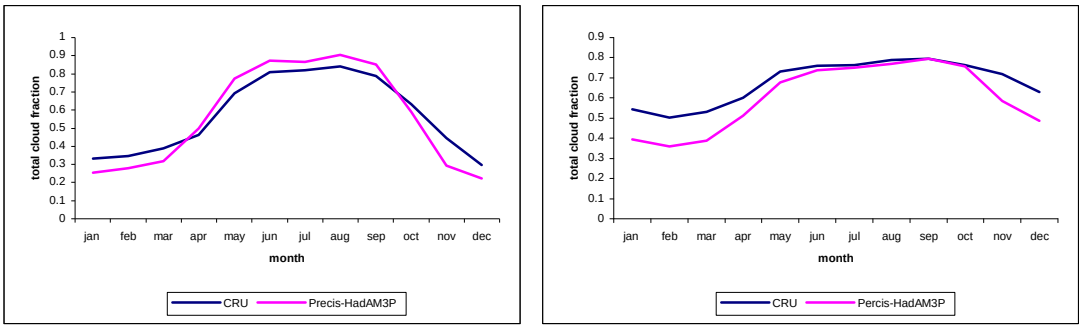

Figure 5.16: Annual Cycle of observed and PRECIS-HadAM3P total cloud fraction (1961-1990) over Central Thailand (left) and Southern (Peninsular) Thailand (right).

Figure 5.17 shows how much agreement during June to September precipitation was found between PRECIS driven by the reanalysis data, ERA40, and the gridded observations in the Central Thailand region. Most of the model overestimates are within a factor of two of the observations except in the month of May. It is found that during the southwest monsoon period, PRECIS has difficulties realistically simulating precipitation in the month of monsoon onset which may be related to the earlier monsoon arrival in central Thailand or to too much convective precipitation simulation.

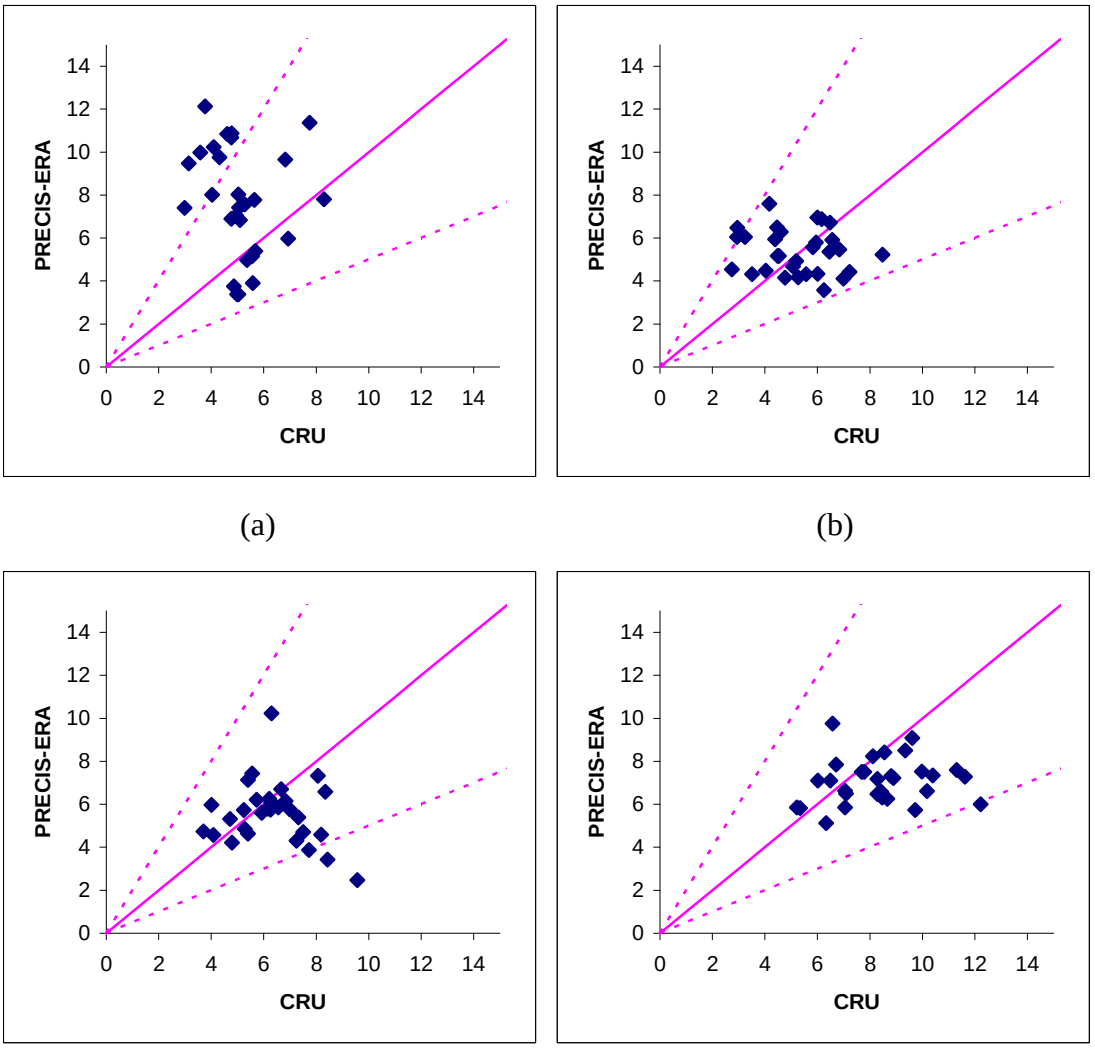

(a) (b)

(c) (d)

Figure 5.17: Observed (CRUTS2.1) and Modelled (PRECIS-ERA40) monthly average precipitation (mm/day) (1961-1990) over Central Thailand in the month of (a) June (b) July (c) August (d) September.

If we now consider equivalent results for peninsular Thailand for the months of May-November, the scattering of the PRECIS-ERA40 and CRUTS2.1 data seem similar each month which would appear to suggest a systematic negative bias in the model (Figure 5.18). The radiation scheme and/or land sea interaction may be related to precipitation underestimation in southern Thailand in particular. Marengo *et al.* (2009) mentioned that the possible effect of local dynamic forcings, for example dry or wet soil, may be dominant over the large-scale SST forcing.

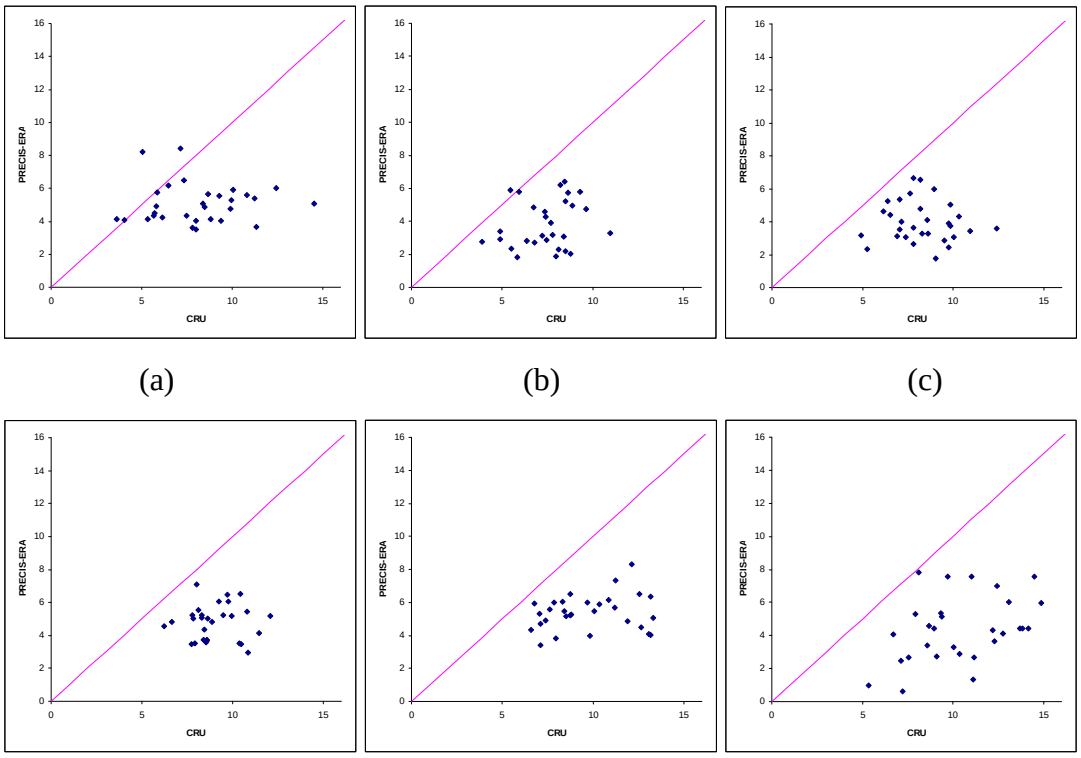

(a) (b) (c)

(d) (e) (f)

Figure 5.18: PRECIS-ERA40 modelled and observed (CRUTS2.1) monthly average precipitation (mm/day) (1961-1990) over peninsular Thailand in the months of (a) May (b) June (c) August (d) September (e) October (f) November [note that July shows the same pattern as June]

In summary, PRECIS simulations run with and without interactive sulphur cycle, show insignificant differences in spatial and point precipitation analysis, moreover, in terms of simulations driven from different initial conditions of HadAM3P, a 150 km resolution version of the Hadley Centre's global atmosphere-only model, using observed time series of HadISST SST and sea-ice for 1960-1990, there is also no significant difference in output (Table 5.1 and 5.2). Applying the grid-to-grid analysis method, there is a striking difference in the sign of bias between the north and south of the domain indicating that model biases over SEA more likely depend on geographical location. In PRECIS simulation over other parts of the world, precipitation bias more likely depends on season, for example, underestimation (overestimation) during summer (winter) possibly responding to hydrostatic restriction as PRECIS fails to realistically simulate convective precipitation (Hudson and Jones, 2002, Alves and Marengo, 2009, Shahgedanova et al., 2010). Generally, RCM simulations show more precipitation than driving GCM simulations because in

the RCM there is more convective and large scale precipitation throughout the seasonal cycle as well as a more active hydrological cycle compared to the driving GCM (Hudson and Jones, 2002). Therefore, the possible cause of the bias would be gridded observation quality and/or RCM error.

PRECIS is able to add value to the driving GCM during the active monsoon season, JJAS (Figure 5.6). The negative bias occurring over the peninsula implied that the convection scheme and/or physical parameterization fails to fully reproduce precipitation over the region. Even with improved boundary conditions, the skill of dynamical downscaling was also controlled by the regional scale forcings which may include orography, land-sea contrast, vegetation cover, lake effects, or they may be anthropogenic for example air pollution, urban heat island, and land and water management. The radiation scheme and/or land sea interaction may be related to precipitation underestimation in southern Thailand in particular. Marengo *et al*. (2009) mentioned that the effect of local dynamic forcing for example of dry or wet soil, may be dominant over the large-scale SST forcing. Applying the point-to-point analysis method, there is evidence that the RCM adds some value to the GCM simulations in reproducing the station data, however, PREICS generates too many low precipitation events and insufficient high precipitation events and these biases are unlikely to be due to large biases in the humidity fields. Hence the bias may be partially related to the tropical region where more optically thick cloud is simulated than observed (Hudson and Jones, 2002); total cloud fraction slightly in excess of the observations was found in this study (Figure5.16) which could be related to an error in the wind and pressure field through the lateral boundaries (Hudson and Jones, 2002).

5.2.4 Surface Temperature

The RCM results, which are available at a resolution of 0.44^{o}x0.44^{o}, are first re-interpolated to the 0.5^{o}x0.5^{o} resolution of the CRUTS2.1 grid.

5.2.4.1 GCM and RCM compared with the gridded CRUTS2.1 observations

Figures-5.22 shows**,** in general, that the GCM and RCM simulations underestimate (overestimate) maximum temperature north (south) of 12^{o}N during JJAS and ON, excluding PRECIS-ECHAM which is too warm in all seasons. . PRECIS-HadAM3P simulated the surface maximum temperature quite realistically over Thailand with a cold bias mostly less than 3°C during JJAS and ON. The RCM simulated surface maximum temperature with a negative bias while the GCM simulated the temperature with positive bias. Biases in maximum temperature are consistent with biases in precipitation, negative (positive) temperature biases were found mostly over Thailand where precipitation was overestimated (Figure 5.4 and 5.22) which is the same finding as Solman et al. (2007). The negative bias is also related to vertical updraft (Figure 5.33). This cold bias is unlikely to be due to gridded observations but more likely due to PRECIS itself. During DJF, all simulations produce overestimated maximum temperature except over the northern Vietnam, Laos and Burma region, while during MAM, all model simulations have a tendency to produce conditions which are too warm, except PRECIS-HadAM3P which underestimates maximum temperature over central Thailand. The difference of regional maximum temperature compared with the gridded observation data set is shown in Figure 5.23 with detail for northern and mainland Thailand. In summary, PRECIS is able to most accurately simulate the maximum temperature field over these regions.

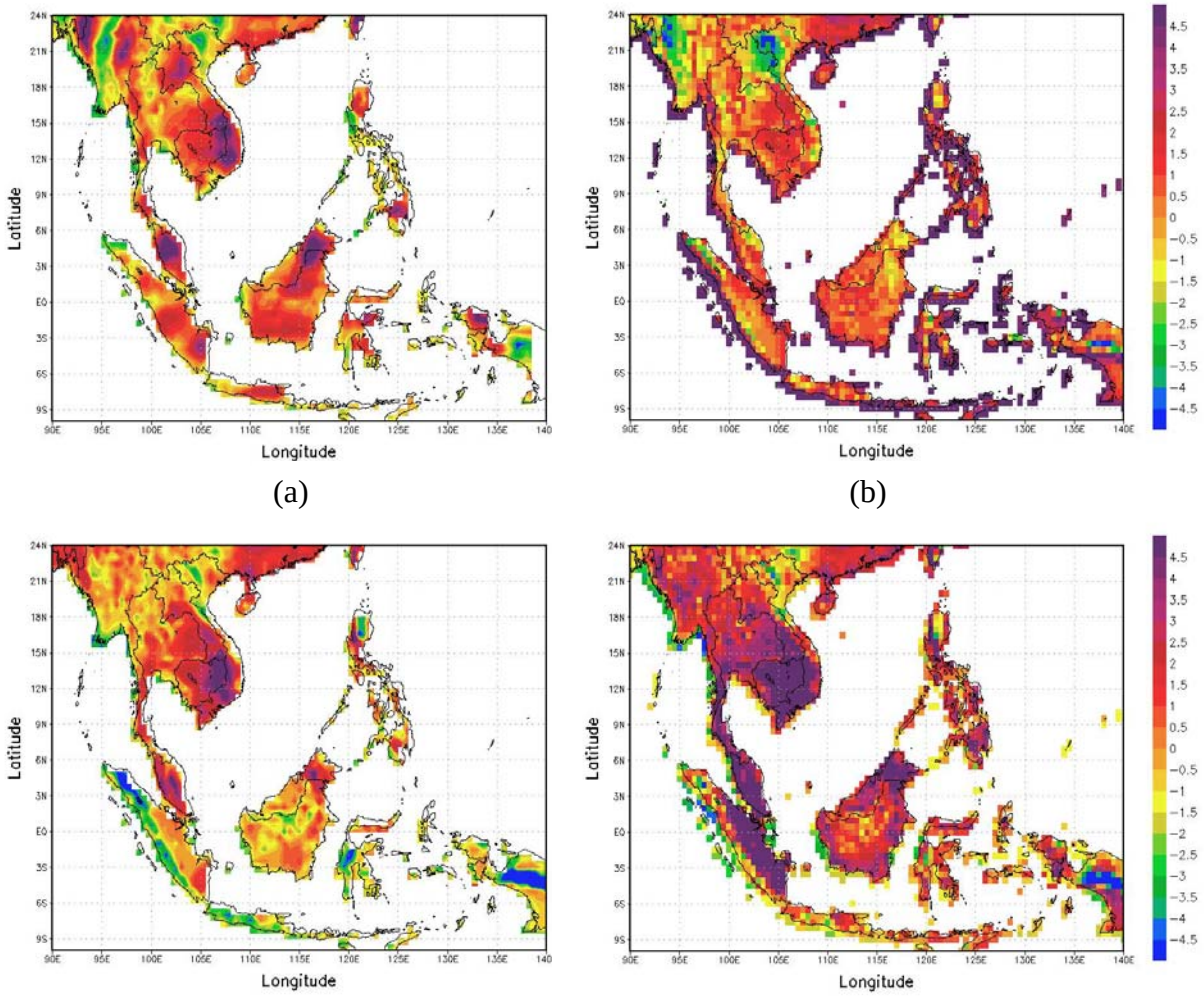

Figure 5.19: Difference between model and observations (CRUTS2.1) of average surface maximum temperature (^{o}C) in the period of 1961-1990 during DJF (a) HadAM3P (b) PRECIS-HadAM3P (c) PRECIS-ERA40 (d) PRECIS-ECHAM4

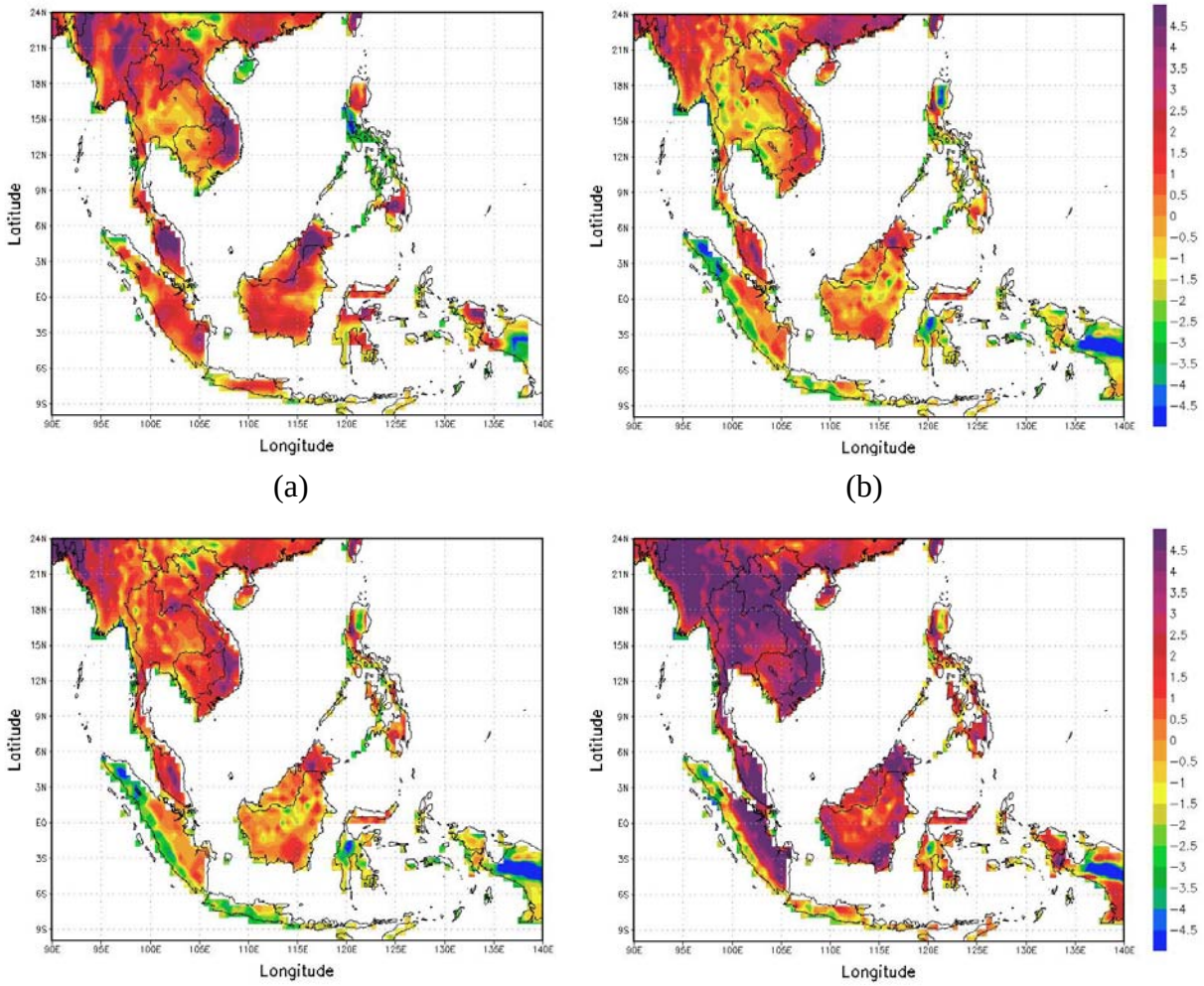

Figure 5.20: Difference between model and observations (CRUTS2.1) of average surface maximum temperature (^{o}C) in the period of 1961-1990 during MAM (a) HadAM3P (b) PRECIS-HadAM3P (c) PRECIS-ERA40 (d) PRECIS-ECHAM4

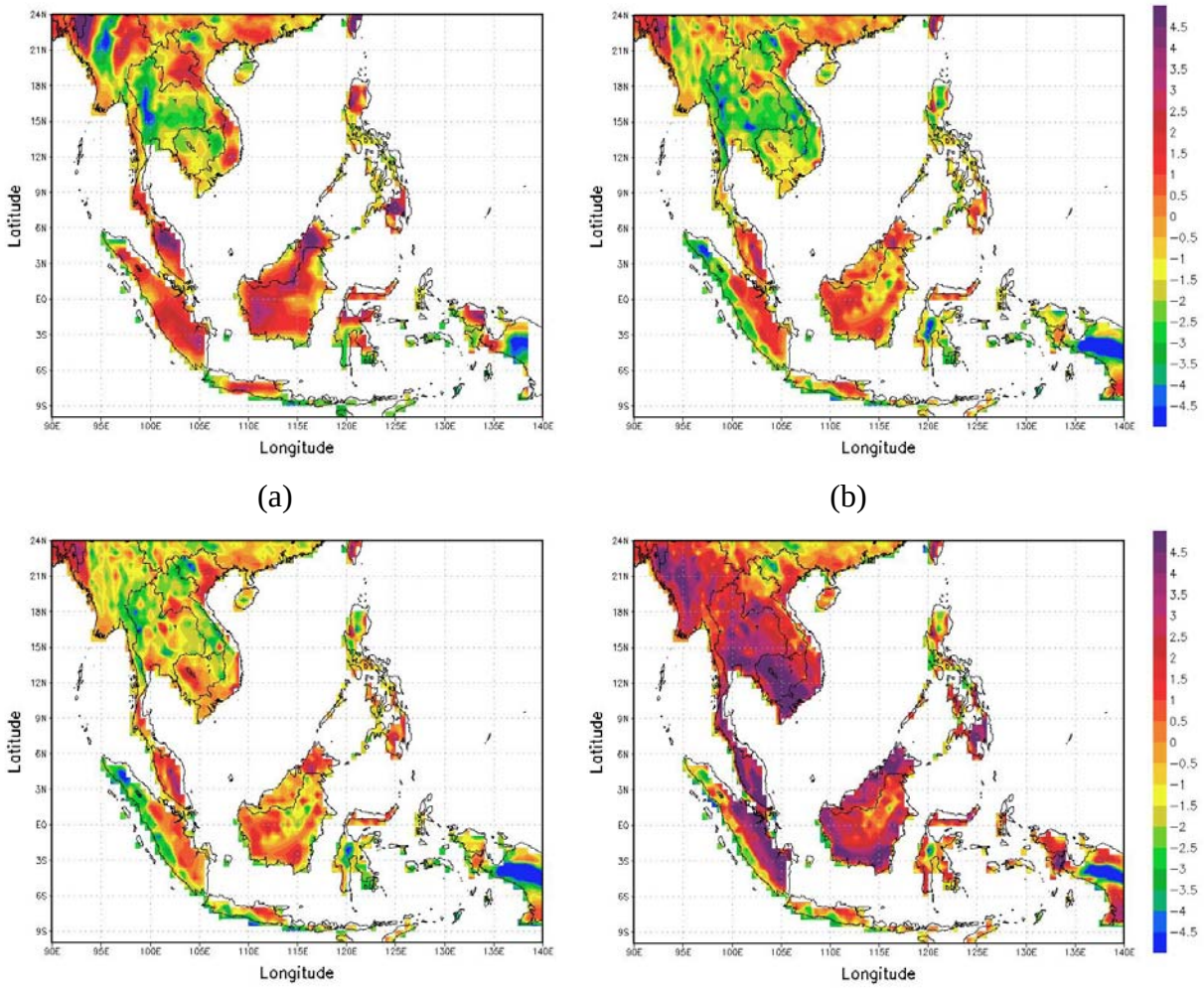

Figure 5.21: Difference between model and observations (CRUTS2.1) of average surface maximum temperature (^{o}C) in the period of 1961-1990 during JJAS (a) HadAM3P (b) PRECIS-HadAM3P (c) PRECIS-ERA40 (d) PRECIS-ECHAM4

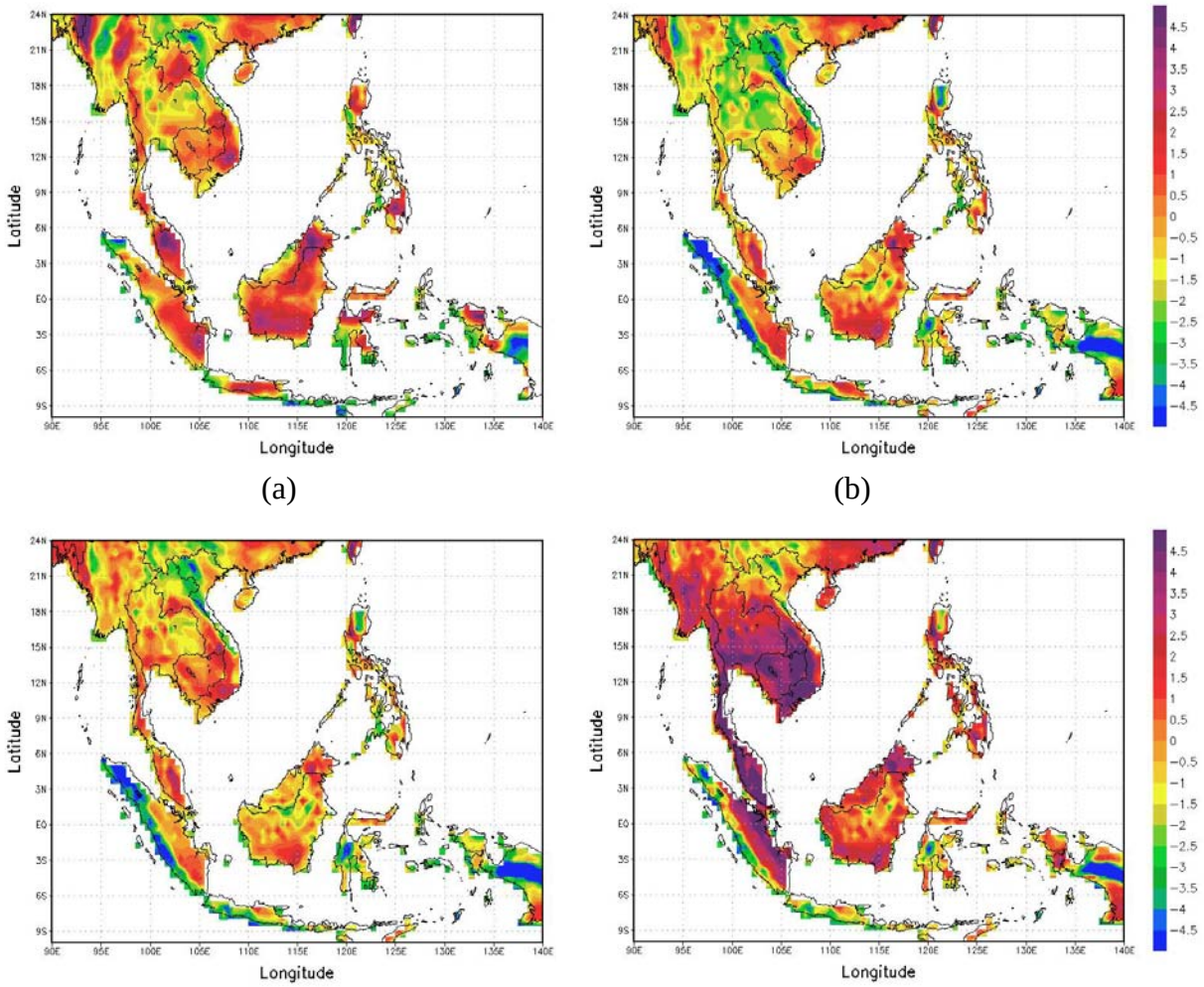

Figure 5.22: Difference between model and observations (CRUTS2.1) of average surface maximum temperature (^{o}C) in the period of 1961-1990 during ON (a) HadAM3P (b) PRECIS-HadAM3P (c) PRECIS-ERA40 (d) PRECIS-ECHAM4

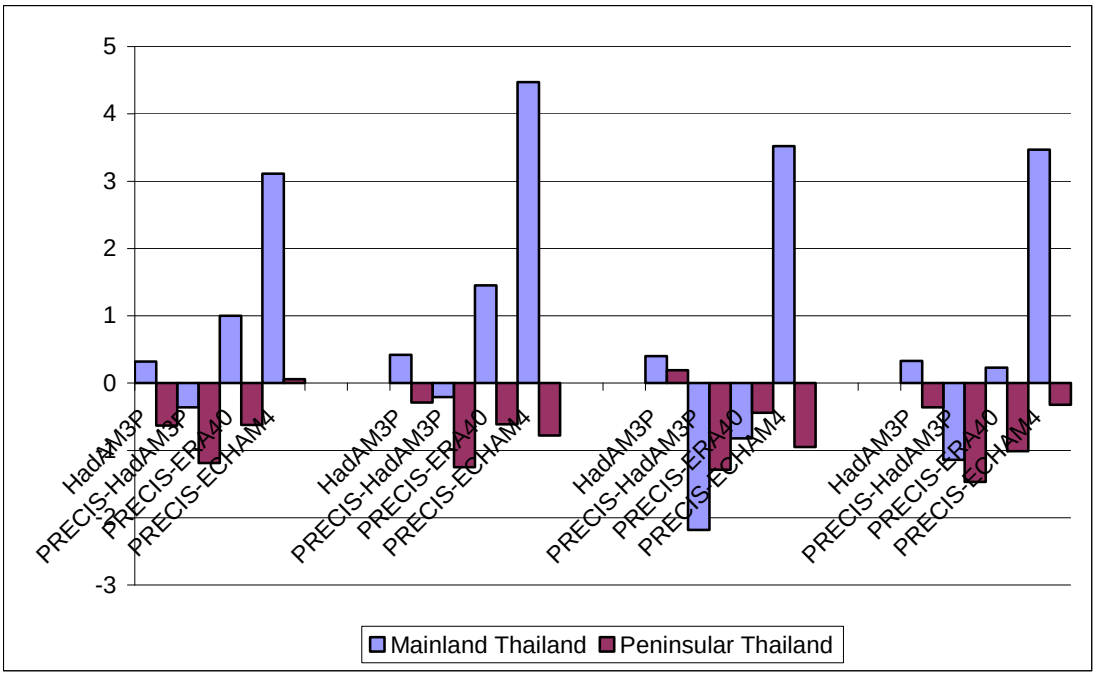

Figure 5.23: The seasonal maximum temperature difference of GCM and RCM compared with the gridded CRUTS2.1. [Note that the four groups in the graph represent the seasons, DJF, MAM, JJAS and ON].

Figures 5.24-5.27 show that**,** in general, all model simulations produce overestimated minimum temperature for the whole domain during DJF, MAM and JJAS. Warm biases were found in both the driving GCM, HadAM3P, and PRECIS with maximum magnitude of 5.5°C, 3°C and 1°C for PRECIS-ECHAM4, PRECIS-ERA40 and PRECIS-HadAM3P respectively (Figure 5.28). Interestingly, the GCM shows smallest (largest) positive bias over mainland (peninsular) Thailand neglecting PRECIS-ECHAM4 simulation (Figure 5.28 and 5.30). This would be an expectation of GCM skill, providing a good simulation of a large scale climate regime over an aggregated area of mainland Thailand while the limitation of GCM skill was found over coastal region. The largest warm bias in PRECIS-ECHAM4 may be due to the insufficiency of driving boundary condition. In summary, the GCM is able to calculate most accurately the minimum temperature over mainland Thailand while PRECIS-HadAM3P and PRECIS-ERA simulate minimum temperature reasonably well over peninsular Thailand.

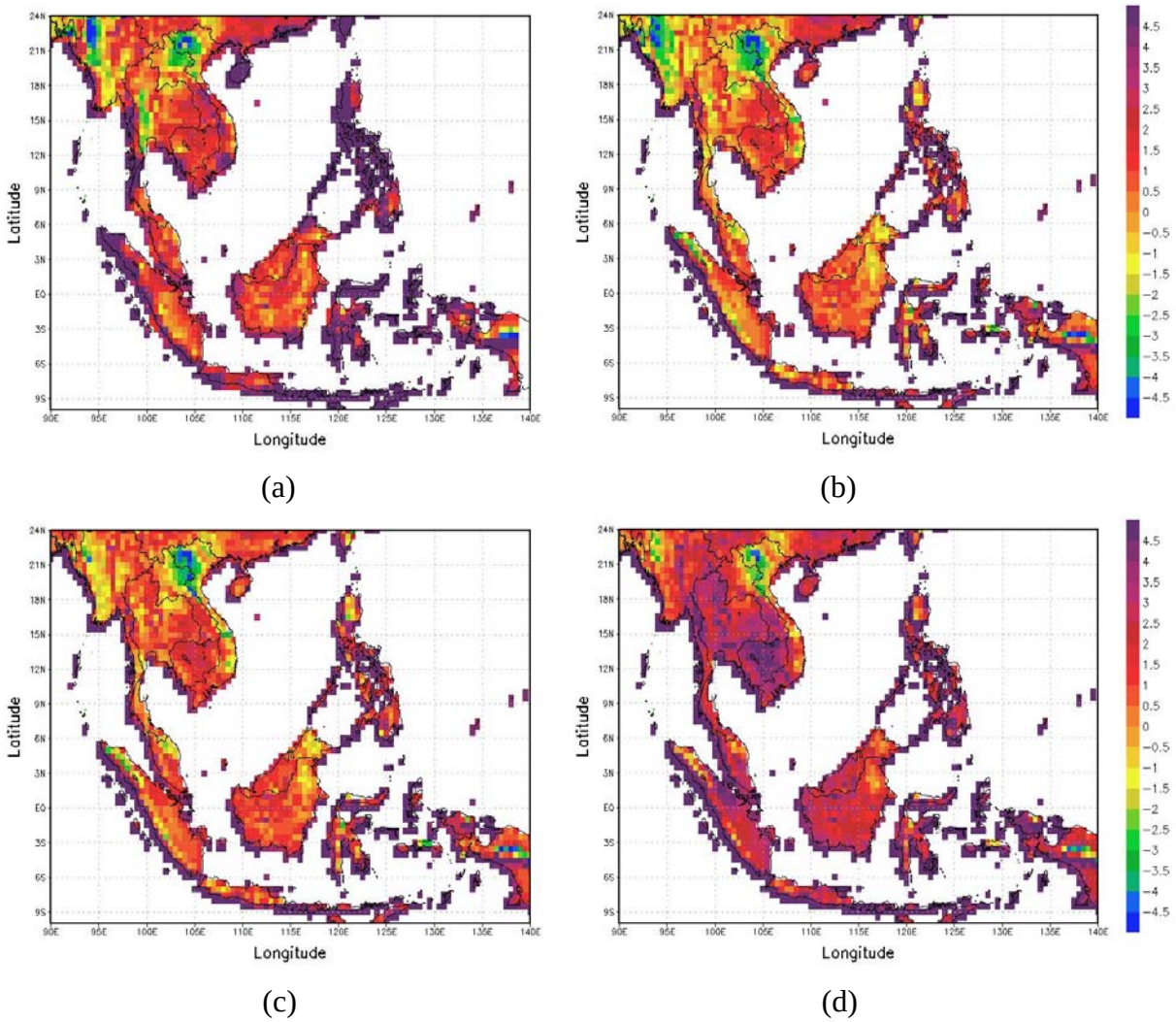

Figure 5.24: Difference between model and observations (CRUTS2.1) of average surface minimum temperature (^{o}C) in the period of 1961-1990 during DJF (a) HadAM3P (b) PRECIS-HadAM3P (c) PRECIS-ERA40 (d) PRECIS-ECHAM4

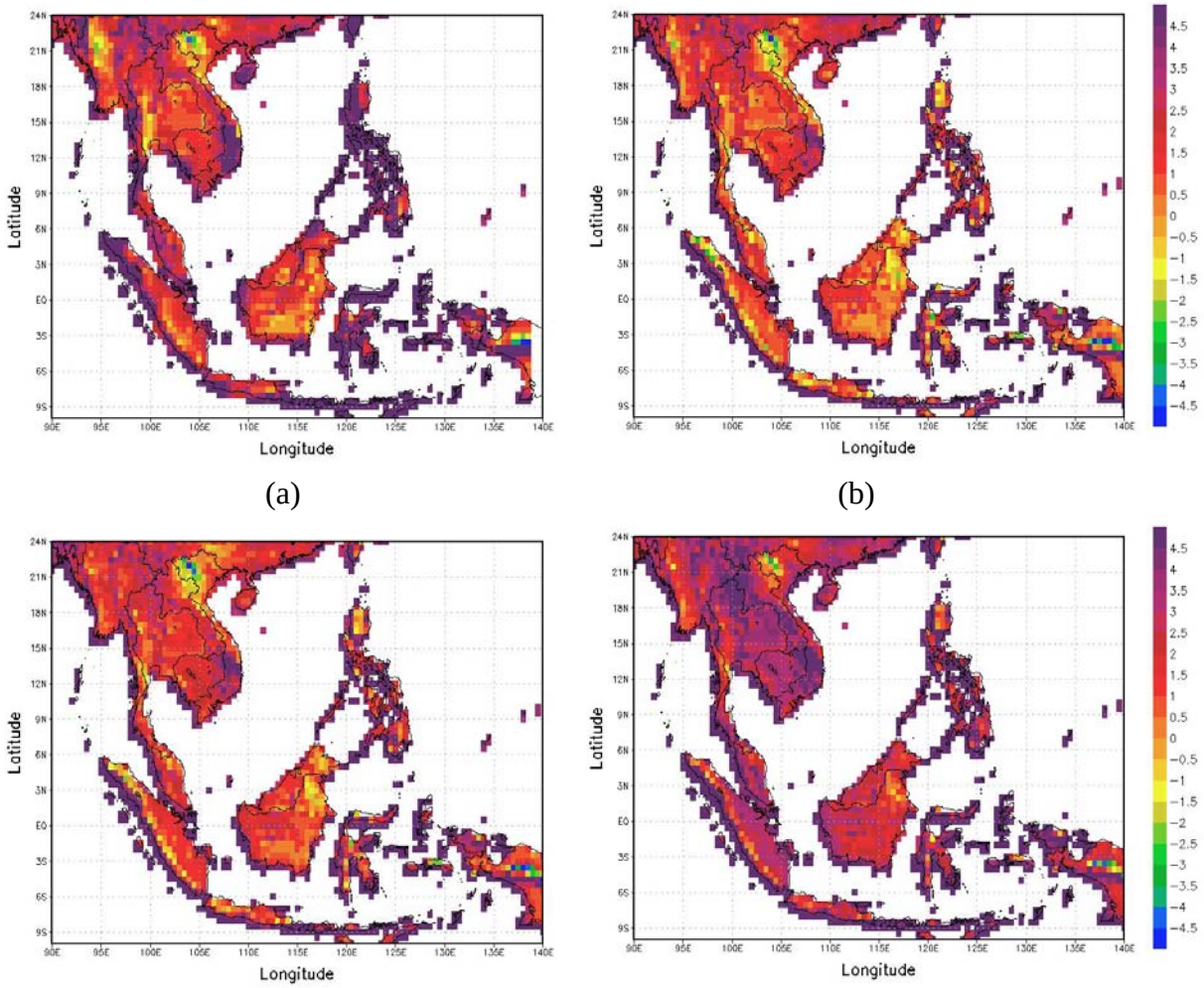

Figure 5.25: Difference between model and observations (CRUTS2.1) of average surface minimum temperature (^{o}C) in the period of 1961-1990 during MAM (a) HadAM3P (b) PRECIS-HadAM3P (c) PRECIS-ERA40 (d) PRECIS-ECHAM4

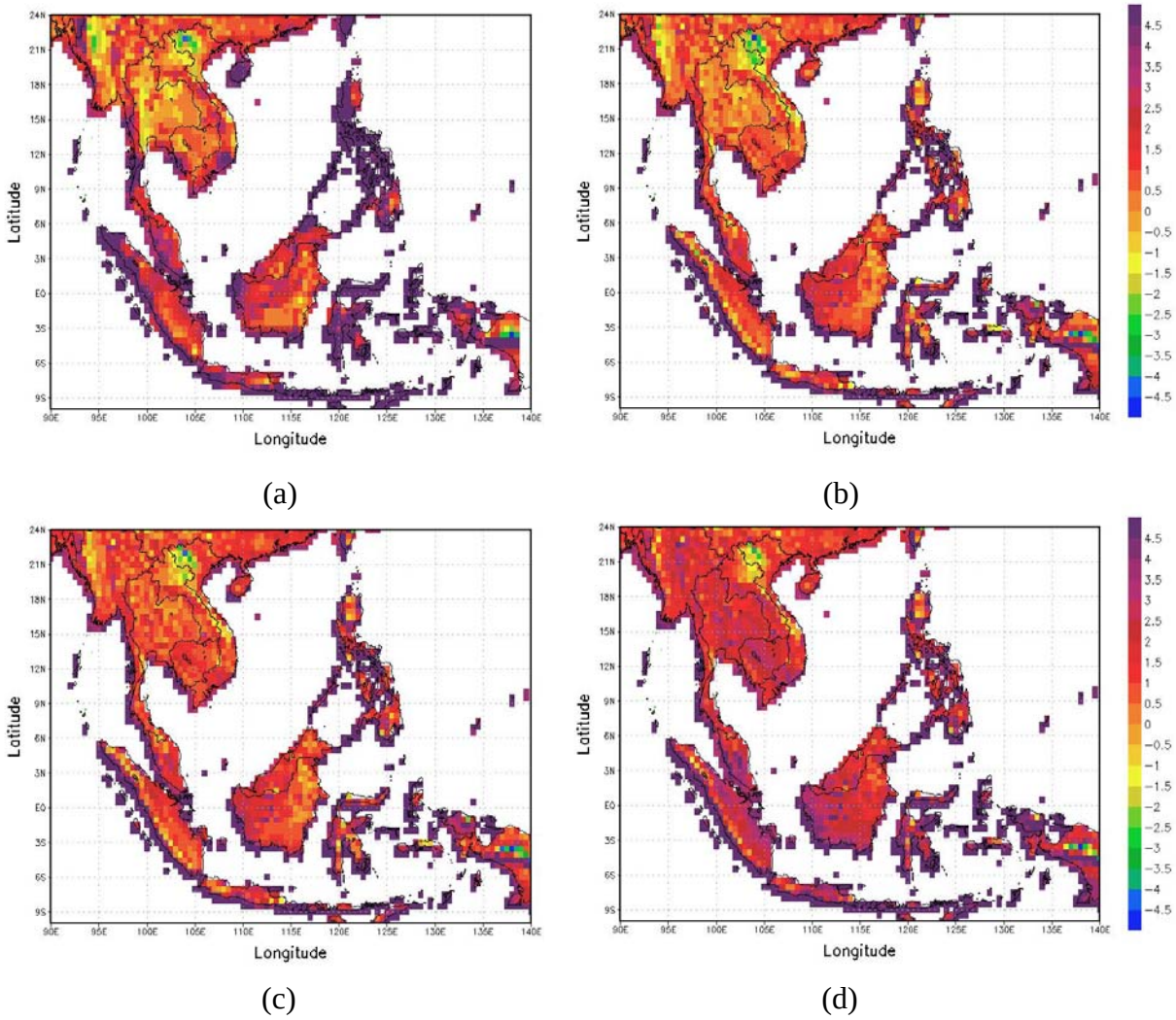

Figure 5.26: Difference between model and observations (CRUTS2.1) of average surface minimum temperature (^{o}C) in the period of 1961-1990 during JJAS (a) HadAM3P (b) PRECIS-HadAM3P (c) PRECIS-ERA40 (d) PRECIS-ECHAM4

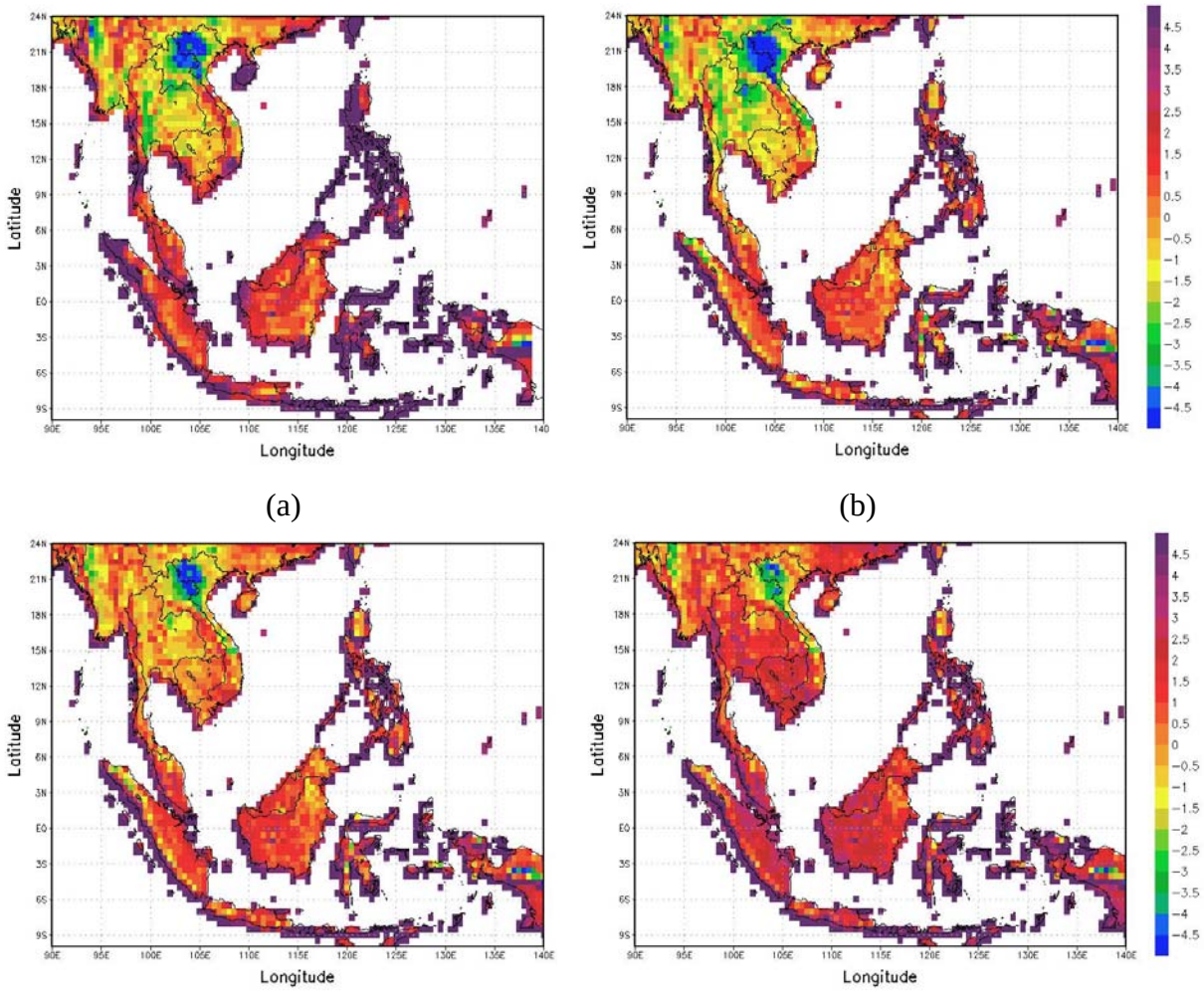

(a) (b)

(c) (d)

Figure 5.27: Difference between model and observations (CRUTS2.1) of average surface minimum temperature (^{o}C) in the period of 1961-1990 during ON (a) HadAM3P (b) PRECIS-HadAM3P (c) PRECIS-ERA40 (d) PRECIS-ECHAM4

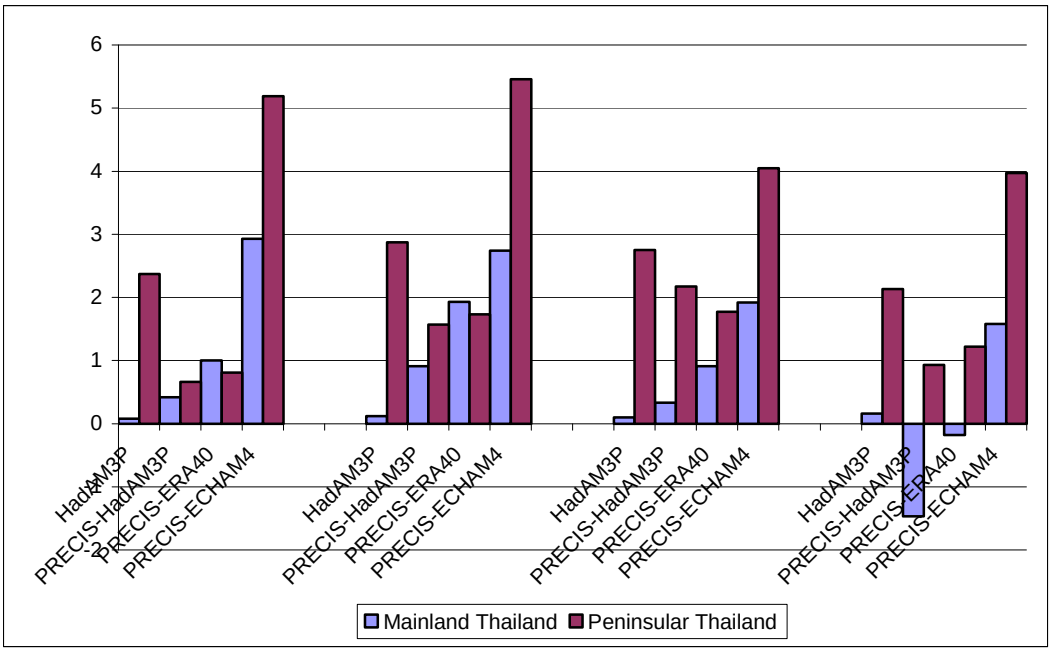

Figure 5.28: The minimum temperature difference between GCM and RCM compared with the gridded CRUTS2.1. [Note that the four groups in the graph represent the seasons, DJF, MAM, JJAS and ON]

5.2.4.2 Model Comparison with available daily station observational datasets

Figure 5.29 shows direct comparisons in maximum and minimum temperature between models and station data, using the point to point analysis method. The surface temperature decreases with higher altitude so the difference in elevation between RCM and station should be primarily considered. The model elevations of the nearest model grid cell at BKK and Ubon are very close to those of the station while the rest are somewhat different (Table 3.3). Moberg and Jones suggested that the RCM temperatures should be adjusted to the station level by assuming an average lapse rate of 6.5°C/km. In that case the surface temperature would be reduced by 1.9°C, 1.7°C and 0.9°C at CM, Phitlok and Surat site, respectively.

At the CM site, both the RCM and GCM calculated minimum temperatures warmer than the observations during the cool season, continuing through to the month of May. Acceptable simulations of minimum temperature are made during the summer monsoon period (Figure 5.29(a) left). Regarding the simulations of maximum

temperature, both RCM and GCM have a cool bias for all months while the RCM is closer to the station observation data (Figure 5.29(a) right). The largest warm bias in minimum temperature from PRECIS-HadAM3P simulation was found in March with a magnitude of 5 °C (about 3°C after including the altitude effect) and the largest cold biases in maximum temperature from HadAM3P (PRECIS-HadAM3P) simulation are 9°C (6°C). This implied that the altitude effect in the GCM might be larger than RCM. In summary, the RCM produced an acceptable simulation in both surface minimum and maximum temperature annual cycle.

At the Phitlok site, both GCM and RCM produce a very accurate simulation of the seasonal cycle of surface temperature (Figure 5.29(b)).

At the BKK site (Figure 5.29(c)), both GCM and RCM overestimate the minimum temperature to a similar extent in most months. The largest biases were found in March of the order of 5°C(4°C) in RCM (GCM). The observed maximum temperature does not vary too much at this station with the GCM underestimating values due to its grid-point. However, significant warm biases in the RCM were found in February to April with magnitudes of 8.8°C, 9.4°C and 5.5°C, respectively. The nearest grid cell elevation is very close to station elevation (Table 3.3) so this is unlikely due to model elevation error. Clearly, the average urban heat island (UHI) effect was found to be strongest in winter which might correspondences to maximum surface temperature increase found on observation (Figure 5.29(c) right) which should result exclusively from anthropogenic energy. The maximum temperature annual cycle at BKK is consistent in pattern with the cycle at CM, Phitlok and Ubon located over mainland Thailand so the implication is that the RCM is inadequate in simulating the UHI effect. One of the other possible causes of RCM overestimation is an unrealistic degree of coastal influence.

At the Ubon site, the RCM is rather poor in accurately simulating minimum temperature over DJFM, withvalues of warm bias of 3.8°C, 5.8°C, 6°C and 3°C which is consistent with the GCM. The PRECIS grid cell altitude is comparable to that of the station, 0.6 m lower. The warm bias in minimum temperature coincides with a dry bias in soil moisture content. RCM performance is generally better during

JJAS and the rest of the months. The maximum temperature annual cycle at this site is consistent with the cycle at the CM site, for example, slightly positive bias in JFMA and less than 5°C negative bias in MJJASON.

At Surat Thani, on the peninsula, both GCM and RCM generally overestimate the minimum temperature to a similar extent, producing small negative and positive biases in their maximum temperature simulations; both capture the relatively low amplitude of the temperature seasonal cycles at this station very well. (Figure 5.29(e)).

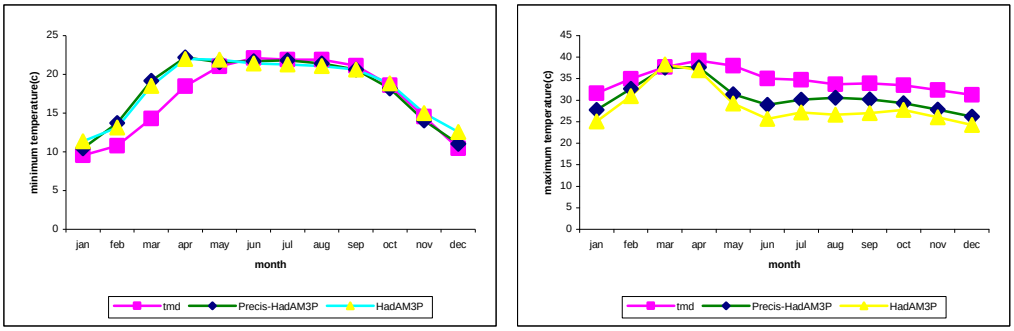

(a)

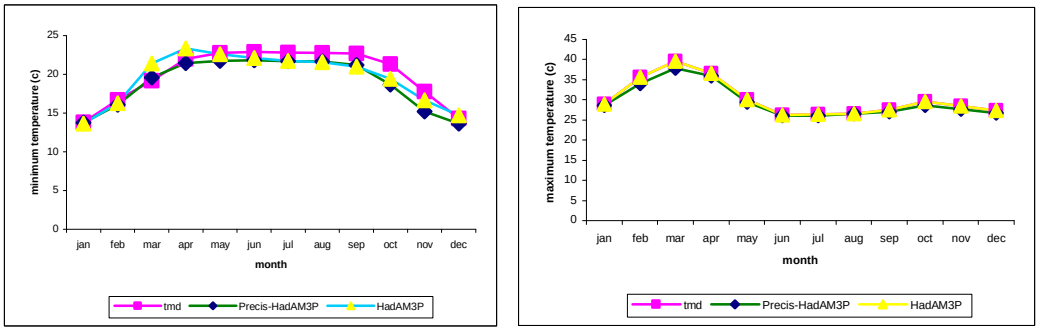

(b)

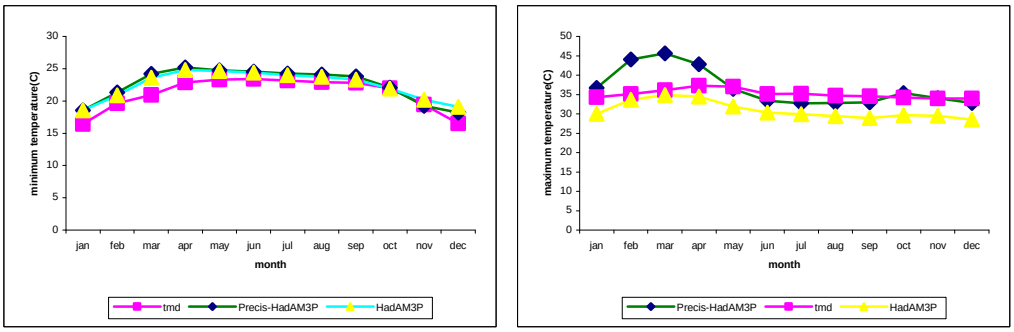

(c)

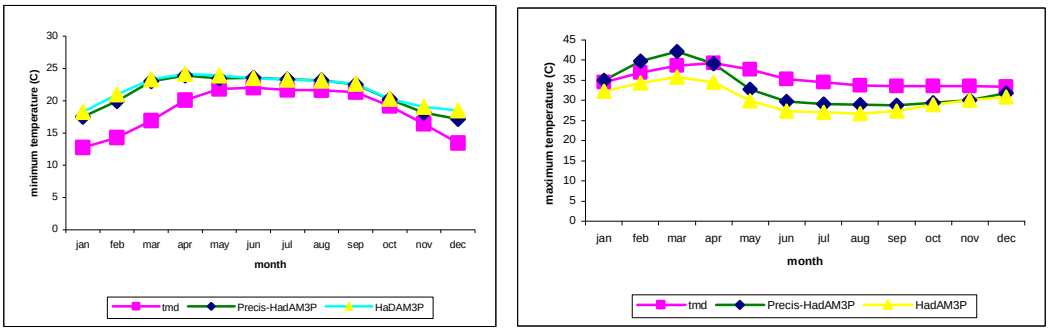

(d)

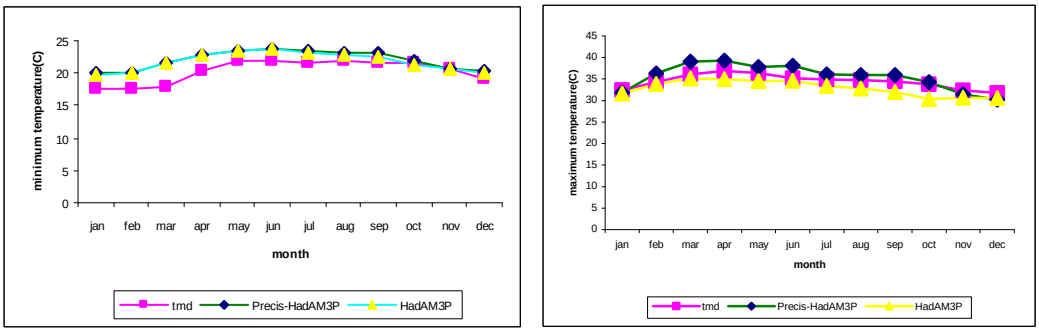

(e)

Figure 5.29: 1961-90 annual cycle of monthly minimum (left) and maximum (right) 1.5m temperature from station data, HadAM3P and PRECIS-HadAM3 at (a) CM (b) Phitlok (c) BKK (d) Ubon (e) Surat

Figure 5.30 (a) shows that the monthly averaged minimum surface temperature over central Thailand obtained from the PRECIS model simulations exhibits a small warm bias during the southwest monsoon season (JJAS) when the magnitudes of the overestimations are 0.33, 0.91 and 1.92^{o}C for PRECIS-HadAM3P, PRECIS-ERA40 and PRECIS-ECHAM4, respectively. The equivalent minimum temperature biases during the cool season (DJF) are 0.42, 1.00 and 2.93^{o}C. It is found that for maximum surface temperature a cold bias exists in PRECIS-HadAM3P and PRECIS-ERA40 for the active monsoon season. Uchiyama et al. (2006) found that the variation in temperature bias, for example, cold bias in the dry season and hot bias in the rainy season, may be linked to incorrect energy partitioning related to the latent heat flux. The GCM, HadAM3P, simulates the minimum temperature more accurately than the other RCM simulation over central Thailand.

All model simulations overestimated the temperature over the peninsula where, the RCMs, excluding PRECIS-ECHAM4, are closer to the absolute value of the observed temperature.

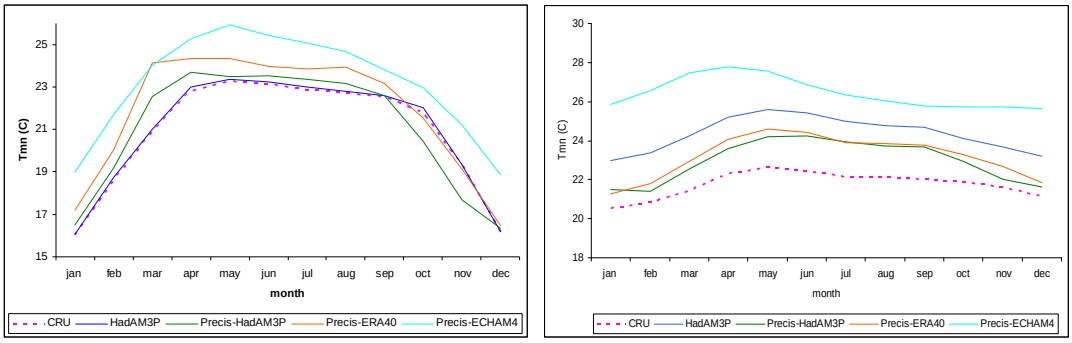

(a)

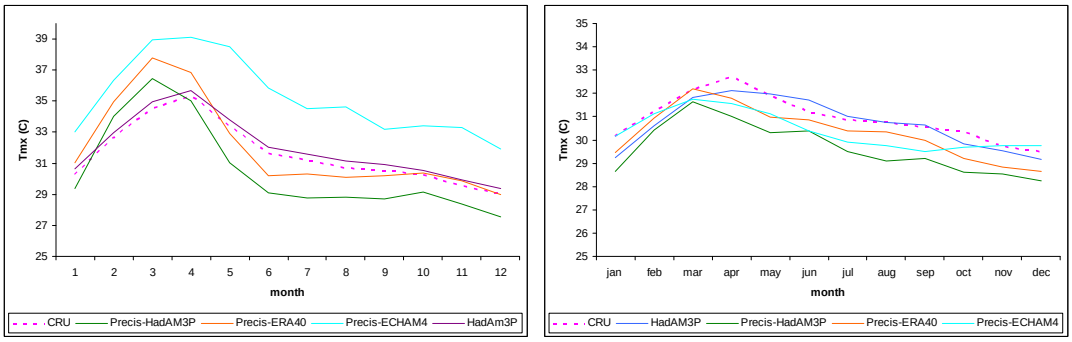

(b)

Figure 5.30: (a) Minimum and (b) maximum 1.5 temperature cycle (1961-1990) from model simulations and gridded observation data set over central Thailand (left) and over Southern Thailand (right).

Figure 5.30(b) shows that the model overestimations of PRECIS-HadAM3P, PRECIS-ERA and PRECIS-ECHAM4 are 1.69 (0.68), 1.78 (0.81) and 4.05 (5.18)^{o}C for JJAS (DJF) respectively over central Thailand while the monthly averaged maximum surface temperature obtained from the PRECIS model simulation exhibits a cold bias for every month in the area of peninsular Thailand. The model underestimations of PRECIS-HadAM3P, PRECIS-ERA and PRECIS-ECHAM4 are 1.3 (1.19), 0.44 (0.62) and 0.96 (0.06)^{o}C for JJAS (DJF) over the peninsula respectively. The GCM generates more accuracy in maximum temperature than the RCM over both central and Southern Thailand.

In general, the RCM provides regional detail in surface temperature while the GCM calculates area averaged surface temperature more accurately than the RCM. Applying grid to grid analysis, the cold bias during JJAS and ON (Figure 5.21 and 5.22) is unlikely due to biases in the gridded observation data itself but likely due to PRECIS itself. The variation in temperature (i.e. cold bias in the rainy season and warm bias in the dry season) may be due to the decrease and increase of latent heat flux for the two seasons which may not be well distinguished by the model (Islam et al., 2007). Applying the point to point analysis, corrected RCM elevation may reduce the bias in surface temperature at some sites, i.e., CM, Phitlok and Surat, however, consistencies of surface temperature annual cycle at the sites located over the mainland were revealed (Figure 5.29) . The positive bias in minimum temperature in JFM (Figure 5.29 (d)) may be related to the radiation scheme. The radiation scheme in both GCM and RCM defined the corresponding gases in a series of spectral bands, for example, carbon dioxide, ozone, methane, nitrous oxide and halocarbons, which over-absorb energy flux relative to the actual climate condition so that the models calculate excessive long-wave energy flux over the region (Mlawer et al., 1997). Another possible cause for the warm bias in minimum temperature is the result of the land surface scheme which may release too much energy heat flux from the soil, compared with reality, during night time. On the other hand, the warm bias in maximum temperature during Feb-Mar (Figure 5.29(c) and 5.29(d)) may be related to unrealistically low soil energy absorption during daytime.

5.2.5 Monsoon onset

This chapter also uses the same monsoon onset criteria as mentioned in Chapter 4 which suggested using five successive rainy days with more than 5 mm each day accompanied by westerly or southwesterly low level winds and easterly upper level winds to determine the monsoon onset (Sangwaldach, 2006). The observation record indicated that the onset of the rainy season in Thailand generally occurs around mid-May. It is assumed that the onset is similar in each year and that the same mechanisms are involved.

The mean 1961-1990 variables show the rainy season over Thailand starts at approximately the same time each year, with just 1 pentad difference. The first appearance of an average resultant westerly wind of strength 4 m/s occurs in the second pentad of May, while the average 250-hPa easterly wind first appears in the third pentad of May (Figure 5.31). The first arrival of the rapid increase in daily mean precipitation appears in the first pentad of May (Figure 5.32). Therefore, the average monsoon onset during 1961-1990, with all three criteria satisfied, occurs in the third pentad of May. Using a similar approach at the end of the rainy season over Thailand shows that this occurs around the third pentad of September.

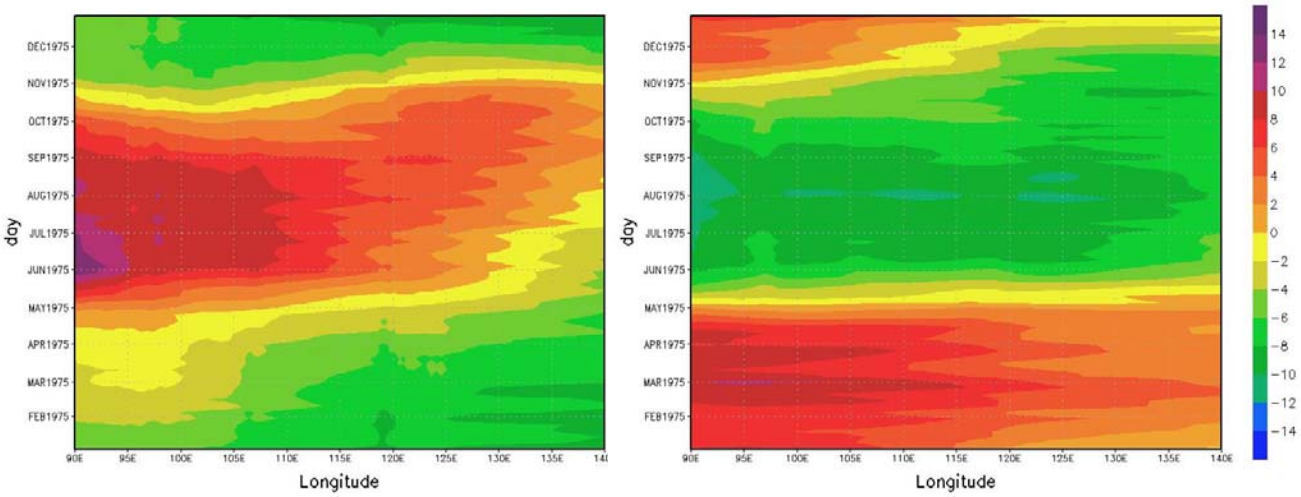

(a) (b)

Figure 5.31: Time-longitude section averaged over 5^{o}N-20^{o}N (the latitude range covering Thailand) of climatological pentad zonal wind (ms^{-1}) from PRECIS-HadAM3P at (a) 850 hPa (b) 250 hPa

Considering the topography of the region of 97.5-105^{o}E, the changing direction in winds when the westerly wind is stronger can be seen during the fourth pentad of May to the third pentad of October in Figure 5.31 representing a change to upslope flow along the mountainous region over western Thailand (Figure 3.1). The 850-hPa westerly winds extend eastward to the whole domain of SE Asia during the period from May until October. The maximum wind speed occurs at 90-95^{o}E, in the Bay of

Bengal, in the period mid-May through mid July accompanied by the peak in precipitation amount.

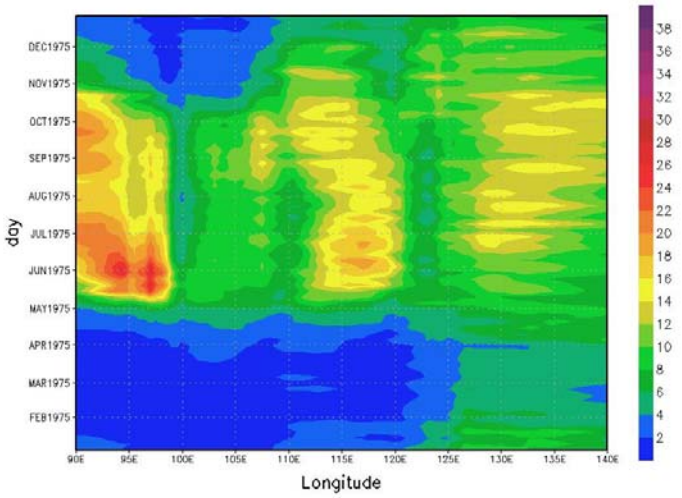

Figure 5.32: Time-longitude section averaged over 5^{o}N-20^{o}N of climatological pentad total precipitation (mm/day) from PRECIS-HadAM3P

Figure 5.33 shows the existence, during the southwest monsoon season, of ascending vertical motion over western Thailand occuring at approximately 97.5^{o}E, associated with highest precipitation amounts. It is shown that the monsoon onset reaches Thailand later by 1.5 day/30 year (Figure 5.34).

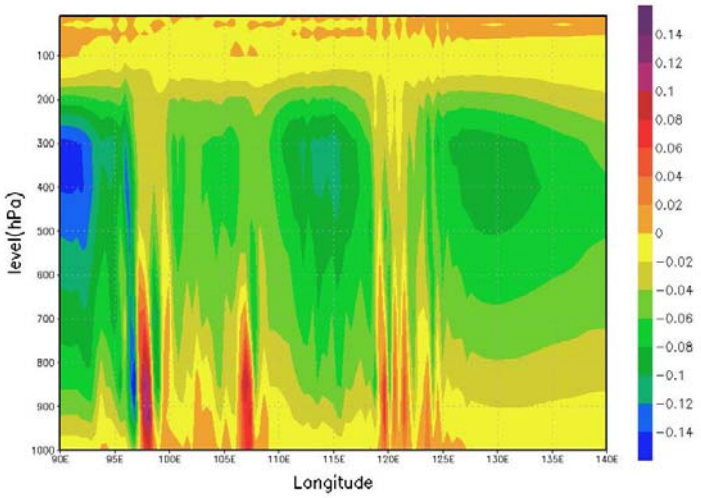

Figure 5.33: Pressure Level-longitude section averaged over 5^{o}N-20^{o}N of climatological vertical wind (ms^{-1}) from PRECIS-HadAM3P during JJAS

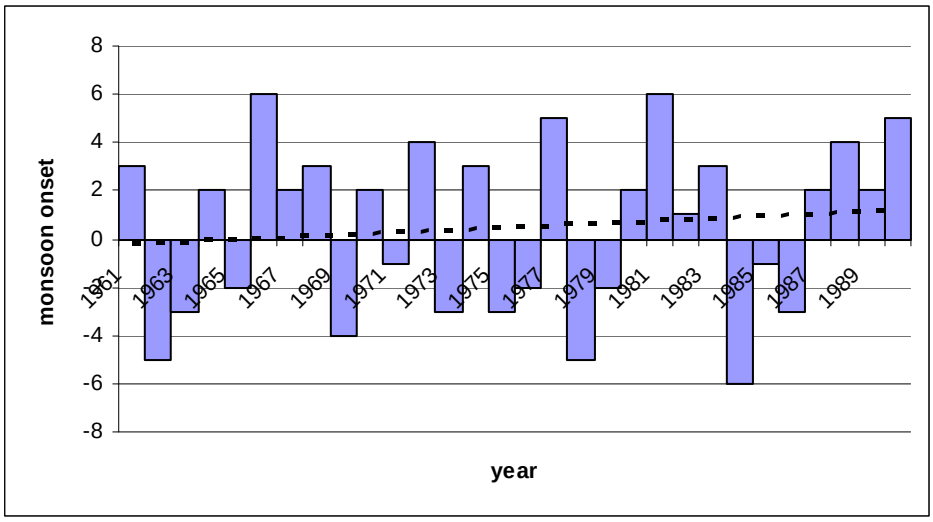

Figure 5.34: Inter-annual variation, 1961-1990, of the date of the south-west monsoon onset from PRECIS-ERA simulation. The y-axis represents the difference in monsoon onset compared with the average onset date (15th May).

The average onset date of the rainy season for the baseline period (1961-1990) from the PRECIS-ERA simulation is 15 May and the standard deviation for the onset is 3 days. The earliest monsoon arrival is 9 May in 1984 and the latest is 21 May in 1966 and 1981. The monsoon arrived earlier than 15th May during the years of El Niño (year in parenthesis) by 3 days (1963), 2 days (1965), 4 days (1969), +4 days(1972), 2 days (1976), +1 day (1982) and 3 days (1986), the positive number meaning the monsoon started later than the average onset date. The monsoon arrived earlier than 15th May during the years of La Niña (year in parenthesis): +2 days (1964), +2 days (1970), 3 days (1973), 3 day (1975), 6 days (1984) and +4 days (1988). From these results there appears to be no link between the ENSO cycle and the monsoon onset over Thailand. During the monsoon active phase the specific humidity increases quite rapidly from May to September (Figure 5.15).

5.3 Summary

This chapter addresses the questions; how well does the RCM capture the main regimes for current Thai climate, which variables do the GCM and RCM simulate realistically, and does the RCM add value to the GCM when compared against daily station and gridded CRUTS2.1 datasets.

All simulations, HadAM3P, PRECIS-HadAM3P and PRECIS-ERA, excluding PRECIS-ECHAM4, produced precipitation patterns consistent with the gridded CRUTS2.1 datasets during JJAS (Figure 5.1). In general, all simulations generated too much precipitation over the area north of 12°N and underestimated precipitation over the area south of this latitude (Figures 5.2-5.5). In detail, the driving GCM, HadAM3P, underestimated absolute precipitation more than the RCM, PRECIS-HadAM3P, does. Considering Thailand specifically, it was found that while the driving GCM HadAM3P simulated precipitation amount more accurately in all seasons over the mainland, PRECIS-HadAM3P did a better job over the peninsula. Daily station data were also used for model validation, to help address the question of potential added value from the RCM. The precipitation annual cycle produced from daily data shown as Figure 5.9 indicated that the RCM is more consistent than the GCM.

The average precipitation annual cycle from both station and model simulation over Thailand shows that there are two peaks, the first one occurs in May and the later one occurs in September in the mainland and in November over peninsular Thailand. Overestimated precipitation in May was found in all simulations and underestimated precipitation in September/November. Precipitation distributions over 5 stations were produced and show the model generates too many low volume precipitation events and insufficient high volume precipitation events. The possible causes inducing this performance were investigated. Regarding the limitations of the observation data, some variables are tested including number of wet days (defined as a day with rain above 1mm), humidity fields, cloud fractions, presence of an El Niño/La Niña event, and monsoon onset. The models calculated too many wet days during March to September compared with CRUTS2.1. The model calculated acceptable cloud fractions over Thailand compared with the observation data. A case study of an El

Niño event in 1982 and La Niña event in 1988 shows weak relations with the anomaly precipitation. The average monsoon onset from model simulation during 1961-1990 is also investigated. It was found that the average monsoon onset occurs in the third pentad of May while the literature review and the result from chapter 4 indicated that the onset occurs in pentad 25-26 (10th May).

In general, compared with the gridded data set, the GCM HadAM3P overestimated seasonal minimum temperature in all four regions in Thailand while all RCM simulations underestimated the temperature (Figure 5.23) in all seasons. Regarding the comparison between the forcing GCM and RCM, it was found that the GCM simulates surface minimum air temperature more realistically over both mainland and peninsular Thailand (Figure 5.30(a)). All model simulations producing surface maximum air temperature overestimate compared with the gridded data set for all seasons over the four regions in Thailand. It was found that the GCM (RCM) simulated maximum temperature more realistically over the mainland (peninsular) Thailand (Figure 5.28). Compared with station observational data, it was found that both HadAM3P and PRECIS-HadAM3P produce similar minimum temperatures in terms of both the annual cycle pattern and the absolute amount.

It was concluded, overall, that HadAM3P and PRECIS are sufficiently good in simulating current Thai climate to be used in analyses of their simulations of potential future regional climate in SEA. These results are considered in the following chapter.

Chapter 6

Future Projections of Climate Change

6.1 Introduction

This chapter contains a discussion of the main characteristics of climate change projections in Thailand and the surrounding area for both the high emission scenario (SRESA2) and the low emission scenario (SRESB2) for the end of the 21st century (2071 to 2100) relative to the period of 1961-1990 produced by the PRECIS-HadAM3 model.

IPCC-AR4 (2007) presents results from a global simulation with the A1B scenario while IPCC-TAR (2001) shows global projections based on SRESA2 and SRESB2 which are the same scenarios as used in this study. The change in global average annual precipitation is +3.9% (with a range of 1.3 to 6.8%) for the A2 scenario and +3.3% (with a range of 1.2 to 6.1%) for the B2 scenario (IPCC-TAR, 2001). These GCM assessments from CSIRO Mk2, CCSR/NIES, ECHAM/OPYC, CGCM1 (average three-member ensemble) and HadCM2 (average four-member ensemble) show reasonable agreement with average precipitation change over SEA of between -5 and 5% in DJF for both the A2 and B2 scenarios as well as for JJA for A2, however there was disagreement in JJA based on the B2 scenario (IPCC-TAR, 2001). Based on an ensemble of GCM simulations, the change in global average annual surface air temperature by the end of the century (JJA and DJF combined) is 3.0°C (with a range of 1.3 to 4.5°C) for the A2 scenario and 2.2°C (with a range of 0.9 to 3.4°C) for the B2 scenario. These GCMs show warming over SEA is less than 40% of the global average annual warming in JJA under both A2 and B2 emission scenarios (IPCC-TAR, 2001). The AOGCMs included in AR4 are CCSM3, CGCM3.1 (T47 and T63), CNRM-CM3, CSIRO-MK3, ECHAM5/MPI-OM, ECHO-G, FGOALS-g1.0, GFDL-CM2.0, GFDL-CM2.1, GISS-EH, GISS-ER, INM-CM3.0, IPSL-CM4, MIROC3.2 (medium and high resolution), MRI-CGCM2.3.2, PCM1, UKMO-HadCM3 and UKMO-HadGEM1. IPCC-AR4 (2007) mentioned that precipitation in DJF is likely to increase over the south of SEA and precipitation in JJA is likely to increase by 5% under the A1B scenario. Moreover, extreme precipitation and winds associated with

tropical cyclones are likely to increase in SEA, in other words, more intense precipitation events (IPCC-AR4). The annual warming for SEA is 2.5°C (with a range of 1.5 to 3.7°C) by the end of 21st century similarly to global mean on the A1B scenario (IPCC-AR40, 2007). The seasonal warming is similar to annual warming.

6.2 Projections of Climate Change

As per the experimental design outlined in chapter 3, PRECIS-A2, PRECIS-B2 and PRECIS-ECHAM4-A2 experiments were undertaken. To enable direct comparisons with experiments for the current climate (1961-1990) presented in chapter 5, these future simulations are also run without a sulphur cycle and results are analyzed in this chapter and compared against IPCC global model findings. In chapter 5 it was demonstrated that PRECIS-ECHAM4 simulations show a fairly poor ability to realistically simulate the current climate over Thailand, relative to the gridded observational data set CRUTS2.1, therefore, in this chapter, only the results from PRECIS-A2 and PRECIS-B2 will be discussed.

6.2.1 Precipitation Projections

Precipitation changes in the global and regional model simulations for 2071-2100 include a pronounced seasonality and considerable variation across the region of SEA (Figures 6.1-6.4). When compared with the precipitation pattern simulated by the forcing global model, HadAM3P, the regional model, PRECIS, is generally consistent with the forcing model in all seasons. The similarity over SEA will be due to the fact that the RCM maintains the large-scale weather systems from the GCM, superimposing finer scale regimes that derive from interactions with the land surface and mesoscale weather processes, for example, moisture flux.

Figure 6.1 shows increases of precipitation during the cool season (DJF) over mainland Thailand, Laos, the northeast Pacific, Borneo and southern Indonesia with a maximum increase of +45% over mainland Thailand for the PRECIS-A2 and +20 % for the PRECIS-B2. In the same season, precipitation decreases are found over peninsular Indochina, the southern South China Sea and Bay of Bengal with a maximum reduction of -40% in both scenarios. Figure 6.2 shows that the area of the

precipitation reduction in the cool season (DJF) is likely to continue decreasing in MAM and the reductions expand over the South China Sea though the Philippines to the northwest Pacific Ocean. However, both scenarios simulate 15-20% increases of precipitation during MAM over the marine continent of Sumatra, Malaysia and Borneo. Precipitation reductions of 30%-5% in MAM were detected for both the A2 and B2 scenario in Thailand excluding some parts of northeastern Thailand. The difference in the summer monsoon period (JJAS) precipitation total at the end of the 21st century relative to the baseline current climate (1961-1990) is depicted in Figure 6.3. Although there are regional details in SEA in the difference between the future (both A2 and B2 scenarios) and current monsoon season simulations, the key change appears to be increases in monsoon season precipitation over the Bay of Bengal, Sumatra, and the Gulf of Thailand through the western North Pacific excluding the area of the South China Sea. In the detail of the SE Asia region, the precipitation projection for the PRECIS-A2 scenario during JJAS suggests a reduction of 15% in monsoon precipitation over part of peninsula Thailand and the southern Philippines and a reduction of up to 45% in some parts of Indonesia. At the same time, precipitation increases are simulated especially in Burma, northern Sumatra Island and by up to +40% in the northern Philippines compared to the 1961-1990 baseline period. Small increases in precipitation in northeast Thailand, Cambodia and Laos of up to 5-10% are projected under both the A2 and B2 scenarios, with the projected change under A2 being slightly larger than under B2. An increase in precipitation was found during ON over all continental SEA, excepting southern Indonesia, with the largest changes, +45%, simulated over Mainland Thailand, the coast of Burma along the Bay of Bengal, northern Laos and Vietnam under the A2 scenario (Figure 6.4).

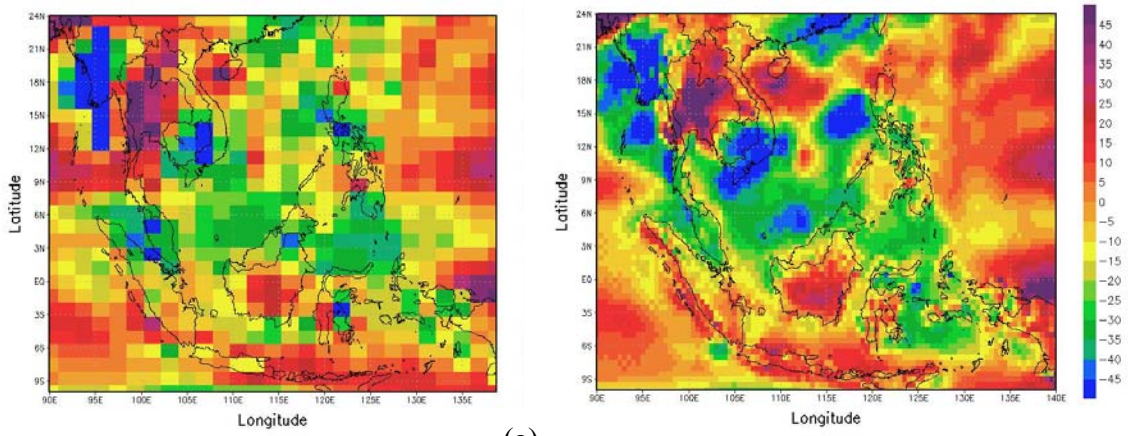

(a)

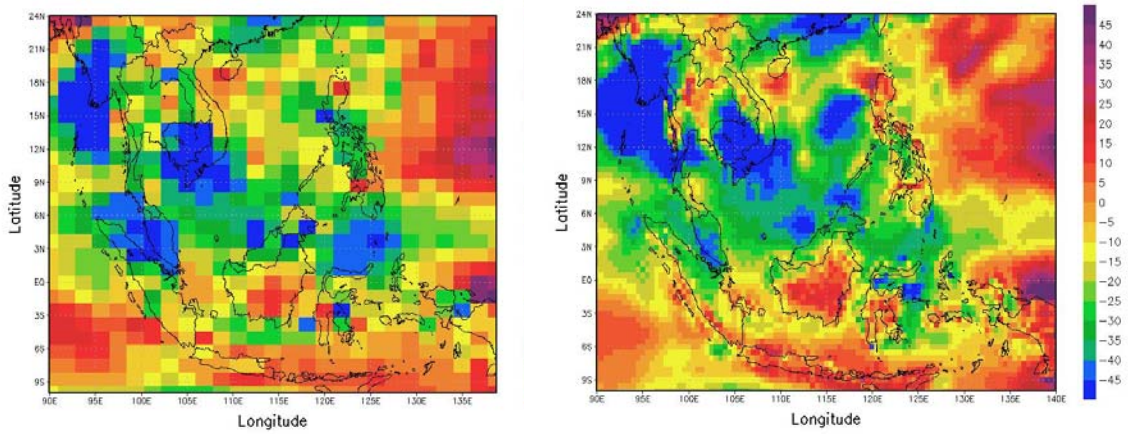

(b)

Figure 6.1: Projected precipitation changes (%) in the cool season (DJF) for 2071–2100 relative to 1961–1990 from GCM-HadAM3P (left) and RCM-PRECIS (right) (a) projections for the PRECIS-A2 scenario (b) projections for the PRECIS- B2 scenario

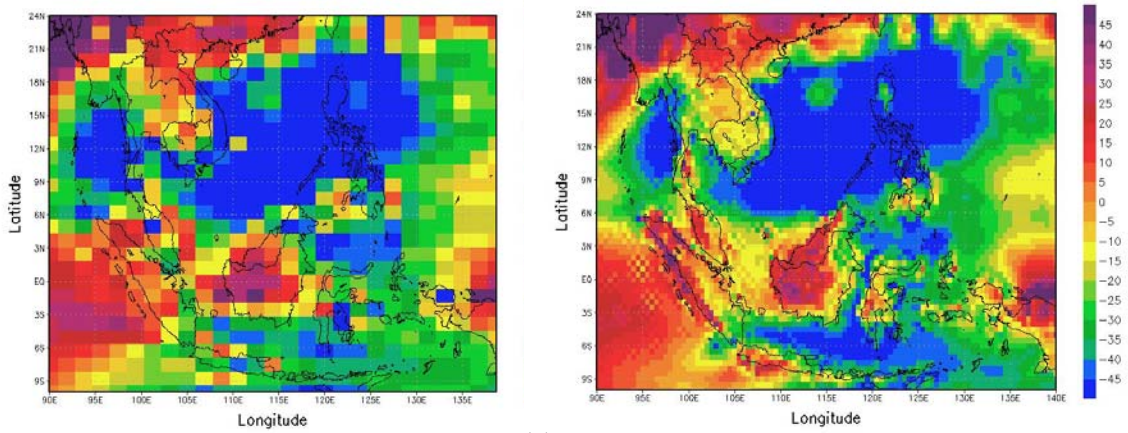

(a)

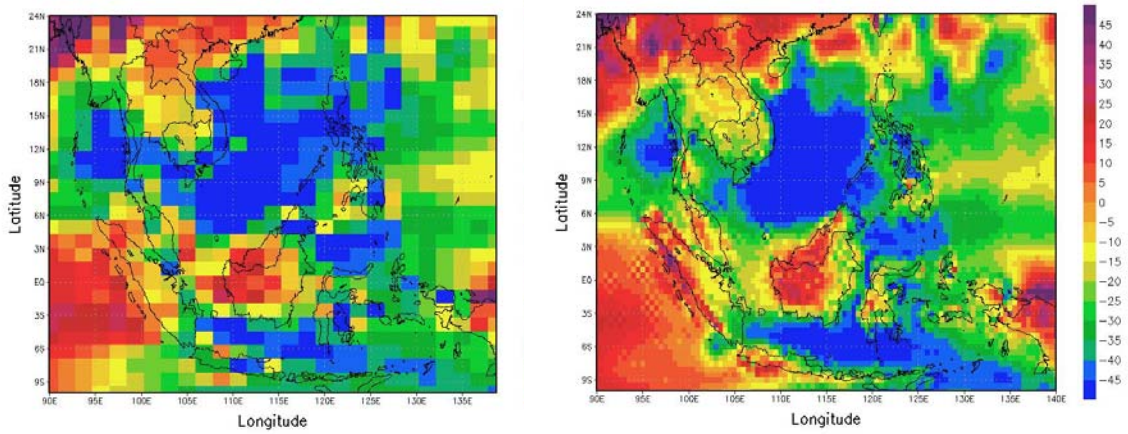

(b)

Figure 6.2: Projected precipitation changes (%) in MAM for 2071–2100 relative to 1961–1990 from GCM-HadAM3P (left) and RCM-PRECIS (right) (a) projections for the PRECIS-A2 scenario (b) projections for the PRECIS- B2 scenario.

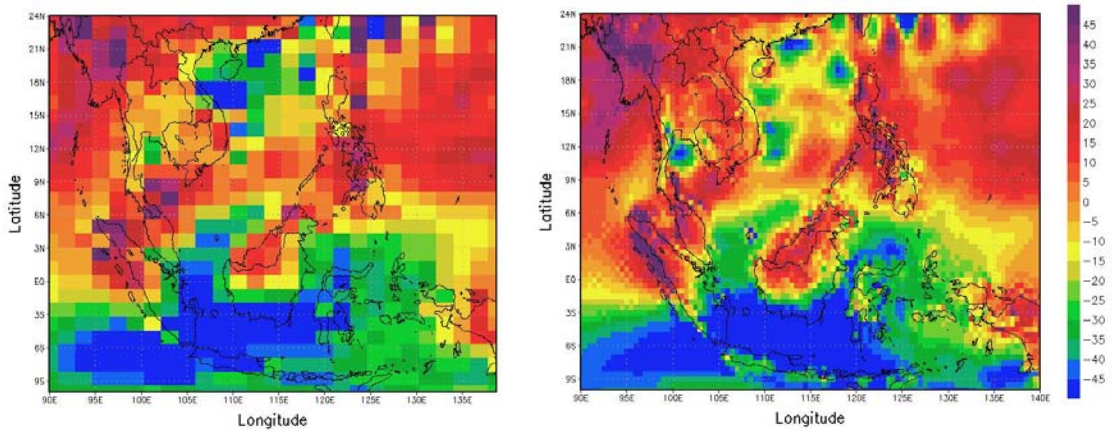

(a)

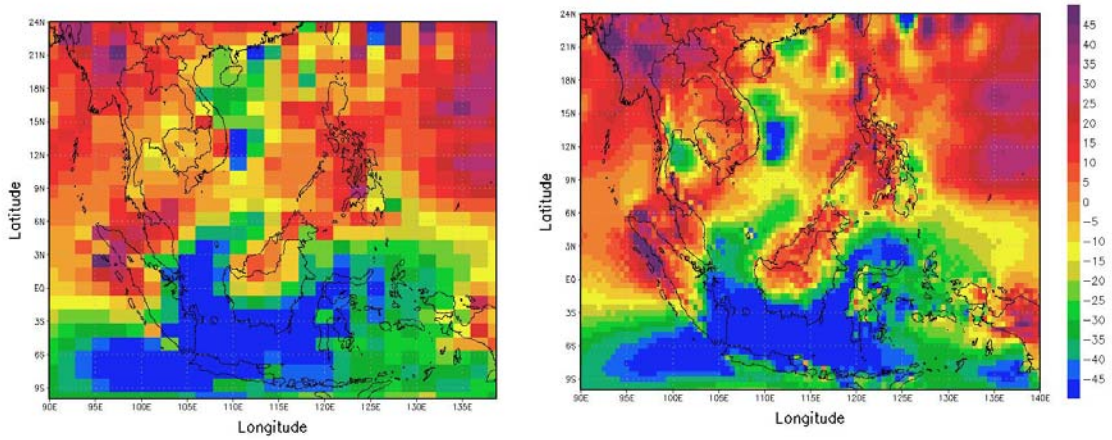

(b)

Figure 6.3: Projected precipitation changes (%) in summer monsoon season (JJAS) for 2071–2100 relative to 1961–1990 from GCM-HadAM3P (left) and RCM-PRECIS (right) (a) projections for the PRECIS-A2 scenario (b) projections for the PRECIS-B2 scenario

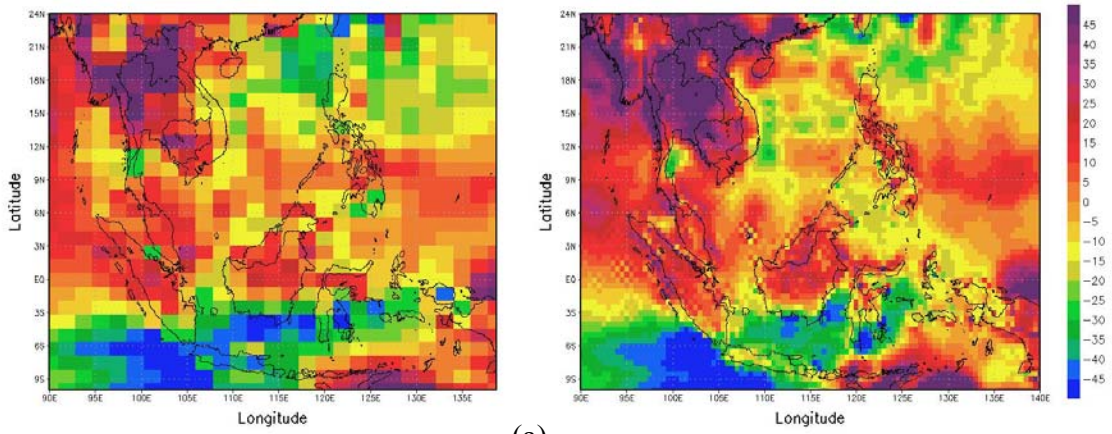

(a)

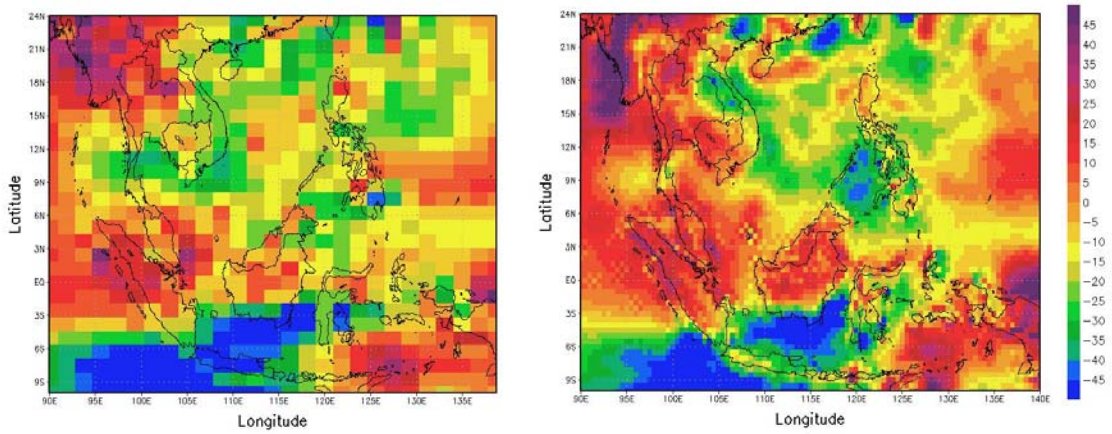

(b)

Figure 6.4: Projected precipitation changes (%) in ON for 2071–2100 relative to 1961–1990 from GCM-HadAM3P (left) and RCM-PRECIS (right) (a) projections for the PRECIS-A2 scenario (b) projections for the PRECIS- B2 scenario.

The regional area averages in total precipitation change over Thailand from driving GCM, HadAM3P and PRECIS under the A2 and B2 scenario are presented in Table 6.1. During DJF, over northern, northeastern and central Thailand PRECIS-A2 produces precipitation increases of 7%, 18% and 61%, respectively and PRECIS-B2 produces a precipitation decrease of -25%, -31% and -10%. In the same season, over the peninsula the two simulations produce a similar precipitation decrease response by -16%. Consistent responses in both A2 and B2 simulations are found in MAM (decreased precipitation) and in JJAS (increased precipitation) throughout Thailand. The magnitudes of the precipitation decreases in MAM under the A2 (B2) scenario

over northern, northeastern, central and southern Thailand are 15% (11%), 5% (9%), 22% (18%) and 10% (8%), respectively. The magnitude of the precipitation increases in JJAS under the A2 (B2) scenario over northern, northeastern, central and southern Thailand are 25% (29%), 8% (8%), 4% (4%) and 14% (13%), respectively. During ON, the two scenarios produce similar responses with increased precipitation throughout Thailand except that PRECIS-B2 produces decreased precipitation over northeast Thailand. The magnitude of the precipitation increases in ON under the A2 (B2) scenario over northern, northeastern, central and southern Thailand are +53% (+15%), +56% (-14%), +49% (+8%) and +17% (+11%), respectively.

When compared with the precipitation patterns simulated by the forcing global model, HadAM3P, the regional results over Thailand from the regional model, PRECIS, can be summarised as follows, supported by Table 6.1.

(i) North; the RCM results are generally consistent with the GCM in every season.

(ii) Northeast; the RCM results are variable with the GCM; consistent with the GCM during DJF and MAM, different to the GCM in JJAS in both A2 and B2 simulations (PRECIS produces changes double those of the GCM) and the A2 simulation is consistent with the GCM during ON.

(iii) Central; the RCM results are generally consistent with the GCM.

(iv) South; the RCM results are generally consistent with the GCM except the B2 simulation during ON.

Focusing upon differences in results between scenarios, there is little to highlight at the annual timescale. Seasonally, DJF and ON results reveal the largest sensitivity to choice of emission scenario; DJF shows negative (positive) changes under B2 (A2) over the mainland regardless of model while ON reveals, in both models, larger positive changes over the mainland under A2.

Table 6.1: Seasonal precipitation change (%) obtained from GCM and RCM simulation in Thailand

Precipitation change (%)	Annual	DJF	MAM	JJAS	ON
Northern Thailand					
HadAM3-A2	9	12	-13	15	53
HadAM3-B2	7	-21	-10	14	16
PRECIS-A2	12	7	-15	25	53
PRECIS-B2	14	-25	-11	29	15
Northeastern Thailand					
HadAM3-A2	-1	6	-1	-5	25
HadAM3-B2	-4	-18	-8	-2	3
PRECIS-A2	8	18	-5	8	56
PRECIS-B2	1	-31	-9	8	-14
Central Thailand					
HadAM3-A2	-4	44	-18	-2	31
HadAM3-B2	-3	-22	-15	3	0
PRECIS-A2	-1	61	-22	4	49
PRECIS-B2	-3	-10	-18	4	8
Southern Thailand					
HadAM3-A2	1	-16	-16	12	5
HadAM3-B2	-5	-33	-20	12	-8
PRECIS-A2	6	-16	-10	14	17
PRECIS-B2	2	-16	-18	13	11

Precipitation seasonal cycles from the future simulations are shown in Figure 6.5 for four regions over Thailand. In general, the absolute monthly precipitation from the GCM future simulation is lower than from the RCM and the changes for the B2 scenario are similar to those for the A2 scenario although with somewhat smaller (larger) amplitude in August-November (April-July). The GCM with both A2 and B2 scenarios produces increased precipitation by 1-2 mm/day during July - September over northern Thailand and by 1 mm/day in northeast, central and southern Thailand. The RCM, under both scenarios, produces increases by 2 mm/day in precipitation during JAS over all regions in Thailand excepting by 1 mm/day in central Thailand (Figure 6.5). The maximum increases in precipitation by 2 (1.5) mm/day were found in September in northern Thailand under the A2 (B2) scenario.

Over **mainland Thailand** the pattern of the future precipitation seasonal cycle is consistent with the baseline; the first peak is in May and the later peak is in September. The precipitation magnitude is significant decreased in May in both A2 and B2 scenarios over mainland Thailand while it is significant increased over northern and northeastern Thailand and small increases over central Thailand in the later peak and during ON. This might be related to a possibility of increased tropical cyclones over SEA which is reported by IPCC-AR4 because 70% of tropical cyclonic disturbance move across Thailand during September to November (Table 3.2). Comparing the A2 and B2 scenarios in May (September), the A2 scenario produces less (more) precipitation than the B2 scenario. Over **peninsular Thailand** a modest precipitation increase stretches from May to November. The magnitude of precipitation from the A2 and B2 scenarios shows no significant difference. The simulated increase in precipitation in September is possibly due to a shift of monsoon period which is discussed later in this section. Moreover, the future vertical velocity simulation during JJAS increases from the period of 1960-1990 to the period of 2071-2100 which implies more ascending air possibly producing more precipitation (Figure 6.6).

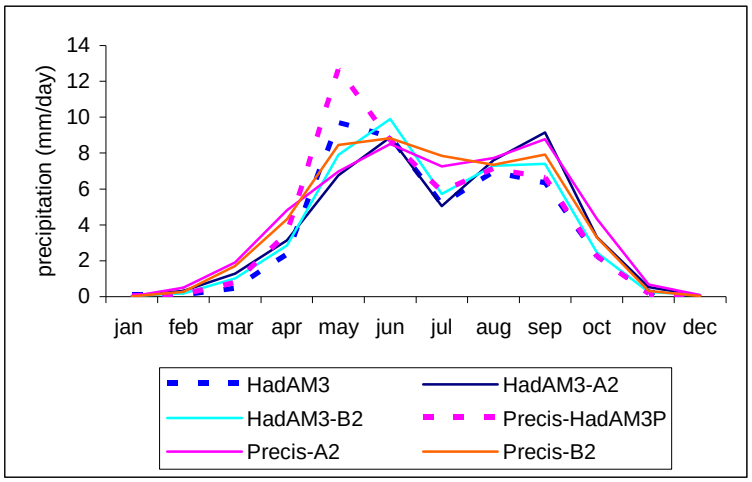

(a)

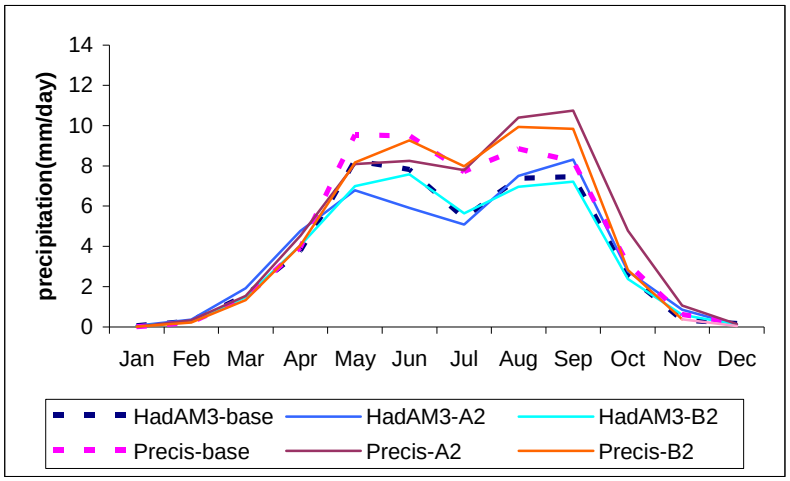

(b)

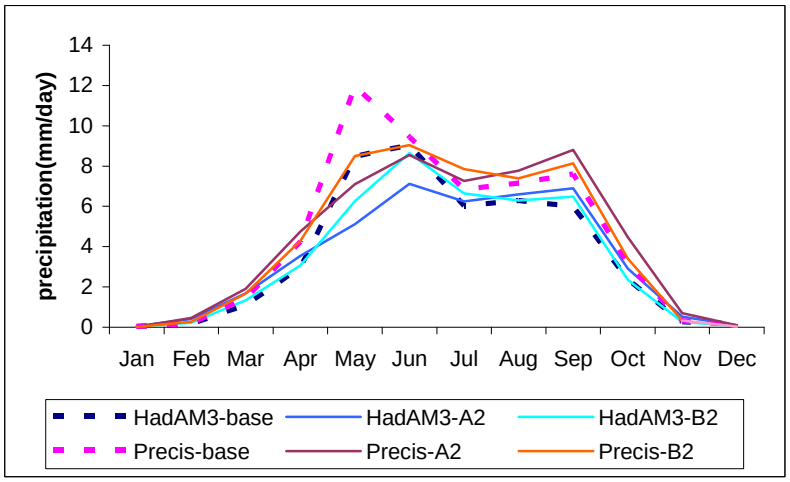

(c)

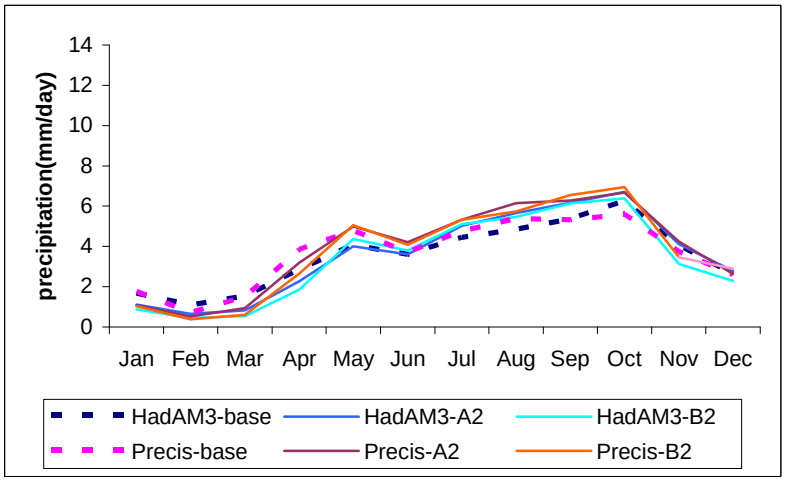

(d)

Figure 6.5 Comparison of 30 year seasonal cycle of baseline (1961-1990) and future (2071-2100) precipitation intensity (mm/day) over (a) northern (b) northeastern (c) central and (d) Peninsular Thailand from HadAM3 and PRECIS.

When we consider the Koppen climate classification, northern, central and northeastern Thailand can be merged into one mainland region under the climate of tropical rainforest (Chapter 3). Specifically, the same criteria to define precipitation change as was used in the IPCC Third Assessment Report, TAR, is used here for defining precipitation projections in Thailand; the precipitation amount changing by greater than 20% is defined as a significant increase/decrease, while the precipitation amount changing between 5%-20% is defined as a small increase/decrease. A change of between -5 to 5% is defined as no significant change. Over **mainland Thailand**, during DJF, the GCM-A2 and RCM-A2 mostly project a small precipitation increase and the GCM-B2 and RCM-B2 agree on a small decrease. During JJAS, the GCM A2 and B2 scenarios project no significant precipitation change while both the RCM A2 and B2 scenarios agree on small precipitation increases during JJAS. Over **peninsular Thailand** the GCM and RCM future simulations agree on small precipitation increases during JJAS and small decreases during DJF (Table 6.1). Some are in agreement with the average precipitation projections published in the most recent IPCC report (IPCC-AR4, 2007) indicated that over SEA an increase in precipitation during DJF of 6% and of 7% during JJA is anticipated under the A1B scenario [the scenario projection between the low emission SRES-B2 and high emission SRES-A2 scenarios].

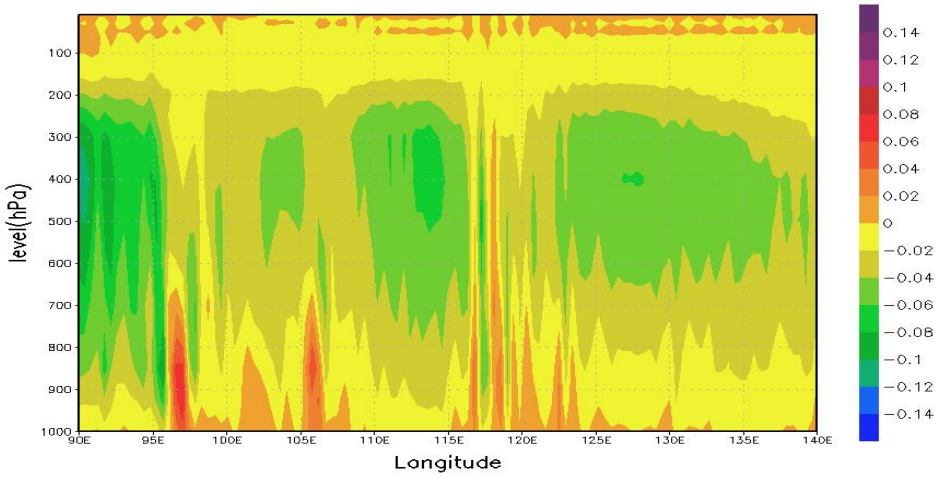

(a)

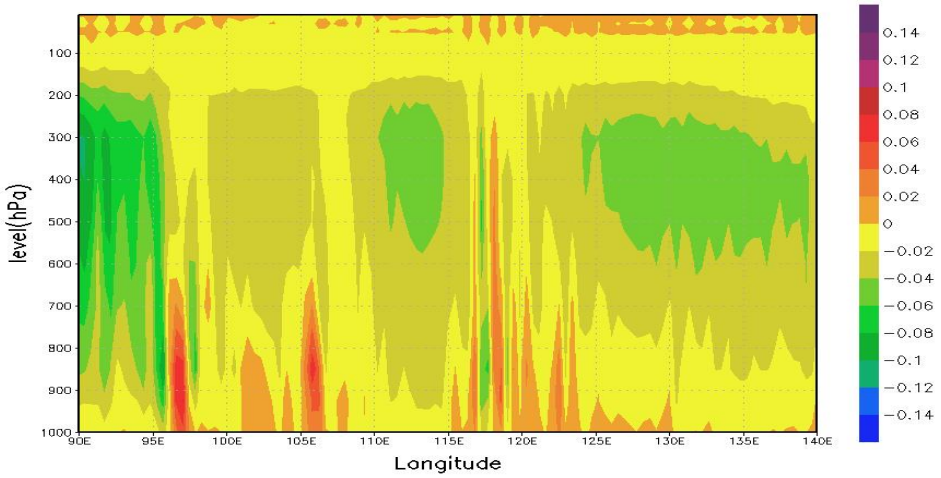

(b)

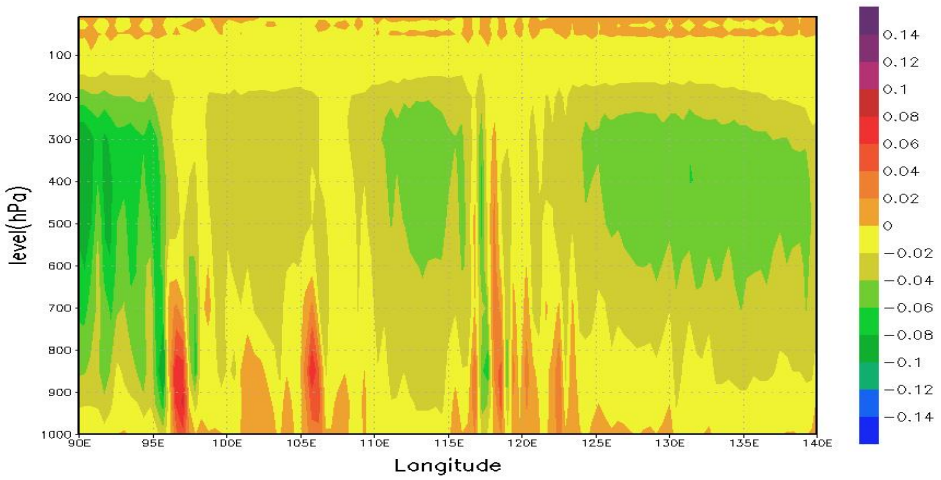

(c)

Figure 6.6: Mean 30 year vertical velocity (ms^{-1}) averaged over a latitude band of 10°S-25°N covering Thailand during JJAS (a) PRECIS-HadAM3 (1961-1990) (b) PRECIS-A2 (2071-2100) (c) PRECIS-B2 (2071-2100)

When we consider Figure 6.7 based on the Koppen climate classification it is found that over the **mainland** the GCM-A2 and B2 simulations produce a reduced number of wet days (days with rain above 1 mm) by 5-8 days during JJAS relative to the baseline period and simulate no change in the number of wet days during DJF. The RCM calculates 2 days decrease, under either emission scenario, in the number of wet days in JJAS and simulates no change in the number of wet days during DJF. Over the **peninsula**, both the GCM A2 and B2 scenarios simulated 9 fewer wet days during DJF than in the baseline period and no change in wet day frequency during JJAS while the RCM simulated a decrease in the number of wet days with magnitude of 5 (9) days in JJAS (DJF).

The RCM (A2 and B2 scenarios) produce average precipitation increases during JJAS with a decrease in the simulated average number of wet days over the mainland and the peninsula. This implies that the amount of precipitation on wet days in the future is larger than the amount during the baseline period.

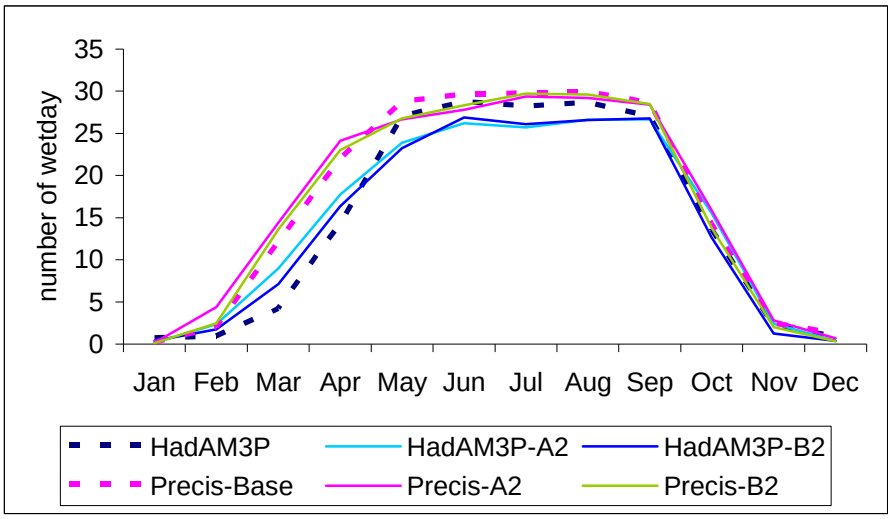

(a)

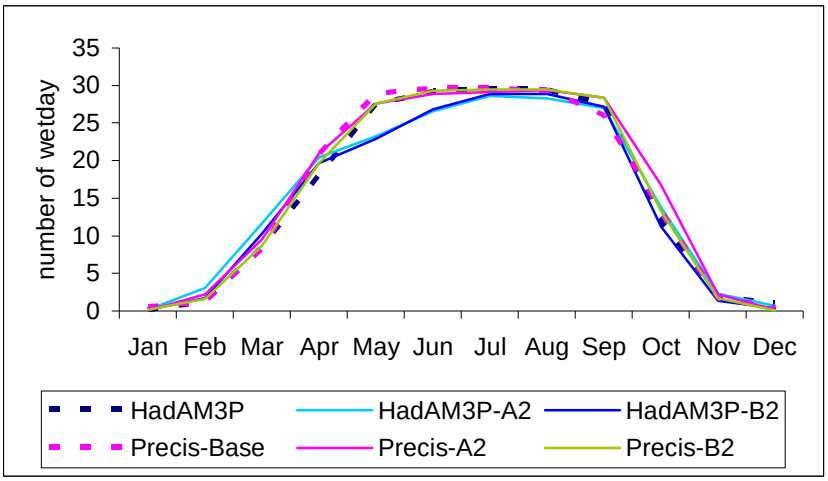

(b)

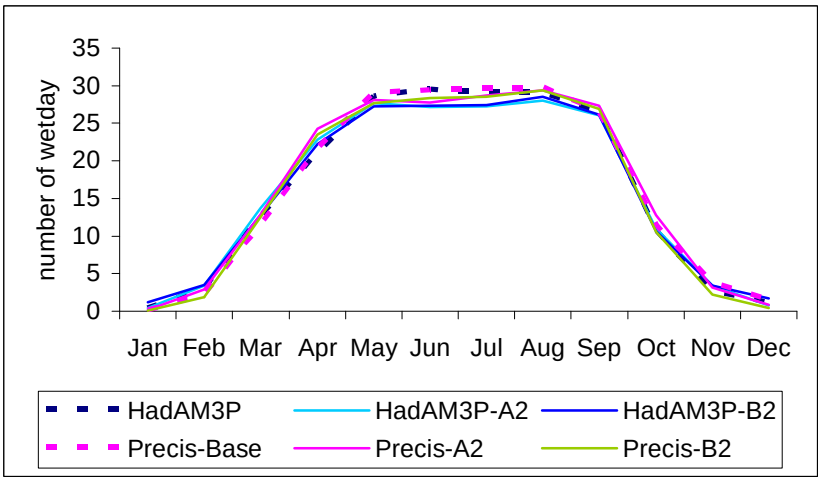

(c)

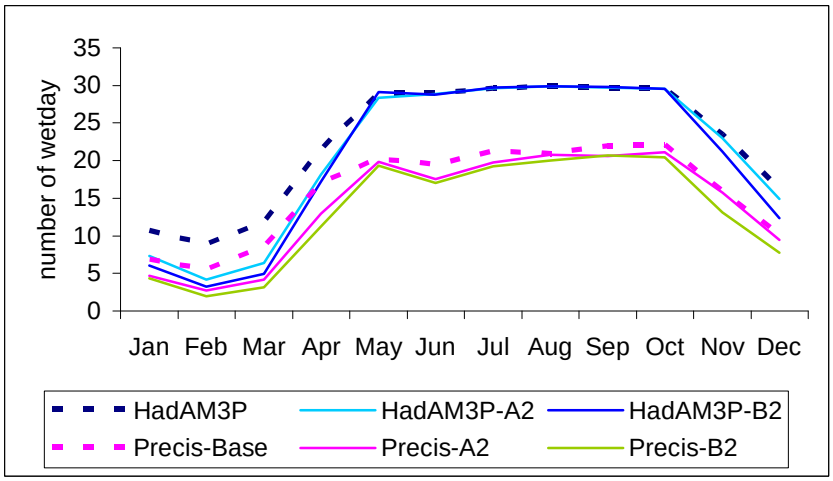

(d)

Figure 6.7: Number of wet days in current and future climate (a) north (b) northeast (c) central (d) Peninsular Thailand

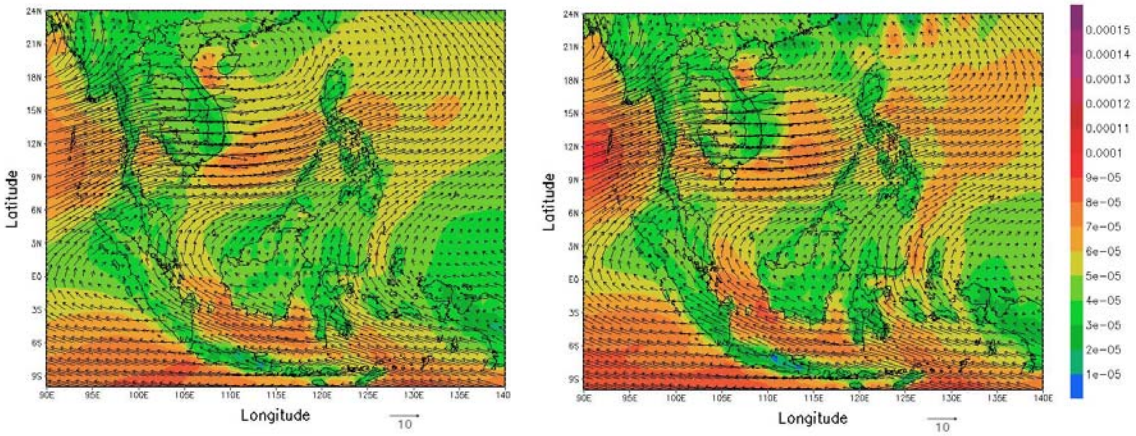

Figure 6.8: Horizontal surface moisture flux (kg m^{-2} s^{-1}) between 1961-1990 from PRECIS-HadAM3P simulation (left) and 2071-2100 from PRECIS-A2 (right) during JJAS.

The future changes in the surface moisture flux during the southwest monsoon season clearly indicate an enhancement of the moisture transport over the Indian Ocean into the Indochina region (Figure 6.8). The specific humidity also increased remarkably over the Indian Ocean (Figure 6.9), which is consistent with the intensified moisture transport. Therefore, the small precipitation increases during JJAS found in the future scenario projections seem to be most associated with a moister atmosphere and increased precipitation intensities. Ueda et al. (2006) showed that the enhanced moisture transport into the Asian monsoon region, associated with the increased moisture sourced from the Arabian Sea though the Indian Ocean into SE Asia, is a key mechanism that is responsible for intensified precipitation in future simulations.

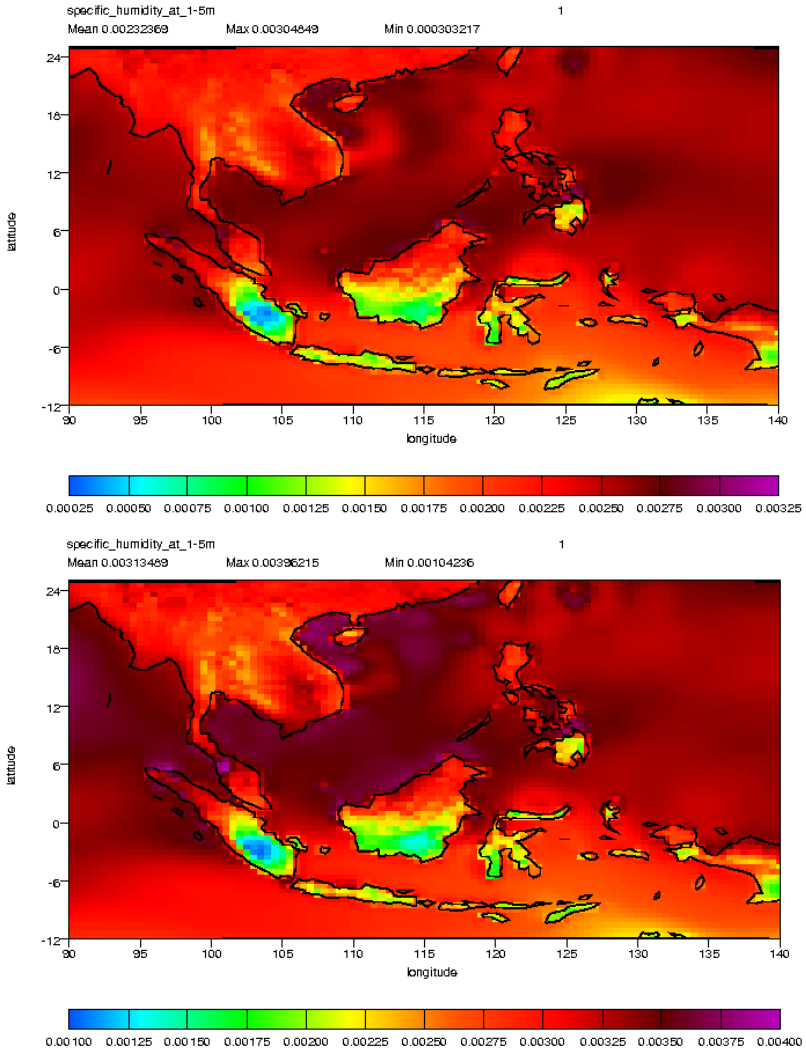

Figure 6.9: Specific humidity (kg kg^{-1}) 1961-1990 from PRECIS-HadAM3P simulations (top) and 2071-2100 from PRECIS-A2 (below) during JJAS.

In conclusion, over the **mainland** PRECIS projects a small precipitation increase (5%-20%) under the A2 and B2 scenarios associated with a 2 day decrease in the simulated average number of wet days during JJAS. The maximum total precipitation increase was found in September with a magnitude of 2 mm/day. During DJF, PRECIS-A2 (B2) mostly projects a small precipitation increase (decrease) associated with no change in the number of wet day under either emission scenario. Over the **peninsula** and under both the A2 and B2 scenarios, PRECIS projects a small precipitation increase associated with a decrease of 5 days per season in the simulated average number of wet days during JJAS and a small decrease in DJF associated with a 9 day per season decrease in wet days. The precipitation increase during JJAS may be related to more likely intense precipitation events, tropical cyclone increase in SEA

(IPCC-AR4) and intensified moisture transport from the Indian Ocean into the Indochina region.

This study found small increases in precipitation during JJAS while the global models reported by the IPCC under the same A2 and B2 scenarios found no significant change., This study agrees, however, with precipitation increases of +6% (with a range of -2% to 10%) in global model precipitation simulations under the A1B scenario. During DJF, this study found a small precipitation increase in some regions of Thailand under the A2 scenario but small increases was found over the whole of Thailand under the B2 scenario; IPCC indicated no significant change in the A2 scenario, disagreement change in the B2 scenario and a 7% increase with a range of -4 to 17% in the A1B scenario.

6.2.2 Surface air temperature projections

6.2.2.1 GCM and RCM comparison

Changes in seasonal maximum surface air temperature from the GCM and RCM are shown in Figures 6.10-6.14. In general, both models produce similar patterns of changes in maximum temperature but with differences over specific areas. During the cool season (DJF) there are considerable maximum temperature differences; the GCM-A2 simulation produces approximately 1^{o}C more warming than RCM-A2 over Burma. In contrast, the RCM-A2 produces approximately 1^{o}C more warming than the GCM-A2 over Cambodia and northeastern Thailand. It is also clear that the RCM-B2 produces 1.5^{o}C higher maximum temperature changes than the GCM-B2 over the Philippines (Figure 6.11). During MAM, there are notable temperature differences (about 1^{o}C higher in the RCM) over eastern Burma, a mountainous area, central Thailand and the coast of western Borneo (Figure 6.12). During JJAS, there are considerable maximum temperature differences (approximately 1^{o}C higher in GCM) over central Thailand and Borneo in the A2 scenario while there is no significant difference in the temperature response over particular regions between the models in the B2 scenario (Figure 6.13). During ON, there is no significant difference in maximum temperature between the GCM and RCM in both A2 and B2 scenarios (Figure 6.14).

6.2.2.2 RCM-A2 and RCM-B2 comparison

In general, the RCM-A2 scenario produces maximum temperature patterns which are generally consistent with the RCM-B2 but with magnitudes 1°C higher in the A2 scenario in all seasons. The largest warming in DJF was found over Burma and parts of peninsular Malaysia (5°C), over mainland Thailand, Laos and southern Borneo (5°C) and in Vietnam (4.5°C) in the RCM-A2 scenario. The largest simulated change in JJAS maximum temperature were found over Indonesia and Borneo, along the equator, with a magnitude of 6.5°C in the A2 scenario and reaching 5°C for the B2. Overall the largest SEA temperature changes occur in JJAS.

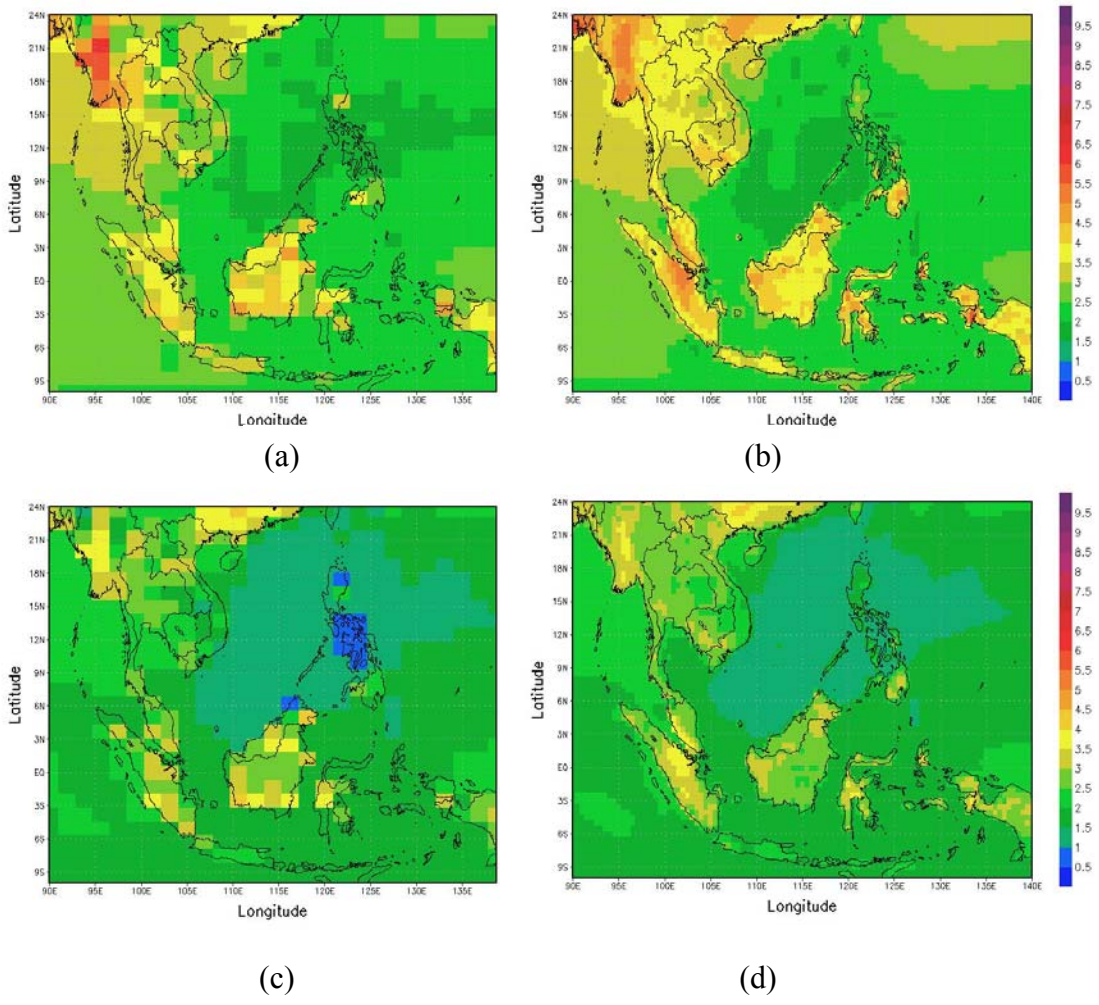

Figure 6.10: Projected changes in cool season (DJF) maximum surface temperature (°C) for 2071–2100 relative to 1961–1990 projections from (a) HadAM3-A2 (b) HadAM3P-B2 (c) PRECIS-A2 (d) PRECIS-B2

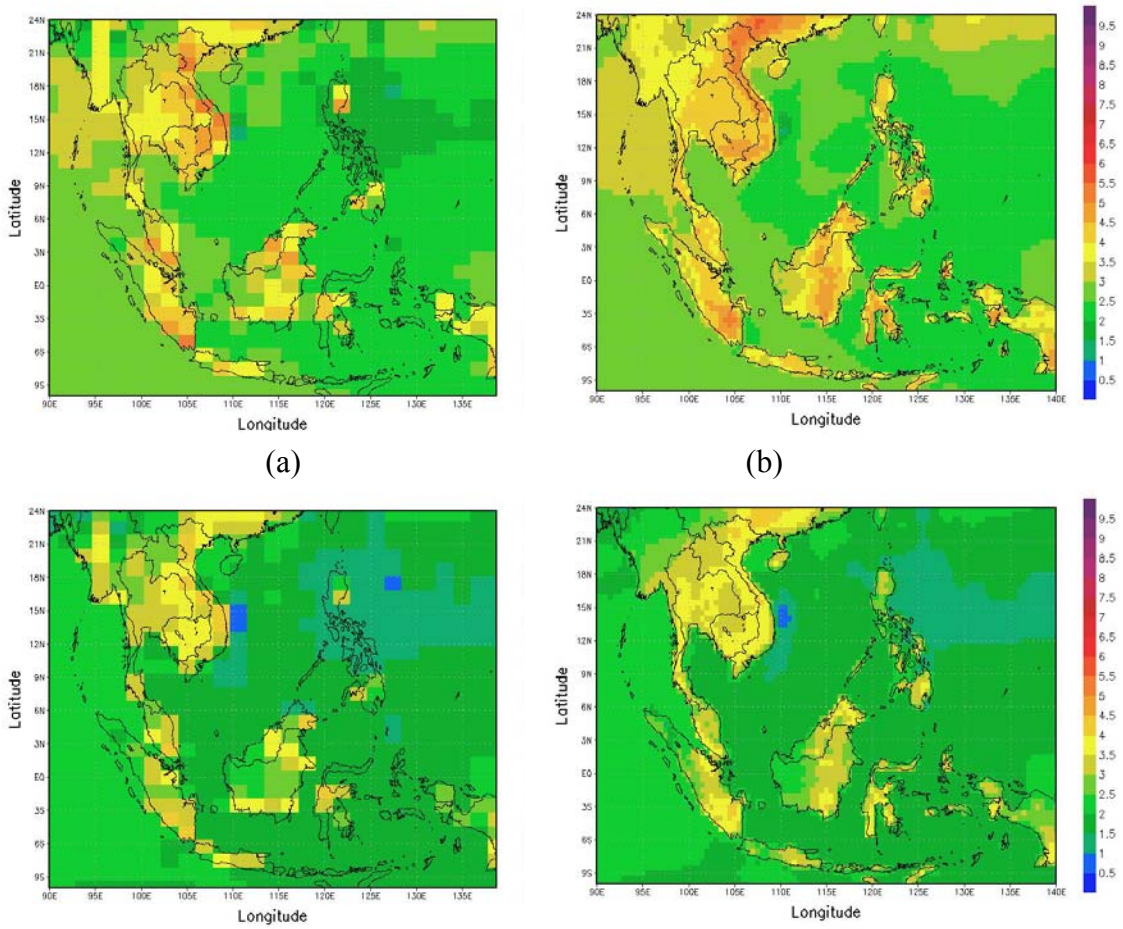

Figure 6.11: Projected changes in MAM maximum surface temperature (°C) for 2071–2100 relative to 1961–1990 projections from (a) HadAM3-A2 (b) HadAM3P-B2 (c) PRECIS-A2 (d) PRECIS-B2

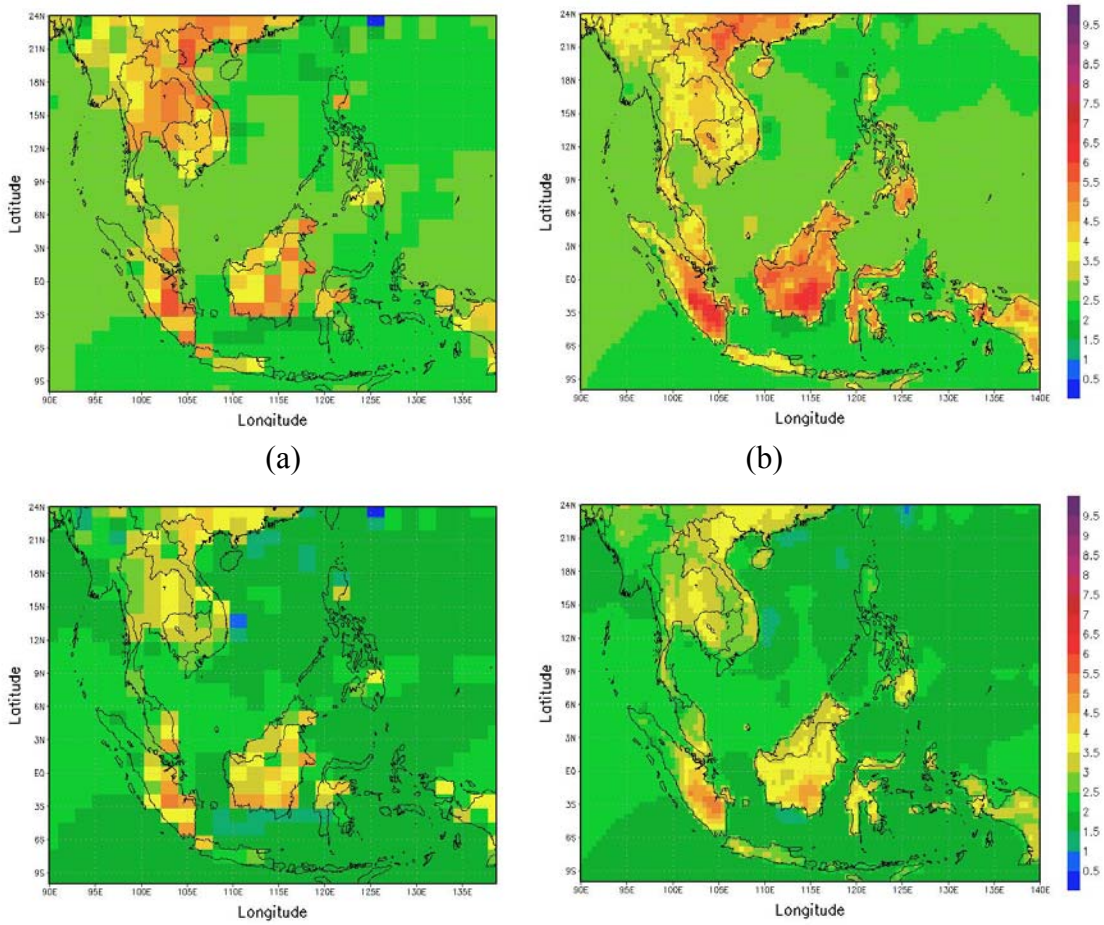

Figure 6.12: Projected changes in summer monsoon (JJAS) maximum surface temperature (°C) for 2071–2100 relative to 1961–1990 projections from (a) HadAM3-A2 (b) HadAM3P-B2 (c) PRECIS-A2 (d) PRECIS-B2

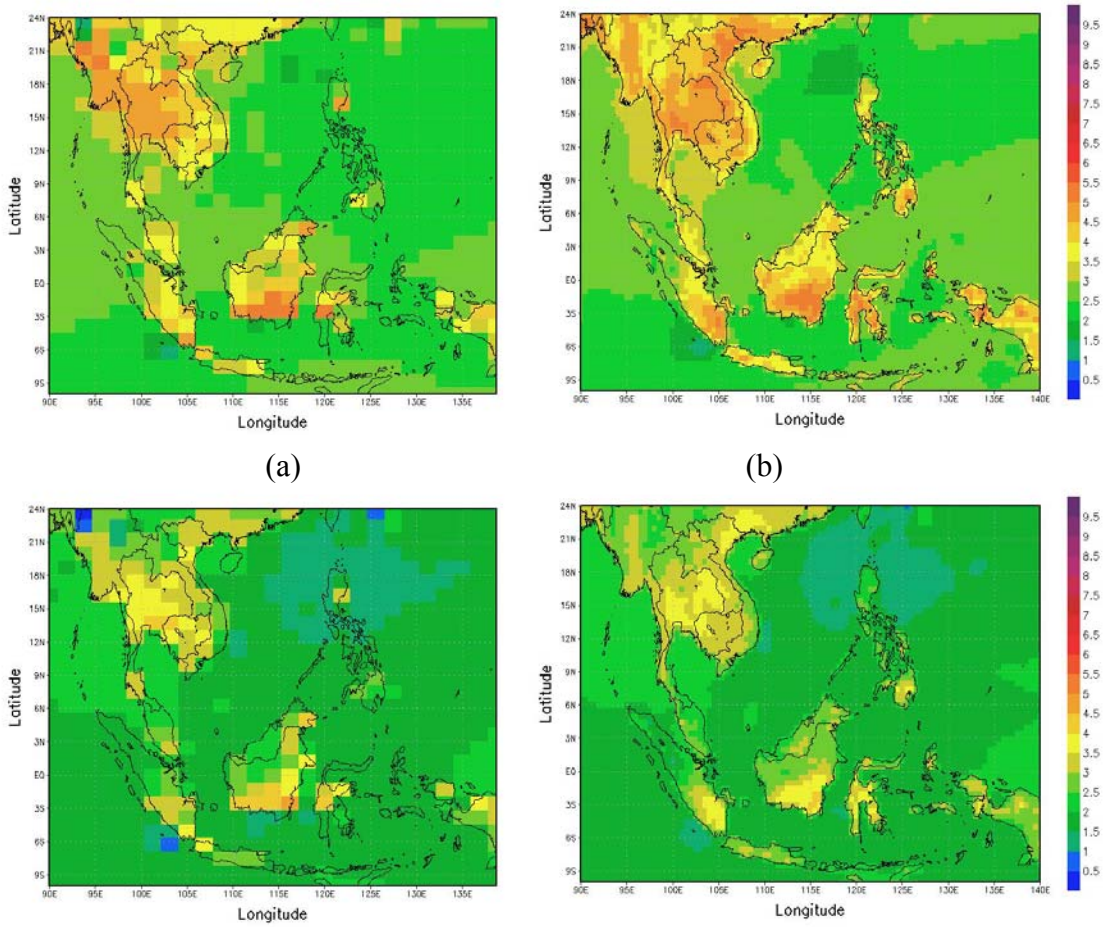

Figure 6.13: Projected changes in ON maximum surface temperature (°C) for 2071–2100 relative to 1961–1990 projections from (a) HadAM3-A2 (b) HadAM3P-B2 (c) PRECIS-A2 (d) PRECIS-B2

Changes in seasonal minimum surface air temperature from the GCM and RCM are shown in Figures 6.14-6.17. The minimum temperature warming patterns are consistent with the maximum temperature patterns; the largest warming in minimum temperature is detected in the same areas as the largest warming in maximum temperature. However, in the regions of largest warming, the minimum temperature change is 0.5°C lower than the warming of maximum temperature. For the SEA region overall, the largest warming in minimum temperature is in DJF.

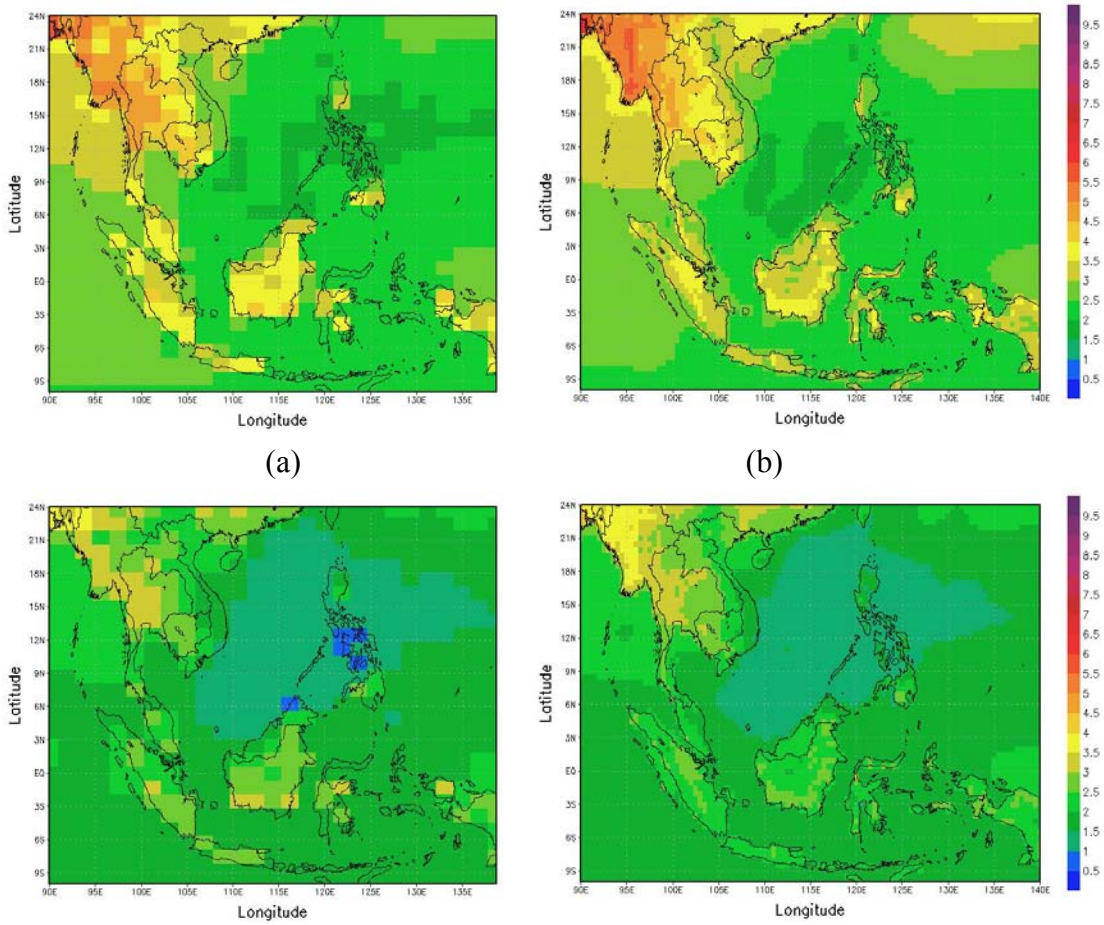

Figure 6.14: Projected changes in cool season (DJF) minimum surface temperature (°C) for 2071–2100 relative to 1961–1990 projections from (a) HadAM3-A2 (b) HadAM3P-B2 (c) PRECIS-A2 (d) PRECIS-B2

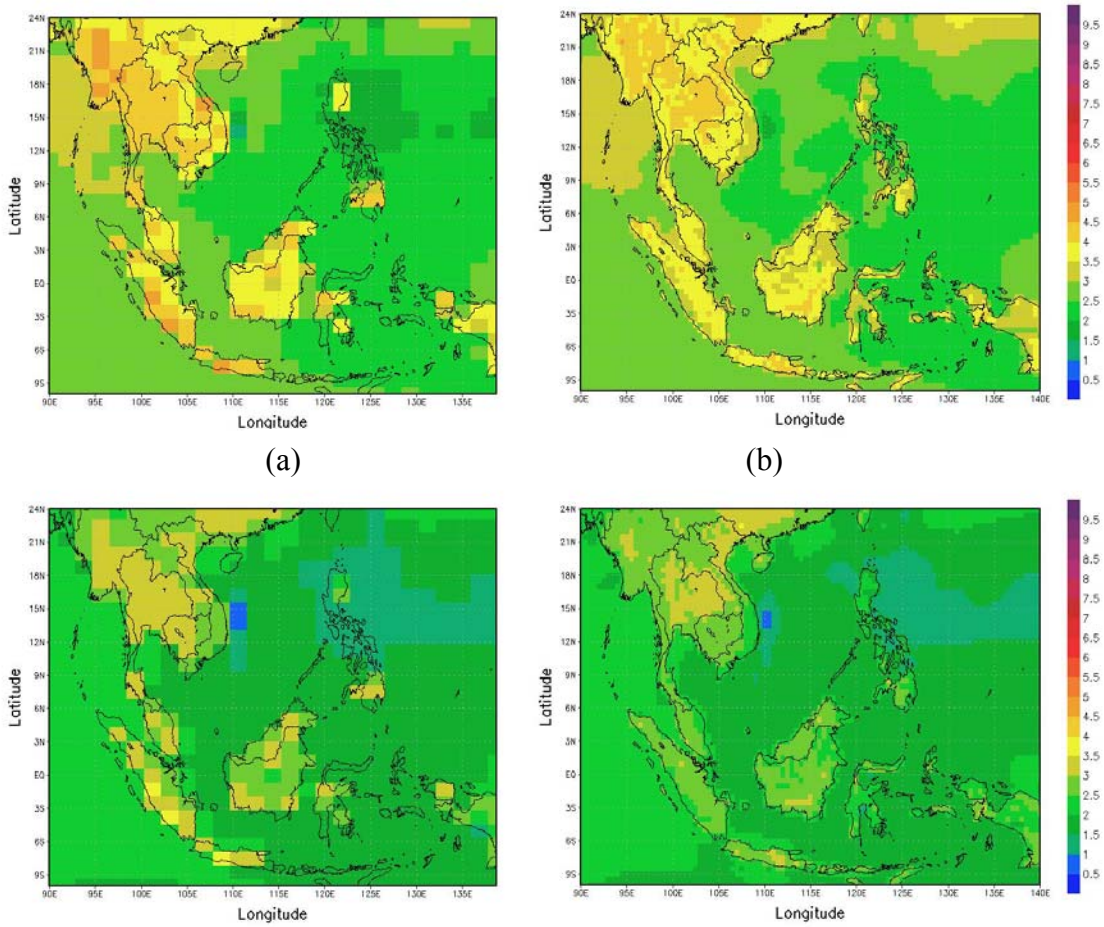

Figure 6.15: Projected changes in MAM minimum surface temperature (°C) for 2071–2100 relative to 1961–1990 projections from (a) HadAM3-A2 (b) HadAM3P-B2 (c) PRECIS-A2 (d) PRECIS-B2

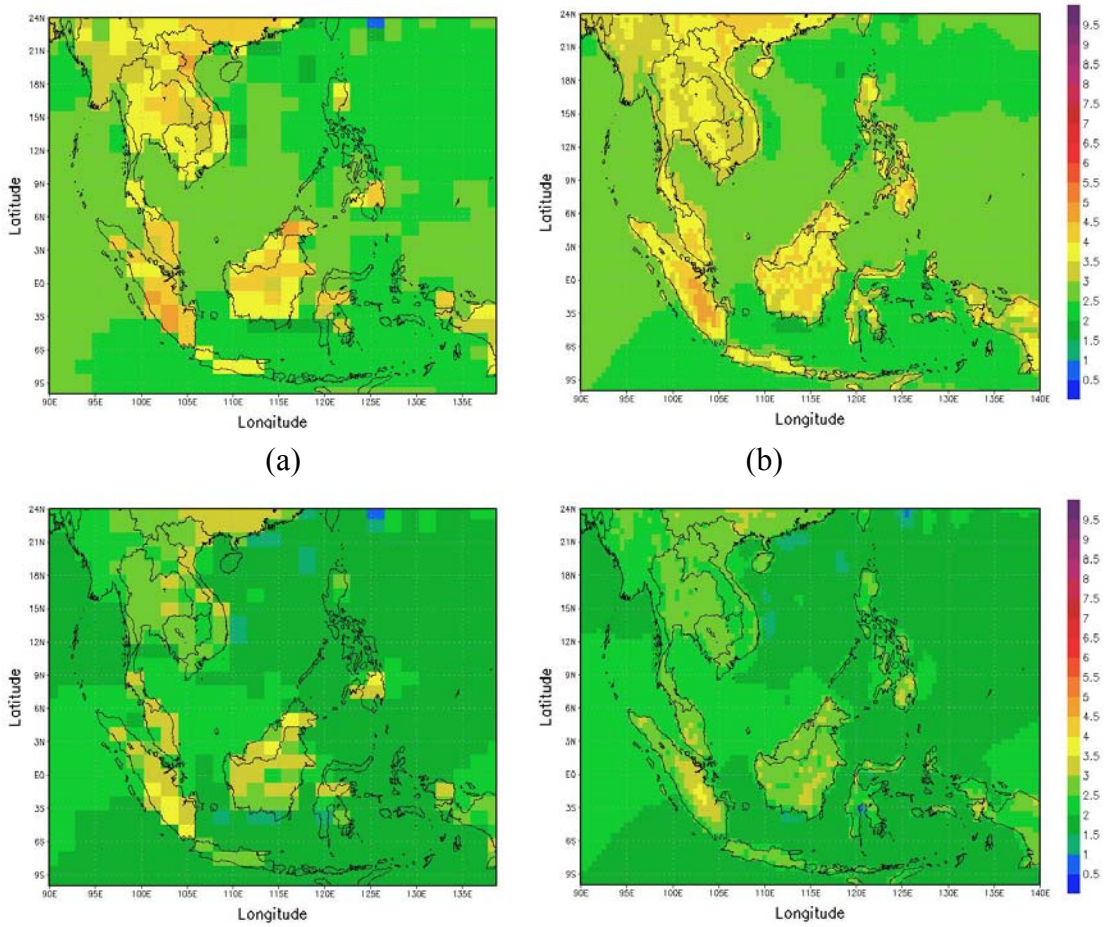

Figure 6.16: Projected changes in summer monsoon (JJAS) minimum surface temperature (°C) for 2071–2100 relative to 1961–1990 projections from (a) HadAM3-A2 (b) HadAM3P-B2 (c) PRECIS-A2 (d) PRECIS-B2

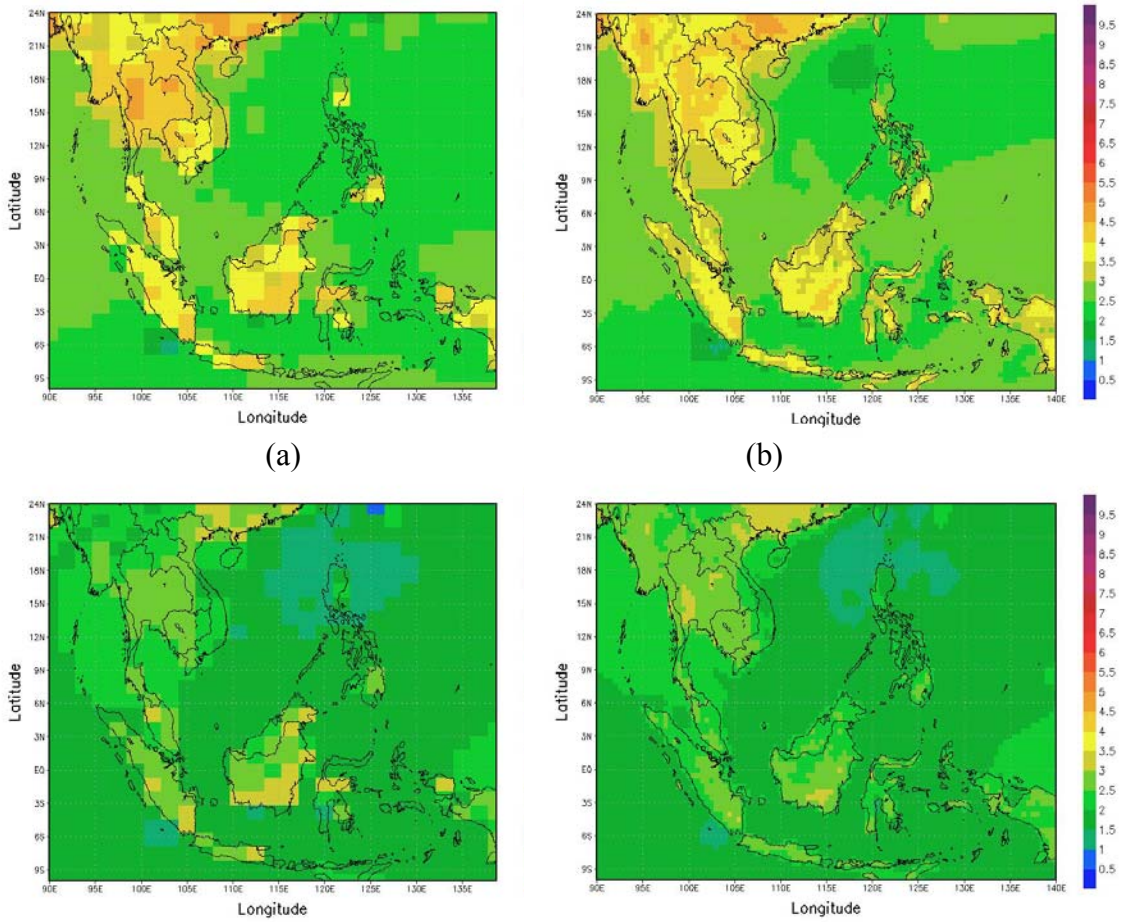

Figure 6.17: Projected changes in ON minimum surface temperature (°C) for 2071–2100 relative to 1961–1990 projections from (a) HadAM3-A2 (b) HadAM3P-B2 (c) PRECIS-A2 (d) PRECIS-B2

Table 6.2: Seasonal temperature warming (^{o}C) obtained from GCM and RCM simulations in Thailand

tmin change (^{o}C)	Annual	DJF	MAM	JJAS	ON
mainland Thailand					
HadAM3-A2	4.2	4.7	4.3	3.7	4.5
HadAM3-B2	3	3.1	3.4	2.8	2.8
PRECIS-A2	4.3	4.3	3.9	3.5	4.2
PRECIS-B2	3.2	3.1	3	2.7	3
Peninsular Thailand					
HadAM3-A2	3.4	3.2	3.5	3.4	3.3
HadAM3-B2	2.5	2.1	2.7	2.6	2.4
PRECIS-A2	3.4	3.4	3.4	3.4	3.5
PRECIS-B2	2.5	2.2	2.5	2.6	2.5
tmax change (^{o}C)					
mainland Thailand					
HadAM3-A2	4.1	3.5	3.6	4.5	4.8
HadAM3-B2	3.1	2.7	3.1	3.1	3.8
PRECIS-A2	3.1	3.4	4.2	4.3	4.5
PRECIS-B2	2.6	2.7	3.6	3.3	3.5
Peninsular Thailand					
HadAM3-A2	3.1	3.1	3.2	3.1	3.1
HadAM3-B2	2.4	2.3	2.6	2.4	2.4
PRECIS-A2	3.4	3.5	3.7	3.2	3.4
PRECIS-B2	2.7	2.6	3.1	2.5	2.6

The warming seen in the seasonal temperatures is reflected in the extreme temperatures also, and both maximum and minimum temperature are getting warmer in the future scenarios.

The seasonal cycle of maximum temperature change (Figure 6.18) differs dramatically between the hot and cool seasons. The largest warming in the mainland region occurs in May and the smallest in March for both A2 and B2 scenarios. The A2 scenario produces a larger warming by approximately 1^{o}C from May to December but a more modest increment during the rest of the year. The GCM and RCM produce a similar degree of warming during the summer monsoon season. Over peninsular

Thailand, the seasonal warming range is a modest 0.5°C in each of the simulations, with the A2 scenario producing a larger warming of about 1°C in each month. The GCM produces less warming than the RCM over the peninsula, most probably due to the relatively coarse GCM spatial resolution being unable to reproduce any land effects on the climate of this area.

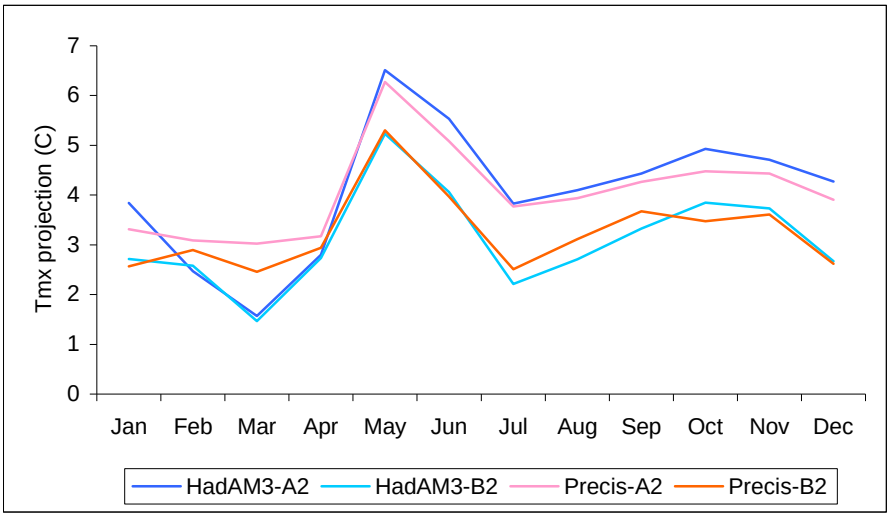

(a)

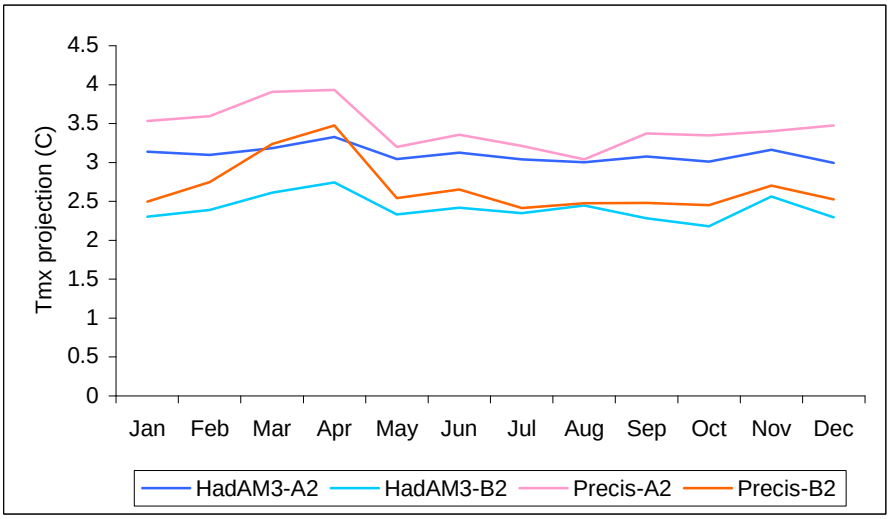

(b)

Figure 6.18: Surface air maximum temperature change projection over (a) mainland Thailand (b) Peninsular Thailand.

The seasonal cycle of minimum temperature change is shown in Figure 6.19. The largest warming in the mainland region, of the order of 5°C, occurs in February, May and November and the smallest in August for both A2 and B2 scenarios. The A2 scenario also produces a 1.5°C larger warming every month. The GCM produces a modestly larger warming than the RCM. Over peninsular Thailand the seasonal cycle in the warming shows a small range, with increases averaging 3.5°C and 2.5°C in the A2 and B2 scenarios respectively.. The A2 scenario produces a larger warming of about 1^{o}C in every month and the GCM and RCM produce comparable warming every month.

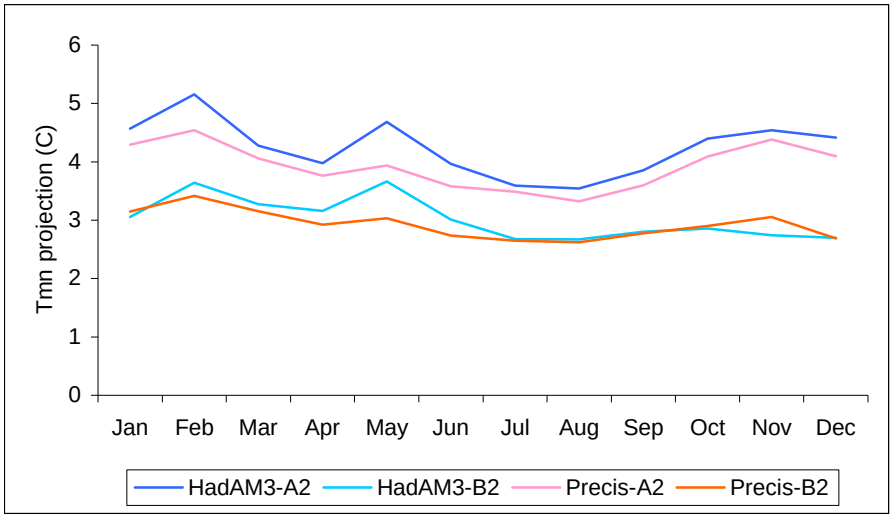

(a)

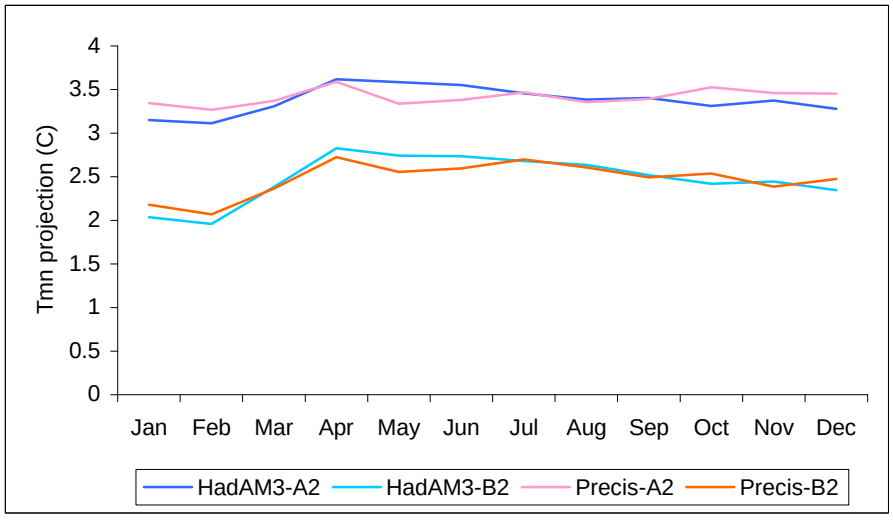

(b)

Figure 6.19: Air surface minimum temperature projection over (a) mainland Thailand (b) Peninsular Thailand

In Thailand specifically, annual temperature change (minimum and maximum combined) over mainland (peninsular) Thailand is approximately 4.2^{o}C (3.4^{o}C) in the A2 scenario and about 3.1^{o}C (2.5^{o}C) in the B2 scenario from the HadAM3 projection. There is a small difference in annual temperature change between the GCM and the RCM of <1^{o}C over the mainland; the annual temperature change over mainland (peninsular) Thailand is about 3.6^{o}C (3.2^{o}C) in the A2 scenario and about 2.8^{o}C (2.5^{o}C) in the B2 scenario in the PRECIS simulation. IPCC-TAR reported that the warming projection over SEA under the A2 and B2 scenario is less than 40% of the global annual average in both DJF and JJA, amounting to 1.8^{o}C under the A2 scenario and 1.3^{o}C under the B2 scenario. Meanwhile the IPCC-AR4 end of the century temperature estimate under the A1B scenario over SEA is 2.5^{o}C with range of 1.6^{o}C to 3.6^{o}C in DJF and 2.4^{o}C with the range of 1.5^{o}C to 3.8^{o}C in JJA.

6.2.3 Changes in extreme events

A key motivation for using RCMs in climate impacts research is the requirement to represent extreme events. By definition, extreme weather often occurs rapidly and over a small geographical extent. Extreme seasonal conditions, such as drought, occur more slowly and with larger geographical extent, and typically depend on fine-scale interactions between the atmosphere and land surface features such as topography that are not well resolved in global models. Thus, regional climate models are potentially better suited to studying these events. Summary statistics for several types of extreme events related to temperature and precipitation are presented in this section.

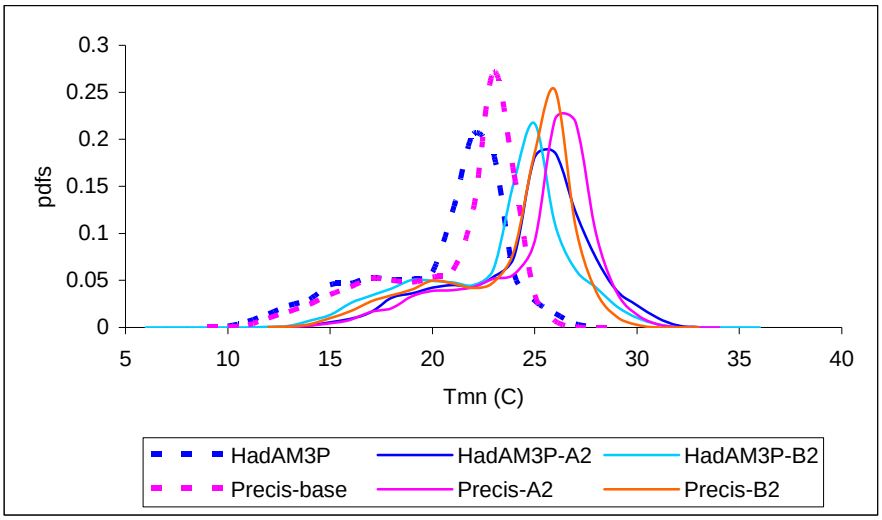

(a)

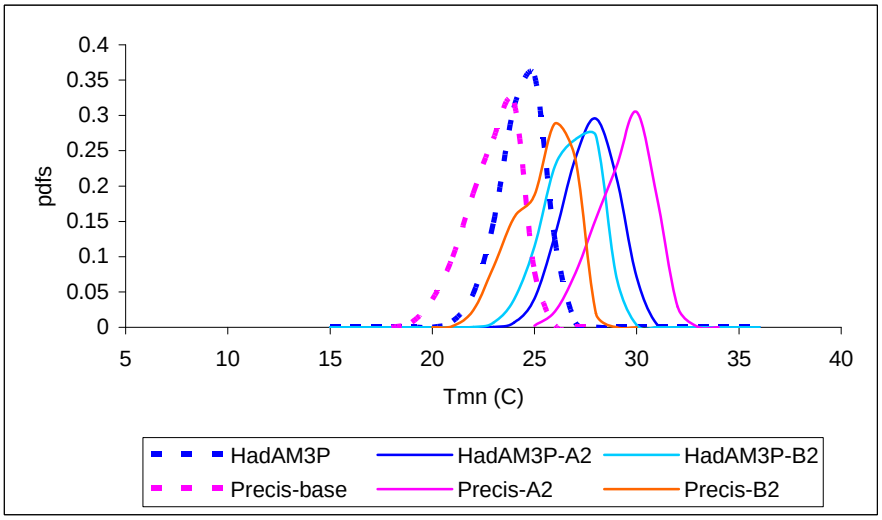

(b)

Figure 6.20: Air surface minimum temperature Pdfs over (a) mainland Thailand (b) Peninsular Thailand under different model simulations.

Simulated daily minimum temperature for the period of 2071 to 2100 is projected to show a shift in the mean of the distribution by about 3.5°C (6.0°C) and 2.8°C (2.3°C) over northern (Southern) Thailand for PRECIS under the A2 scenario and B2 scenario, respectively. Considering the distribution of the temperature change, the difference of the standard deviation appears to be about 0.1°C wider (absolute standard deviation about 3.2°C over northern Thailand and 1.3°C over the peninsula).

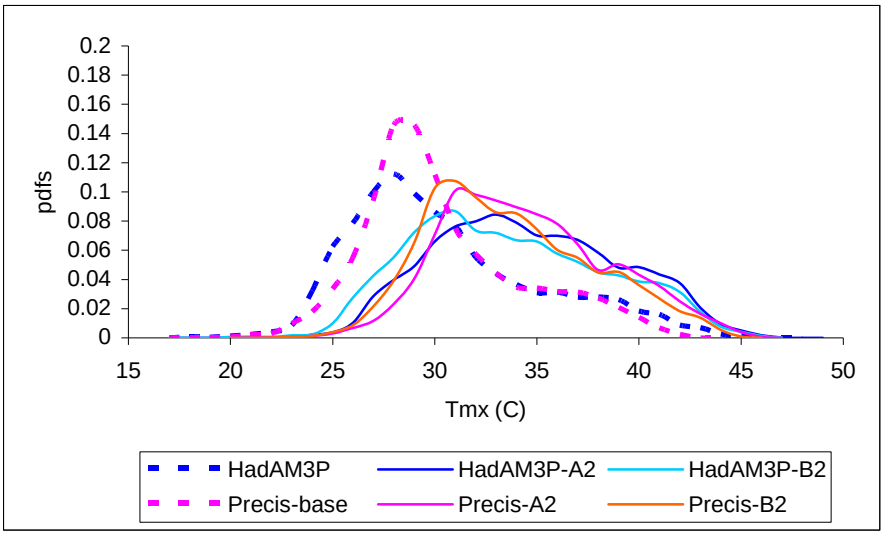

(a)

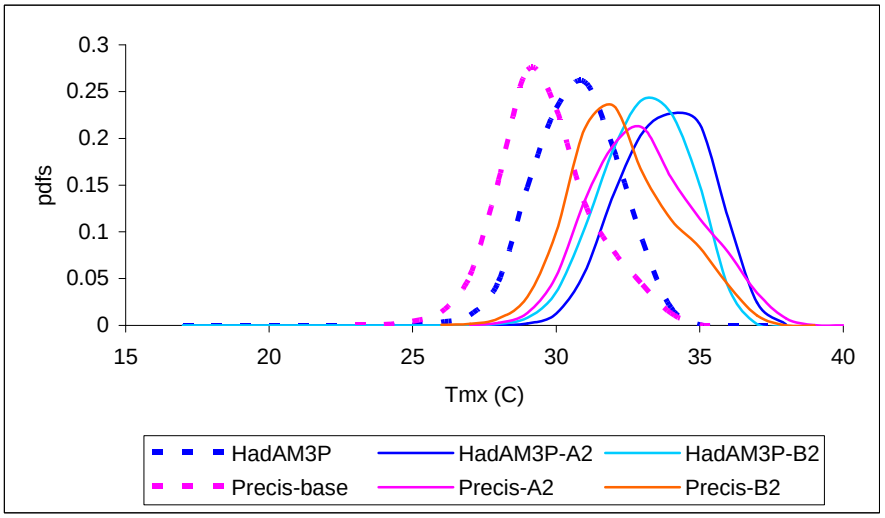

(b)

Figure 6.21: Air surface maximum temperature Pdfs over (a) mainland Thailand (b) Peninsular Thailand under different model simulations.

Simulated daily maximum temperatures for the period 2071-2100 show a shift in the mean of the distribution by about +3.0°C (+3.6°C) and 2.3°C (2.6°C) over northern (Southern) Thailand for the A2 scenario and B2 scenario, respectively, as shown in Figure 6.21. Considering the distribution of the temperature change, the difference of the standard deviation appears to be about 0.1-0.2°C wider (the absolute standard deviation is 3.9°C over northern Thailand and 1.6°C over the peninsula according to PRECIS-HadAM3).

The increase in daily maximum temperature is greater than the increase in daily minimum which leads to an increased mean diurnal temperature range. The results indicate an increase in the 95th percentile of maximum temperature to 41.7°C in northern Thailand and 36.4°C in the peninsula region while the baseline value are 36.7°C and 32.6°C.

Considering temperature extremes with specific temperature thresholds, hot and cold events can be divided into days above and below a threshold. TMD defined a hot day to be a day with temperature >35°C and a cold day to be a day with temperature <16 °C. Rising daily maximum temperatures result in an increase in the number of days exceeding a predefined threshold value, such as, ≥35°C. In a similar way, the numbers of days with minimum temperatures below a specific threshold (eg.≤16°C) are expected to decrease in all seasons (Table 6.3). Bell et al. (2004) indicated that the increase in daily minimum temperature is associated with decrease in days below freezing and prolonged cold events occur less often and are shorter and warmer on average over California, a climatically complex region.

Table 6.3: Absolute number of hot days (≥35°C) and cold nights (≤ 16°C) in total during each season for 1961-1990 and 2071-2100.

number of hot days	DJF	MAM	JJAS	ON
mainland Thailand				
PRECIS-HadAM3P	13	44	1	0
PRECIS-A2	39	73	31	18
PRECIS-B2	29	69	20	9
peninsular Thailand				
PRECIS-HadAM3P	0	0	0	0
PRECIS-A2	15	52	13	2
PRECIS-B2	3	39	4	0
number of cold days				
mainland Thailand				
PRECIS-HadAM3P	35	0	0	13
PRECIS-A2	5	0	0	1
PRECIS-B2	9	0	0	3
peninsular Thailand				
PRECIS-HadAM3P	0	0	0	0
PRECIS-A2	0	0	0	0
PRECIS-B2	0	0	0	0

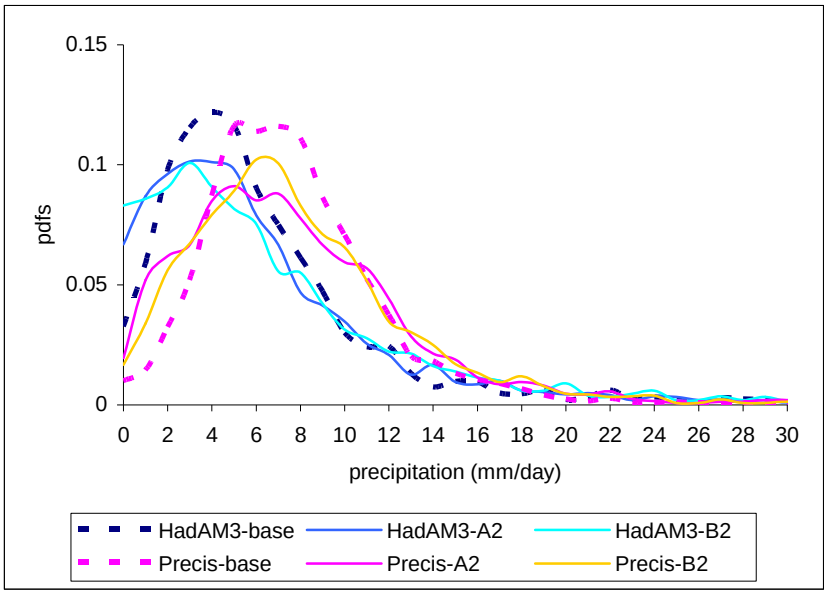

(a)

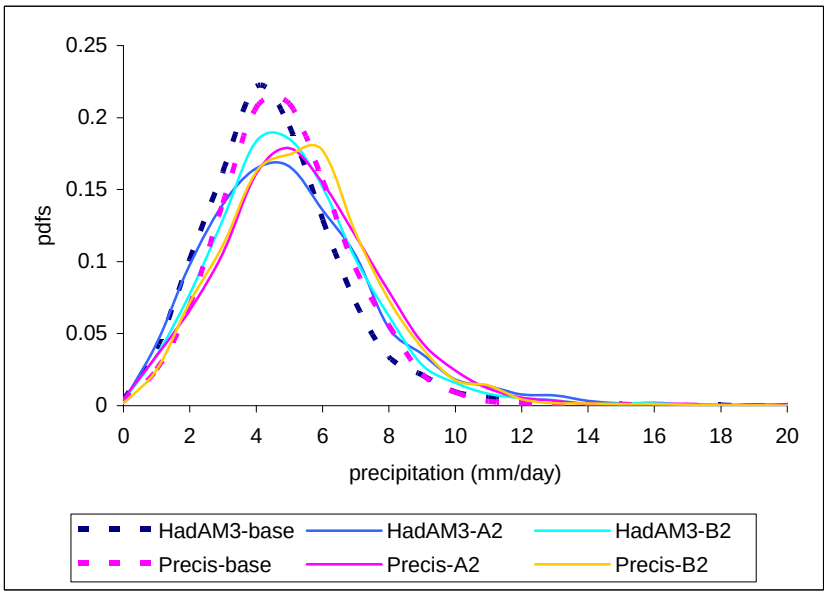

(b)

Figure 6.22: Frequency distributions of daily precipitation over land during JJAS over (a) northern (b) peninsular Thailand. The dashed lines show baseline simulations (1961-1990). Solid lines show future simulations (2071-2100)

Figure 6.22 presents changes in frequency distribution of daily precipitation from 1961–1990 to 2071–2100 during the rainy (JJAS) season. Due to the pdfs similarity over the mainland, the northern region is considered as a whole. Changes in frequency of daily precipitation are slightly different between the A2 and B2 scenarios. For northern Thailand, during JJAS, the number of days with daily precipitation below

3.5(3) and above 11(12.5) mm/day tends to increase in the A2 (B2) scenario, with a broader standard deviation. The extreme precipitation, over the 95th percentile, of precipitation increases from 15.7mm/day to 17.8 and 17.1 mm/day in the A2 and B2 scenarios, respectively. For peninsular Thailand the number of days with daily precipitation above 6.5 (5.5) mm/day tends to increase in the A2 (B2) scenario during the active southwest monsoon accompanying a +10% precipitation amount increase. The extreme precipitation, over the 95th percentile, of precipitation shifts from 8.2 to 9.6 and 9.2 mm/day for the A2 and B2 projections.

In terms of the most damaging extreme events in Thailand, this study found that the 95th percentile daily precipitation intensity increased by up to 2 mm/day which might be associated with hot day increases being larger than cold day decreases. These two conditions, hotter and wetter, may more likely lead to severe storms and floods.

6.2.4 Monsoon onset

The rainy season over Thailand extends from mid-May to mid-September (Tanaka, 1992; Murakami and Matsumoto, 1994; Sangwaldach, 2006). The 30 year monthly mean specific humidity at 1.5 m over Thailand (Figure 6.23) shows a rapid increase between February and May. The largest specific humidity occurs from May to September. Approximately 70-80% of the total annual precipitation in Thailand occurs during this period, with the onset of monsoon occurring in mid-May and the wettest month occurring in September. Surface specific humidity remains essentially constant for the whole monsoon season.

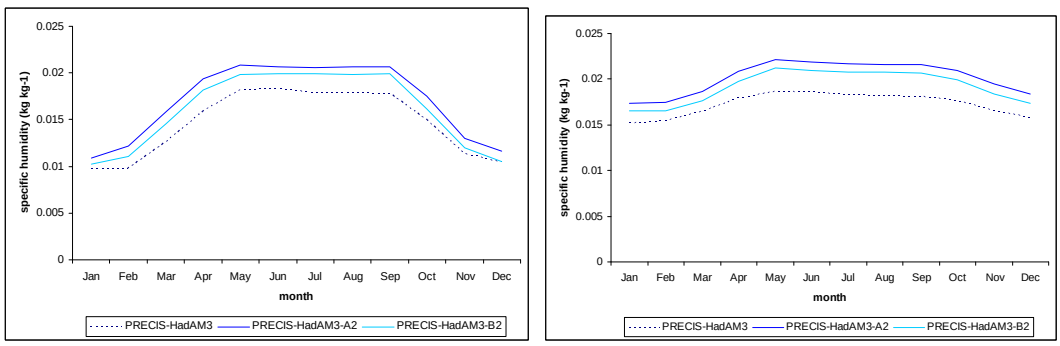

Figure 6.23: 30 year monthly mean specific humidity (kg/kg) at 1.5 m over mainland Thailand (left) and southern Thailand (right) from PRECIS during 2071-2100.

From the PRECIS-A2 simulation, the first appearance of an average resultant 850 hPa westerly wind of strength 4 m/s occurs in the fourth pentad of May (Figure 6.24a), while an average 250 hPa easterly wind first appears in the third pentad of May (Figure 6.24b) and the first appearance of an average precipitation greater than 6 mm/day occurs in the first pentad of May (Figure 6.26a). Based on the same criteria to justify the monsoon onset date as used in Chapters 4 and 5, PRECIS-A2 simulates average monsoon onset during 2071-2100 in the fourth pentad of May.

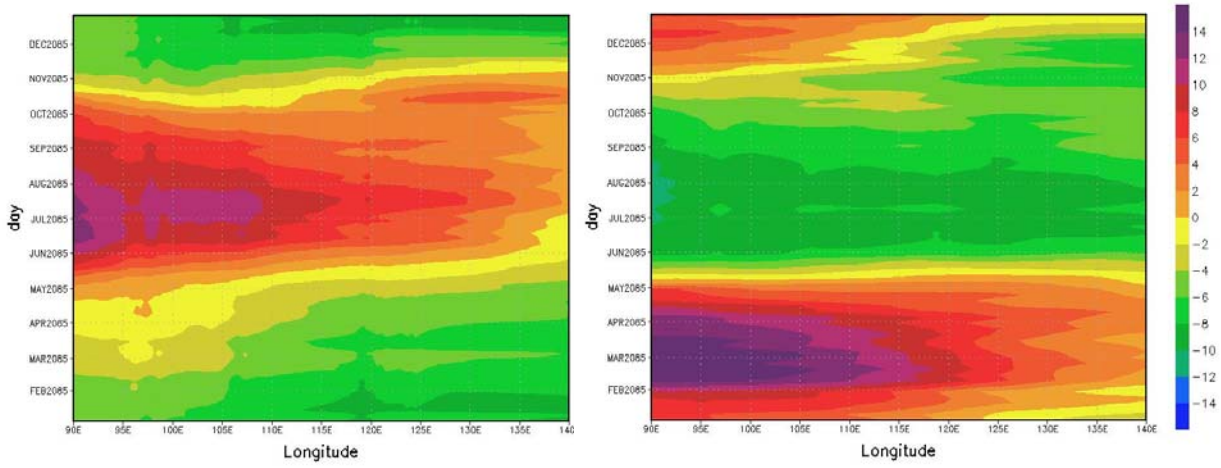

(a) (b)

Figure 6.24: Time-longitude section averaged over 5^{o}N-20^{o}N of climatological pentad zonal wind (ms^{-1}) from PRECIS-A2 at (a) 850 hPa (b) 250 hPa

On the other hand, from the PRECIS-B2 simulation, the first appearance of an average resultant 850 hPa westerly wind of strength 4 m/s occurs in the fourth pentad of May (Figure 6.25a), while the average 250 hPa easterly wind first surprisingly appears in the third pentad of May (Figure 6.25b) and the arrival of an average precipitation greater than 6 mm/day occurs in the second pentad of May (Figure 6.26b). The PRECIS-B2 simulation therefore produces an average monsoon onset during 2071-2100 which also occurs in the fourth pentad of May. Therefore, the projection of monsoon onset for the end of this century is one pentad (5 days) later than the average monsoon onset during 1961-1990. From statistical analysis, the monsoon onset date averaged over the 1961-1990 period over Thailand was approximately 11th May with a standard deviation of 8 days (section 4.2.7). The

monsoon possibly arrives in Thailand, by the end of this century, in the range of the second pentad of May to the first pentad of June. The latter might lead to a more prolonged drought period which could affect rice cultivation.

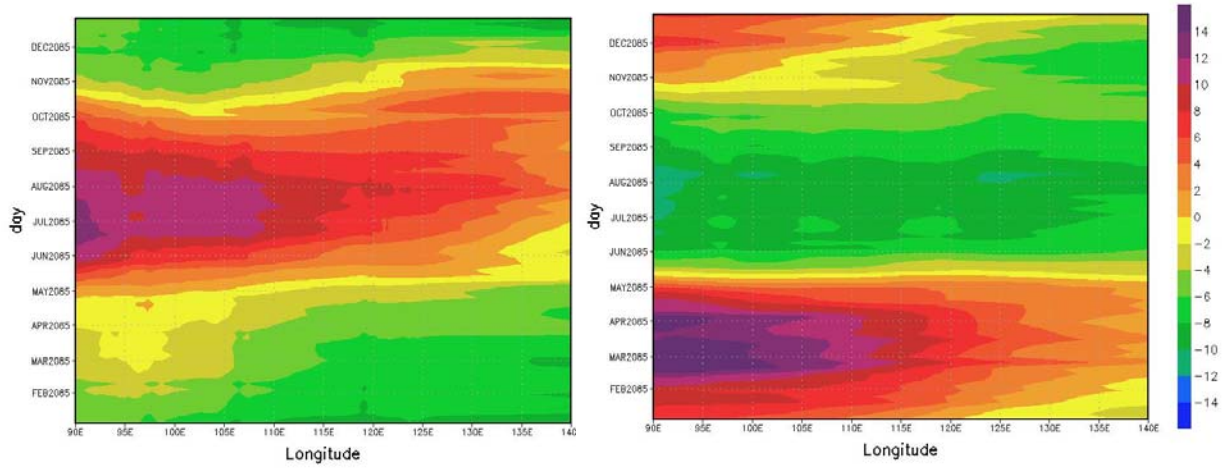

(a) (b)

Figure 6.25: Time-longitude section averaged over 5^{o}N-20^{o}N of climatological pentad zonal wind (ms^{-1}) from PRECIS-B2 at (a) 850 hPa (b) 250 hPa

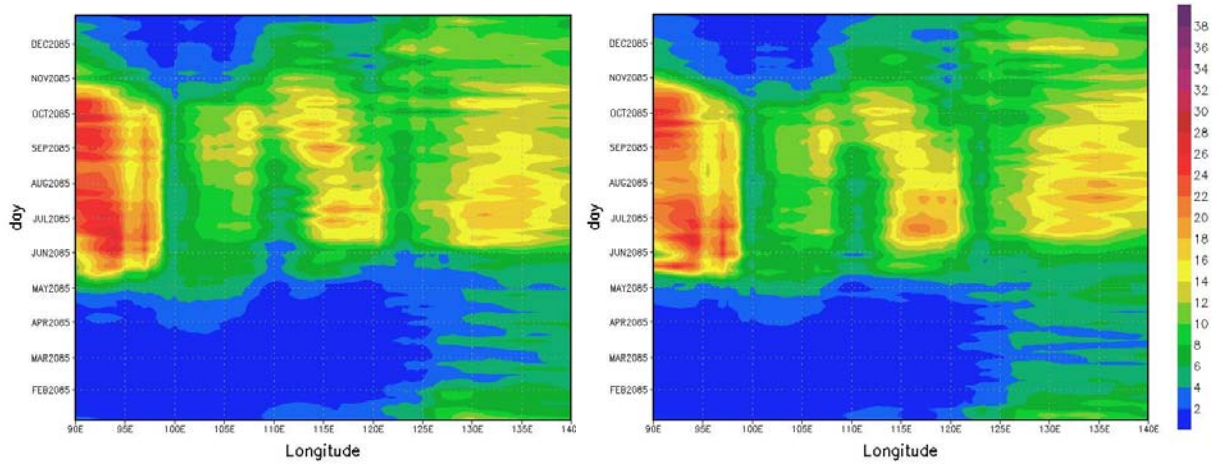

(a) (b)

Figure 6.26: Time-longitude section averaged over 5^{o}N-20^{o}N of climatological pentad total precipitation (mm/day) from (a) PRECIS-A2 (b) PRECIS-B2

6.3 Summary

Over **mainland Thailand**, during DJF, the precipitation projection from the A2 emission scenario shows a small increase and the precipitation projection from the B2 emission scenario shows a small decrease (Figure 6.1). During JJAS the GCM A2 and B2 scenarios both project no significant precipitation changes while the RCM A2 and B2 scenarios project small precipitation increases. Over the **peninsula** all simulations, GCM-A2, GCM-B2, RCM-A2 and RCM-B2, project small precipitation decreases during DJF and small increases during JJAS (Table 6.1).

The increase in precipitation during JJAS occurs in association with a either an unchanging or decreased number of wet days, implying that the average amount of precipitation on wet days in the future is larger than the amount in the baseline period. Moreover, the future vertical velocity simulations during JJAS are increased compared with the baseline period. The specific humidity also increased remarkably over the Indian Ocean which is consistent with intensified moisture transport. Therefore, the small precipitation increases during JJAS found in the future scenario projections seem to be most associated with higher moisture in the atmosphere and increased precipitation intensities. Intensive precipitation events, i.e., tropical cyclones, are likely to be associated with the JJAS precipitation increase. In terms of small precipitation changes (both positive and negative) in DJF, this does not imply a significant climate change impact in Thailand because precipitation during this season is relatively low. On the other hand, a small precipitation decrease during MAM and a small precipitation increase during JJAS (Table 6.1) is an important climate change in a country which has fluctuated from severe droughts to severe floods. Most recently severe floods occurred in October-November, 2009, when over 40 cities on the mainland, including Bangkok, were affected with 21,901 damaged houses, 1.2 million km^2 of agriculture damage and 11 deaths. Another severe flood occurred over southern Thailand in the period 23 March - 3 April, 2011 while precipitation was below normal level causing drought during 1 November, 2009 to 28 February, 2010 over 29 cities in Thailand (http://www.thaiwater.net/web/index.php/archive.html, in Thai).

In general, for the SEA region, both GCM and RCM produce similar patterns of changes in maximum and minimum temperature but with small differences over specific areas. The warming according to the RCM is about 1^{o}C higher than with the GCM. The difference in warming between RCM-A2 and RCM-B2 is about the same amount, 1^{o}C. The RCM A2 and B2 simulations show warming over both the mainland and peninsular Thailand, greater than the average annual warming (3.0^{o}C for A2 and 2.2^{o}C for B2), in DJF and JJAS in both A2 and B2 scenarios. The warming over the mainland is higher than over the peninsula by 0.9^{o}C in DJF and by 0.1^{o}C in JJAS. This warming is consistent with the 4^{o}C global average-temperature rise proposed by IPCC, however, it is greater than the agreement in most GCMs under the A2 and B2 scenario in IPCC-TAR (2001) and most AOGCMs under the A1B scenario in IPCC-AR4 (2007). IPCC-TAR (2001) reported a warming projection over SEA under the A2 and B2 scenarios of less than 40% of the global average annual warming in both DJF and JJA, namely 1.8^{o}C under the A2 scenario and 1.3^{o}C under the B2 scenario. IPCC-AR4 temperature increase under the A1B scenario over SEA is 2.5^{o}C with a range of 1.6^{o}C to 3.6^{o}C in DJF and 2.4^{o}C with a range of 1.5^{o}C to 3.8^{o}C in JJA.

In general, the annual minimum temperature change over mainland (peninsular) Thailand is about 4.2^{o}C (3.4^{o}C) under the A2 scenario and about 3.1^{o}C (2.5^{o}C) under the B2 scenario. There is an interesting difference in annual maximum temperature change between the GCM and the RCM of up to 1^{o}C over the mainland. The annual maximum temperature change over mainland (peninsular) Thailand is about 3.6^{o}C (3.2^{o}C) in the A2 scenario and about 2.8^{o}C (2.5^{o}C) from B2. This high warming could lead to rain forest loss in northern Thailand either through drought stress on vegetation or through uncontrolled spread of forest fire. Thailand produces only 0.8% of the world's carbon dioxide emissions, and has a lower per capita emission rate than the global average. However, with a global average temperature increase of 4^{o}C, the proportion of CO_2 emissions remaining in the atmosphere could rise to 70%. The warming would also have an effect on water availability by reducing river run-off and sea level rise would threaten to submerge Bangkok.

PRECIS-A2 and PRECIS-B2 both simulate average monsoon onset during 2071-2100 in the fourth pentad of May. Therefore, the monsoon projection for the end of this century is for monsoon onset to occur one pentad later than the average monsoon onset during the baseline period 1961-1990 (the third pentad of May).

Thailand is home to about 64 million people, the majority living in rural and agricultural areas. Agriculture employs 49% of the population and contributes 10% of GDP (http://www.nso.go.th/). Moreover, tourism along the coastline plays an important role in the Thai economy, providing 6% of GDP. As capital city, Bangkok is home to 15% of the Thai population and serves as the economic, political and social centre. Therefore climate change threatens all three important sectors of Thailand's economy: agriculture, tourism, and trade. The effects of climate change, including higher surface temperatures, floods, and droughts put Thailand's rice crop at risk. In this study, it is projected that a warming of 1.5°C-4.3°C by the end of this century will occur, affecting rice productivity. One degree of warming will destroy the rice crops that are central to the economy, and a few centimeters of sea level rise will submerge the capital city and devastate coastal tourism. This study also found that the wet season will be wetter through fewer wet days but more intense precipitation events and that the dry season will be drier and longer; an action plan is needed to mitigate against and adapt to this climate change. One mitigation measure must be urgent global action to significantly reduce greenhouse gas emissions from vehicles and energy use.

Chapter 7
Conclusions and Recommendations

7.1 Conclusions

Thailand is located on the Indochina peninsula and is a country of complex and contrasting topography, including the mountainous north, the high plateau in the north-east, the lowland plains in central regions and the peninsula in the south. The country has coastal borders with the Andaman Sea and the Gulf of Thailand and the climate is also influenced by the Bay of Bengal and the South China Sea. Southern Thailand includes the narrowest part of Indochina in the form of a long peninsula with a width of just 0.7° longitude. Coarse resolution GCMs clearly struggle to resolve some of the climatic influences of all this complex topography. It is essential that higher resolution climate modelling is trialled, in application to Thailand, to test its capability to simulate the Thai climate more faithfully and to project possible climate futures.

This project first tried to develop new knowledge about the recent climate of Thailand by using daily surface station observations from the Thai Meteorology Department (TMD) and a high resolution monthly gridded dataset (CRUTS2.1) covering the period 1961-90. Brief details of CRUTS2.1 are provided in chapter 3 and full details are available in Mitchell and Jones (2005). There is no previous literature documenting the application of CRUTS2.1 specifically to Thailand. The CRUTS2.1 gridded dataset was based on 36 stations in Thailand and is used to summarise the spatial variation in Thai climate seasonality and to provide a good resource to assist with verification of the climate model output.

Using the above observational data over the period 1961-1990, it is found that the climate over peninsular Thailand can be clearly distinguished from the climate over the mainland. It was shown that the annual/JJAS precipitation over the **mainland region** has decreased by 0.13/0.76 mm/year respectively, over this period; the dominant precipitation season is JJAS, the SEA summer monsoon, contributing 60-70 % of the annual rain; the number of rain days (≥1 mm) in JJAS is also shown to have decreased in this region by approximately 10 days over the period which supports the

findings of other studies. For instance, Manton et al. (2001) also found that the number of rain days had decreased significantly at one station located in northern Thailand and at another station located in southern Thailand over 1961-1998, and the proportion of precipitation from extreme events had increased at the Nan station, located in northern Thailand. In this thesis, minimum temperatures over the mainland are shown to have increased by approximately 1^{o}C in MAM and DJF during the 1961-1990 period, higher than the linear global warming trend over 1956-2005 of 0.13^{o}C per decade (IPCC-AR4, 2007) while maximum temperatures have increased by. 0.47^{o}C (0.02^{o}C)/30 years in MAM (DJF). Regarding the spatial minimum and maximum temperature pattern in Thailand, the area showing a warming trend appears larger in 1961-1970 compared with 1981-1990. The trend in mainland Thailand diurnal temperature range (DTR) reveals a decrease in MAM and DJF. This decrease in DTR is caused by temperatures increasing faster at night than during the day. The estimated average summer monsoon onset date (1961-1990) is shown in this thesis to be 11th May and would appear to be happening insignificantly later by the end of the 1961-90 period (1 day/30 year). The monsoon onset date can be seen to vary, over the 1961-90 period, between 10 days later and 13 days earlier than the mean for the period.

The annual precipitation over the **southern region** of Thailand shows a faster rate of decrease in some seasons than over the mainland region, 0.66, 0.28 and 2.44 mm/month-year in annual, JJAS and ON 1961-90 data respectively; the precipitation during JJAS (ON) in this region contributes approximately 40 (30) % of the annual rain and the number of rain days is shown to have decreased by approximately 10 days over the 1961-90 period. This finding is consistent with Mention et. al. (2000) who showed that Prachuap Khiri Khan, one of the stations in southern Thailand, demonstrates a significant decrease in rain days over 1961-1998. The minimum and maximum temperatures over southern Thailand show relatively small changes through the year. The minimum and maximum temperatures are shown to be increasing at 1.6^{o}C (0.7^{o}C) /30 years and 0.46^{o}C (1^{o}C) /30 years in MAM (DJF) respectively over the 1961-1990 period. The DTR is shown to have decreased at a rate of 1^{o}C /30 years in MAM and increased at a rate of 0.25^{o}C /30 years in DJF. The average monsoon onset (1961-1990) date is the 10th May, slightly earlier than over the

mainland region. The inter-annual variability in onset over southern Thailand is similar to that over mainland Thailand.

In terms of tropical depressions, analyzing the impact of cyclonic disturbances on individual station precipitation in this study found that there is a statistically significant difference in precipitation over both the mainland and the peninsula, therefore, depression frequency statistically significantly increases precipitation. Moreover, it was found that the relationship between the number of wet days and precipitation amount for all five sites analysed is a simple linear function. The decrease in the number of wet days is therefore a key factor in inducing the precipitation decrease during JJAS.

In this thesis it was shown in section 4.2.4 that there is no sign of precipitation change over the mainland during La Niña events, however, there is a statistically significant decrease of precipitation during El Niño years at the Chiang Mai site during JJAS and a statistically significant intensification of precipitation during La Niña years at Surat Thani during ON. There are no statistically significant differences in precipitation found between any pair of these ENSO events during DJF and MAM seasons over 1961-1990. This indicates that the precipitation during the DJF and MAM seasons is not influenced by the ENSO phenomenon. Meanwhile, in El Niño years, tropical depression activity during neutral years and El Niño years over Thailand is comparable during the period July-November whereas during La Niña years, the number of depressions in Thailand is generally above average.

A case study of the major El Niño event in 1982 using the gridded CRU dataset showed that precipitation during JJAS was slightly lower than average (1961-1990) over Thailand. Over peninsular Thailand, there is no significant anomaly detected during ON, a period when 30% of the precipitation occurs on average. A case study of the 1988 La Niña event showed that increased precipitation is observed over western Thailand in July while during November decreased precipitation occurred over the peninsula. No other significant anomalies occur in Thailand in the remaining months during this La Niña event.

PRECIS simulations run with and without an interactive sulphur cycle show insignificant differences in spatial and point precipitation analysis, moreover, in terms of simulations driven from different initial conditions of HadAM3P, a 150 km resolution version of the Hadley Centre's global atmosphere-only model, using observed time series of HadISST SST and sea-ice for 1960-1990, there is also no significant difference in output (Table 5.1 and 5.2). Both PRECIS and HadAM3 produce precipitation spatial patterns for the current climate (1961-90) which are in general consistent with the gridded CRUTS2.1 dataset, but with the models overestimating precipitation over the area north of 12°N and underestimating precipitation over the area to the south. Comparison between the driving GCM, HadAM3P, and PRECIS over Thailand specifically, shows that HadAM3P simulates the precipitation amount in all seasons better over the mainland than PRECIS while the latter simulates the precipitation amount more accurately over peninsular Thailand. This shows that PRECIS has the capability to resolve features in a complex area, as shown in Figure 7.1; the coarser resolution of HadAM3 assumes that the peninsular is in fact sea. Over another region affected by the southwest monsoon, India, Kumar et al. (2006) found that PRECIS can capture the spatial pattern of the summer monsoon along the windward side of the Western Ghats. With respect to Thailand, the average daily precipitation during JJAS over 1961-1990 simulated by the RCM added more detail, in particular, over the coastline. It was found that PRECIS-ERA simulates total precipitation amount in JJAS with much lower error of 20-30% than ERA. This indicates that, in the summer monsoon season, the dynamical downscaling performed by PRECIS–ERA40 results in more accurately simulated precipitation amounts over this geographical area. The ERA40 strongly underestimated total precipitation mainly results from the coarse resolution, 2.5 x 2.5 degree, and may be related to (i) underestimation of atmospheric surface wind speed (ii) inaccurate cloud radiation and (iii) error of tropical deep convection cloud and low level cloud amount in particular over this geographic area which are improved with skill of PRECIS.

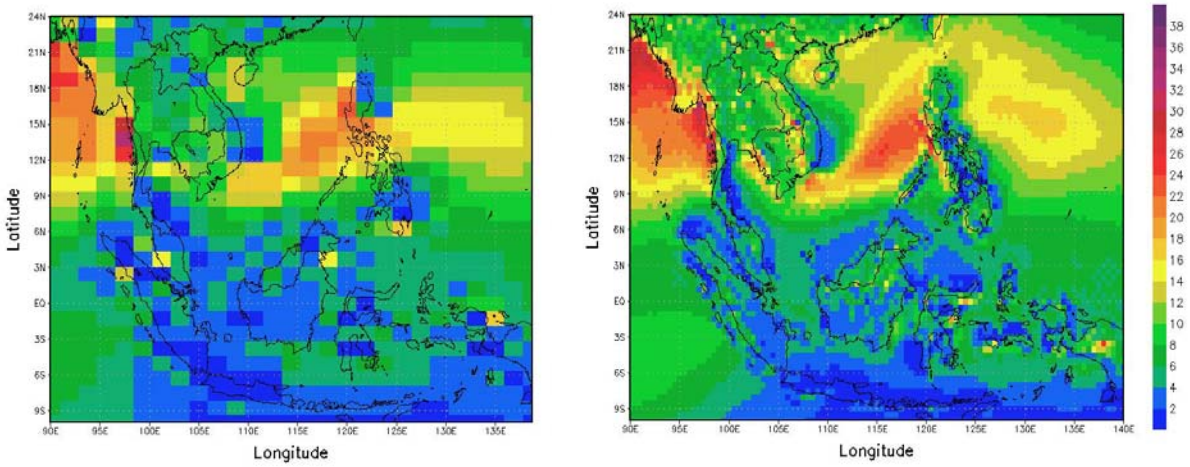

(a) (b)

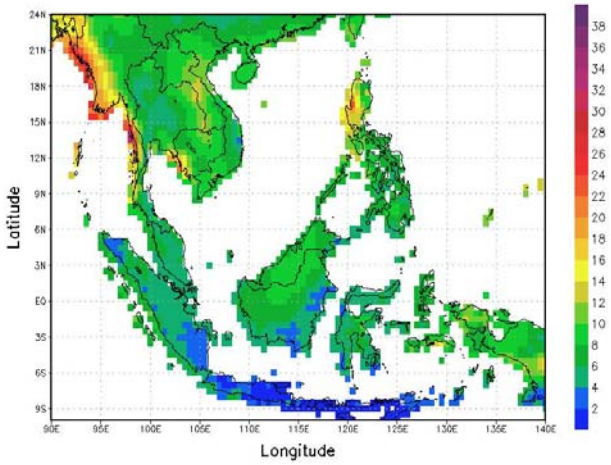

(c)

Figure 7.1: Spatial distribution of average precipitation (mm/day) during JJAS (1961-1990) from (a) GCM, HadAM3P (b) RCM, PRECIS-HadAM3P (c) CRUTS2.1

Applying the grid-to-grid analysis method, there is a striking precipitation difference in the sign of the model bias between the north and south of the domain (Figures 5.2-5.5) indicating that the bias over SEA depends on geographical location. In PRECIS simulations over other parts of the world, precipitation bias more commonly depends on season, for example, underestimation (overestimation) during summer (winter) possibly responding to the hydrostatic restriction which leads to PRECIS failing to adequately simulate convective precipitation (Hudson and Jones, 2002, Alves and Marengo, 2009, Shahgedanova et al., 2010). Generally, RCM simulations show more precipitation than driving GCM simulations because in the RCM there is more

convective and large scale precipitation throughout the seasonal cycle as well as a more active hydrological cycle compared to the driving GCM (Hudson and Jones, 2002). The possible cause of the Thailand bias would not be expected to be the quality of the gridded observation dataset because the reliability of the interpolation method over SEA has been assessed by New et al. (2002). The negative bias occurring over the peninsula implied that the convection scheme and/or the physical parameterization fail to adequately reproduce precipitation over the region, perhaps also implying that 50km resolution remains insufficient in resolving the complexity of the peninsula. Even with improved boundary conditions, the skill of dynamical downscaling was also constrained by the regional scale forcings which may include orography, land-sea contrast, vegetation cover, lake effects, or they may be anthropogenic in origin, for example local air pollution, urban heat island, and land and water management.

Point precipitation distributions at the five surface observing stations were simulated using PRECIS and these showed that the model generates too many low precipitation events and insufficient high precipitation events. These limitations are unlikely to be due to large biases in the humidity fields but may be partially related to the tropical region where more optically thick cloud occurs in the model than in the observations (Hudson and Jones, 2002); total cloud fraction slightly in excess of the observations was found in this study and may result from an error in the wind and pressure field through the lateral boundaries (Hudson and Jones, 2002). It was also shown that PRECIS calculated too many wet days during the period March to September when compared to CRUTS2.1.

Atsamon (2006) showed that ENSO is influential with respect to temperature anomalies in Thailand. Some other studies found that El Niño is also associated with decreased precipitation in Thailand (eg Kulkarni, 1997) but others demonstrated no such effect. So this study investigated a case study El Niño event in 1982 and La Niña event in 1988 revealing weak relationships with precipitation anomaly Sirabaha (2004) indicated that Thailand is considered to be less affected by ENSO compared with the other countries of the maritime continent.

In the thesis it was shown that the average PRECIS monsoon onset in the ‘current climate’ occurs in the third pentad of May and the end of the rainy season over

Thailand occurs around the third pentad of September. This is consistent with the literature review and with the observational analyses shown in chapter 4.

In general, compared with the gridded observational data set, HadAM3P overestimates seasonal minimum temperature (Tmn) in all four regions of Thailand while all PRECIS simulations underestimate the minimum temperature for all seasons, the latter agreeing with the underestimate in temperature simulated by the NWP-MM5 as a RCM (Kreasuwan et al., 2009). Using the RegCM3 regional climate model to simulate a case study in JJA 1996 and 1997, Kieu Thi Xin (2004) also found that the model underestimated temperature by 2^{o}C.

Regarding the comparison between HadAM3P and PRECIS, it is found that the GCM simulates surface maximum air temperature (Tmx) more realistically over both the mainland and peninsular Thailand, and conversely that PRECIS simulates the minimum temperature more realistically over peninsular Thailand (Figure 5.23 and 5.28). In conclusion, the GCM produces more accurate temperature and precipitation over the mainland of Thailand while the RCM produce those variables more accurately over the peninsula. In general, the RCM provides regional detail in surface temperature while the GCM calculates area averages of surface temperature more accurately than the RCM. Applying grid to grid analysis, the cold bias during JJAS and ON is unlikely to be due to gridded observation but more likely due to PRECIS itself. The variation in temperature (i.e. cold bias in the rainy season and warm bias in the dry season) may be due to the decrease and increase of latent heat flux for the two seasons which may not be well distinguished by the model (Islam et al., 2007). Applying point to point analysis, corrected RCM elevation may reduce the bias in surface temperature at some sites, i.e., CM, Phitlok and Surat. The positive bias in minimum temperature in JFM may be related to the radiation scheme; the scheme in both GCM and RCM defined the corresponding gases in a series of spectral bands, for example, carbon dioxide, ozone, methane, nitrous oxide and halocarbons, which absorb energy fluxes more than in actual climatic conditions so that the models calculate excessive energy fluxes for longwave radiation over the region (Mlawer et al., 1997). Another possible cause for the warm bias in minimum temperature is the land surface scheme which may release heat energy flux from soil to surface more than is the case in actual climatic conditions during the night time. On the other hand,

the warm bias in maximum temperature during Feb-Mar may be related to soil energy absorption which is less than in actual conditions during the daytime. Interestingly, the GCM shows smallest (largest) positive bias over mainland (Peninsular) Thailand. This would be an expectation of GCM skill, realistically simulating the large scale climate regime over an aggregate area of mainland Thailand while being less successful over coastal regions.

In summary, the RCM produced an acceptable simulation of both the surface minimum and maximum temperature annual cycle. A similar surface temperature annual cycle at the sites located over the mainland was detected (Figure 5.29). The positive bias in minimum temperature may be related to the radiation scheme (as discussed above). At an urban site, BKK, significant warm biases in the RCM were found in February to April with magnitudes of 8.8°C, 9.4°C and 5.5°C, respectively although the nearest grid cell elevation is very similar to the station elevation. The maximum temperature annual cycle at BKK has a pattern which is consistent with the cycle at CM, Phit and Ubon located over mainland Thailand which implies that the RCM has an inadequate UHI effect, as one would expect from the 50km resolution. One of the other possible causes of RCM overestimation is due to insufficient coastal influence in the model, again partly as a function of spatial resolution.

The results emerging from the validation of the models in the baseline period provided sufficient encouragement to progress onto the simulations of possible future climate in the SEA region and in Thailand in particular. Based on the Koppen climate classification, climate projections were classified in two geographical areas, mainland and peninsular Thailand, and the results are summarised in Table 7.1.

In the PRECIS simulations of possible future climate over Thailand and SEA it was found that the HadAM3 A2 and B2 simulations projected no significant change of precipitation over mainland Thailand specifically in JJAS while the PRECIS A2 and B2 simulations mostly produce small precipitation increases in the same months over mainland. The GCM A2 and the RCM A2 simulations produce small precipitation increases during DJF while both GCM-B2 and RCM-B2 mostly produce small precipitation decreases during DJF over mainland. Over the peninsula of Thailand the GCM and RCM show small precipitation increases (decrease) during JJAS (DJF).

Some are in agreement with the average precipitation projections published in the most recent IPCC report (IPCC-AR4, 2007) indicated that over SEA an increase in precipitation during DJF of 6% and of 7% during JJA is anticipated under the A1B scenario [the scenario projection between the low emission SRES-B2 and high emission SRES-A2 scenarios].

Across the SEA region, both the GCM and RCM produce similar general spatial changes in maximum and minimum temperature, under the two emission scenarios, but with differences of detail over specific areas. The RCM A2 and B2 simulations show warming over both (continental) mainland and (maritime) peninsular Thailand which are greater than the average annual warming (3.0^{o}C for A2 and 2.2^{o}C for B2) in DJF and JJAS and are greater than the agreement in most GCMs under the A2 and B2 scenario in IPCC-TAR (2001) and most AOGCMs under the A1B scenario in IPCC-AR4 (2007). IPCC-TAR (2001) reported a warming projection over SEA under the A2 and B2 scenarios of less than 40% of the global average annual warming in both DJF and JJA, namely 1.8^{o}C under the A2 scenario and 1.3^{o}C under the B2 scenario. IPCC-AR4 temperature increase under the A1B scenario over SEA is 2.5^{o}C with a range of 1.6^{o}C to 3.6^{o}C in DJF and 2.4^{o}C with a range of 1.5^{o}C to 3.8^{o}C in JJA.

In this thesis it was found that the increase in precipitation during JJAS over mainland and peninsular Thailand occurs with a decreased number of wet days implying that the amount of precipitation on wet days in the future will increase compared to the baseline period. Moreover, the future vertical velocity simulation during JJAS shows an increase compared with the baseline period, hinting at enhanced convection. The specific humidity also increased remarkably over the Indian Ocean which is consistent with warming and greater atmospheric moisture holding capacity plus the possibility of intensified moisture transport. Therefore, the small precipitation increases during JJAS found in the future scenario projections seem to be mostly associated with a more humid atmosphere and increased precipitation intensities.

PRECIS-A2 and PRECIS-B2 both simulate average monsoon onset during 2071-2100 in the fourth pentad of May. Therefore, the monsoon projection for the end of this century is for monsoon onset to occur one pentad later than the average monsoon onset during the baseline period 1961-1990.

Table 7.1: Climate projections over mainland and peninsular Thailand during the period of 2071-2100 compared with the period 1961-1990.

(note that: precipitation amount change of greater than 20% is a 'Large increase' (++), increase with a change between 5 and 20% is a 'Small increase' (+), a change between −5 and 5% is a 'No change' (0), decrease with a change between −5 and −20% is a 'Small decrease' (-), decrease with a change of less than −20% is a 'Large decrease'(--), and disagreement with average change is 'Inconsistent sign' (i), IPCC-TAR, 2001) and IPCC shows warming projection as mean surface temperature. Tmn (Tmx) is surface minimum (maximum) temperature).

Model	Precipitation change (%)		Tmn change (°C)		Tmx change (°C)	
	DJF	JJAS	DJF	JJAS	DJF	JJAS
Mainland						
HadAM3P-A2	+	0	4.7	3.7	3.5	4.5
HadAM3P-B2	-	0	3.1	2.8	2.7	3.1
PRECIS-A2	+	+	4.3	3.5	3.4	4.3
PRECIS-B2	-	+	3.1	2.7	2.7	3.3
Peninsula						
HadAM3P-A2	-	+	3.2	3.4	3.1	3.1
HadAM3P-B2	-	+	2.1	2.6	2.3	2.4
PRECIS-A2	-	+	3.4	3.4	3.5	3.2
PRECIS-B2	-	+	2.2	2.6	2.6	2.5
SEA						
GCMs-A2	0	0	1.8	1.8	1.8	1.8
GCMs-B2	0	i	1.3	1.3	1.3	1.3
(IPCC-Tar, 2001)						
SEA						
GCMs-A1B	6	7	2.5	2.4	2.5	2.4
(IPCC-AR4, 2007)						

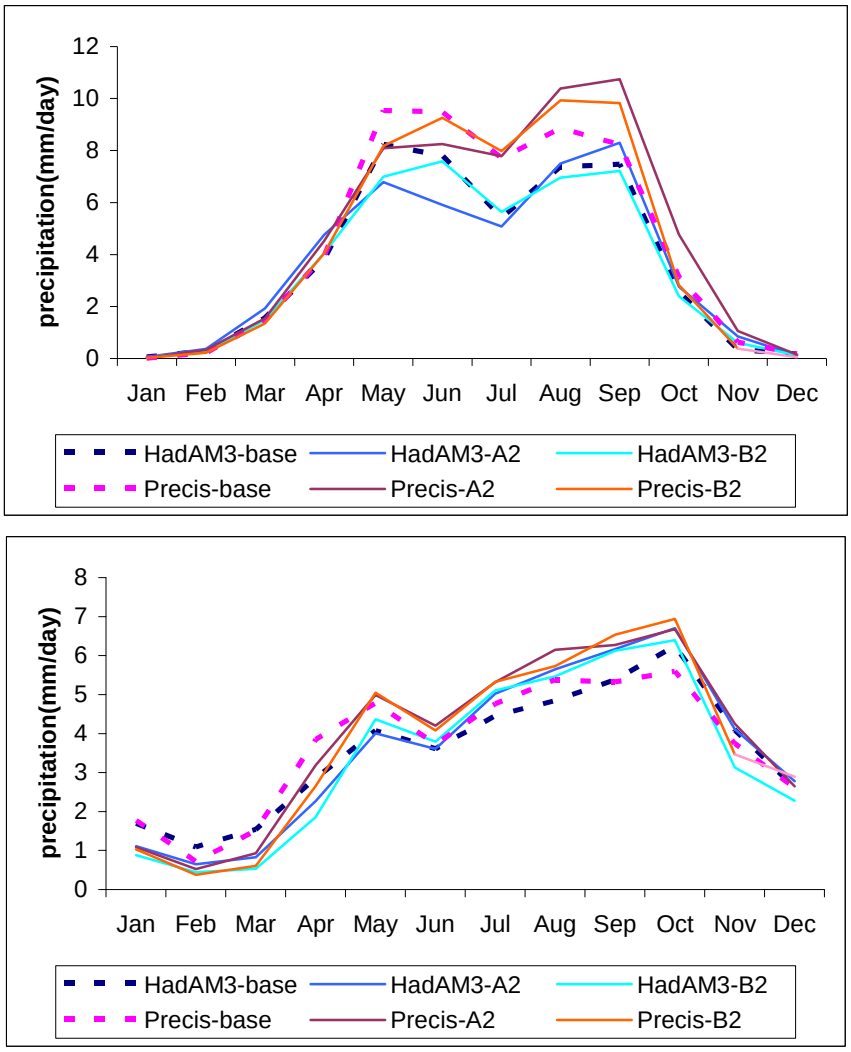

Figure 7.2: 30 year seasonal cycle of baseline (1961-1990) and future (A2/B2 2071-2100) precipitation intensity (mm/day) over northeastern (top) and Peninsular Thailand (bottom) produced by HadAM3P and PRECIS.

In general, the original project objective in this study addressed specific questions in section 2.2 as follows.

Analysing limited observation data indicated that that the climate over peninsular Thailand can be clearly distinguished from the climate over the mainland. Annual precipitation over the peninsular shows a faster rate of decrease in some seasons than over the mainland region. The number of rain days is shown to have decreased in both regions over the 1961-90 period. The minimum temperature has increased rapidly than the maximum temperature in mainland and peninsula in MAM and DJF

excepting over the peninsula in DJF. The average monsoon onset date (1961-1990) over the peninsula is one day earlier than the mainland region and would appear to be happening insignificantly later by the end of 1961-1990 period. It was also confirmed that tropical depression frequency statistically significantly increases precipitation and the relationship between the number of wet days and precipitation amount for all five sites analysed is a simple linear function. It was shown that rainfall during the DJF and MAM seasons is not influenced by the ENSO phenomenon and El Niño (La Niña) events can be lead to statistical significant precipitation decrease (increase) during JJAS (ON) at a northern (southern) station.

PRECIS is able to capture precipitation for current climate in SEA. Applying the grid-to-grid analysis method, the displayed spatial JJAS precipitation patterns are similar, with more detail provided by the PRECIS simulation compared with HadAM3P itself and the model simulations realistically simulate the heavy precipitation over the Bay of Bengal coast. With respect to Thailand, the average daily precipitation during JJAS over 1961-1990 simulated by the RCM adds more detail, in particular, over the coastline but is insignificant in adding further value over the southern region. The model simulations show a modest "added value" of using the RCM over the GCM during the active monsoon season, JJAS (Figure 5.6(c)). There is a striking difference in the sign of bias between the north and south of the domain indicating that model biases over SEA more likely depend on geographical location. The underestimation in precipitation arounds the equator over marine continents implied that the convection scheme and/or the physical parameterization fail to faithfully reproduce precipitation over the region. Moreover, the radiation scheme and/or land sea interaction may be related to precipitation underestimation in southern Thailand in particular. PRECIS model simulates total precipitation amount fairly accurately through an underestimate of precipitation intensity but an overestimate of wet day frequency. Compared with station observation data, the model generally simulates too many low precipitation events and insufficient high precipitation events. This bias may be partially related to the tropical region where more optically thick cloud is simulated than observed which total cloud fraction slightly in excess of the observations was found in this study (Figure5.16) which could be related to an error in the wind and pressure field through the lateral boundaries (Hudson and Jones, 2002). Annual precipitation cycle revealed that RCM generated too much precipitation during the monsoon onset, May,

meanwhile the model generated inadequate precipitation in some local scale in Thailand during JJAS. The RCM has a difficulty to accurately simulate humidity fields over this geographic area (Figure 5.11). The model produced vapour pressure reasonably over the largely marine environment of the peninsula which suggests a deficiency in the simulation of the water cycle, perhaps through land-atmosphere interactions, over more continental areas. The strengths in the output of PRECIS is adding value of the driving GCM, however, in some cases HadAM3P is performing better than PRECIS producing less precipitation than the RCM, for example, in the onset month of May in northern, northeastern and central Thailand. This is related to that RCM there is more convective and large scale precipitation throughout the seasonal cycle as well as a more active hydrological cycle compared to the driving GCM. Therefore, RCM is likely to reproduce the convection which is activated at the lee-side foot of two mountainous regions located in western and central Thailand during the daytime and to extend that precipitation during the night time over inland regions far downwind from the mountains themselves. Moreover, the driving GCM is able to calculate most accurately the minimum and maximum surface temperature over mainland Thailand (Figure 5.30). This would be an expectation of GCM skill, providing a good simulation of a large scale climate regime over an aggregated area of mainland Thailand while the limitation of GCM skill was found over coastal region. PRECIS-ECHAM4 simulations reveal largest underestimation in precipitation and surface temperature which may be due to the insufficiency of driving boundary condition.

PRECIS A2 and B2 simulations mostly produce small precipitation increases in JJAS over all region in Thailand meanwhile PRECIS A2 (B2) simulations produce small precipitation increases (decrease) during DJF over mainland Thailand and RCM under either emission scenario produce small decrease during DJF over peninsular Thailand. Some are in agreement with the average precipitation projections published in the most recent IPCC report (IPCC-AR4, 2007) under the A1B scenario [the scenario projection between the low emission SRES-B2 and high emission SRES-A2 scenarios]. PRECIS A2 and B2 simulations show warming over both (continental) mainland and (maritime) peninsular Thailand which are greater than the average annual warming in DJF and JJAS and are greater than the agreement in most GCMs under the A2 and B2 scenario in IPCC-TAR (2001) and most AOGCMs under the

A1B scenario in IPCC-AR4 (2007). The results indicated an increase in the 95th percentile of maximum temperature to 41.7°C in northern Thailand and 36.4°C in the peninsula region while the baseline value are 36.7°C and 32.6°C. This study found that the 95th percentile daily precipitation intensity increased by up to 2 mm/day which might be associated with hot day increases being larger than cold day decreases. These two conditions, hotter and wetter, may more likely lead to severe storms and floods. RCM is able to realistically captured period of southwest monsoon active and monsoon onset and the projection of monsoon onset for the end of this century is one pentad (5 days) later than the average monsoon onset during 1961-1990.

7.2 Limitations and Recommendations

In this study, just five surface observation stations distributed over Thailand were used to study recent Thai climate due to the costs associated with accessing the larger network; the Thai Meteorology Department makes a charge, even for educational purposes, of approximately £7,000 for the larger dataset. Without personal contact, the process to obtain the data set took fourteen months to complete. To more fully validate the RCM performance and document local climatic variation in Thailand, more local scale data is ideally needed. There was only one station in the peninsular considered in this study, however this site can be used to represent the general climate in the southern area. The specific geographic area which it would be particularly valuable to test further is in the peninsula of Thailand because this is a challenging area to simulate for an RCM.

Specifically studying extreme events such as tropical cyclones, heavy precipitation and drought are also recommended as these were beyond the scope of this thesis; in this study it was found that the precipitation is likely to change in terms of intensity which is in agreement with the IPCC-AR4 (2007). Approximately one third of Thailand's area is used for agricultural production. Crop yield, for example of rice, is associated with climate change. Using PRECIS forced with ECHAM4, Agarwal (2009) projected the future climate to drive a crop model over the Mekong basin and found that the reduction in yield reached 18, 28 and 24% in the region during the

2020s, 2050s and 2080s, respectively, compared to the average yield of years 1997-2006. This sort of work is also desperately needed in Thailand.

The WHS, Wilson and Henderson-Sellers, land use dataset (global coverage, 1x1 degree gridded data) was used in the PRECIS modelling reported in this thesis. Some of the SEA PRECIS modelling consortium undertook sensitivity studies with respect to land use impacts. The latter was not specifically done for Thailand and this would be an interesting study to carry out so as to improve the model's skill in representing the climate of Thailand, using more realistic terrain and land use data.

The office of the National Economic and Social Development Board has responsibility for adaptation in Thailand. Regarding climate change issues, the office receives full details from the Office of National Resources and Environmental Policy and Planning (ONEP), interacting with the communities (i.e. private organisations and government) and has already joined the United Nations Framework Convention on Climate Change, UNFCCC. The ONEP has responsibility for writing a national report for UNFCC and contributing to the framework of climate change in Thailand, including reduction of greenhouse gas emissions (Mitigation) and reacting to the impacts caused by climate change (Adaptation). My thesis will be given to the Office of the higher Education Commission and it will be distributed to the organisations which are involved this issue.

Forest fires are a long-term problem at the local scale in northern Thailand, occurring every year during February-March during the relatively dry period controlled by the northeast monsoon. In the 2007 El Niño year, measurements of particulate matter (PM_{10}) exceeded the threshold level for health impact security ($383\mu g/m^3$) in Chiang Mai province and nearby areas (source: Pollution Control Department, PCD). It is unclear what the main cause of this event is but possibilities are forest fires, pollution from tourism and the effect of El Niño. This is a regional scale event and if it should be repeated regularly then important climatic radiative forcing might occur. Studying the possible impact of climate change on such events, together with associated feedbacks, would therefore also be a valuable next step.

References

Agarwal A. (2009). "Forecasting rice yield under climate change scenarios and evaluation of agro-adaptation measures for Mekong basin region: a simulation study." Earth and Environmental Science **6**.

Allan Richard P., Mark A. Ringer, J. Alison Pamment, and Anthony Slingo (2004). "Simulation of the Earth's radiation budget by the European Centre for Medium-Range Weather Forecasts 40-year reanalysis (ERA40)". Journal of Geophysical Research **109:** (D18107), doi:10.1029/2004JD004816

Arnell, N. W., D. A. Hudson, et al. (2003). "Climate change scenarios from a regional climate model: Estimating change in runoff in southern Africa." Journal of Geophysical Research-Atmospheres **108**(D16): -.

Atsamon A , S. Limjirakan and T. Sriburi (2006) "Assessment of extreme weather events along the coastal areas of Thailand" Eighth Conference on Coastal Atmospheric and Oceanic Prediction and Processes Eighth Symposium on the Urban Environment, Thailand.

Beraki AF (2005). Climate change scenario simulations over Eritrea by using a fine resolution limited area climate model: temperature and moisture sensitivity. Department of Geography, Geoinformatics and Meteorology. Eritrea, University of Pretoria. **Masters Thesis,etd-02102006-152327**.

Bell, G.D. and Halphert, M.S. (1998) "Climate assessment for 1997". Bulletin of the American Meteorological Society **79**: S1-s50.

Betts, R. A. (2000). "Offset of the potential carbon sink from boreal forestation by decreases in surface albedo." Nature **408**: 187-189.

Betts, R. A., P.M. Cox, S.E. Lee and F.I. Woodward, (1997). "Contrasting physiological structural vegetation feedbacks in climate change simulations." Nature **387**: 796-799.

Bhaskaran, B., J.M. Murphy and R.G. Jones, (1998). "Intraseasonal Oscillation in the Indian Summer Monsoon Simulated by Global and nested Regional Climate Models." Mon. Wea. Rev. **126**: 3124–3134.

Bhaskaran, B. a. J. F. B. M. (1998). "Simulated changes in southeast Asian monsoon precipitation resulting from anthropogenic emissions." Int. J. Climatology **18**: 1455-1462.

Bjerknes, J.A. (1969). "Atmospheric teleconnections from the equatorial Pacific, Ibid. **97**: 163-172

Boochabun, K., Tych, W., Chappell, N.A., Carling P.A., Lorsirirat K., and Pa-Obsaeng, S. (2004). "Statistical modelling of rainfall and river flow in Thailand." Journal of the Geological Society of Indi. **64**: 503-515.

Braganza K, Karoly DJ, Arblaster JM (2004). "Diurnal temperature range as an index of global climate change during the twentieth century." Geophys Res Lett **31**:L13217

Bringfelt, B., Räisänen, J., Gollvik, S., Lindström, G., Graham, L. P., and Ullerstig, A. (2001). "The land surface treatment for the Rossby Centre Regional Atmospheric Climate Model version 2 (RCA2)." Reports Meteorology and Climatology **98**: 40 pp, Swedish Meteorological and Hydrological Institute, Norrköping, Sweden.

Challinor, A. J., Wheeler, T. R., Slingo J. M., Craufurd, P. Q., Grimes D. I. F. (2005). "Simulation of Crop Yields Using ERA-40: Limits to Skill and Nonstationarity in Weather–Yield Relationships." Journal of applied meteorology **44**; 516-534

Challinor, A. J., T. R. Wheeler, P. Q. Craufurd, C. A. T. Ferro and D. B. Stephenson, (2007). "Adaptation of crops to climate change through genotypic responses to mean and extreme temperatures." Agriculture Ecosystems and Environment, **119** (1-2): 190-204.

Chang C.P. and Lau K.M. (1982). "Short term planetary-scale interactions over the tropics and mid-latitudes during northern winter. Part I: Contrasts between active and interactive periods." Monthly Weather Review **110**: 933-946.

Chen, Tsing-Chang, Jin-ho Yoon (2000). "Interannual Variation in Indochina Summer Monsoon Rainfall Possible Mechanism." J. Climate **13**: 1979–1986.

Chokngamwong R. and L. S. Chiu (2008). "Thailand Daily Rainfall and Comparison with TRMM Products." J. Hydrometeorology **9**(2): 256-266.

Chotamonsak Chakrit, Eric P. Salath´e Jr, Jiemjai Kreasuwan, Somporn Chantara and Kingkeo Siriwitayakorn (2011). "Projected climate change over Southeast Asia simulated using a WRF regional climate model" Atmos. Sci. Let., (wileyonlinelibrary.com) DOI: 10.1002/asl.313

Christensen J.H. and Kuhry P (2000). "High resolution regional climate model validation and permafrost simulation for the East- European Russian Arctic." J. Geophys. Res. **105**: 29647-29658.

Christensen JH, Christensen OB, Lopez P, van Meijgaard E, Botzet M. (1996). "The HIRHAM4 regional atmospheric climate model." DMI Technical Report 96-4. Available from DMI, Lyngbyvej 100,

Christensen, O. B. and J. H. Christensen (2004). "Intensification of extreme European summer precipitation in a warmer climate." Global and Planetary Change **44**(1-4): 107-117.

Christensen J. H. and O. B. Christensen. (2007) "A summary of the PRUDENCE model projections of changes in European climate by the end of this century," Climatic Change **81**: 7–30.

Cox P.M., R. A. B., C.B. Bunton, R.L.H. Essery, P.R. Rowntree and J. Smith, (1999). "The impact of new land surface physics on the GCM simulation of climate and climate sensitivity." Clim Dyn. **15** 183–203.

Cubasch, U., G. A. Meehl, G. J. Boer, R. J. Stouffer, M. Dix, A. Noda, C. A. Senior, S. Raper and K. S. Yap, (2001). Projections of Future Climate Change, in Climate Change 2001 : The Scientific Basis. Contribution of Working Group I to the Third Assessment Report of the Intergovernmental Panel on Climate Change, edited by J. T. Houghton, Y. Ding, D. J. Griggs, M. Noguer, P. J. van der Linden, X. Dai, K. Maskell, and C. A. Johnson, Cambridge Univ. Press, New York, 881 pp.

Cullen, M. J. P. (1993). "The Unified Forecast/Climate Model." Meteor. Mag. **122**: 81-94.

Dai, A. (2006). "Precipitation characteristics in eighteen coupled climate models." Journal of Climate **19** (18): 4605-4630

Davidson, N. E., J. L. McBride, and B. J. McAvaney (1983). "The onset of the Australian monsoon during winter MONEX: Synoptic aspects." Mon. Wea. Rev. **111**: 496–516.

Davies, H.C. (1976). “A lateral boundary formulation for multi-level prediction models.” Quart. J. R. Meteor. Soc. **102**: 405-418.

Dethloff K., Glushak K., Rinke A., and Handorf D. (2010) “Antarctic 20th century accumulation changes based on regional climate model simulations.” Advances in Meteorology **2010**: Article ID 327172, doi:10.1155/2010/415632.

Dickinson, R.E. (1984) “ Modeling evapotranspiration for three-dimensional global climate models. Climate Processes and Climate Sensitivity.” Geophys. Monogr.2**9:** 58-72.

Dickinson, R. E., Errico, R.M., Giorgi, F., Bates, G. T. (1989). “A regional climate model for western United States.” Clim. Change **15**: 383-422.

Ding Y. (1994). "Monsoons over China." Kluwer Academic Publisher: 419.

Diskinson, R.E, P.J. Kennedy, A.Henderson-Sellers and M.Wilson. (1986). "Biosphere-Atmosphere Transfer Scheme (BATS) for the NCAR Community Climate Model". NCAR/TN-275+STR, 69

Dong B, Valdes PJ. (1998). “Modeling the Asian summer monsoon rainfall and Eurasian winter/spring snow mass.” Quarterly Journal of the Royal Meteorological Society **12**: 2567–2596.

Douville H, Royer JF. (1996). “Sensitivity of the Asian summer monsoon to an anomalous Eurasian snow cover within the Metro-France GCM.” Climate Dynamics **12**: 449–466.

D¨oscher R, Will´en U, Jones C, Rutgersson A, Meier HEM, Hansson M, Graham LP. (2002). "The development of the coupled regional ocean-atmosphere model RCAO." Boreal Environmental Research **7**: 183–192.

Druyan Leonard M., Jinming Feng, Kerry H. Cook, Yongkang Xue, Matthew Fulakeza, Samson M. Hagos, Abdourahamane Konare, Wilfran Moufouma-Okia, David P. Rowell, Edward K. Vizy and Seidou Sanda Ibrah. (2009).” The WAMME regional model intercomparison study.” Clim. Dyn., DOI :10.1007/s00382-009-0676-7

Edwards J. M. and Slingo A. (1996). "Studies with a flexible new radiation code. I: Choosing a configuration for a large-scale model." Q. J. R. Meteorol. Soc. **122**: 689–719.

Erda, L., X.Wei, J. Hui, X. Yinlong, L. Yue, B. Liping and X. Liyong (2005). "Climate change impacts on crop yield and quality with CO_2 fertilization in China." Philos. T. Roy. Soc. B. **360**:2149-2154.

Fasullo J. (2004). “A stratified diagnosis of the Indian monsoon-Eurasia snow cover relationship.” Journal of Climate **17**: 1110–1122.

Fasullo J, Webster PJ. (2003). "A hydrological definition of Indian monsoon onset and withdrawal". Journal of Climate **16**: 3200–3211.

Feser, F. and H. von Storch (2008). "A dynamical downscaling case study for typhoons in Southeast Asia using a regional climate model." Monthly Weather Review **136**(5): 1806-1815.

Fischer E.M. and Christoph S. (2009) "Future changes in daily summer temperature variability: driving processes and role for temperature extremes." Climate Dynamics **33**(7-8): 917-935

Frei, C., J. H. Christensen, M. De´que´, D. Jacob, R. G. Jones, and P. L. Vidale (2003). "Daily precipitation statistics in regional climate models: Evaluation and intercomparison for the European Alps." J. Geophys. Res**:108(D3)**: 4124.doi:10.1029/2002JD002287.

Frei C, Schöll R, Fukutome S, Schmidli J, Vidale PL. (2006). "Future change of precipitation extremes in Europe: An intercomparison of scenarios from regional climate models." Journal of Geophysical Research **111:** D06105, doi:10.1029/2005JD005965.

Fowell Martin (2006) “Water–land–atmosphere interactions” DOI: 10.1256/wea.122.04

Gibson J. K., P. K., S. Uppala, A. Hernández, A Nomura and E. Serrano (1997). ERA description, ECMWF Reanalysis Project Report Series 1, ECMWF, Reading**:** 66.

Gillett NP, Allan RJ, Ansell TJ (2005). "Detection of external influence on sea level pressure with a multimodel ensemble." Geophys Res Lett **32**:L19714

Giorgi, F., L.O. Mearns, C. Shields and L. McDaniel (1998). "Regional nested model simulations of present day and 2┐ CO2 climate over the Central Plains of the U.S." Clim. Change **40**: 457–493.

Giogi, F.; Mearns, L. O. (1999). “Regional climate modelling revisited. An introduction to the special issue.” J. Geophys. Res. **104**: 6335-6352.

Giorgi F. and M.R. Marinucci (1996). "Improvements in the simulation of surface climatology over the European region with a nested modeling system." Geophys. Res. Lett. **23**: 273–276.

Giorgi F. and X. Bi (2000). "A study of internal variability of a regional climate model." J. Geophys. Res. **105**: 29503–29521.

Goodison B.E., Louie P.Y.T. and Yang D (1998). "WMO solid precipiation measurement intercomparison: final report." Instruments and observing methood report **67**, World Meteorological Organization.

Gordon, C., C. Cooper, C.A. Senior, H.T. Banks, J.M. Gregory, T.C. Johns, J.F.B. Mitchell and R.A. Wood, (2000). "The simulation of SST, sea ice extents and ocean heat transports in a version of the Hadley Centre coupled model without flux adjustments." Clim. Dyn **16**: 147-168.

Gregory, D., G.J. Shutts, and J.R. Mitchell, (1998). "A new gravity-wave-drag scheme incorporating anisotropic orography and low-level wave breaking: Impact upon the climate of the UK Meteorological Office Unified Model." Quart. J. Roy. Meteor. Soc. **124**: 463-494.

Griffiths, G. M., L. E. Chambers, et al. (2005). "Change in mean temperature as a predictor of extreme temperature change in the Asia-Pacific region." International Journal of Climatology **25**(10): 1301-1330.

Halpert M.S. and Ropleweski C.F. (1992). "Surface temperature patterns associated with the Southern Oscillation." Journal of Climate **5**: 577-593.

Hasternrath, S. (1991) “Climate Dynamics of the Tropics.” Kluwer Academic, Boston, USA, 488

Hassell, D. a. R. G. J. (1999). Simulating climatic change of the southern Asian monsoon using a nested regional climate model (HadRM2), Hadley Centre for Climate Prediction and Research, London Road, Bracknell, UK.

Hennessey, K.J., P.H. Whetton, J.J. Katzfey, J.L. McGregor, R.N. Jones, C.M. Page, and K.C. Nguyen (1998) "Fine Resolution Climate Change Scenarios for New South Wales." Annual mReport, 1997/98, CSIRO, Australia, 48pp.

Henson, R. (2002). The Rough Guide to Weather, Rough Guides Ltd, London.

Holton, J. R., J.A. Curry, and J. A. Pyle (2003). Monsoons. Encyclopedia of the Atmospheric Sciences., Elsevier Science Ltd., Oxford, UK.

Hori, M.E., and H. Ueda. (2006). "Impact of global warming on the East Asian winter monsoon as realized by nine coupled atmospheric-ocean GCMs." Geophys. Res. Lett., **33** (3), L03713, doi:10 1029/2005GL024961

Houghton, J. T. (2001). Climate change 2001 : the scientific basis : contribution of Working Group I to the third assessment report of the Intergovernmental Panel on Climate Change /edited by J.T. Houghton ... [et al.], Cambridge: Cambridge University Press.

Houze, R. A., Geotis, S.G., Marks, F.D. and West, A.K. (1981). "Winter monsoon convection in the vixinity of Morth Beroneo 1. Structure and time variation of the clouds and precipitation." Monthly Weather Review **109**: 1595-1614.

Hudson DA and Jones RG (2002). Regional climate model simulations of present-day and future climates of southern Africa, Bracknell: Met Office (Note 39).

Huntingford, C. J., R.G. Prudhomme, C. Lamb, R. Gash, J.H.C. and Jones, D.A. (2003). "Regional climatemodel predictions of extreme rainfall for a changing climate." Quarter. J. Royal Mete. Soc. **129**(590): 1607– 1621.

Hulme, M., Mitchell, J., Ingram, W.J., Lowe, J.E., Johns, T.C., New, M., Viner, D. (1999). "Global change scenarios for global impact studies." Global Environmental Change **9**, S3–S20.

Im, E. S., J. B. Ahn, et al. (2008). "Sensitivity of the regional climate of East/Southeast Asia to convective parameterizations in the RegCM3 modelling system. Part 1: Focus on the Korean peninsula." International Journal of Climatology **28**(14): 1861-1877.

Ingram W. J., W. S., and Edwards J., (1997). Radiation Unified Model documentation paper 23 (v3), Meteorological Office, UK.

IPCC (1997). The Regional Impacts of Climate Change: An Assessment of Vulnerability, University Press, Cambridge.

IPCC (2001)**.** Climate Change 2001: The Scientific Basis, University Press, Cambridge.

IPCC (2007). Climate Change 2007: The Physical Science Basis, Cambridge University Press, Cambridge.

Islam, Md. and Uyeda, H. (2006). "Use of TRMM in determining the climatic characteristics of rainfall over Bangladesh." Remote Sensing of Environment **108**: 264–276.

Islam MN and Uyeda H. (2007). "Use of TRMM in determining the climatic characteristics of rainfall over Bangladesh." Remote Sensing of Environment,Elsevier Science. **108**(3): 264–276

JA, B. (1969). "Atmospheric teleconnections from the equatorial Pacific." Mon Wea Rev **97**: 163–172.

Jacob D (2001). "A note to the simulation of the annual and interannual variability of the water budget over the Baltic Sea drainage basin. Meteorol Atmos Phys **77**: 61–73

Jacobsen, I., and E. Heise. (1982). “A new economic method for the computation of the surface temperature in numerical models.” Beitr. Phys. Atm. **55**: 128-141.

Ji, Y., and A. D. Vernekar (1997). "Simulation of the Asian summer monsoons of 1987 and 1988 with a regional model nested in a global GCM." J. Climate **10**: 1965-1977.

Johns, T.C., Gregory, J.M., Ingram, W.J., Johnson, C.E., Jones, A., Lowe, J.A., Mitchell, J.F.B., Roberts, D.L., Sexton, D.M.H., Stevenson, D.S., Tett, S.F.B., Woodage, M.J. (2003). "Anthropogenic climate change for 1860 to 2100 simulated with the HadCM3 model under up-dated emissions scenarios." Climate Dynamics **20**: 583–612.

Jones, R. G., D. Hassel and K. Ward (1999). First results from the Hadley Centre’s new regional climate model including effects of enhanced resolution, DETR report, March 1999, Hadley Centre for Climate Prediction and Research, London Road, Bracknell, UK.

Jones, R. G., J.M. Murphy, M. Noguer and A.B. Keen (1997). "Simulation of climate change over Europe using a nested regional climate model. II: Comparison of driving and regional model responses to a doubling of carbon dioxide." Quart. J. R.. Met. Soc. **123**: 265–292.

Jones, R. G., Noguer, M., Hassell, D.C., Hudson, D., Wilson, S.S., Jenkins, G.J., and Mitchell, J.F.B. (2004). Generating high resolution climate change scenarios using PRECIS, Met Office Hadley Centre, Exeter, UK.

Jones, T. C., and Coauthors. (2003) “Anthropogenic climate change for 1860 to 2100 simulated with the HadCM3 model under updated emission scenarios.” Climate Dyn. **20**, 583–612.

Joseph, P. V., J. Eisheid, and R. J. Pyle, (1994). "Interannual variability of the onset of the Indian summer monsoon and its association with atmospheric features, El Niño, and sea surface temperature anomalies." J. Climate **7**: 81-105.

Kaas E. and P. Frich (1995). "Diurnal temperature range and cloud cover in the Nordic countries: observed trends and estimates for the future." Atmospheric Research **37**: 211–228.

Kain, J., and Fritsch, J. M. (1990) “A one dimensional entraining/detraining plume models and its application to convective parameterization.” J. Atmos. Sci. **47**: 2784-2802.

Kalnay, E., M. Kanamitsu, R. Kistler,W. Collins, D. Deaven, L. Gandin, M. Iredell, S. Saha, G. White, J. Woollen, Y. Zhu, M. Chelliah, W. Ebisuzaki, W. Higgins, J. Janowiak, K.C. Mo, C. Ropelewski, J. Wang, A. Leetmaa, R. Reynolds, R. Jenne and

D. Joseph and . (1996). "The NCEP/NCAR 40-Year Reanalysis Project." Bull. Am. Met. Soc. **77**: 437–471.

Karoly DJ, Wu Q (2005). "Detection of regional surface temperature trends." J Clim**18**: 4337–4343

Kato, H., K. Nishizawa, H. Hirakuchi, S. Kadokura, N. Oshima and F. Giorgi (2001). "Performance of the RegCM2.5/NCAR-CSM nested system for the simulation of climate change in East Asia caused by global warming." J. Met. Soc. Japan **19:**99-121

Kemball Cook, S., and B. Wang (2001). "Equatorial waves and air–sea interaction in the boreal summer intraseasonal oscillation." J. Climate **14:** 2923–2942.

Kessler, E. (1969) “On the distribution and continuity of water substance in atmospheric circulation models.” Meteor. Monographs **10**

Kiehl, J. T. (1996). “Description of the NCAR Community Climate Model (CCM3)” Tech. Note, NCAR/TN-420+STR, 152 pp

Kieu Thi Xin, L. D., Hole Thi Minh ha (2004). Improving simulation of Southeast Asia rainfall using RegCM3 and problem for the tropical region. the 6th International GAME Conf., Kyoto, Japan.

Kiladis, G., Meehl, G. and Weickmann (1994). "The large scale circulation associated with westerly wind bursts and deep convection over the western equatorial Pacific." Journal of Geophysical Research **99**: 18527-18544.

Kousky VE, R. C. (1989). "Extremes in the Southern Oscillation and their relationship to precipitation anomalies with emphasis on the South American region." Rev Bras Meteor **4**: 351–363.

Kreasuwan J.,Chodamornsuk C., Ratjiranukool P., Wirunvedchayan O., Panseuk P. and amnuaylawjarun T. (2009) "Climate Change Simulation for Thailand by the MM5-Regional Climate Model." The First China-Thailand Joint Seminar on Climate Change, 23-24 March, Bangkok, Thailand.

Kripalani, R.H., Singh, S.V., Panchwagh, N. and Brikshavana, M. (1995). "Variability of the summer monsoon rainfall over Thailand—comparison with features over India." Int. J. Climatol. **15**: 657–672.

Kripalani R.H. and Kulkarni A. (1997). "Rainfall variability over South-East Asia-connections with Indian monsoon and ENSO extremes: New perspectives." International Journal of Climatology **17**: 1155-1168.

Krishnan, R., C. Zhang, M. Sugi. (2000). "Dynamics of Breaks in the Indian Summer Monsoon." J. Atmos. Sci., **57**, 1354–1372.

Kumar, K. R., A. K. Sahai, et al. (2006). "High-resolution climate change scenarios for India for the 21st century." Current Science **90**(3): 334-345.

Kuo-Ying Wang and D. E. Shallcross (2005). "Simulation of the Taiwan Climate Using the Hadley Centre PRECIS Regional Climate Modeling System: The 1979-1981 Results." Terrestrial, Atmospheric and Oceanic Sciences **16**(5): 1017-1043.

Lau K.M. and Yang S. (1996). "Seasonal variation, abrupt transition, and interseasonal variability associated with the Asian summer monsoon in the GLA GCM." Journal of Climate **9**: 965-985.

Lau, N. C., Philander, S.G.H. and Nath, M.J. (1992). "Simulation of ENSO-like phenomena with a low-resolution coupled GCM of the global ocean and atmosphere." Journal of Climate **5**: 284-307.

Leung L.R., e. a. and . (2003). "Regional climate research needs and opportunities." Bull. Amer. Meteor. Soc. **84**: 89-95.

Lin Erda, X. W., Ju Hui, Xu Yinlong, Li Yue, Bai Liping, and Xie Liyong, (2005). "Climate change impacts on crop yield and quality with CO2 fertilization in China." Philos Trans R Soc Lond B Biol Sci. **360**(1463): 2149–2154.

Liu Y., Chan C. L., Chow K. C. and Ding Y. (2006). "Ten-year climatology of summer monsoon over south china and its surroundings simulated from a regional climate model." Int. J. Climatol. **26**: 141–157

Liu, X. D. and Chen, B. D. (2000) "Climatic warming in the Tibetan Plateau during recent decades." Int. J. Climatol. **20**: 1729–1742

L¨uthi D, Cress A, Davies HC, Frei C, Sch¨ar C (1996). "Interannual variability and regional climate simulations." Theoretical and Applied Climatology **53**: 185–209.

Manton, M.J., P.M. Dellaa-Marta, M.R. Haylock, K.J. Hennessy, N. Nicholls, L, E, Chambers, D.A. Collins, G. Daw, A.Finet, D. Gunawan, K. Inape, H. Isobe, T.S. Kestin, P.Lefale, C.H. Leyu, T. Lwin, L.Maitrepierre, N. Oprasitwong, C.M. Page, J.Pahalad, N. Plummer, M.J. Salinger, R. Suppiah, V.L. Tran, B. Trewin, I. Tibig and D. Yee. (2001). “Trends in extreme daily rainfall and temperature in southeast Asia and the south Pacific: 1961-1998, J.Climatol.**21**:269-284

Marengo J. and T. Ambrizzi (2006). Use of regional climate models in impacts assessments and adaptations studies from continental to regional and local scales: The CREAS (Regional Climate Change Scenarios for South America) initiative in South America. Proceedings of 8 ICSHMO,April 24-28,2006, Foz do Iguaçu, Brazil.

Martineu P. (2005). An assessment of the PRECIS Regional Climate Modelling System – Simulations over North America using PRECIS., Research activities in Atmospheric and Oceanic Modelling, WMO/TD, edited by J. Côté**:** No. 35, 7-21.

Maslanik, J. A., A.H. Lynch and M. Serreze (2000). "A case study simulation of Arctic regional climate in a coupled model." J. Climate. **13**: 383-401.

Matsumoto, J. (1997). "Seasonal Transition of Summer Rainy Season over Indochina and Adjacent Monsoon Region." Adv. Atmos. Sci. **14**: 231-245.

McGregor G. R. and NIEUWOLT S. (1998). Tropical climatology: an introduction to the climates of the low latitudes, John Wiley & Sons, Chichester.

McGregor, J. L., J.J. Katzfey and K.C. Nguyen (1998). "Fine resolution simulations of climate change for southeast Asia. Final report for a Research Project commissioned by Southeast Asian Regional Committee for START (SARCS)." CSIRO Atmospheric Research. **15**: 35.

McGregor, J. L., J.J. Katzfey and K.C. Nguyen (1999). Recent regional climate modelling experiments at CSIRO. In: Research Activities in Atmospheric and Oceanic Modelling, H. Ritchie (ed). (CAS/JSC Working Group on Numerical Experimentation Report ; 28; WMO/TD – no. 942) [Geneva]: WMO**:** 7.37–7.38.

McIntyre, M. E. (1980). "An introduction to the generalized Lagrangianmean description of wave, mean flow interactions." Pure Appl. Geophys. Res. Lett. **118**: 152–176.

Mearns, L. (2004). NARCCAP North American Regional Climate Change Assessment Program A Multiple AOGCM and RCM Climate Scenario Project over North America. AGU Fall Meeting, San Francisco, USA.

Mearns, L. O., Giorgi, F., Shields, C., L. McDaniel, (2003). "Climate scenarios for the Southeast US based on GCM and regional modelling simulations." Climatic Change **60**: 7-35.

Mearns, L. O., W. Easterling, and C. Hays, (2001). "Comparison of agricultural impacts of climate change calculated from high and low resolution climate model scenarios: part I: the uncertainty due to spatial scale." Clim. Change (in press).

Mitchell, J. F. B., D. J. Karoly, G. C. Hegerl, F. W. Zwiers, M. R. Allen, and J. Marengo (2001) " Detection of climate change and attribution of causes." Climate Change 2001*: The Scientific Basis,*Cambridge University Press, J. T. Houghton et al., Eds., 695–738.

Mlawer, E. J., S. J. Taubman, P. D. Brown, M. J. Iacono, and S. A. Clough (1997). "Radiative transfer for inhomogeneous atmosphere: RRTM, a validated correlated-k model for the longwave". J. Geophys. Res. **102** (D14): 16663-16682.

Moberg A. and P. D. Jones (2004). "Regional climate model simulations of daily maximum and minimum near-surface temperatures across Europe compared with observed station data 1961-1990." Climate Dynamics **23**(7-8): 695-715.

Morita, T., J. Robinson, J. Alcamo, D. Zhou, N. Nakicenovic (2001). Greenhouse Gas Emission Mitigation Scenarios and Implications, Chapter 2, Climate Change 2001: Mitigation, Third Assessment Report, 115-167. Working Group III of the Intergovernmental Panel on Climate Change, IPCC, Geneva, Switzerland. (ISBN 0-521-01502-2)

Murakami T. and J. Matsumoto (1994). "Summer monsoon over the Asian continent and the western North Pacific." J. Meteor. Soc. Japan **72**: 719–745.

New, M. G., M. Hulme, and P. D. Jones., (1999). "Representing twentieth century space-time climate variability. Part I: Development of a 1961-1990 mean monthly terrestrial climatology." Journal of Climate **12**: 829-856.

Newell RE, K. J., Vincent DG, Boer GJ (1972). "The general circulation of the tropical atmosphere and interaction with extratropical latitudes." Massachusetts: MIT Press: 258.

Nicholls N, M. J., and Ormerod RJ., (1982). "On predicting the onset of the Australian wet season at Darwin." Monthly Weather Review **110**: 14–17.

Nieuwolt, S. (1981). The Climates of Continental Southeast Asia. In: World Survey of Climatology, Amsterdam, Oxford, New York.

Noguer M., R. G. J., and Murphy J.M., (1998). "Sources of systematic errors in the climatology of a nested regional climate model (RCM) over Europe." Clim. Dyn. **14**: 691–712.

Moufouma-Okia, W. and D. P. Rowell. (2010). "Impact of soil moisture initialisation and lateral boundary conditions on regional climate model simulations of the West African Monsoon." Clim Dyn **35**:213–229

Pai D, Rajeevan M. (2007). “Indian summer monsoon onset: Variability and prediction.” National Climate Centre Research Report 6, India Meteorological Dept: Pune, India.

Pal, J. S., Small, E. E., Eltahir, E. A. B. (2000). “Simulation of regional-scale water energy budgets: Representation of subgrid cloud and precipitation process within RegCM.” Journal of Geophysical Research **105**: 29579-29594.

Palmer, T. N., G.J. Shutts, R. Swinbank, (1986). "Alleviation of a systematic westerly bias in general circulation and numerical weather prediction models through an orographic gravity wave drag parameterization." Quart. J. Roy. Meteor. Soc. **112**: 1001-1039.

Pan, Z., J.H. Christensen, R.W. Arritt, W.J. Gutowski, Jr., E.S. Takle, and F. Otieno, (2001). "Evaluation of uncertainties in regional climate change simulations." J. Geophys. Res. **106**: 17,735–17,752.

Peel M. C., B. L. F., and T. A. McMahon, (2007). "Updated world K¨oppen-Geiger climate classification map, Hydrol." Earth Syst. Sci. **11**: 1633–1644
Pielke, R. A., Sr., R.L. Walko, L. Steyaert, P.L. Vidale, G.E. Liston and W.A. Lyons (1999). "The influence of anthropogenic landscape changes on weather in south Florida." Mon. Wea. Rev. **127**: 1663-1673.

Polanski S., Rinke A., and Dethloff K. (2010) “Validation of the HIRHAM-Simulated Indian Summer Monsoon Circulation” Advances in Meteorology, Volume 2010, Article ID 415632, doi:10.1155/2010/415632

Qian WH, Lee DK (2000). “ Seasonal march of Asian summer monsoon.” Int J Climatol **20**: 1371–1378

Quadir, D. A., M. L. Shrestha, et al. (2004). "Variations of surface air temperature over the land areas in and around the Bay of Bengal." Natural Hazards **31**(2): 561-584.

Quah LC (1988). "ENSO and anti-ENSO related precipitation response over Malaysian Region". *A working paper presented at the WMO/ASCA winter monsoon workshop*. Kuala Lumpur, 27 June-2 July.

Ramage C. (1971). Monsoon meteorology, International Geophysics Series Vol. 15, Academic Press, San Diego.

Rasch, P. J., and Kristjánsson, J. E. (1998) “A comparison of the CCM3 model climate using diagnosed and predicted condensate parameterizations.” J. Climate **11**: 1587-1614.

Rasmusson EM, A. P. (1985). Interannual climate variability associated with the El Ni~no=Southern oscillation.
Coupled Ocean–Atmosphere Models. Amsterdam, Elsevier Science Publishers B.V.

Rasmusson EM, C. T. (1982). "Variations in tropical sea surface temperature and surface wind fields associated with the Southern oscillation=El Ni~no." MonWea Rev **110**: 354–384.

Rinke A., and Dethloff K. (2008) “Simulated circum-Arctic climate changes by the end of the 21st century.” Global and PlanetaryChange, **62**: 173–186.

Ritter, B., and J. Geleyn (1992) “A comprehensive radiation scheme for numerical weather prediction models with potential applications in climate simulations.” Mon. Wea. Rev. **120**: 303–325

Roeckner E, Arpe K, Bengtsson L, Christoph M, Claussen M, D¨umenil L, Esch M, Giorgetta M, Schlese U, SchulzweidaU. (1996). "The atmospheric general circulation model ECHAM4: Model description and simulation of present-day climate." Report No. 218. Max Planck Institut f¨ur Meteorologie: Hamburg, 90.

Roongroj Chokngamwong and Long Chiu (2006). "Trmm and Thailand daily guage rainfall comparison." 20th Conference on Hydrology Wednesday.

Roy N.S. and Kaur S. (2000). "Climatology of monsoon rains of Burma." Interantional Journal of Climatology **20**: 913-928.

Rummukainen, M., J. Räisänen, B. Bringfelt, A. Ullerstig, A. Omstedt, U. Willén, U. Hansson and C. Jones, (2001). "A regional climate model for northern Europe: model

description and results from the downscaling of two GCM control simulations." Clim. Dyn **17**: 339–359.

Saeed S., Sheikh M. M., Saeed S.F. (2006). “Simulations of 1992 Flood in River Jhelum using high resolution regional climate model, PRECIS to study the underlying physical process involved in the extreme precipitation event.” Pakistan Journal of Meteorology **3** (6):35-55

Saji N. H. and S.-P. Xie (2006). "Tropical Indian Ocean variability in the IPCC 20th-century climate simulations." Journal of Climate **13**: 4397-4417

Sangwaldach, P., Wongwises, P., Exell, R.H.B., and Sukawat, D. (2006). The Surface Features of Southwest Monsoon Onset over Thailand. The 2ndJoint International Conference on Sustainable Energy and Environment (SEE 2006), 21-23 November , Swissôtel Nai Lert Park, Bangkok, Thailand.

Sass, B. H., Rontu, L, and Räisänen, P. (1994). “HIRLAM-2 Radiation Scheme: Documentation and Tests.” HIRLAM Technical Report, **16**: 43pp., SMHI, SE-60176, Norrköping.

Sathiyamoorthy, V., P. K. Pal, et al. (2004). "Influence of the Upper-Tropospheric Wind Shear upon Cloud Radiative Forcing in the Asian Monsoon Region." Journal of Climate **17**(14): 2725-2735.

Satomura (2000). "Dirurnal variation of precipitation over the Indo-China Peninsula: Two-dimensional numerical simulation." Journal of the Meteorological Society of Japan **78** (4): 461-475

Savijärvi, H. (1990). “Fast radiation parameterization schemes for mesoscale and short-range forecast models.”, J. Appl. Meteor. **29**: 437-447.

Seiler C. (2009). "Implementation and validation of a RCM for Bolivia." : http://precis.metoffice.com/Useful_Links/Publications

Siniarovina U. and Engardt (2005). “High-resolution model simulations of anthropogenic sulphate and sulphur dioxide in Southeast Asia.” Atmospheric Environment **39**(11): 2021-2034

Sirabaha, H. S. H. (2004). The Influence of El Nino Southern Ocsillation on Climate in Southeast Asia. Environmental Sciences. Norwich, University of East Anglia. **PhD:** 336.

Slingo, J. (1999). "The Indian summer Monsoon and its variability, Beyond El Nino: decadal variability in the climate system." A. Navarra, Ed., Springer-Verlag: 103-118.

Smith, R. N. B. (1990). "A scheme for predicting layer clouds and their water content in a general circulation model." Quarterly Journal of the Royal Meteorological Society **116**: 435-460.

Smith, R. N. B. (1993). Experience and developments with the layer cloud and boundary layer mixing schemes in the UK Meteorological Office Unified Model. In Proceedings of the ECMWF/GCSS Workshop on Parameterisation of the Cloud-Topped Boundary Layer, 8-11 June 1993, European Centre for Medium-Range Weather Forecasts,Reading, England.

Soares W. and Marengo JA. (2009). "Assessments of moisture fluxes east of the Andes in South America in a global warming scenario." Int. J. Climatol. **29**:1395–1414.

Stone, M. C., R. H. Hotchkiss, C. M. Hubbard, T. A. Fontaine, L. O. Mearns, and J. G. Arnold (2001). "Impacts of Climate Change on Missouri River Basin Water Yield." J. of American Water Resources Association. **37**(5): 1119--1130.

Stone, M. C., R. H. Hotchkiss, and L. O. Mearns (2003). "Water yield responses to high and low spatial resolution climate change scenarios in the Missouri River Basin." Geophys. Res. Lett. **30**: 1186-1189.

Stott, P.A. (2003). "Attribution of regional-scale temperature changes to anthropogenic and natural causes." Geophys Res Lett **30**: 1728

Stratton, R. A. (1999). "A high resolution AMIP integration using the Hadley Centre model HadAM2b." Clim. Dyn. **15**: 9–28.

Takahashi HG and Yasunari T (2006). "A Climatological Monsoon Break in Rainfall over Indochina--A Singularity in the Seasonal March of the Asian Summer Monsoon." Journal of Climate **19**(8): 1545-1556.

Takahashi K. and Arakawa H. (1981). World survey of climatology ; Climates of Southern and Western Asia, Amsterdam Oxford : Elsevier Scientific, 1981.

Tanaka, M., J. (1992). "Intraseasonal oscillation and the onset and retreat dares of the summer monsoon over east, southeast Asia and the western Pacific region using GMS high cloud amount data." Meteor. Soc. Japan **70**: 613–629.

Taylor K.E. and J. E. Penner (1994). “Response of the climate system to atmospheric aerosols and greenhouse gases.” Nature **369**, 734-737

Tiedtke, M. (1989) “A comprehensive mass flux scheme for cumulus parameterization in large-scale models.” Mon. Wea. Rev. **117**: 1779-1800.

Tonsuwonnont Pathathai (2006). “Heat Island and Electrical Energy Consumption in Urban Area.**”** MS Thesis, Asian Institute of Technology.

Torsri1 Kritanai, Mega Octaviani1, Kasemsan Manomaiphiboon1 (2009). “Regional Climate Modeling with 60-km Grid Resolution on Temperature for Thailand Using RegCM3 Model with Two Different Driving Meteorological Datasets”. 7th Eco-Energy and Materials Science and Engineering Symposium, Chiang Mai, Thailand 19-22 Nov

Tran H, Uchihama D, Ochi S and Yasuoka Y (2006). "Assessment with satellite data of the urban heat island effects in Asian mega cities" Int. J. Appl. Earth Obs. Geoinf. **8**: 34–48

Ueda, H., A. Iwai, K. Kuwako, and M. E. Hori (2006). "Impact of anthropogenic forcing on the Asian summer monsoon as simulated by 8 GCMs" Geophs. Res. Lett, **33**, L06703, doi:10.1029/2005GL025336.

Uppala, S. M., P.W. Kållberg, A.J. Simmons, U. Andrae, V. da Costa Bechtold, M. Fiorino, J.K Gibson, J. Haseler, A. Hernandez, G.A. Kelly, X. Li, K. Onogi, S. Saarinen, N. Sokka, R.P. Allan, E. Andersson, K. Arpe, M.A. Balmaseda, A.C.M. Beljaars, L. van de Berg, J. Bidlot, N. Bormann, S. Caires, F. Chevallier, A. Dethof, M. Dragosavac, M. Fisher, M. Fuentes, S. Hagemann, E. Hólm, B.J. Hoskins, L. Isaksen, P.A.E.M. Janssen, R. Jenne, A.P. McNally, J.-F. Mahfouf, J.-J. Morcrette, N.A Rayner, R.W. Saunders, P. Simon, A. Sterl, K.E. Trenberth, A. Untch, D. Vasiljevic, P. Viterbo and J. Woollen (2005). "The ERA-40 reanalysis." Quart. J. Roy. Meteor. Soc. **131**: 2961-3012.
V. D. Pope, M. L. G., P. R. Rowntree, and R. A. Stratton, (2000). "The impact of new physical parametrizations in the Hadley Centre climate model: HadAM3." Climate Dynamics **16**: 123-146.

Vecchi, G. A., and D. E. Harrison (2002). "Monsoon breaks and subseasonal sea surface temperature variability in the Bay of Bengal
" J. Climate **15**: 1485–1493.

Vidale PL, L¨uthi D, Frei C, Seneviratne S, Sch¨ar C. (2003). "Predictability and uncertainty in a regional climate model." Journal of Geophysical Research **108**(D18): 4586, DOI: 10.1029/2002JD002810.

Waliser and Gautier (1993). "A satellite-derived Climatology of the ITCZ." Journal of Climate **6**: 2162-2174.

Wang B, K. I.-S., and Li J-Y, (2004). "Ensemble simulation of Asian-Australian monsoon variability by 11 AGCMs." J Climate **17**: 803–818.

Wang C. and Weisberg R.H. (2000). "The 1997-98 El Nino evolution relative to previous El Nino event." Journal of Climate **13**: 488-501.

Wang, Q.J., R.J. Nathan, R.J. Moran, and B. James (1999). "Impact of climate Changes on the Security of the Water Supply of the Campaspe System". Proceedings of the 25th Hydrology and Water Resources Symposium, **1**, 6-8 July, Brisbane, Institution of Engineers, Australia, Water99 Joint Congress, pp. 135-140.

Warner, T. T., R. A. Peterson, and R. E. Treadon (1997). "A tutorial on lateral boundary conditions as a basic and potentially serious limitation to numerical weather prediction." Bull. Amer. Meteor. Soc. **78**: 2599–2617.

Webster P. J. and S. Yang (1992). "Monsoon and ENSO: Selectively Interactive Systems." Quart. J. Roy. Meteor. Soc. **118**: 877-926.

Webster, P. J., Magana, V.O., Palmer, T.N., Shukla, J., Tomas, R.A., Yanai, M, and Yasunari, T. (1998). "Monsoons Processes, predictability and the prospects fo prediction." Journal of Geophysical Research **103**: 14451-14510.

Wilby, R.L. and T.M.L. Wigley (1997). "Downscaling general circulation model output: a review of methods and limitations." Prog. Phys. Geography. **21**: 530-548.

Wilson C.A. and R. Swinbank (1997). Gravity Wave Drag, Unified Model Documentation Paper 22, version 2.0.

Wilson D.R. and Ballard S.P. (1999). "A microphysically based precipitation scheme for the UK Meteorological Office Unified Model." Q.J.R. Meteorol. Soc. **125**: 1607-1636.

Wilson M.F. and A. Henderson-Sellers. (1985). "A Global Archive of Land Cover and Soils Data for Use in General Circulation Climate Models." Journal of Climatology **5**: 119-143.

Wilson, S., Hassell, D., Hein, D., Jones, R., and Taylor, R. (2005). Installing and using the Hadley Centre regional climate modelling system, PRECIS. Version 1.3., Met Office Hadley Centre, Exeter, UK.

Ye H. and Bao Z. (2001). "Lagged teleconnections between snow depth in northern Eurasia, rainfall in southeast Asia and sea-surface temperatures over the tropical Pacific Ocean." Int. J. Clim. **21**:1607-1621.

Ye H., Bao Z. and Feng X. (2005) "Connections of Siberian snow onset dates to the following summer's monsoon conditions over southeast asia" Int. J. Clim. **25**:1567-1584

Zhang C. and J. Gottschalck (2002). "SST anomalies of ENSO and the Madden–Julian oscillation in the equatorial Pacific." J. Climate **15**: 2429–2445.

Zhang, Y., Y. L. Xu, et al. (2006). "A future climate scenario of regional changes in extreme climate events over China using the PRECIS climate model." Geophysical Research Letters **33**(24): -.

Zhang, Yongsheng, Tim Li, Bin Wang, Guoxiong Wu (2002). "Onset of the Summer Monsoon over the Indochina Peninsula: Climatology and Interannual Variations". J. Climate **15**: 3206–3221.

Zhou, N. F., Y. Q. Yu, et al. (2006). "Simulations of the 100-hPa South Asian High and Precipitation over East Asia with IPCC Coupled GCMs." Advances in Atmospheric Sciences **23**(3): 375-390.

Zwiers FW, Zhang X (2003). "Towards regional climate change detection." J Clim **16**: 793–797